Investigation of Chromosome Segregation and Protein Targeting in *Staphylococcus aureus*

Untersuchungen zur Chromosomen-Segregation und Protein-Sortierung in *Staphylococcus aureus*

Dissertation

der Mathematisch-Naturwissenschaftlichen Fakultät

der Eberhard Karls Universität Tübingen

zur Erlangung des Grades eines

Doktors der Naturwissenschaften

(Dr. rer. nat.)

vorgelegt von

Wenqi Yu

aus Shanghai, China

Tübingen

2012

Tag der mündlichen Qualifikation:	14.03.2012
Dekan:	Prof. Dr. Wolfgang Rosenstiel
1. Berichterstatter:	Prof. Dr. Friedrich Götz
2. Berichterstatter:	Prof. Dr. Andreas Peschel

Table of Contents

Abbreviations

aa	Amino acid
agr	Accessory gene regulator
Appr.	Approximate
bp	Base pair
CA-MRSA	Community-acquired methicillin-resistant *Staphylococcus aureus*
CL	Cardiolipin
CWS	Cell wall sorting signal
DAPI	4'-6-diamidino-2-phenylindole
DNA	Deoxyribonucleic acid
Fig.	Figure
Fla	Flavomycin
FnBPB	Fibronectin binding protein B
GFP	Green fluorescent protein
h	Hour
kb	Kilobase
kD	Kilodalton
lip	Lipase
Mbp	Millions of base pairs
mCh	mCherry
MSSA	methicillin-sensitive *Staphylococcus aureus*
NAO	10-*N*-nonyl-acridine orange
OD	Optical density
oriC	Origin of replication
Pc	Penicillin G
PG	Phosphatidylglycerol
PP	Propeptide
RF	Red fluorescence
sfGFP	Super-folder GFP
smc	Structural maintenance of chromosomes
SP	Signal peptide
Spa	Protein A
SrtA	Sortase A
ter	Terminus of replication
Topo IV	DNA topoisomerase IV

TSB	Tryptic soy broth
Van-FL	BODIPY® FL vancomycin
WT	Wild type
YFP	Yellow fluorescent protein
µM	Micromolar
µm	Micrometer

Amino acid code

A	Ala	Alanine	I	Ile	Isoleucine	R	Arg	Arginine
C	Cys	Cysteine	K	Lys	Lysine	S	Ser	Serine
D	Asp	Aspartic acid	L	Leu	Leucine	T	Thr	Threonine
E	Glu	Glutamic acid	M	Met	Methionine	V	Val	Valine
F	Phe	Phenylalanine	N	Asn	Asparagine	W	Trp	Tryptophan
G	Gly	Glycine	P	Pro	Proline	Y	Tyr	Tyrosine
H	His	Histidine	Q	Gln	Glutamine			

Symbols

Δ	Deletion
°C	Grad Celsius
::	Insertion
µ	Micro
α	Anti

Summary

The thesis addressed bacterial cell biological topics of *Staphylococcus aureus*, one of the most important human pathogens. Insights into essential cellular processes, such as chromosome segregation, could serve as a basis for developing new antibiotic targets. The first part deals with chromosome segregation in *S. aureus*. In contrast to rod-shaped model bacteria, an *S. aureus smc* (structural maintenance of chromosomes) mutant was not lethal, and had only mild deficiency in chromosome organization and segregation. Double mutations of *smc* and *spoIIIE* encoding an active DNA translocase resulted in severe growth defect and chromosome segregation impairment. Further, the SMC proteins localized as dynamic foci in a cell cycle dependent manner in *S. aureus*. These results unravel the differences in chromosome dynamics in the spherical staphylococcal cells compared to the model in rods and implies some yet unknown mechanisms. The second part deals with the localization of surface proteins that play key roles in *S. aureus* pathogenicity. A fluorescence microscopic method was developed to directly monitor the localization of secreted and cell wall anchored surface proteins in *S. aureus*. Dependent on the presence of signal peptides alone or together with the cell wall sorting sequence the red fluorescent protein mCherry could be targeted into the cytosol, the supernatant and the cell envelope respectively; in all cases mCherry exhibited bright fluorescence. In staphylococci two types of signal peptides (SP) can be distinguished: the +YSIRK motif SP_{lip} and the −YSIRK motif SP_{sasF}. MCherry-hybrids supplied with the SP_{lip} were always expressed higher than those with SP_{sasF}. Further, mCherry-hybrids with SP_{lip} preferentially localized at the cross wall, while those with SP_{sasF} preferentially localized at the peripheral wall. Interestingly, when treated with sub-lethal concentrations of penicillin or moenomycin, both mCherry-fusions with different SPs were concentrated at the cross wall. The effect is most likely due to antibiotic mediated increase of free anchoring sites (Lipid II) at the cross wall, the substrate of Sortase A (SrtA); SrtA was required for this shift. In the last part (in cooperation with the research group of Dr. Proikas-Cezanne), the invasion of *S. aureus* into non-phagocytic cells (human osteosarcoma U2OS cell line stably expressing GFP-WIPI-1) triggering host autophagic response was investigated. It was found that the invading *S. aureus* USA300, HG001, SA113 could stimulate autophagy, and became entrapped in intracellular autophagosome-like vesicles. *Agr*-positive *S. aureus* strains were more efficiently entrapped than *agr*-negative cells. The entrapped *S. aureus* still undergo cell division. Likely, the invading *S. aureus* become entrapped in autophagosome-like vesicles and are dedicated for lysosomal degradation in non-professional host cells.

Zusammenfassung

Die Doktorarbeit behandelt ein Thema der bakteriellen Zellbiologie bei *Staphylococcus aureus*, einer der wichtigsten humanpathogenen Arten. Einblicke in die grundlegenden zellulären Prozessen, wie z. B. Chromosomensegregation, könnten als Grundlage für die Entwicklung neuer Angriffsorte für Antibiotika dienen. Der erste Teil befasst sich mit der Chromosomen-Segregation in *S. aureus*. Im Gegensatz zu stäbchenförmigen Modell-Bakterien, war in *S. aureus* eine SMC-Mutante (structural maintenance of chromosomes) nicht letal, und hatte nur leichte Mängel in der Organisation und Segregation der Chromosomen. Eine Doppel-Mutante von SMC und SpoIIIE, letztere codiert für eine aktive DNA-Translokase, führte zu schwerwiegenden Defekten in Wachstum und Chromosomensegregation. Ferner waren die SMC-Proteine als dynamische Punkte (foci) in einer Zellzyklus-abhängigen Weise in *S. aureus* lokalisiert. Diese Ergebnisse zeigen, dass es deutliche Unterschiede in der Chromosomen-Dynamik zwischen den sphärischen Staphylokokken den stäbchenförmigen Bakterien gibt und lassen auf noch unbekannte Mechanismen schließen. Der zweite Teil beschäftigt sich mit der Lokalisierung der Oberfläche Proteine, die in *S. aureus* eine Schlüsselrolle in der Pathogenität spielen. Es wurde ein fluoreszenzmikroskopisches Verfahren entwickelt, um direkt die Lokalisierung von sekretierten und Zellwand verankerten Oberflächenproteinen bei *S. aureus* verfolgen zu können. Je nach dem, ob das rot fluoreszierendes Protein mCherry allein, mit dem Signalpeptide, oder zusammen mit der Zellwand-Sortierungssequenz fusioniert wurde, war mCherry etweder im Cytosol, dem Überstand oder der Zellwand lokalisiert; in allen Fällen zeigte mCherry helle Fluoreszenz. In Staphylokokken können zwei Arten von Signalpeptiden (SP) unterschieden werden: mit einem (+YSIRK) Motiv (SP_{lip}) und ohne einem (−YSIRK) Motiv (SP_{sasF}). mCherry-Hybride mit (+YSIRK) Motiv waren immer höher exprimiert als als jene ohne (−YSIRK) Motiv (SP_{sasF}). Ferner waren mCherry-Hybride mit SP_{lip} bevorzugt in der Querwand, während diejenigen mit SP_{sasF} bevorzugt in der peripheren Wand lokalisiert. Bei Behandlung mit subletalen Konzentrationen von Penicillin oder Moenomycin, waren beide SP-mCherry Fusionen in der Querwand konzentriert. Der Effekt ist höchstwahrscheinlich auf die Antibiotika-vermittelte Erhöhung der freien Ankerplätze (Lipid II), dem Substrat der Sortase A (SrtA), an der Querwand zurückzuführen. SrtA war für diesen Effekt notwendig. Im letzten Teil (in Zusammenarbeit mit der Arbeitsgruppe Dr. Proikas-Cezanne), wurde die Invasion von *S. aureus* in nicht-phagozytierenden Zellen (human osteosarcoma U2OS cell line stably expressing GFP-WIPI-1) und die Auslösung von Autophagocytose-Reaktionen untersucht. Es stellte sich heraus, dass die eingedrungenen *S.*

aureus USA300, HG001, SA113 Zellen Autophagie auslösten und in und in intrazellulären Autophagosom-ähnlichen Vesikeln eingeschlossen waren. *Agr*-positive *S. aureus* Stämme wurden effizienter als *agr*-negativen Zellen eingeschlossen. Die eingeschlossenen *S. aureus* Zellen teilten sich noch. Wahrscheinlich werden die eindringenden *S. aureus* Zellen in Autophagosom-ähnliche Vesikel eingefangen und dem lysosomalen Abbau in de nicht-professionellen Wirtszellen zugeführt.

List of publications

a) Publications from the current thesis

1. **Yu W**, Herbert S, Graumann PL, Götz F. (2010) Contribution of SMC (structural maintenance of chromosomes) and SpoIIIE to chromosome segregation in Staphylococci. *J Bacteriol.* 192 (15): 4067-4073.
2. **Yu W**, Götz F. (2012) Cell Wall Antibiotics Provoke Accumulation of Anchored mCherry in the Cross Wall of *Staphylococcus aureus*. *PLoS ONE* 7(1): e30076.
3. Mauthe M, **Yu W**, Krut O, Kroenke M, Götz F, Robenek H, Proikas-Cezanne T. (2012) WIPI-1 positive autophagosome-like vesicles entrap pathogenic *Staphylococcus aureus* for lysosomal degradation. *Int J Cell Biol,* in press.

b) Publications and manuscripts <u>not</u> from the current thesis

1. Lin P, Hu T, Hu J, **Yu W**, Han C, Zhang J, Qin G, Yu K, Götz F, Shen X, Jiang H, Qu D. (2010) Characterization of peptide deformylase homologues from *Staphylococcus epidermidis*. *Microbiology*.156: 3194-202.
2. Schlag M, Biswas R, Krismer B, Kohler T, Zoll S, **Yu W**, Schwarz H, Peschel A, Götz F. (2010) Role of staphylococcal wall teichoic acid in targeting the major autolysin Atl. *Mol Microbiol.* 75(4): 864-873.
3. Wu Y, Xu T, Wang J, Liu J, **Yu W**, Lou Q, Zhu T, He N, Ben H, Hu J, Götz F, Qu D. (2012) The two-component signal transduction system ArlRS regulates *Staphylococcus epidermidis* biofilm formation in an *ica*-dependent manner. *PLoS ONE* submitted.
4. Schuster S, Nega M, **Yu W**, Schreiber F, Götz F, Zhang F. The role of the serum components on bacterial adhesion at OEG/PEG SAM coated gold substrates. Manuscript in preparation.

Contribution to publications

Yu W, Herbert S, Graumann PL, Götz F. (2010) Contribution of SMC (structural maintenance of chromosomes) and SpoIIIE to chromosome segregation in Staphylococci. *J Bacteriol.* 192 (15): 4067-4073.
I conceived and designed the experiments, performed the experiments, analyzed the data and wrote the paper. Herbert S provided the DKO1.6 triple mutants; Graumann PL and Götz F gave me supervision and suggestions for every step.

Yu W, Götz F. (2012) Cell Wall Antibiotics Provoke Accumulation of Anchored mCherry in the Cross Wall of *Staphylococcus aureus*. *PLoS ONE* 7(1): e30076.
For this part, I conceived and designed the experiments, performed the experiments, analyzed the data and wrote the paper. Götz F gave me supervision and suggestions for every step.

Mauthe M, **Yu W**, Krut O, Kroenke M, Götz F, Robenek H, Proikas-Cezanne T. (2012) WIPI-1 positive autophagosome-like vesicles entrap pathogenic *Staphylococcus aureus* for lysosomal degradation. *Int J Cell Biol,* in press.
For the cooperation with the research group of Dr. Proikas-Cezanne, I constructed pC-tuf-ppmch and provided different staphylococcal strains with this fluroscence-gene expressing plasmid. I also contributed to data analysis and paper writing.

General Introduction

1. The *Staphylococcus* genus

The *Staphylococcus* genus (*Firmicutes, Bacilli, Bacillales* and *Staphylococcaceae*) belongs to the Gram-positive bacteria with a low DNA G+C content (33-40%) (Götz, 2006). The beautiful name '*Staphylococcus*' (derived from the Greek, σταφυλή, *staphylē*, 'bunch of grapes' and κόκκος, *kókkos*, 'granule') illustrates the round (cocci) and the clustering (grape-like) morphology of this bacteria genus. Members of the *Staphylococcus* genus are facultative anaerobic, immotile, nonspore-forming and with a genome of about 2-3 Mbp. The natural habitats of *Staphylococcus* include the skin, skin glands, and mucous membranes of mammals and birds. Among around 40 species identified so far in this genus, the pathogenic species *Staphylococcus aureus* and *Staphylococcus epidermidis* are most intensively studied. Compared to *S. epidermidis* that is often implicated in the chronic nosocomial infections, *S. aureus* can cause more invasive and acute infections, such as toxic shock syndrome, staphylococcal scalded skin syndrome, osteomyelitis, septic arthritis, or endocarditis. To become a successful pathogen, *S. aureus* employs a variety of strategies to colonize and invade the host and evade the host immune defense, such as secreting numbers of enzymes (protease, nuclease, lipase, hyaluronidase, *etc*.) and toxins (enterotoxins, leukocidin, hemolysins, exfoliative toxin A and B, toxic shock syndrome toxin 1, *etc*.) to break down the host cells and tissues, expressing surface proteins as adherence factors to proliferate both extra- and intracellularly (fibronectin-binding proteins FnbpA/B, fibrinogen-binding proteins ClfA/B, *etc*.), modifying its surface to escape from the innate immune response, or changing its lifestyles to survive in different ecological niches (biofilm formation, small colony variant, etc.) (Becker *et al.*, 2007, Fedtke *et al.*, 2004, Foster, 2005, Proctor *et al.*, 2006). The increased emergence of highly virulent and multiple antibiotics resistant stains of *S. aureus* (MRSA, VRSA) in the recent years further emphasize the research on staphylococci.

2. Visualizing *Staphylococcus*

In the traditional microbiology textbook, the bacterial cell is regarded to be amorphous, or as 'bag of enzymes', as it has neither nucleus nor clear cellular structures. But obviously thousands of biological processes take place orderly in such a 'tiny bag' almost every second. How could this be achieved? The first time I learnt '*Staphylococcus*', I wondered why *Staphylococcus* is round and grape-like? How do staphylococci divide? With all these questions in mind, I became interested in the newly emerged research field, the 'bacterial cell

biology', which studies the bacterial subcellular architectures and bacterial cell cycle (Gitai, 2005). Especially in the last twenty years, with the aid of the fast developments in microscopic visualization techniques, it is evident now that despite of its diminutive cell size, the bacterial cell is exquisitely organized, precisely coordinated and highly dynamic! So far, most of the bacterial cell biology studies have been focused on the 'model organisms', such as *Escherichia coli* or *Bacillus subtilis*. There are relatively few reports on the spherical staphylococcal cells, which indeed have a unique cell division mode compared to the rod-shaped model organisms.

During my PhD study, I have been interested in visualizing staphylococcal cells and understanding the biology of the human pathogen *S. aureus* by using genetic and microscopic techniques. The thesis is composed of three parts. The first part is about the staphylococcal chromosome distribution and segregation; the second part is about the localized secretion and anchoring of staphylococcal surface proteins. In the third part, *S. aureus* invasion to the host eukaryotic cells inducing autophagic response was visualized and analyzed.

Part I Staphylococcal chromosome segregation

Introduction

1. Bacterial chromosome segregation

After DNA replication, the sister chromosomes separate from each other and each daughter cell receives equivalent DNA. This process must be spatially and temporally well defined to ensure faithful reproduction. Compared to the elaborate process of mitosis in the eukaryotic cell, much less is known about the bacterial cell division and chromosome segregation. Yet as the most widespread and abundant organisms on the earth, bacteria adopted elegant features for the fast and accurate reproduction.

1) Chromosome organization

Most of the bacterial genomes consist of double stranded DNA in the circular form and are about several Mbp in size. In *E. coli*, the physical length of its genomic DNA is about 1000 times the length of the cell. To fit in to the tiny bacterial cell, the bacterial chromosome is highly condensed and compact in a structure known as the nucleoid. The bacterial nucleoids have no nuclear membrane, and have a diffuse appearance in the cytoplasm (**Fig.I-1A**). However, the nucleoids are not just a plate of 'spaghetti', they are in fact spatially and orderly organized (**Fig. I-1B**). Webb et al. inserted a large number of *lacO* sites into the chromosome of *B. subtilis* at the sites of interest, e.g. the origin of replication (*oriC*) or the terminus of replication (*ter*); and then expressed the LacI-GFP fusion that bound to the *lacO* sites. The resulting fluorescent pictures illustrated the localization of *oriC* or *ter* in the cell (Webb *et al.*, 1997). Similar experiments and fluorescence in situ hybridization (FISH) in *E. coli* and *Caulobacter* show that the bacterial chromosome is spatially localized like its gene locus's position in the genome; furthermore, the orientation of the chromosome differed from bacteria to bacteria (Jensen & Shapiro, 1999, Teleman *et al.*, 1998, Lau *et al.*, 2003, Viollier *et al.*, 2004, Nielsen *et al.*, 2006b, Wang *et al.*, 2006) (**Fig. I-1B**). For example, the *oriC* localized at one cell pole in *B. subtilis* but at the mid-cell *in E. coli.*

2) Models of bacterial chromosome segregation

A. Replicon model

The traditional and most popular view about bacterial chromosome segregation is the replicon model (Jacob F, 1963). It was proposed that the newly replicated *oriC* regions were attached

to the cell membrane. The growth between the attachment sites of sister *oriC* regions drove the separation of the sister chromosomes passively.

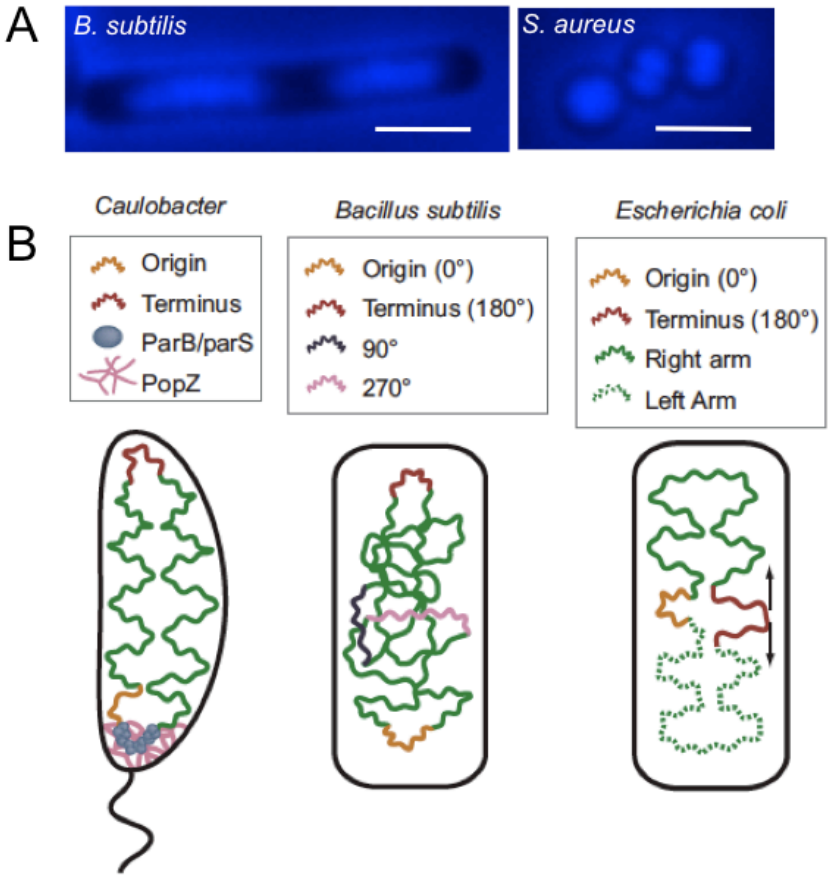

Fig. I-1. Chromosome distribution in bacteria. (A) Chromosome distribution in *B. subtilis* and *S. aureus* revealed by DAPI staining; scale bar, 2 µm. **(B)** Chromosome organization in *Caulobacter*, *B. subtilis* and *E.coli;* figure adapted from (Toro & Shapiro, 2010).

B. Driving force model

As demonstrated by the DNA tagging technology, it is now clear that the separation of newly replicated nucleoids is much faster than the speed of cell elongation (Webb et al., 1997, Jensen & Shapiro, 1999, Teleman et al., 1998, Viollier et al., 2004, Gordon *et al.*, 1997, Mohl & Gober, 1997). Meanwhile, the sister chromosomes segregate progressively while the replication is still ongoing (Viollier et al., 2004, Nielsen *et al.*, 2006a). It was therefore hypothesized that some sort of motors generated the driving force for the chromosome segregation. The hypothesized motors include the DNA polymerase (Lemon & Grossman, 2001), the RNA polymerase (Dworkin & Losick, 2002), 'transertion' (the coupled process of transcription, translation, insertion of membrane associated proteins) (Woldringh, 2002), or the conformational entropy of the sister chromosomes (Jun & Wright, 2010). The actin-like

MreB protein has also been suggested to be involved in the bacterial chromosome segregation (Gitai *et al.*, 2005, Kruse *et al.*, 2006, Soufo & Graumann, 2003).

C. Mitotic-like model

The observation that many bacterial chromosomes encode homologs of the active partitioning proteins (ParABS system) from low copy number plasmids (F and P1) suggested the existence of bacteria mitotic-like apparatus. ParA ('Soj' in *B. subtilis*) is a Walker type ATPase that can polymerize over the nucleoid (Surtees & Funnell, 2003). *ParS* is a centromeric DNA sequence that distributes in the proximity of *oriC*. ParB ('Spo0J' in *B. subtilis*) protein binds specifically to the *parS* sequence. It was shown recently that in *Caulobacter crescentus,* ParB moved the centromere (*oriC*) to the opposite cell pole by depolymerizing ParA, in a way that was similar to eukaryotic spindles (Ptacin *et al.*, 2010).

To sum up the above theories about bacterial chromosome segregation, every model is supported by some observations but there seems no common mechanism that could be applied to explain the various observations in the different bacteria. The mechanisms of bacterial chromosome segregation are rather diverse and redundant (Errington *et al.*, 2005), which remains as one of the most mysterious process in the cell.

3) Coordinating bacterial chromosome segregation and cell division

A. Min system.

The MinCDE system is the first mechanism that has been discovered to control the right placement of the division septum in the mid of the cell. MinD is an ATPse that forms complex with MinC, which inhibits the FtsZ-ring formation. In *E. coli*, MinCD oscillate from cell pole to pole with the help of MinE (Hu & Lutkenhaus, 1999, Raskin & de Boer, 1999). In *B. subtilis*, MinCD stably localize to both cell poles by DivIVA, which in turn, binds to the negatively curved membranes (Lenarcic *et al.*, 2009, Marston & Errington, 1999, Marston *et al.*, 1998, Ramamurthi & Losick, 2009).

B. Nucleoid occlusion

Another system that regulates the position of cell division is the nucleoid occlusion effect. The Noc protein in *B. subtilis* and the SlmA protein in *E. coli* were found to play crucial roles in coordinating cell division and chromosome segregation by preventing cell division over the nucleoids (Wu & Errington, 2004, Bernhardt & de Boer, 2005). Deletion of *noc* or *slmA* led to

the bisection of the chromosome by the division septum under certain conditions. Double mutants of *noc* and *min* or *slmA* and *min* were synthetic-lethal. Both Noc and SlmA were found to bind to special DNA sequence in the chromosome. SlmA inhibited the cell division by inhibiting the FtsZ ring formation (Bernhardt & de Boer, 2005, Cho *et al.*, 2011); while the molecular target of Noc is still elusive. Interestingly, Noc and SlmA have no sequence or structural similarity and are found restricted in certain bacterial classes (Noc found in Gram-positive *Firmicute*, SlmA found in Gram-negative phylum *Proteobacteria*). Notably, some other unknown mechanisms are likely existed, as suggested by the observation that Z-ring can still form in the DNA-free space when both Noc and Min system are absent (Wu & Errington, 2011).

2. Role of bacterial condensins (SMC) in chromosome segregation

SMC (structure maintenance of chromosomes) proteins are known to play central roles in the chromatin biology in the living organisms (Hirano, 2006). In bacteria, known as bacterial condensins, SMC complexes are found to be crucial in various aspects of bacterial chromosome dynamics, such as chromosome condensation, packaging, partitioning and DNA repair (Britton *et al.*, 1998, Dervyn *et al.*, 2004, Graumann, 2000, Lindow *et al.*, 2002, Moriya *et al.*, 1998, Volkov *et al.*, 2003). Three families of SMC complexes have been identified in bacteria. The SMC-ScpAB complex (Mascarenhas *et al.*, 2002, Soppa *et al.*, 2002) is found in many bacteria and archaea. The MukBEF complex (Danilova *et al.*, 2007, Niki *et al.*, 1991, Petrushenko *et al.*, 2006) is found only in enterobacteria and some other γ-proteobacteria, and the newly identified MksBEF (MukBEF-like SMC proteins) complex is found scattering over the phylogenetic tree and often coexists with SMC-ScpAB or MukBEF (Petrushenko *et al.*, 2011).

B. subtilis SMC protein and its functional analog MukB protein in *E. coli* are composed of two head regions at N- and C- termini, setting up an ATPase domain, separated by two heptad-rich regions forming a single internal long coiled-coil that are connected by a flexible hinge domain in the middle. Homodimerized SMC proteins linked by the hinge domain (Hirano & Hirano, 2002) form a ring-like structure with ScpA and ScpB while MukB forms complex with MukF and MukE correspondingly (Mascarenhas et al., 2002, She *et al.*, 2007) (**Fig. I-2A**). It has been shown that the MukBEF complex binds and bridges distant DNA fragments to compact the chromosome on a large scale (Petrushenko *et al.*, 2010).

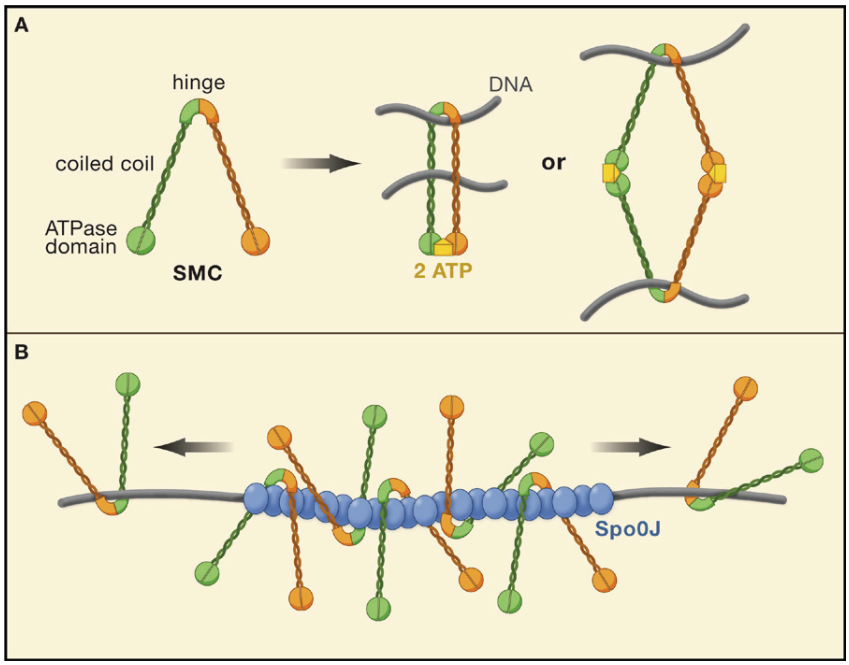

Fig. I-2. (A) Structure of SMC complex. **(B)** SMC is recruited to the *oriC* region by Spo0J-*parS*. Figure adapted from (Thanbichler, 2009).

The mutant of *B. subtilis smc* shows a severe temperature sensitive lethal phenotype with irregular chromosome organization and chromosome segregation defects (Britton et al., 1998, Moriya et al., 1998). It is proposed that the pleiotropic phenotype of *smc* mutant was primarily due to its function in chromosome condensation (Britton et al., 1998). Recently it has been found that in *B. subtilis,* the localization of SMC proteins near the *oriC* region is mediated by the nucleoprotein complex of Spo0J (ParB) bound to *parS* sites, which distributes around the *oriC* region (Gruber & Errington, 2009, Sullivan *et al.*, 2009). The *oriC*-proximal localization of SMC protein is pivotal but not essential for its function, as an SMC mutant has much more severe defect in chromosome segregation than a Spo0J mutant (Britton et al., 1998). It is suggested that instead of global condensation of the chromosomes, the enrichment of SMC near the *oriC* region by ParB-ParS facilitate efficient chromosome segregation by compacting the nascent DNA as it emerges from the replisome (Gruber & Errington, 2009, Sullivan et al., 2009) (**Fig. I-2B**).

Despite of low sequence similarity with SMC in *B. subtilis*, the *E. coli mukB* mutant shows similar phenotype. MukB also colocalizes with the *oriC* region (Danilova et al., 2007). However, *E. coli* lacks the ParABS system. The mechanism of targeting MukB is not known yet. On the other hand, a direct physical and functional interaction between the MukB hinge domain and the DNA binding subunit of decatenase (DNA topoisomerase IV, Topo IV) has

been reported recently (Hayama & Marians, 2010, Li *et al.*, 2010). The interaction appears to be crucial for the functions of both proteins, and the cooperation between decatenation and condensation is vital for proper chromosome segregation in *E. coli*. Whether *B. subtilis* SMC interact directly with Topo IV remains to be investigated. Yet there is evidence that over-expression of Topo IV can partially rescue the growth and DNA condensation defect of the *smc* mutant, but not the DNA segregation defect in *B. subtilis* (Tadesse *et al.*, 2005). In summary, how the bacterial condensins promote the nascent sister chromosomes segregation is still not very clear.

3. Role of DNA translocases (SpoIIIE and SftA) in chromosome segregation

The involvement of SpoIIIE in chromosome segregation was first identified during sporulation in *B. subtilis* (Wu & Errington, 1994). It is required for active translocation of the bulk chromosome into the forespore across the fused septal membranes (Burton *et al.*, 2007). SpoIIIE consists of an N-terminal transmembrane domain responsible for membrane anchoring and the C-terminal ATPase and DNA translocation domain. The function of SpoIIIE in postseptational chromosome partitioning renders it as a backup mechanism to rescue the nucleoids that have been trapped by the division septum when chromosome segregation was perturbed in vegetative cells (Sharpe & Errington, 1995). Consequently, the double mutant of *smc* and *spoIIIE* had a synergistic lethal phenotype in *B. subtilis* (Britton & Grossman, 1999). The combination of *E. coli mukB* null mutation and truncation of *ftsK* encoding the homolog protein to SpoIIIE resulted in a similar synergistic lethal phenotype (Yu *et al.*, 1998).

Recently it has been found in *B. subtilis* that a second FtsK/SpoIIIE like protein, SftA (septum-associated FtsK-like translocase of DNA) coordinates chromosome translocation to ensure maximum chromosome segregation, however, at a different stage of cell division than SpoIIIE (Biller & Burkholder, 2009, Kaimer *et al.*, 2009). SftA contains the C-terminal DNA binding and ATPase domain; but instead of the N-terminal transmembrane domain in SpoIIIE, it has a soluble domain. SftA translocates chromosomes before septation while SpoIIIE comes into play postseptationally when chromosomes are trapped by the septal membrane. Like *B. subtilis spoIIIE* mutants, the *sftA* mutants had a synergistic lethal defect with an *smc* deletion (Kaimer et al., 2009). The *sftA/spoIIIE* double mutant undergoes normal growth while the defect in chromosome segregation is exacerbated significantly compared to both single mutants (Kaimer et al., 2009).

4. Staphylococcal chromosome segregation and cell division

Compared to the intensive investigations on chromosome segregation in the 'model organisms', very little is known about staphylococcal chromosome organization and dynamics.

Since *Staphylococcus* is closely related to *Bacillus*, some of the findings from *Bacillus* can be applied to *Staphylococcus* as well. But it is not always the case. As mentioned above, the DivIVA protein in *B. subtilis* performs the role as the cell pole anchor for the MinD protein, which prevents cell division at the cell poles. Interestingly, the homolog of DivIVA is also presented in *Staphylococcus* that apparently has no cell pole. The deletion of *divIVA* gene in *S. aureus* shows no detectable phenotype (Pinho & Errington, 2004). Another study on the role of Noc protein in *S. aureus* shows that in the Noc deleted cells there is an increase in bisected chromosomes by the division septum. Further, the FtsZ ring placement is no longer perpendicular to the previous division plane (Veiga *et al.*, 2011). Therefore it is proposed that the axis of chromosome segregation has a role in determining the division plane placement in *Staphylococcus* (Veiga et al., 2011). However, the *noc* deletion mutant is still viable, indicating the complexity of the mechanisms in maintaining proper chromosome segregation.

A summary and comparison of different proteins involved in chromosome segregation and cell morphogenesis among *B. subtilis, E. coli* and *S. aureus* is listed in **Table 1**.

Table 1. Comparison of proteins involved in chromosome segregation and cell morphogenesis among *B. subtilis, E. coli* and *S. aureus*

Name			**Function**
B. subtilis	*E. coli*	*S. aureus*	
ParA/Soj	no	no	Regulate DNA replication via DnaA in *B. subtilis;* Form polymers and its depolymerization moves chromosome to the cell pole in *Caulobacter*
ParB/Spo0J	no	SAOUHSC_00342	Binds to *parS* sequence scattering near *oriC*, interact with ParA, SMC in *B. subtilis*
Smc	MukB	SAOUHSC_01204	Chromosome condensation, partitioning
ScpA	MukF	SAOUHSC_01589	ScpA (MukF) and ScpB (MukE) form complex with SMC (MukB)
ScpB	MukE	SAOUHSC_01588	
SpoIIIE	FtsK	SAOUHSC_01253	Pump the chromosome across the fused membrane in *B. subtilis*; resolve sister chromosome dimers in *E. coli*
SftA	γ-domain-containing FtsK DNA translocases paralog	SAOUHSC_01857	Pump the chromosome before septation
MinC	MinC	no	Prevent Z-ring formation at cell poles
MinD	MinD	no	
DivIVA	no	SAOUHSC_01158	Bind MinCD at cell pole in vegetative growth; adaptor linking RacA-DNA to membrane at one cell pole during sporulation in *B. subtilis*
YpsB (DivIVA paralog)	no	SAOUHSC_01462	Late divisome protein
Noc	SlmA	SAOUHSC_03049	Nucleoid occlusion effector
MreB	MreB	no	Bacterial cytoskeleton protein, involved in many cellular process, including chromosome segregation
MreC	MreC	SAOUHSC_01759	Rod shape determining protein
MreD	MreD	SAOUHSC_01758	Rod shape determining protein
RodZ	RodZ	SAOUHSC_02404	Rod shape determining protein

5. Aim of the study

While little is known about chromosome organization and dynamics in *Staphylococcus* so far, its spherical cell shape and the special consecutive perpendicular division mode (Giesbrecht *et al.*, 1998, Tzagoloff & Novick, 1977, Zapun *et al.*, 2008) render it an attractive organism for the chromosome and bacterial cell cycle research. Moreover, the important status of *S. aureus* as one of the most prominent human pathogens highlights the significance of studying essential cellular processes that could serve as a basis for antibiotic target development (Götz, 2004, Haydon *et al.*, 2008).

In the current study, we aimed to get a first glimpse of the molecular mechanisms underlying chromosome segregation in *S. aureus*. We present the intriguing findings towards the functions of SMC and SpoIIIE in chromosome segregation in *S. aureus*. The subcellular localization of SMC was also studied.

Results

1. *S. aureus smc* mutant was not impaired in growth

Genome analysis revealed that there was one single *smc* gene locus presented in all the staphylococcal genomes available so far. *S. aureus smc* (SAOUHSC_01204) encodes a 1,188 amino-acid polypeptide with calculated molecular mass of 136.7 kD that shares 42.8% similarity with *B. subtilis* SMC and consists of the typical domain structures of SMC protein family analyzed by ClustalW2 alignment and SMART (Simple Modular Architecture Research Tool). During our previous work, a transposon Tn*917* mutagenesis library was constructed in an *S. aureus* double knock out stain (DKO1) where two genes encoding 'lipopolysaccharide modification acyltransferase' and 'acyltransferase' were deleted (Herbert *et al.*, 2007). One insertion mutant (DKO1.6) was identified of carrying Tn*917* at nucleotides 1078-1087 within the *smc* gene. In order to study the function of SMC involved in chromosome organization and segregation, *smc*::Tn*917* was phage-transduced into wild type (WT) *S. aureus* strain SA113, generating a single *smc*::Tn*917* mutant **(Fig. I-3A)**. Phage transductions were performed at 23°C to decrease the probability of suppressor mutations. Isolated mutants were confirmed by sequencing. Surprisingly, SA113 *smc*::Tn*917* showed similar growth behavior as WT cells both on TSA (tryptic soy broth agar) plates and in TSB liquid medium at all three temperatures (30°C, 37°C and 42°C) tested **(Fig. I-4)**. These observations were in contrast to the previous findings in *B. subtilis*. The *B. subtilis* Δ*smc* was

temperature sensitive lethal in rich medium and could only grow at 23°C in this medium (Britton et al., 1998, Moriya et al., 1998). In the genome of *S. aureus*, *smc* is located directly upstream of *ftsY, p13* and *ffh,* the genes encoding components of signal recognition particle protein translocation system. In order to rule out the possible polar effect of Tn917 on the downstream genes' expression, a marker-less partial deletion *smc* mutant was constructed **(Fig. I-3B)**. A 1.3 kb fragment of *smc* gene at its 3' was left intact due to the consideration that it contains a potential protomtor controlling the downstream genes' expression. SA113 Δ*smc* exhibited the same growth curve as SA113 *smc*::Tn*917* (data not shown).

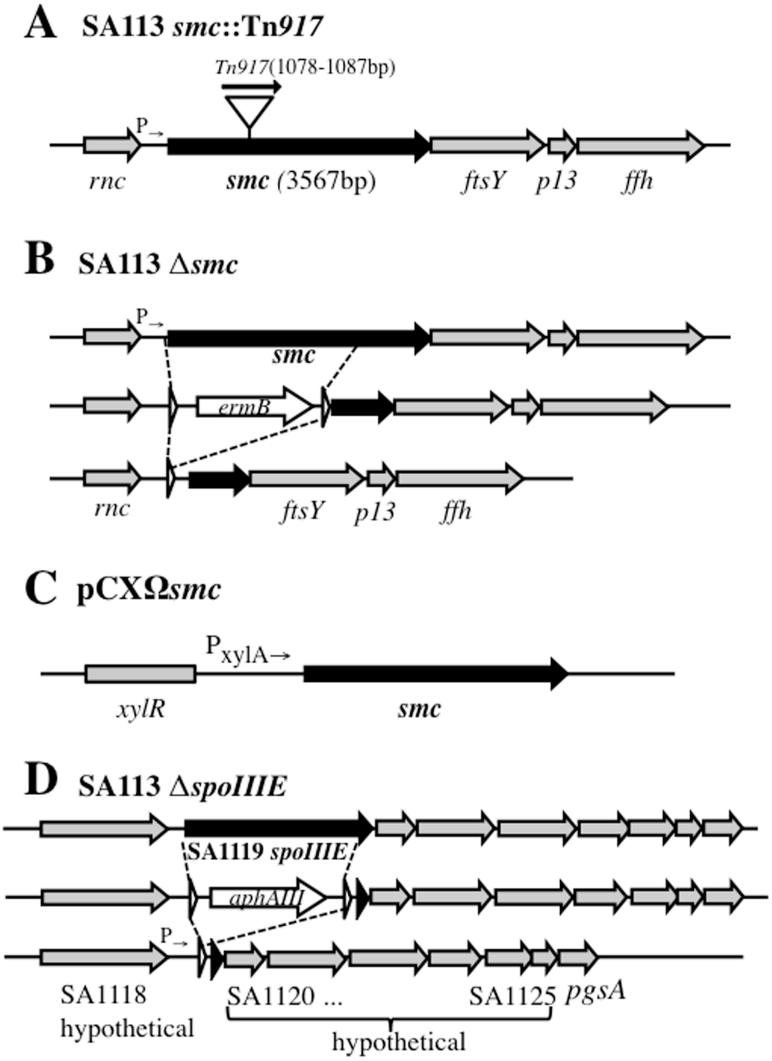

Fig. I-3. (A) Tn*917* insertion site in SA113 *smc::Tn917.* **(B)** Construction of SA113 Δ*smc;* the *smc* coding sequence except 1294 bp at 3' was replaced by *ermB* cassette flanked with *lox* sites that was further removed by Cre recombinase. **(C)** Schema of pCXΩ*smc;* the *smc* gene was cloned into pCX15 (Wieland *et al.*, 1995), under the transcriptional control of xylose promoter/operator system. **(D)** Construction of SA113 Δ*spoIIIE;* the *spoIIIE* coding sequence except 68 bp at 3' was replaced by *aphAIII* cassette flanked with *lox* sites and further removed by Cre recombinase; white arrowheads represented *lox* sites.

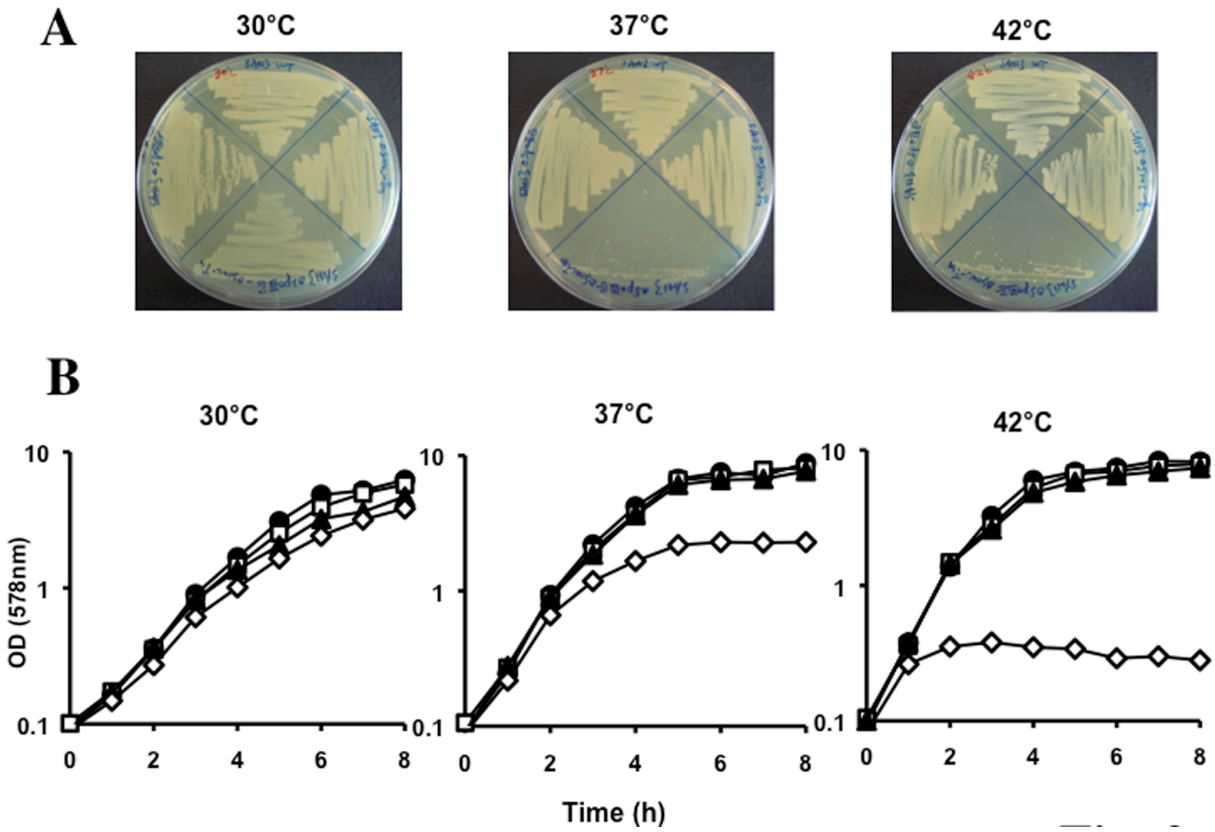

Fig. I-4. (A) Growth comparison of SA113 WT (up), *smc::Tn917* (right), Δ*spoIIIE* (left) and *smc::Tn917*/Δ*spoIIIE* (down) on TSB-Agar plates at 30°C, 37°C and 42°C for 24 h. **(B)** Growth in TSB rich medium. WT (●); *smc::Tn917* (□); Δ*spoIIIE* (▲); *smc::Tn917*/Δ*spoIIIE* (◇).

2. *S. aureus smc* mutant showed chromosome segregation deficiency, which was reduced at higher temperature.

Next, we sought to verify if the loss of functional SMC would affect chromosome segregation in *S. aureus*. Samples were taken from exponentially growing cultures at three temperatures for fluorescent microscopy examination (Leica DM5500B). DNA was stained with DAPI (4'-6-diamidino-2-phenylindole), cell membrane was labeled with FM1-43 and cell wall was labeled with BODIPY® FL vancomycin (Van-FL) to visualize different cellular structures. While in the rod-shaped *E. coli* and *B. subtilis*, it seemed that the chromosome occupies approximately three fourths of the cell volume **(Fig. I-1A)** (Britton et al., 1998, Moriya et al., 1998), in *S. aureus* the chromosome almost fills the entire cell compartment as demonstrated by DAPI staining **(Fig. I-1A, I-5A)**. In SA113 *smc*::Tn*917,* about 10% of the cells were devoid of nucleoids; they appeared as anucleate cells (‘black cells’ stained with DAPI) that indicated defects in chromosome segregation **(Fig. I-5B).** The anucleate cells were also

observed in SA113-DKO1.6 that carried *smc*::Tn*917* but not in SA113-DKO1, confirming that the chromosome segregation defect was due to the mutation in *smc* gene. In SA113 *smc*::Tn*917*, 'half black cells' were observed (2% of 911 cells counted at 30°C) which were composed of one anucleate hemisphere and one normal hemisphere with regular chromosome content and morphology **(Fig. I-5B, arrow)**. We assume that this kind of 'half black cell' would be able to further divide into one anucleate daughter cell and one normal daughter cell as the cross wall could correctly form in the middle of the cell [**Fig. I-5B**; staining with Van-FL (green)] and single spherical anucleate cells were observed frequently **(Table 2)**. Further, anucleate diplococci (i.e. **Fig. I-6B**, yellow arrow) were observed although at a low rate of 0.12% (2 pairs of black diplococci out of 1634 cells counted). It is yet difficult to distinguish whether these anucleate diplococci were divided from one anucleate cell or they were divided from two 'half black cells' and afterwards detached from tetrads composing two normal cells and these two anucleate cells. Intriguingly, quantitative analysis revealed that the percentage of anucleate cells decreased by three fold at 42°C in *smc*::Tn*917* **(Table 2)**, suggesting that the defect of chromosome segregation caused by SMC mutation could be relieved by higher growth temperature. SA113 Δ*smc* exhibited similar rate in chromosome segregation deficiency **(Table 2).** The chromosome segregation defect in *S. aureus smc*::Tn*917* or Δ*smc* could be largely complemented by plasmid-encoded SMC, which is controlled by xylose inducible promoter (pCXΩ*smc*) (Wieland et al., 1995)**(Fig. I-3C, Table 2)**. Notably, no other aberrant chromosome distribution or abnormal cell shape could be found in *S. aureus smc*::Tn*917* and Δ*smc* mutants except for the anucleate cells **(Table 2).** Thus, SMC's function as condensin appeared to be less critical in *S. aureus* in contrast to *B. subtilis* SMC or *E. coli* MukB.

Table 2. Quantitive analysis of irregular chromosome appearance from mid-log phase culture[1].

	Strain	Total cells counted	Anucleate cells[2]	'CUT' phenotype[2]	Uneven distribution[2]	Increased/ decreased content[2]	Big/small cells[2, 3]
30°C	WT	911	0.3	no[4]	no	0.2/ no	no
	Δ*smc*	1258	9.4	no	0.3	0.3/ no	no
	smc::Tn917	881	10.4	no	0.3	0.3/ no	no
	smc::Tn917+ pCXΩ*smc*	1316	2.3	no	0.5	0.3/ no	0.1/ no
	Δ*spoIIIE*	975	0.7	no	0.4	0.5/ no	no /0.1
	smc::Tn917/Δ*spoIIIE*	802	4.8	1.9	10.7	3.2/6.1	1.6/4.5
37°C	WT	1023	0.3	no	0.7	0.6/ no	no
	Δ*smc*	1144	7.9	no	0.7	0.5/ no	no /0.3
	smc::Tn917	851	7.2	no	0.8	0.7/0.2	no /0.2
	smc::Tn917+ pCXΩ*smc*	1216	1.8	no	0.7	0.7/0.3	no /0.3
	Δ*spoIIIE*	732	0.4	no	0.7	0.8/ no	no /0.1
	smc::Tn917/Δ*spoIIIE*	826	6.4	1.7	20.8	5.3/6.2	2.9/4.5
42°C	WT	987	0.3	no	1.5	1.5/0.8	no /0.7
	Δ*smc*	1240	2.5	no	1.4	1.8/1.0	no /0.9
	smc::Tn917	922	3.5	no	1.5	2.0/0.9	no /1.1
	smc::Tn917+ pCXΩ*smc*	1232	1.7	no	1.5	1.9/1.2	0.3/1.1
	Δ*spoIIIE*	890	0.3	no	1.6	2.1/1.0	no /0.9
	smc::Tn917/Δ*spoIIIE*	681	6.2	2.0	28.5	5.3/11.2	4.0/7.0

[1]Data were summarized from three independent experiments.
[2]Data presented in percentage.
[3]Big cells: ≥1.5 μm diameter; small cells: ≤0.5 μm diameter.
[4]no: not observed within the total number of cells counted.

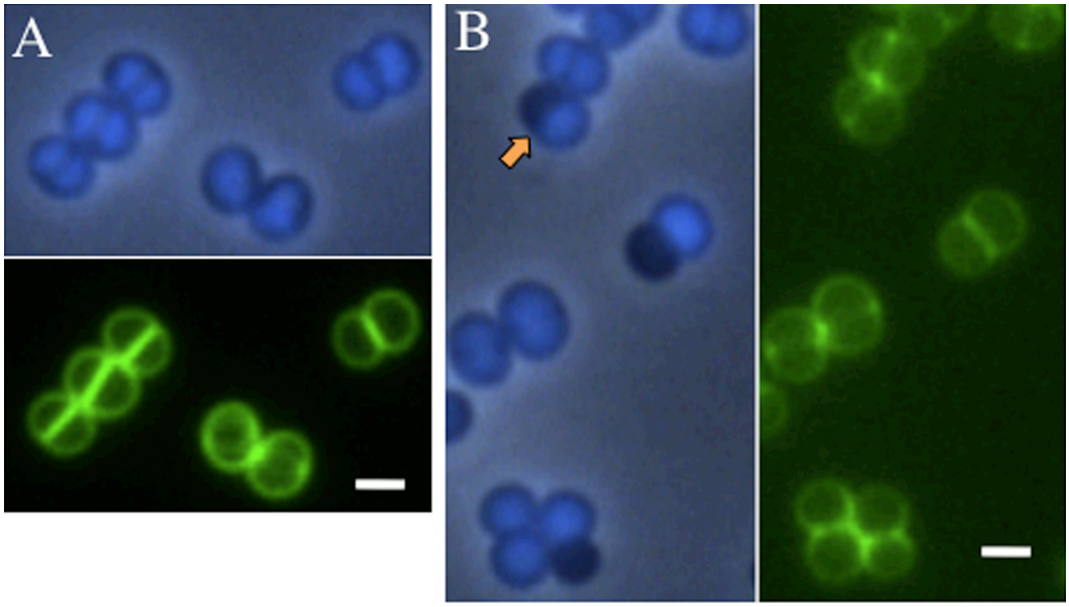

Fig. I-5. Chromosome distribution in SA113 WT and SA113 *smc::Tn917* from mid-log phase TSB cultures at 30°C. (A) SA113 WT, newly formed equatorial rings could be visualized in two tilted cells. **(B)** SA113 *smc::Tn917*; the arrow indicated 'half black cell'. Cell wall was stained with Van-FL (green), chromosome was stained with DAPI (blue) and visualized under phase contrast-fluorescent merging mode; scale bar=1 μm.

3. *S. aureus smc/spoIIIE* double mutant was temperature sensitive and had severe defect in chromosome distribution and segregation

Earlier studies showed that the DNA translocase SpoIIIE could rescue the trapped chromosome from septum membrane during vegetative growth in *B. subtilis* (Sharpe & Errington, 1995). In order to evaluate the function of SpoIIIE in *S. aureus,* a SA113 *spoIIIE* null deletion mutant was constructed *via* double-cross homologous recombination by using a counter-selection vector pKOR1 (Bae & Schneewind, 2006). A majority of the *spoIIIE* reading frame except 68 bp at 3' (that contains Shine-Dalgarno sequence of the downstream gene) was replaced with *aphAIII* cassette that renders kanamycin resistance **(Fig. I-3D).** The *aphAIII* cassette was flanked with *lox* sites and was further removed by Cre recombinase (Leibig *et al.*, 2008). Afterwards, *smc::Tn917* was transduced into SA113Δ*spoIIIE* resulting in SA113 *smc/spoIIIE* double mutant. Consistent with previous findings in *B. subtilis* (Sharpe & Errington, 1995)*, S. aureus spoIIIE* single mutant cells had neither a significant growth disadvantage **(Fig. I-4)** nor an obvious defect in chromosome distribution compared to WT (data not shown).

However, distinct from *B. subtilis,* in *S. aureus* a viable *smc/spoIIIE* double mutant could be isolated. Growth curves showed that the SA113 *smc/spoIIIE* double mutants were temperature sensitive **(Fig. I-4)**. Colonies can only be formed at low temperatures on TSA plates. In liquid medium, SA113 *smc/spoIIIE* double mutant could grow to OD_{578} of 2.2 after 8 hours at 30°C whereas the growth ceased after only two generations (growing for 2 hours to OD_{578} of 0.4) at 42°C. Shifting the culture from 24°C to 42°C resulted in rapid growth cessation. To examine the morphological changes in SA113 *smc/spoIIIE* double mutant, samples were taken at early (1.5 h) and late (5 h) growth phase after diluting overnight cultures into fresh TSB medium and incubated at various temperatures. At early growth phase, the SA113 *smc/spoIIIE* double mutant had distorted chromosome organization and heterogeneous cell sizes as depicted in **Fig. I-6B-D** and quantified in **Table 2**. Approximate 2% of the cells showed the so-called 'guillotine effect' or 'CUT' phenotype that occurred when the chromosome was bisected by the septal membrane **(Fig. I-6, orange arrows, Table 2)**, which was not observed in WT cells or *smc* single mutants. The percentage could not be exactly counted due to the limitation of two-dimensional microscopy technique. 4-6% of the double mutant cells were anucleate, which did not increase significantly compared to the *smc* single mutant **(Table 2)**. The chromosome distribution was heterogeneous in the *smc/spoIIIE* double mutant. While always the same staining method was applied, three fold more mutant cells appeared to contain increased amount of DNA compared to WT (bright blue cells in **Fig. I-6C and D, white**

arrows). More significantly, about 11% of the mutant cells showed decreased content of DNA (**Fig. I-6**, yellow arrowheads), which was ten fold higher than WT or the single mutants. The most severe irregular morphology was the unevenly distributed chromosomes that accumulated punctately in nearly 30% of the mutant cells (**Fig. I-6**, orange arrowheads). These aberrant chromosomal morphological changes suggested that the *smc/spoIIIE* double mutant was greatly deficient not only in chromosome segregation but also in chromosome structure maintenance; the defect in chromosome structure appeared even more severe than the segregation defect. The SA113 *smc/spoIIIE* double mutant also had heterogeneous cell sizes; cells appeared as big (≥1.5 μm diameter) as well as small (≤0.5 μm diameter) cells **(Table 2)**. The heterogeneous cell sizes are probably indirect consequence of the *smc/spoIIIE* mutations since there is no significant correlation between cell size change and the degree of chromosomal disorder (**Table 2**), and second the defect in chromosome structure and segregation may interfere with many other cellular processes that affect cell size. At late growth stage, the chromosome structure was severely disrupted, the cells eventually lysed and more cell debris were produced at 42°C (data not shown). However, at 30°C, although the irregular chromosome disorder aggravated and the cell size differentiated more obviously than earlier growth phase, there were still considerable amounts of normal cells with regular chromosome structure (data not shown).

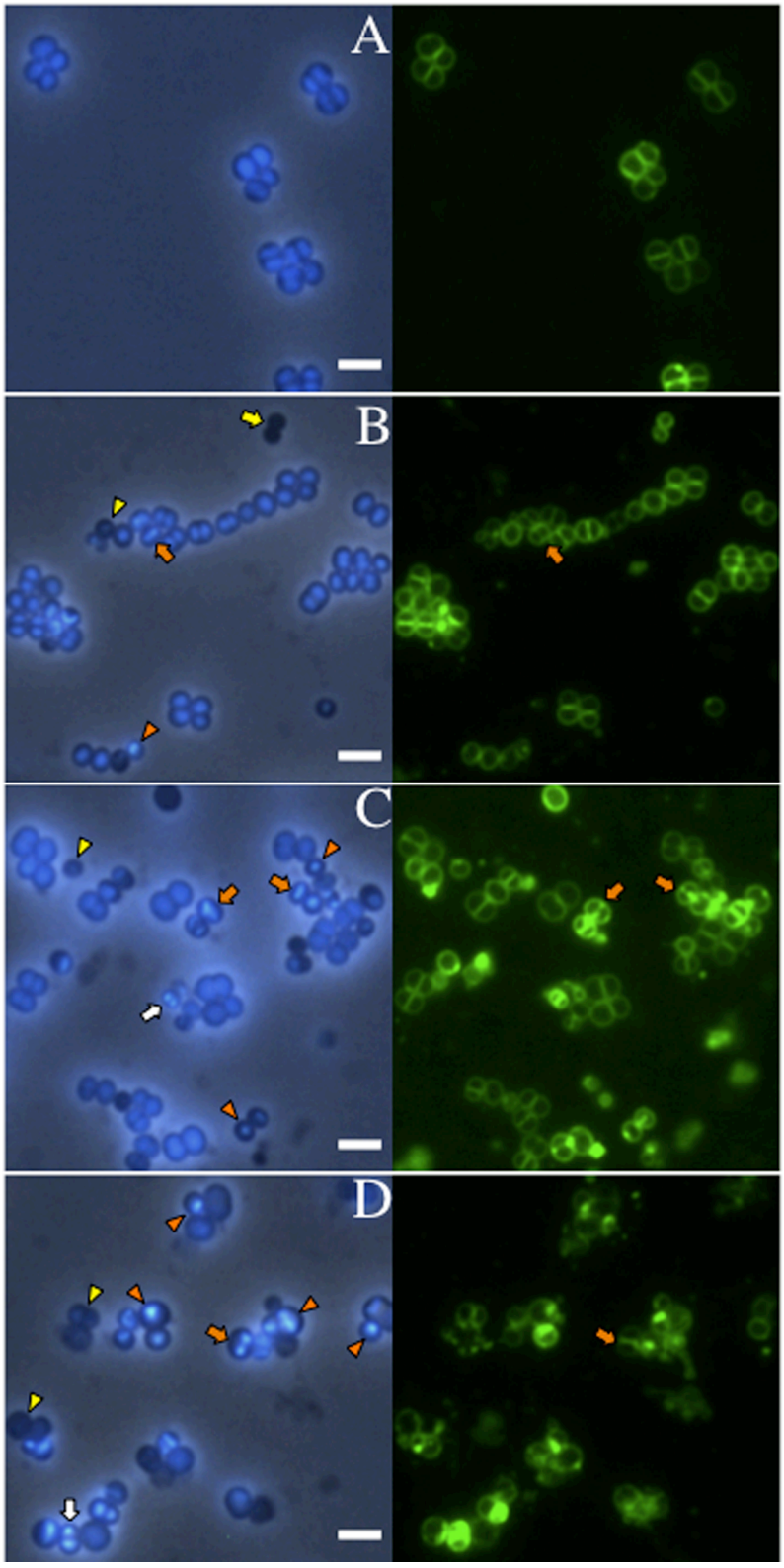

Fig. I-6. Altered chromosome morphology aggravated at higher temperatures in SA113 *smc*::Tn*917/*Δ*spoIIIE*. (A) SA113 WT grown for 1.5h at 42°C. **(B)-(D)** SA113 *smc*::Tn*917/*Δ*spoIIIE* grown for 1.5 h after diluting the overnight culture into fresh TSB medium at 30°C, 37°C, and 42°C respectively; DNA was stained with DAPI (blue), cell membrane was labeled with FM1-43 (green); orange arrows indicated examples of 'guillotine effect' or 'CUT' phenotype: yellow arrow indicated anucleate diplococci; white arrows indicated increased DNA content; yellow arrowheads indicated decreased DNA content; orange arrowheads showed the unevenly distributed nucleoid; scale bar=2 μm.

4. *S. aureus* SMC protein localized as two foci prior to septum formation

To better understand its function, we sought to follow the localization of the SMC protein in *S. aureus*. The SMC was fused at its C-terminus with the super-folder GFP (sfGFP), a fairly bright GFP variant (Pedelacq *et al.*, 2006). A short linker (L) composed of four glycines was between SMC and sfGFP. The fusion was cloned into the pCX vector and expressed under xylose inducible promoter (pCX-smc-sfgfp) **(Fig. I-7A)**. As a control, sfGFP was fused to a staphylococcal lipase propeptide (PP) in pCX vector (pCX-pp-sfgfp). Both plasmids were transformed into *S. aureus* SA113 Δ*smc*. As shown in **Fig. I-7B**, the defect of chromosome segregation in Δ*smc* can be largely complemented by pCX-smc or pCX-smc-sfgfp, but not by pCX-pp-sfgfp, indicating that the SMC-sfGFP fusion was functional. At 30°C, SMC localized as two or four foci in the living cells **(Fig. I-7C)**. One foci can also be visualized, but at low frequency. A close comparison of the SMC foci and septum formation showed that two foci often appeared before septation in one single cell (‘1’). After the first round of division, two foci were allocated into each daughter cell (‘2’). Before the second round of division, two foci reappeared and separated to the ‘cell pole’ in each daughter cell (‘3’), generating two single daughter cells containing two SMC foci again (‘1’). Hence, the localization of SMC foci was dynamic and cell cycle dependent. The SMC foci localization was reminiscent of the Spo0J-YFP localization in *S. aureus* from a recent publication **(Fig. I-7D)** (Veiga et al., 2011). Moreover, the localization of SMC as clear foci was only observed at 30°C, but not at 37°C or 42°C. Likely, the protein was too much over-expressed at higher temperatures.

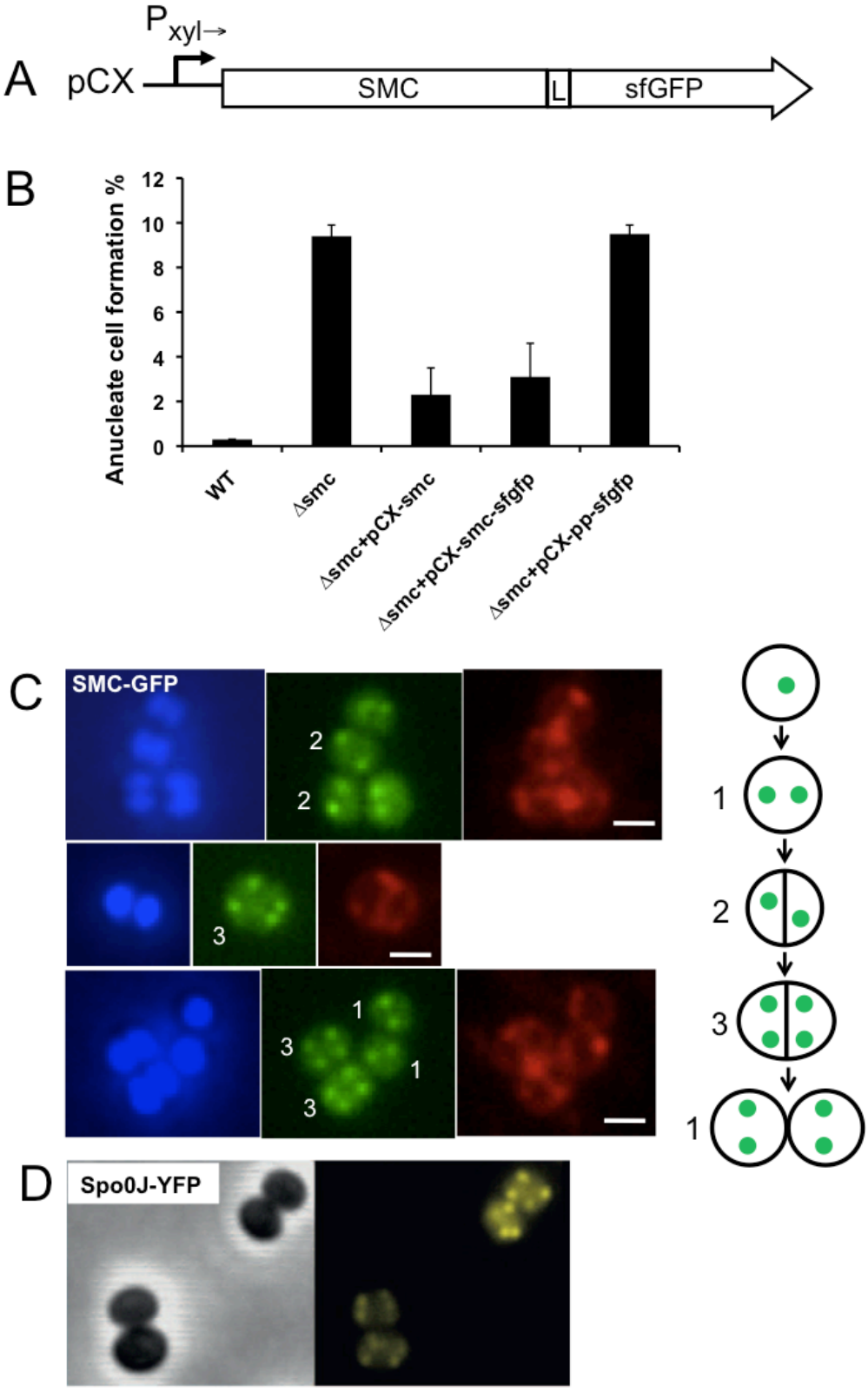

Fig. I-7. Dynamic localization of *S. aureus* SMC at 30°C. (A) Construction of pCX-smc-sfgfp fusion plasmid. (**B)** Percentage of anucleate cell formation at 30°C in SA113 WT, Δ*smc,* Δ*smc* complemented by pCX-smc, pCX-smc-sfgfp, or pCX-pp-sfgfp. **(C)** Subcellular localization of SMC-sfGFP, the cartoon images depict the cell cycle dependent localization of SMC foci; DNA was stained with DAPI (blue), cell membrane was labeled with nile red (red) scale bar=1 μm. **(D)** Subcellular localization of Spo0J-YFP, images adapted from (Veiga et al., 2011).

5. Over-expression *B. subtillus* MreB protein in staphylococci had neither effect on cell morphology or chromosome organization

In the course of cooperation with Prof. Graumann (University of Freiburg), an over-expression construct that aimed at expressing *B. subtillus* MreB protein in staphylococci was made **(Fig. I-8A)**. In this construct, the BsMreB was fused with YFP at its N-terminus. The fusion was cloned under xylose inducible promoter in pTX plasmid backbone (Peschel *et al.*, 1996). Over-expression of YFP-BsMreB in both *S. aureus* and *S. carnosus* had neither obvious influence on cell morphology nor on chromosome distribution **(Fig. I-8B)**. The YFP-BsMreB formed short lines that distributed randomly in the staphylococcal cell **(Fig. I-8B)**, indicating that MreB formed polymers. It remains to be elucidated whether the over-expression of BsMreB affects the cell wall biosnythesis in the staphylococcal cell.

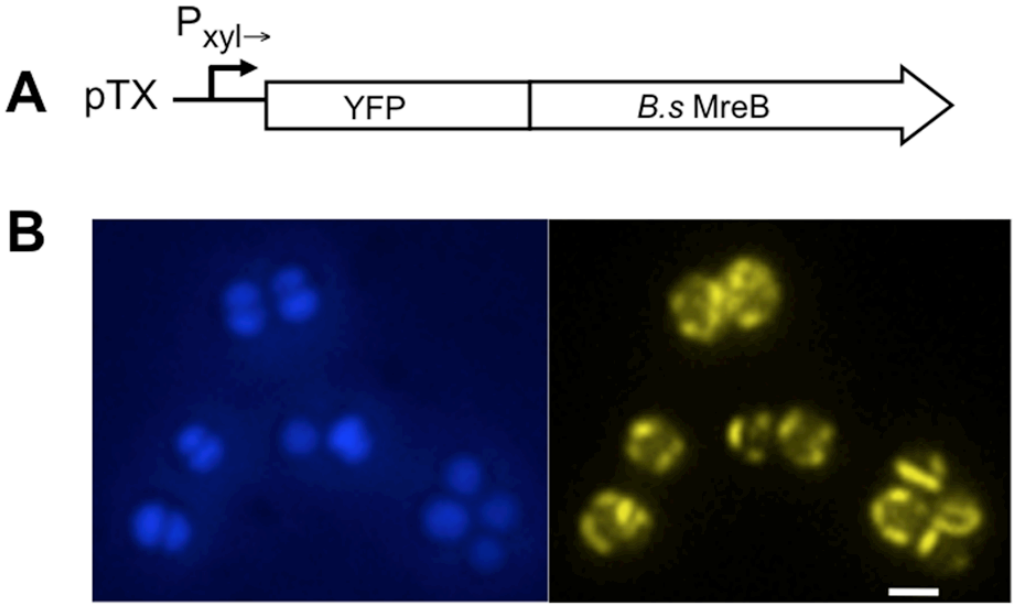

Fig. I-8. (A) Schema of pTX-YFP-BsMreB, the YFP-BsMreB fusion was cloned under the transcriptional control of xylose promoter/operator system. **(B)** Over-expression of YFP-BsMreB in *S. aureus* SA113 with 0.5% xylose induction for 1 h during mid-log phase growth.

Discussion

Why is the effect of *smc* mutation in *S. aureus* less severe than that in rod shaped bacteria? Firstly, the discrepancy could be explained partially by the morphologic difference between rods and cocci. Given that *E. coli* or *B. subtilis* are 1.1 to 1.5 μm wide and 2.0 to 6.0 μm long, the staphylococcal cell is only half size (0.5–1.5 μm in diameter) of a bacillus cell (Götz, 2006). Besides, *S. aureus* has a much smaller cell volume of 0.15 μm^3 compared to *E. coli* with 0.5 - 0.7 μm^3 (Kubitschek, 1990, Pilavtepe-Çelik *et al.*, 2008). Despite different genome sizes between *B. subtilis* and *S. aureus*, (4.1 Mbp *vs* 2.9 Mbp, respectively) (Kuroda *et al.*, 2001, Trevors, 1996), the small staphylococcal cell size becomes spatially limiting for the nucleoids; therefore decondensed chromosomes were not observed in *S. aureus smc* mutant cells. Secondly, as chromosome segregation is one of the most important cellular processes, bacteria must have employed redundant mechanisms. Other factors may play important roles during chromosome segregation in the spherical cells. Interestingly, the defect of chromosome segregation in the *S. aureus smc* mutant was reduced at higher growth temperatures where the growth rate was accelerated. As a consequence, the cellular processes, such as chromosome replication, transcription and translation are faster as well. It is possible that one or more combined cellular processes provide the driving force to optimize chromosome segregation in staphylococci (Draper & Gober, 2002, Jun & Wright, 2010). From this aspect, the 'driving force' theory seems applicable in staphylococci.

On the other hand, the trial in finding factors that determine the axis of the sister chromosomes partitioning is not ceasing. As mentioned before, the deletion of *divIVA* gene that encodes the division site selection protein DivIVA in *S. aureus* shows no apparent phenotype unexpectedly (Pinho & Errington, 2004). YpsB, the paralog of DivIVA, is also presented in *S. aureus* **(Table 1).** YpsB is found to be a late divisome protein in *B. subtilis* (Tavares *et al.*, 2008). Moreover, YpsB is also found to interact with ScpA, one component of the bacterial SMC condensin complex (Dervyn et al., 2004). The function of YpsB in *Staphylococcus* is not known yet. As depicted in **Fig. I-7C, D**, the SMC foci localization is reminiscent to that of Spo0J. Presumably, the SMC complex is recruited by Spo0J-*parS* to the oriC proximal region in *S. aureus*, in a similar manner described in *B. subtilis* and *Streptococcus pneumoniae.* Accordingly, the movement of SMC foci could represent the dynamics of the *oriC* region. The question is then how the nascent replicated *oriC* region separate from each other prior to septum formation in the hemispherical daughter cell. Importantly, *Staphylococcus* divide in a perpendicular manner by shifting the division plane 90° to the previous one (Tzagoloff & Novick, 1977). The understanding of how

Staphylococcus segregates the sister chromosomes would provide critical clues for the mechanism of how this bacterium set up the division planes.

Compared to SA113 *smc* and *spoIIIE* single mutants, the highly distorted chromosome arrangement in *S. aureus smc/spoIIIE* double mutants indicated that SpoIIIE compensated SMC's function in chromosome segregation to a large extent. The aggravated chromosome segregation defect in *smc/spoIIIE* double mutant disclosed the chromosome maintenance deficiency in *smc* single mutant, since it is unlikely that SpoIIIE had a direct role in chromosome organization. In other words, the optimal chromosome segregation facilitates proper chromosome organization in *S. aureus*. While the number of anucleate cells decreased with increased temperature in *smc* single mutant, the effect was reversed in the *smc/spoIIIE* double mutant, where the number of anucleate cells was slightly increased at higher temperature. Interestingly, an earlier transcriptomic data of heat shock response in *S. aureus* showed that *spoIIIE* was 2.15 fold higher transcribed at 48°C (Fleury *et al.*, 2009). This finding could explain that the defect in *smc* single mutant is in part compensated by over-expression of SpoIIIE. Different from *B. subtilis* or *E. coli, S. aureus smc/spoIIIE* double mutants are viable at low temperature; yet possible suppressor mutations could not be excluded. Nevertheless, the distinction underlies that some other factors are involved in guaranteeing maximum chromosome segregation in staphylococci. It is recently found that SftA, the soluable DNA translocase, affects the chromosome segregation in *B. subtilis* (Biller & Burkholder, 2009, Kaimer et al., 2009). Homologous proteins to *B. subtilis* SftA with conserved domain structures are present in all staphylococcal genomes, sharing 33.3% identity. It would be interesting to evaluate the function of SftA in staphylococci. Yet while we were trying to characterize SftA in *S. aureus,* another research group seemed to be already advanced in this respect. So we had to quit the study in this direction. Another interesting candidate would be DNA topoisomerase IV (Topo IV), as over-expression of Topo IV can partially rescue the growth and DNA condensation defect of the *smc* mutant (Tadesse et al., 2005).

Taken together, we have obtained a first insight into chromosome segregation in staphylococcus and presented intriguing results towards the genetic interaction of SMC and SpoIIIE, two critical factors involved in chromosomal dynamics. These findings shed light on different mechanisms of chromosome dynamics in the spherical staphylococcal cells in contrast to the model in rods, which definitely deserves future investigation.

Part II Using cell wall anchored mCherry to monitor staphylococcal surface protein sorting

Introduction

1. Staphylococcal surface proteins and the sorting pathway

Surface anchored proteins of *Staphylococcus aureus* represent a group of proteins that are exposed on the bacterial cell envelope and covalently anchored to the staphylococcal cell wall peptidoglycan (Schneewind *et al.*, 1992). Many of the surface proteins belong to the MSCRAMM family (microbial surface components recognizing adhesive matrix molecules), which play key roles in colonization and adhesion of *S. aureus* (Foster & Höök, 1998).

The process of anchoring surface proteins to the staphylococcal cell wall, termed the 'sorting pathway', includes three steps **(Fig. II-1)** (Marraffini *et al.*, 2006): translocation, sorting and incorporation into mature peptidoglycan. Anchored proteins are distinguished by a C-terminal cell wall sorting signal (CWS). The N-terminal signal peptide directs the polypeptide into the Sec secretory translocon. Sortase A (SrtA) (Mazmanian *et al.*, 1999), a membrane-bound transpeptidase, performs the sorting reaction by cleaving the amide bond between threonine and glycine within the LPXTG motif, which results in the acyl intermediate. The peptidoglycan precursor, Lipid II, serves as the substrate for the sorting reaction, which is the tethering of the C-terminal threonine of the surface protein to lipid II by an amide bond. Lipid II tethered with the surface proteins is finally incorporated into mature peptidoglycan by the penicillin binding proteins (Perry *et al.*, 2002).

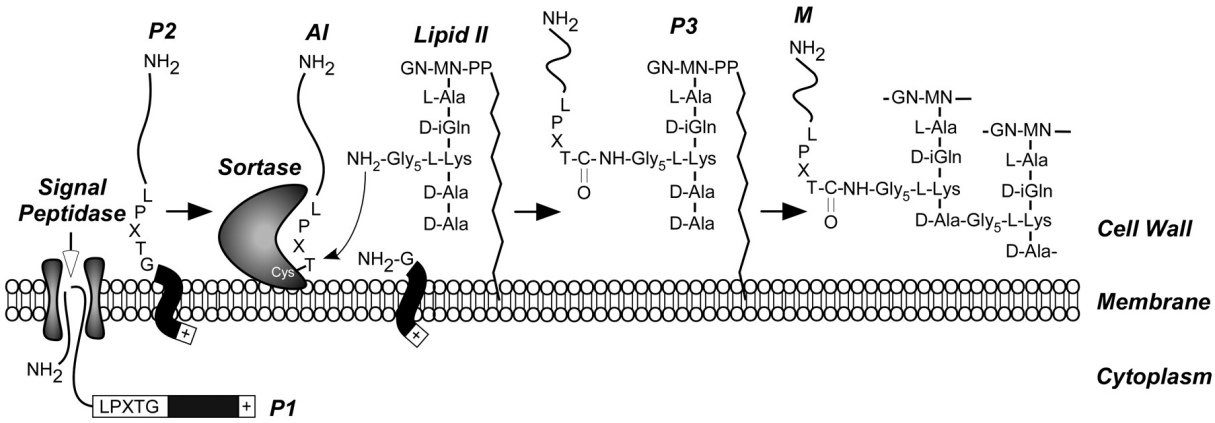

Fig. II-1. Cell wall sorting pathway of surface proteins in gram-positive bacteria. Figure adapted from (Marraffini et al., 2006).

2. Signal peptide with YSIRK-motif

Previously, we have described that the N-terminal signal peptides of staphylococcal lipases harbor a conserved motif - Ser, Ile, Arg and Lys - designated as the SIRK-motif (Rosenstein & Götz, 2000). This motif (termed as YSIRK/GS) is later found conserved in many, but not all surface proteins. SP with the YSIRK/GS motif promotes the secretion of surface proteins (Bae & Schneewind, 2003). In *Streptococcus pyogenes* (Carlsson *et al.*, 2006) and in *S. aureus* (DeDent *et al.*, 2008), the SP (+YSIRK-motif) has a function in directing surface proteins to different surface localizations. In *S. aureus*, SP (+YSIRK) directs the secretion and anchoring of surface proteins at septum (cross wall), while the SP (−YSIRK) leads the secretion and anchoring of surface proteins more to the cell pole (DeDent et al., 2008). It has also been shown that three transmembrane proteins, namely Spd (surface protein display) proteins, are involved in the surface display of protein A, one of the predominant surface proteins carrying SP (+YSIRK) (Frankel *et al.*, 2010). The expression level and surface display of protein A (Spa) are largely reduced in each *spd* mutant. Moreover, *spd* mutants affect the expression of surface proteins with SP (+YSIRK). Interestingly, the *spd* mutants exhibit an increased abundance of visible cross walls and thickened cross walls. Yet, how cross wall formation affects the surface display of surface proteins remains unclear.

3. Aims of the study

Conventionally, immunofluorescence microscopy has been applied to surface proteins localization studies, as the cell surface immobilized proteins have relatively easy and stable access to antibodies (DeDent *et al.*, 2007, Hahn & Cole, 1963). However, immunofluorescence microscopy has a certain intrinsic limitation that especially impedes the subcellular and high throughput studies. For example, antibodies cannot penetrate into the septum without cell wall permeabilization; yet cell wall permeabilization using cell wall hydrolase or detergents often leads to the release of surface proteins with the risk of artifacts. Further, a large numbers of specific antibodies are needed in order to study various surface proteins' localization, which is laborious and time consuming. Particularly in *S. aureus* immunofluorescence is extremely hindered by protein A, the IgG binding protein.

In this study, we aimed at developing a direct visualization method for monitoring the surface proteins anchoring process. The red fluorescent protein mCherry was fused with signal peptides +/−YSIRK and was targeted to the cell wall, which enabled us to visualize the cross and peripheral wall localization pattern rather than using immunofluorescence microscopy.

Further, with this tool in hand, we intended to study the influence of cell wall antibiotics on the targeting of cell wall anchored mCherry.

Results

1. Defined mCh-fusion proteins are targeted in an active form to distinct subcellular compartments

Previously, we have anchored staphylococcal lipase to staphylococcal cell wall in an active form (Strauss & Götz, 1996). Anchored lipase could be extracted from the cell wall, together with covalently tethered peptidoglycan (Müller-Anstett *et al.*, 2010). Based on these results, we asked if mCherry could be immobilized to staphylococcal peptidoglycan while maintaining stable fluorescence. The mature lipase was replaced by mCherry in pCX30Δ82, generating pCX-mCh-cw1 (**Fig. II-2A**). The protein domain order in this construct was, the N-terminal signal peptide (SP_{lip}) and propeptide (PP_{lip}) of lipase, mCherry, and the C-terminal cell wall sorting sequence (CWS) of FnBPB (fibronectin binding protein B). CWS consisted of the LPXTG motif, followed by a hydrophobic domain and a positively charged tail (Strauss & Götz, 1996). To differentiate the effect of SP (+/−YSIRK), the signal peptide of surface protein SasF (SP_{sasF}), a non-YSIRK SP was used to substitute SP_{lip}, resulting in pCX-mCh-cw2 **(Fig. II-2B)**. Moreover, hybrids mCh-sec1&2 lacking C-terminal CWS, as well as hybrid mCh-cyto lacking both SP and CWS, were constructed **(Fig. II-2C-E)**. All the fusions were carried out under the xylose inducible and glucose repressible *Pxyl* promoter of the pCX15 vector backbone (Wieland et al., 1995). Importantly, it was necessary to keep the PP_{lip} in the fusion with mCherry in all the constructs, since PP_{lip} significantly promotes the fusion partners' secretion, stability and activity (Demleitner & Götz, 1994, Sturmfels *et al.*, 2001). Expressing mCherry without PP_{lip} showed drastically reduced fluorescence (see results below).

To test if mCh-hybrids were functional, the plasmids were transformed into *S. aureus* SA113 WT and its *srtA* deletion mutant (Δ*srtA*). After xylose induction, different cell fractions were collected for mCherry expression (indicated by fluorescence intensity measurement). As shown in **Fig. II-3A**, the supernatant of WT-sec1 exhibited the highest red fluorescence (RF) signals, which were set as 100%. WT-sec2 showed the second highest RF intensity of about 50%. WT-cw1, WT-cw2 and WT-cyto had little RF in the supernatant**,** while the Δ*srtA*-cw1 or Δ*srtA*-cw2 showed 10-15% RF intensity. All constructs (anchored or secreted mCh-

hybrids) with SP_{lip} (+YSIRK motif) exhibited significantly higher fluorescence intensity than those with SP_{sasF} (-YSIRK motif). The same results were obtained in SA113 Δ*spa* (data not shown), where the protein levels could be accessed by Western blotting without the interference of protein A. Indeed, the protein level of different constructs **(Fig. II-3B)** correlated with their fluorescence profiles, except for Δ*srtA*-cw1 and Δ*srtA*-cw2 where mCh-cw was released into the supernatant with the unprocessed C-terminal CWS. Possibly, the unprocessed CWS interfered with the correct folding of mCherry; therefore, the fluorescence emission was reduced to some extent. Nevertheless, the fusions with SP_{lip} (+YSIRK) were always expressed at higher level than that with SP_{sasF} (-YSIRK) **(Fig. II-3B)**.

Once covalently anchored to peptidoglycan, surface proteins are immobilized and can only be released by peptidoglycan hydrolyses (Marraffini et al., 2006, Strauss & Götz, 1996). Lysostaphin, the glycyl-glycine endopeptidase, cleaves specifically the pentaglycine cross bridges in staphylococcal peptidoglycan, and thereby releases the surface proteins that are linked to pentaglycine bridges. WT-cw1 released the highest amount of RF by lysostaphin treatment, indicating that mCherry was largely peptidoglycan-immobilized. In WT-cw2 five-fold less RF was released **(Fig. II-3A)**. In the pellet fraction after lysostaphin treatment, WT-cyto displayed the highest fluorescence, indicating that without SPs, mCh-fusion proteins were not secreted but remained in the cytosol **(Fig. 11-3A)**. SA113 WT (pCX30Δ82) showed no fluorescence in all cell fractions, like the negative controls, which were SA113 without plasmid or solely the medium (data not shown). To test if mCh-hybrids were functional in different staphylococcal species, all constructs were transformed into *S. carnosus* TM300 and its *srtA* deletion mutant; we obtained similar results as with *S. aureus* strains (data not shown).

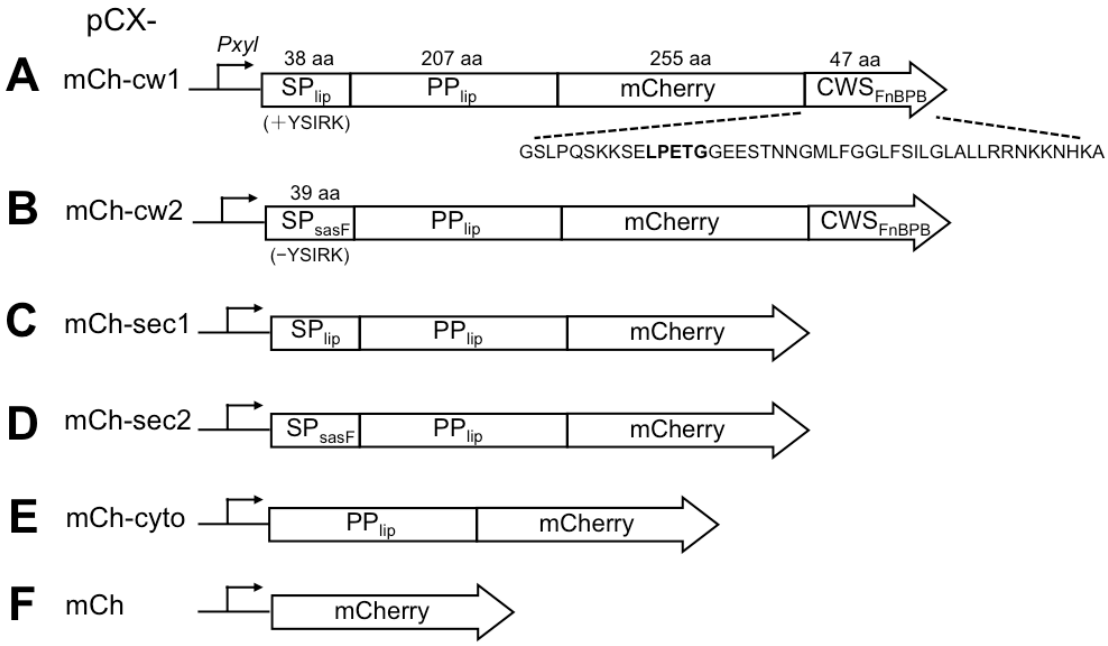

Fig. II-2. Schematic representation of mCh-hybrids. SP, signal peptide; PP, propeptide; CWS, cell wall sorting signal; mCh: mCherry; lip, lipase. The amino acid sequence of CWS was indicated. The parent plasmid was pCX30 and all mCh-fusion constructs were under control of the xylose-inducible promoter, P*xyl*.

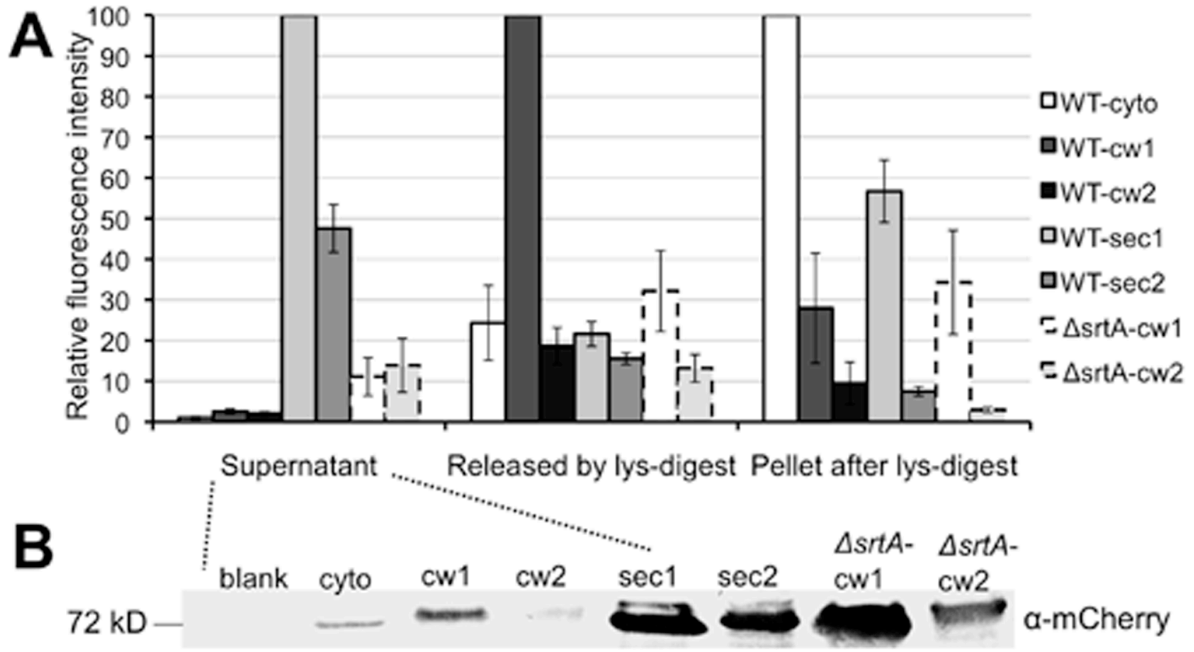

Fig. II-3. Monitoring mCh-hybrids. (A) Fluorescence intensity comparison of mCh-hybrids from different cell fractions. WT-cyto, SA113 (pCX-mCh-cyto); WT-cw1 or 2, SA113 (pCX-mCh-cw1) or (pCX-mCh-cw2); WT-sec1 or 2, SA113 (pCX-mCh-sec1) or (pCX-mCh-sec2); Δ*srtA*-cw1 or 2, SA113 Δ*srtA* (pCX-mCh-cw1) or (pCX-mCh-cw2); lys, lysostaphin. **(B)** Western blotting of mCh-hybrid proteins in the culture supernatant of protein A deficient mutant SA113 Δ*spa*. Blank, SA113 Δ*spa* without plasmid; cyto, SA113 Δ*spa* (pCX-mCh-cyto); cw1 or 2, SA113 Δ*spa* (pCX-mCh-cw1) or (pCX-mCh-cw2); sec1 or 2, SA113 Δ*spa* (pCX-mCh-sec1) or (pCX-mCh-sec2); Δ*srtA*-cw1 or 2, SA113 Δ*spa*Δ*srtA* (pCX-mCh-cw1) or (pCX-mCh-cw2).

2. GFP results and the function of lipase propeptide

At the same time, series of GFP hybrid plasmids were constructed in the same way as the mCh-fusions **(Fig. II-4)**. However, the attempt to secret GFPmut3 (Cormack *et al.*, 1996) failed, because GFPmut3 lost fluorescence when it was translocated via the Sec secretory pathway **(Fig. II-6A)**, similar to the observation with GFPuv in *E. coli* (Feilmeier *et al.*, 2000). It has been reported recently that a new GFP variant, the super-folder GFP (sfGFP) (Pedelacq et al., 2006), can be translocated through the Sec secretory pathway in *E. coli* while maintaining fluorescence (Dinh & Bernhardt, 2011). Compared to GFPmut3, sfGFP displayed remarkable brighter fluorescence when it was expressed in the cytoplasm of *S. aureus* **(Fig. II-5)**. However, the fluorescence of secreted sfGFP-fusions was still fairly low, despite that the sfGFP-fusions were secreted in a higher amount than the GFPmut3-fusions **(Fig. II-6)**. In comparison, the secreted mCh-fusions showed 7-13 fold higher fluorescence intensity than GFP-fusions while the difference in the protein amount was not that remarkable **(Fig. II-6)**. Western blotting results revealed that the secreted GFP-sec fusions (ppGFP-sec1, ppGFP-sec2, ppsfGFP-sec1, and ppsfGFP-sec2) migrated slightly higher than ppGFP or ppsfGFP **(Fig. II-6B, arrows)**. In contrast, the secreted mCh-sec fusions (ppmCh-sec1, ppmCh-sec2) had similar size as mCh-cyto (ppmCh) **(Fig. II-6B, arrows)**. This indicated that the majority of the secreted GFP-fusions were still tethered with signal peptides whereas the mCh-fusions were not. Thus, it appeared that the secreted GFP-fusions could not be processed and fold correctly to be fluorescent after Sec-dependent secretion.

It is also worthwhile to note the functions of the lipase propeptide found from the comparative study of the mCh/GFP-fusions with or without PP_{lip}. When expressed in the cytoplasm without SP, GFPmut3 fused with PP_{lip} showed three fold higher fluorescence than GFPmut3 alone **(Fig. II-5)**. Similar results that PP_{lip} enhanced the fluorescence were also observed with mCherry (data not shown). In the case of sfGFP, the addition of PP_{lip} did not increase its fluorescence **(Fig. II-5).** Very likely sfGFP alone can already fold at 'super' and maximum efficiency. More interestingly, in the absence of SP, the PP_{lip}-GFP fusion protein could be detected in the supernatant, while GFP alone without PP_{lip} could not **(Fig. II-6B)**. Clearly, PP_{lip} can promote protein secretion even without SP.

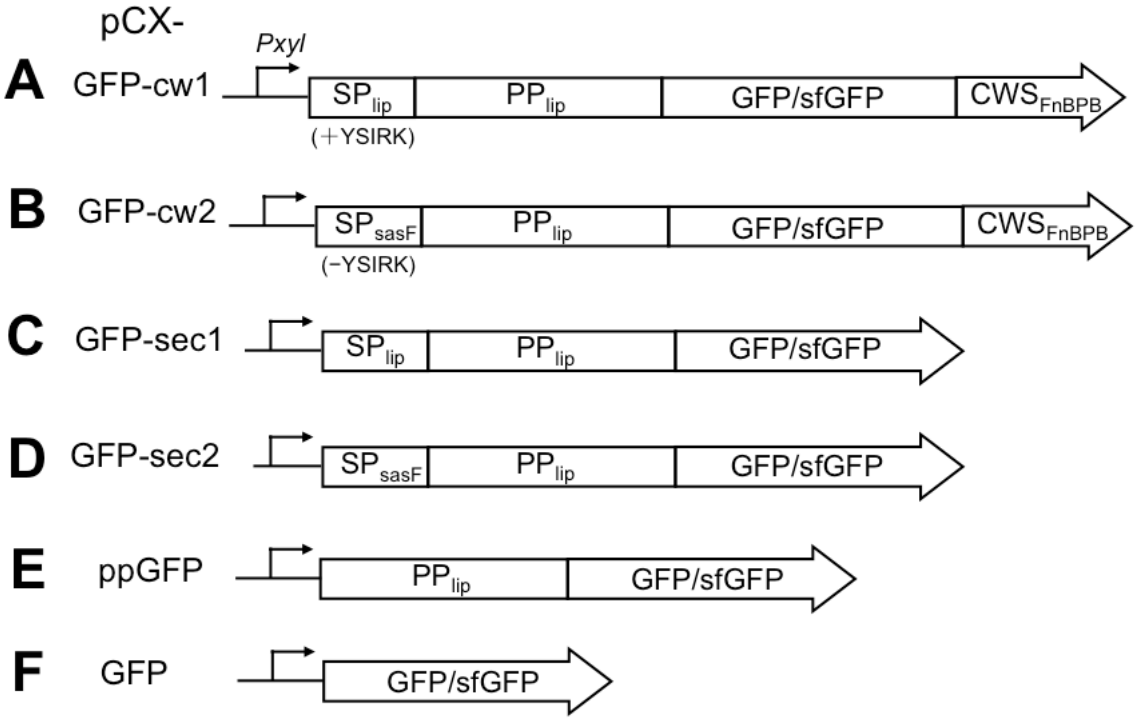

Fig. II-4. Schematic representation of pCX-GFP-hybrids. All of the pCX-GFP-hybrids were constructed in the same order as the mCh-hybrids under P*xyl* promoter. GFP, GFPmut3; sfGFP, super-folder GFP.

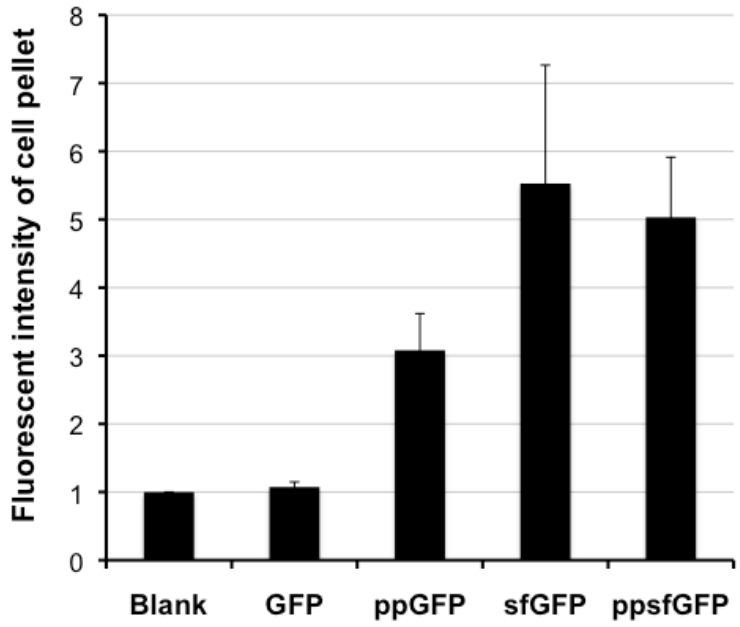

Fig. II-5. Fluorescence intensity of the cell pellet from GFP-hybrids. The vertical axis indicated the ratio of the fluorescence intensity compared to the blank. Blank, SA113 without plasmid; GFP, SA113 (pCX-GFPmut3); ppGFP, SA113 (pCX-ppGFPmut3); sfGFP, SA113 (pCX-sfGFP); ppsfGFP, SA113 (pCX-ppsfGFP).

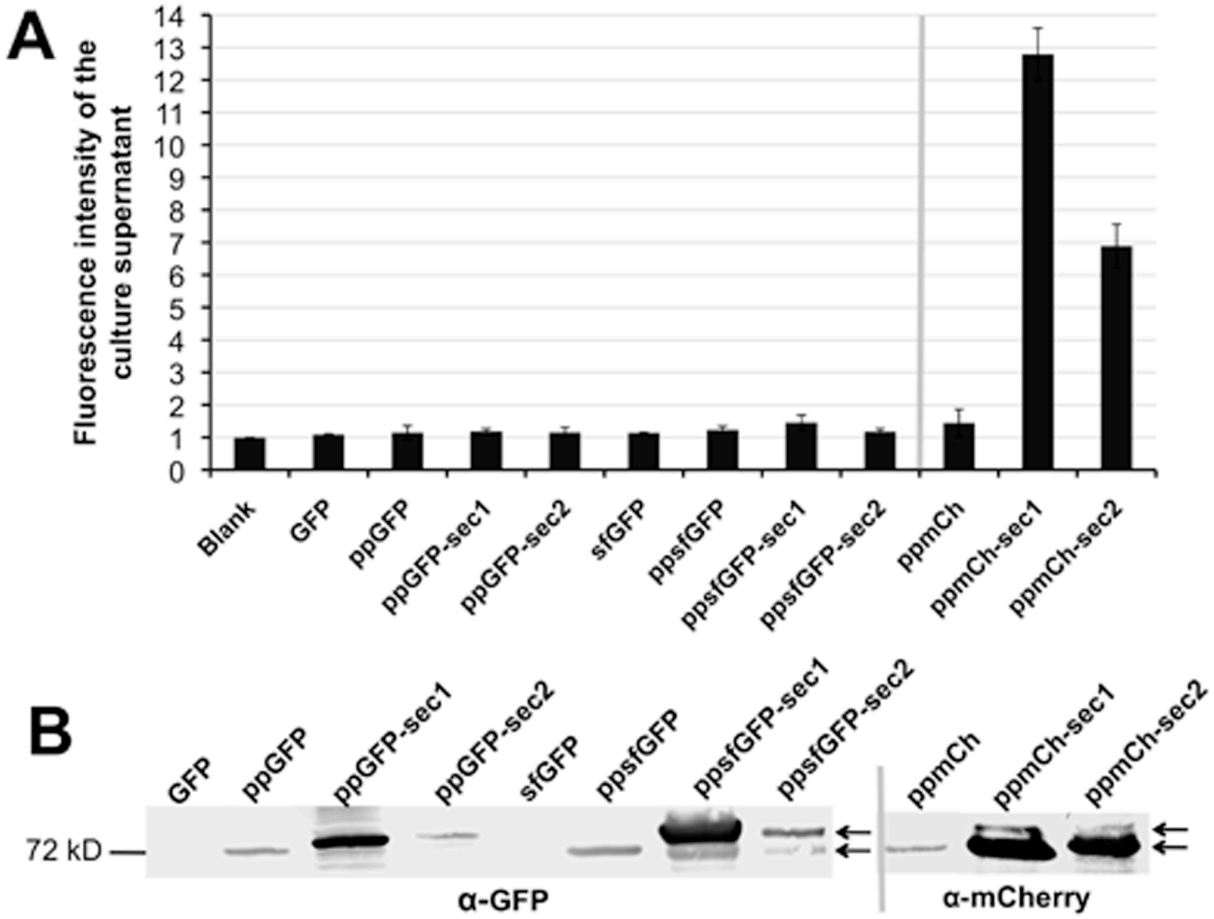

Fig. II-6. Fluorescence intensity and Western blotting comparison between secreted GFP- and mCh-hybrids. (A) Fluorescence intensity of the culture supernatant from GFP/mCh-hybrids. The vertical axis indicated the ratio of the fluorescence intensity compared to the blank. **(B)** Western blotting of the filtered culture supernatant from GFP/mCh-hybrids. Blank, SA113 Δ*spa* without plasmid; GFP, SA113 Δ*spa* (pCX-GFPmut3); ppGFP, SA113 Δ*spa* (pCX-ppGFPmut3); ppGFP-sec1, SA113 Δ*spa* (pCX-GFPmut3-sec1); ppGFP-sec2, SA113 Δ*spa* (pCX-GFPmut3-sec2); sfGFP, SA113 Δ*spa* (pCX-sfGFP); ppsfGFP, SA113 Δ*spa* (pCX-ppsfGFP); ppsfGFP-sec1, SA113 Δ*spa* (pCX-sfGFP-sec1); ppsfGFP-sec2, SA113 Δ*spa* (pCX-sfGFP-sec2); ppmCh, SA113 Δ*spa* (pCX-mCh-cyto); ppmCh-sec1, SA113 Δ*spa* (pCX-mCh-sec1); ppmCh-sec2, SA113 Δ*spa* (pCX-mCh-sec2). Arrows indicated the unprocessed (upper band) or the processed (lower band) form of the secreted GFP/mCh fusions. Note that there were no protein bands at 25 kD (size of GFP protein) in the lanes of GFP and sfGFP.

3. mCh-hybrids provide useful tools to visualize the effect of SP (+/− YSIRK-motif)

In earlier studies it was suggested that SP (+YSIRK) directs the secretion and anchoring of surface proteins at the division septum, whereas the surface proteins with SP (−YSIRK) are secreted and incorporated at the cell pole (Carlsson et al., 2006, DeDent et al., 2008). To test if the spatial difference of SP (+/−YSIRK) can be visualized by mCh-hybrids, we compared the mCh-fusions with SP_{lip} (+YSIRK) and SP_{sasF} (−YSIRK). Indeed, the localization patterns of the SA113 (pCX-mCh-cw1) and SA113 (pCX-mCh-cw2) clones differed from each other.

The mCh-cw1 clone exhibited patchy circumferential RF and especially bright RF at the cross wall (**Fig. II-7A**); often, two foci adjacent to the new cross wall were observed **(Fig. II-7A, arrowhead).** In contrast, in the mCh-cw2 clone RF distributed homogeneously at the peripheral cell wall (**Fig. II-7B**); little RF was seen in the cross wall, even after two daughter cells split **(Fig. II-7B, arrowheads).** Quantification of colocalization analysis of Van-FL (green fluorescence of cell wall staining) and mCh-cw (RF) revealed that mCh-cw1 colocalized with nearly 50% of the total cross walls, while mCh-cw2 colocalized with only 6% of total visible cross walls **(Fig. II-11B)**.

The effect of SPs (+/−YSIRK) can also be visualized by the secretion patterns of SA113 (pCX-mCh-sec1) and SA113 (pCX-mCh-sec2). In mCh-sec2, most of RF was outside and surrounding the cells as a diffuse halo while absent at the cross walls **(Fig. II-7D, arrowheads)**, which indicated a peripheral secretion pattern. In contrast, mCh-sec1 exhibited spot-like foci particularly at or near the (future) division septum **(Fig. II-7C, arrowheads)**. The different localization pattern between SA113 (pCX-mCh-sec1) and SA113 (pCX-mCh-sec2) was in agreement with earlier observations that SPs (+/−YSIRK) probably direct the secretion of surface proteins to different sites (Carlsson et al., 2006, DeDent et al., 2008). In the cytoplasmic expressed mCh-hybrids of SA113 (pCX-mCh-cyto), RF was uniformly distributed within the cells **(Fig. II-7E)**.

Interestingly, the expression of mCh-cw2 led to a mild reduction in the cross-wall formation compared to WT or WT-mCh-cw1 **(Fig. II-11A)**. Moreover, expression of WT-mCh-cw2 tended to form bigger cell clusters **(Fig. II-9B)** while WT or WT-mCh-cw1 appeared as typical dispersed diplococci, tetrad-cocci or small clusters in liquid culture **(Fig. II-9A)**. Cluster formation was not observed in Δ*srtA*-mCh-cw2 or WT-mCh-sec2 (data not shown). Reduced cross-wall formation and clustering were probably due to the over-expression of mCh-cw2; but conversely, even mCh-cw1 caused a higher protein expression **(Fig. II-3B)**, the cell morphology was indistinguishable from WT. Hence, reduced cross-wall formation and clustering were not only because of over-expression, but rather related with an intrinsic peripheral anchoring feature exerted by SP (−YSIRK).

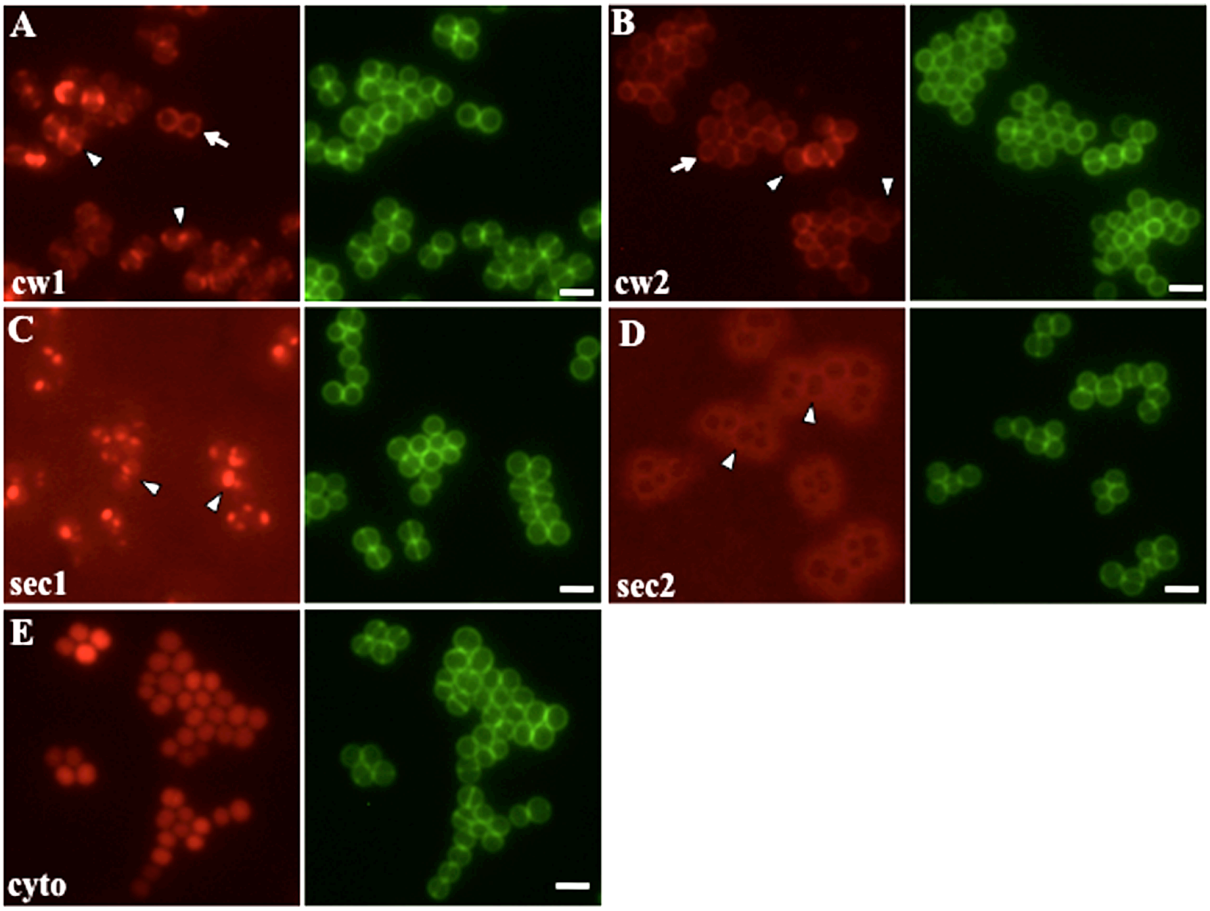

Fig. II-7. Subcellular localization of mCh-hybrid proteins in SA113. (A) pCX-mCh-cw1. **(B)** pCX-mCh-cw2. **(C)** pCX-mCh-sec1. **(D)** pCX-mCh-sec2. **(E)** pCX-mCh-cyto. Arrows in (A) and (B), cell surface localized mCh-cw; arrowheads in (A) and (B), fluorescence localized at the cross wall in (A), but absent from the cross wall in (B). Arrowheads in (C), RF foci close to the initial sites of the cross walls; arrowheads in (D), halo-like RF distribution absent from the cross wall. Images (A), (C) and (E) were taken after one hour of xylose induction; images (B) and (D) were taken after two hours of induction. Green: Van-FL staining (cell wall); scale bar, 2 μm.

4. Penicillin and moenomycin direct mCh-cw to the cross wall, irrespective of SP type

Several cell wall biosynthesis antibiotics interfere with the protein anchoring reaction (Perry et al., 2002, Ton-That & Schneewind, 1999). It has been shown that for example penicillin G, vancomycin, moenomycin, bacitracin and tunicamycin inhibit the tethering of surface proteins with lipid II. Considering that the surface proteins anchoring process is closely related to both protein secretion and cell wall biosynthesis, we examined whether these cell wall antibiotics affect the localization of secretion or anchoring. Gallidermin (Kellner *et al.*, 1988), a lantibiotic that specifically binds to lipid II (Brötz *et al.*, 1998), and D-cycloserine, which prevents D-Ala-D-Ala terminus synthesis of the muropeptides (Lambert & Neuhaus, 1972), were also tested. As shown in **Fig. II-8A**, overnight cultures of SA113 (pCX-mCh-cw) were

diluted into fresh BO medium. Antibiotics were added at 0.1 OD_{578}, followed by two hours of incubation before xylose induction. Samples for microscopy examination were collected after one and two hours of xylose induction. The sub-lethal concentrations of various antibiotics were determined experimentally when the bacterial growth was slightly retarded but not completely inhibited, allowing protein synthesis to proceed.

Among all of the antibiotics tested, penicillin G (Pc) and moenomycin (synonym: flavomycin, Fla) strikingly altered the localization pattern of mCh-cw. In **Fig. II-8B,** both mCh-cw1 and mCh-cw2 became almost exclusively localized at the cross-wall in Pc or Fla treated cells after one-hour xylose induction. The cross-wall localized fluorescence was further intensified and accumulated at the cross-wall after two-hours' xylose induction (**Fig. II-8C**). In comparison, the fluorescence of mCh-cw1 enriched at the cross-wall while mCh-cw2 increased fluorescence at the peripheral wall in the untreated cells after two hours' induction (**Fig. II-8C-a2, d2**). These observations implied that penicillin or flavomycin provoked the newly synthesized mCh-cw hybrid proteins to be targeted to the cross-wall irrespective of SP-type (with or without YSIRK motif). Additionally, the cell clusters of mCh-cw2 were disrupted by the treatment of penicillin or flavomycin (**Fig. II-9C, D**), indicating that the peripheral localization tendency exerted by SP_{sasF} (−YSIRK) was abrogated by penicillin and moenomycin.

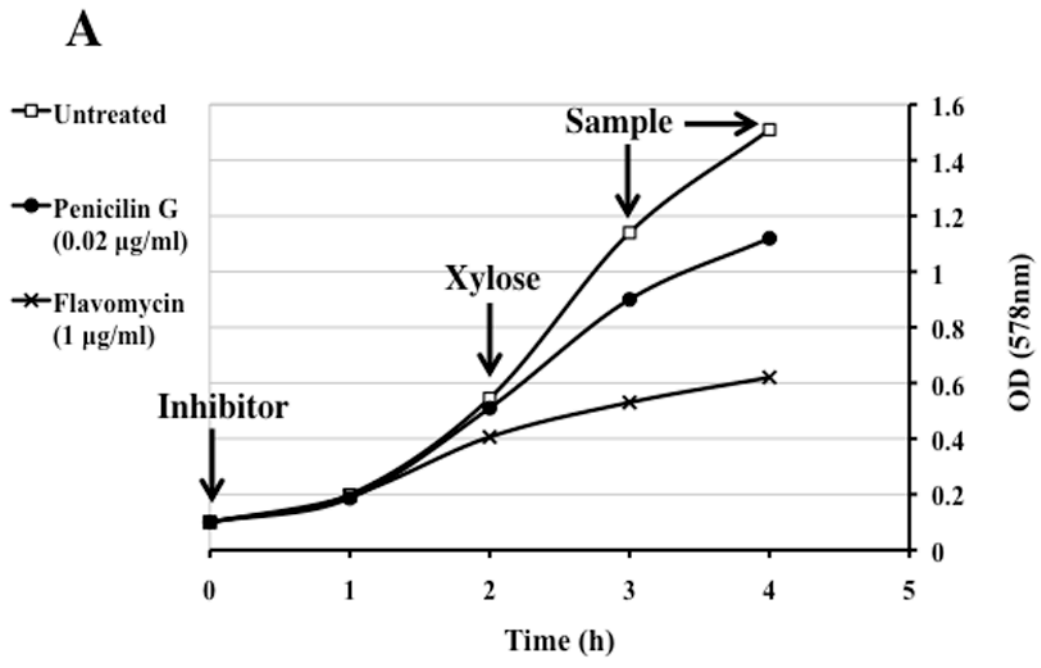

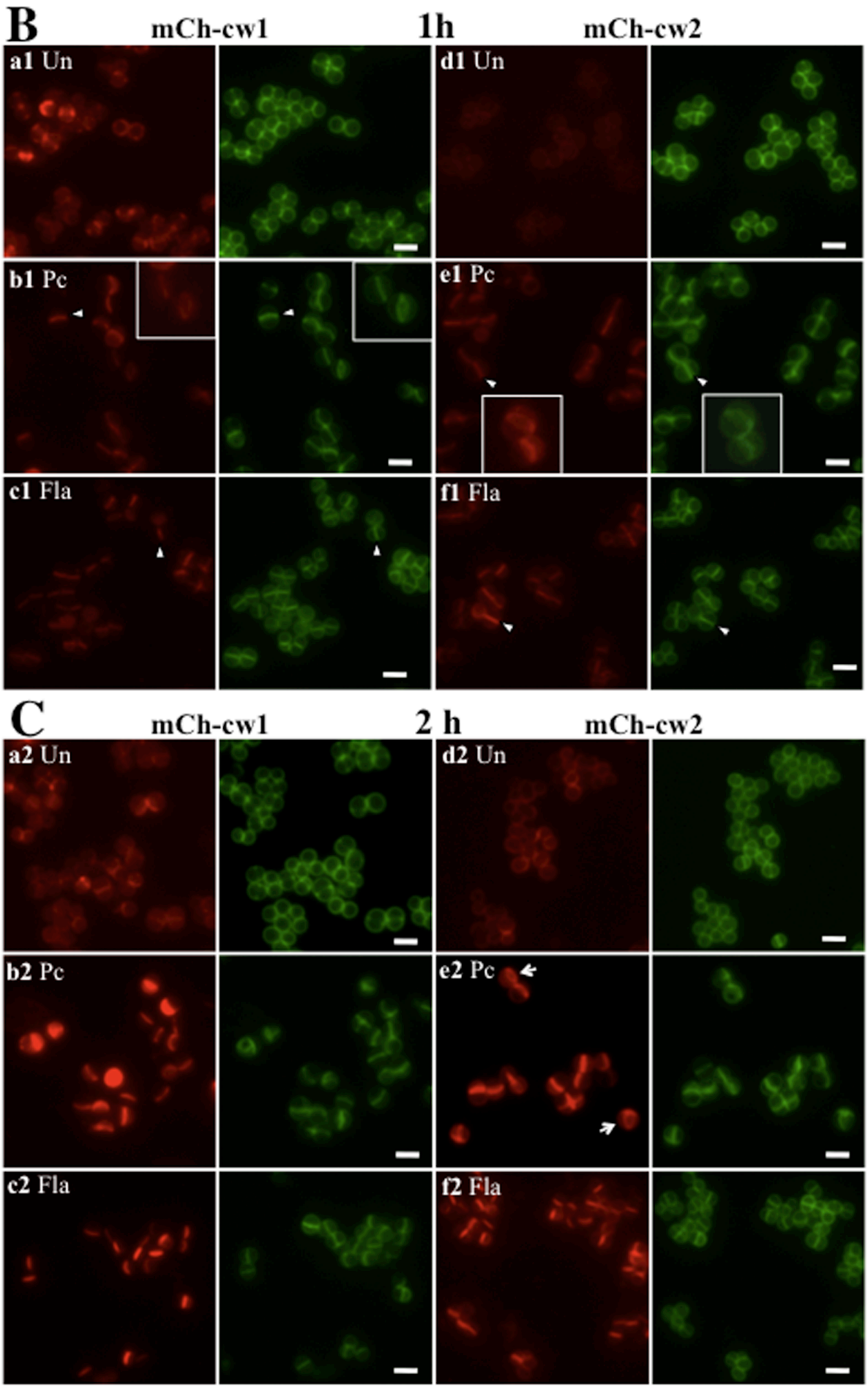
B
mCh-cw1
1h
mCh-cw2
a1 Un
d1 Un
b1 Pc
e1 Pc
c1 Fla
f1 Fla
C
mCh-cw1
2 h
mCh-cw2
a2 Un
d2 Un
b2 Pc
e2 Pc
c2 Fla
f2 Fla

Fig. II-8 Penicillin and moenomycin direct mCh-cw to the cross wall, irrespective of SP type. (A) Schematic representation of antibiotics treatment assay. Untreated (□); treated with penicillin (0.02 μg/ml) (●); treated with moenomycin (flavomycin, Fla) (1 μg/ml) (×). **(B)-(C)** Influence of penicillin (Pc) and moenomycin (Fla) on the subcellular localization of mCh-cw hybrid proteins. (B) Samples taken after one hour's xylose induction; (C). Samples taken after two hours' induction. Arrowheads indicated the cross wall accumulation of mCh-cw that corresponded to the intensified Van-FL staining; arrows and the enlarged images indicated the ring-like distribution; scale bar, 2 μm.

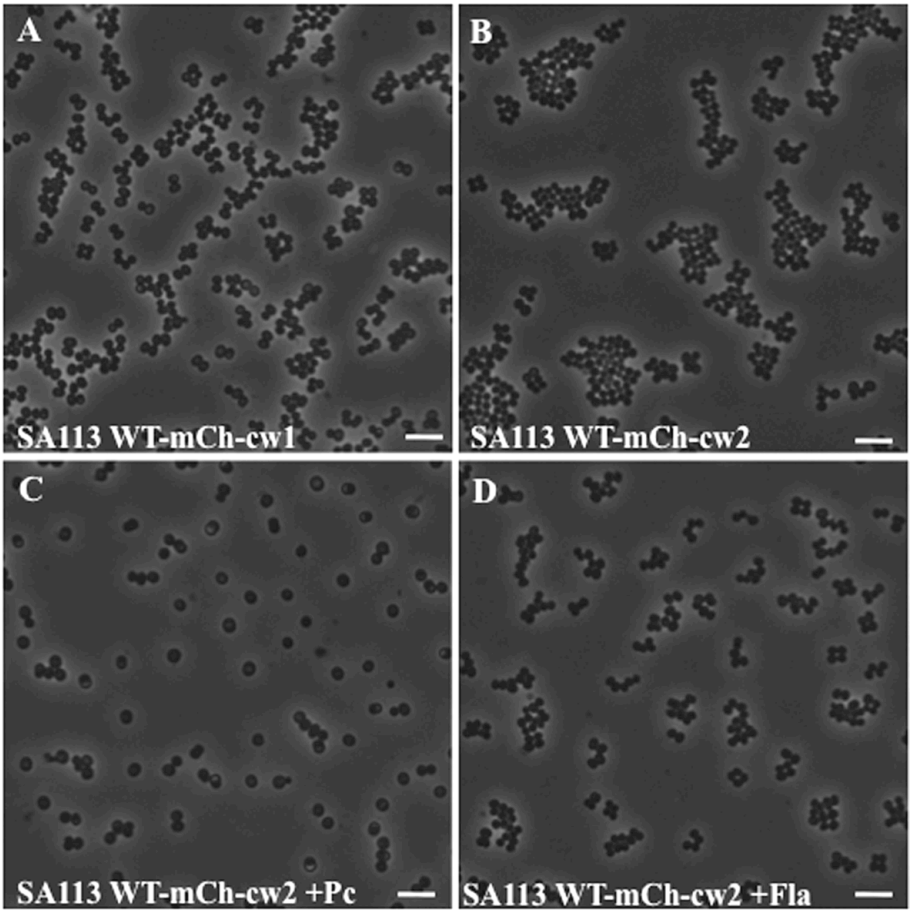

Fig. II-9. Phase contrast images of SA113 WT harboring pCX-mCh-cw after one hour's xylose induction. (**A)** SA113 WT carrying pCX-mCh-cw1. **(B)** SA113 WT carrying pCX-mCh-cw2. **(C)** SA113 WT carrying pCX-mCh-cw2 with penicillin (Pc) treatment. (**D)** SA113 WT carrying pCX-mCh-cw2 with moenomycin (Fla) treatment. Samples were taken from fluid culture without washing or fixation before microscopy examination; scale bar, 5 μm.

5. Penicillin and moenomycin induce Van-FL accumulation at the cross wall

In the presence of penicillin or moenomycin, we found that not only mCh-cw but also Van-FL that recognizes free -D-Ala-D-Ala of lipid II or uncrosslinked murein in the cell wall was accumulated at the cross wall while simultaneously disappearing from the side wall. To evaluate the significance, the relative fluorescence intensity of Van-FL at the cross wall was quantified. The fluorescence profile of a line that is perpendicular to the cross wall and across its middle point was compared between untreated and antibiotics treated cells (**Fig. II-10A**). Only cells with a 'cross wall line' (a closed septum before cell split) were measured. The max amplitude (the major peak) indicated the fluorescence intensity at the cross wall. The two small peaks indicated the peripheral (side) wall fluorescence intensity. Generally, penicillin- or moenomycin-treated cells displayed higher fluorescence (RF and Van-FL) at the cross wall and lower fluorescence at the peripheral wall when compared to untreated cells (**Fig. II-10A**). To avoid the error of staining or imaging difference, the value of max amplitude was divided by the mean Van-FL fluorescence intensity value of the same cell. **Fig. II-10B** showed the average ratio (cross wall intensity/mean intensity) of 150 cells from three independent experiments in each group. The data showed that both penicillin and moenomycin significantly intensified Van-FL staining at the cross wall compared to the untreated cells.

We also quantified the percentage of visible cross wall formation and the rate of cross wall localized mCh-cw (RF) in antibiotic treated and untreated cells (**Fig. II-11**). The percentage of visible cross walls was the ratio of visible cross wall numbers (when Van-FL staining appeared as a line at the septum before daughter cells split) in a cell population versus the total cell numbers of the same cell population. Percentage of cross wall localized RF was the ratio of numbers of line-like cross wall localized RF versus line-like cross walls (visible by Van-FL staining) in the same cell population. Both penicillin and moenomycin treatment led to a significantly higher percentage of visible cross wall formation (**Fig. II-11A**) and an increased percentage of RF localizing at the cross wall in SA113 carrying either pCX-mCh-cw1 or pCX-mCh-cw2 (**Fig. II-11B**). The effect was more pronounced in the mCh-cw2 clone. In the untreated cells, mCh-cw2 colocalized with only 6% of the cross walls, while in penicillin or moenomycin treated cells, the percentage rose to 76% and 95% respectively, implying that mCh-cw2 colocalized with almost every visible cross wall in the moenomycin treated cells.

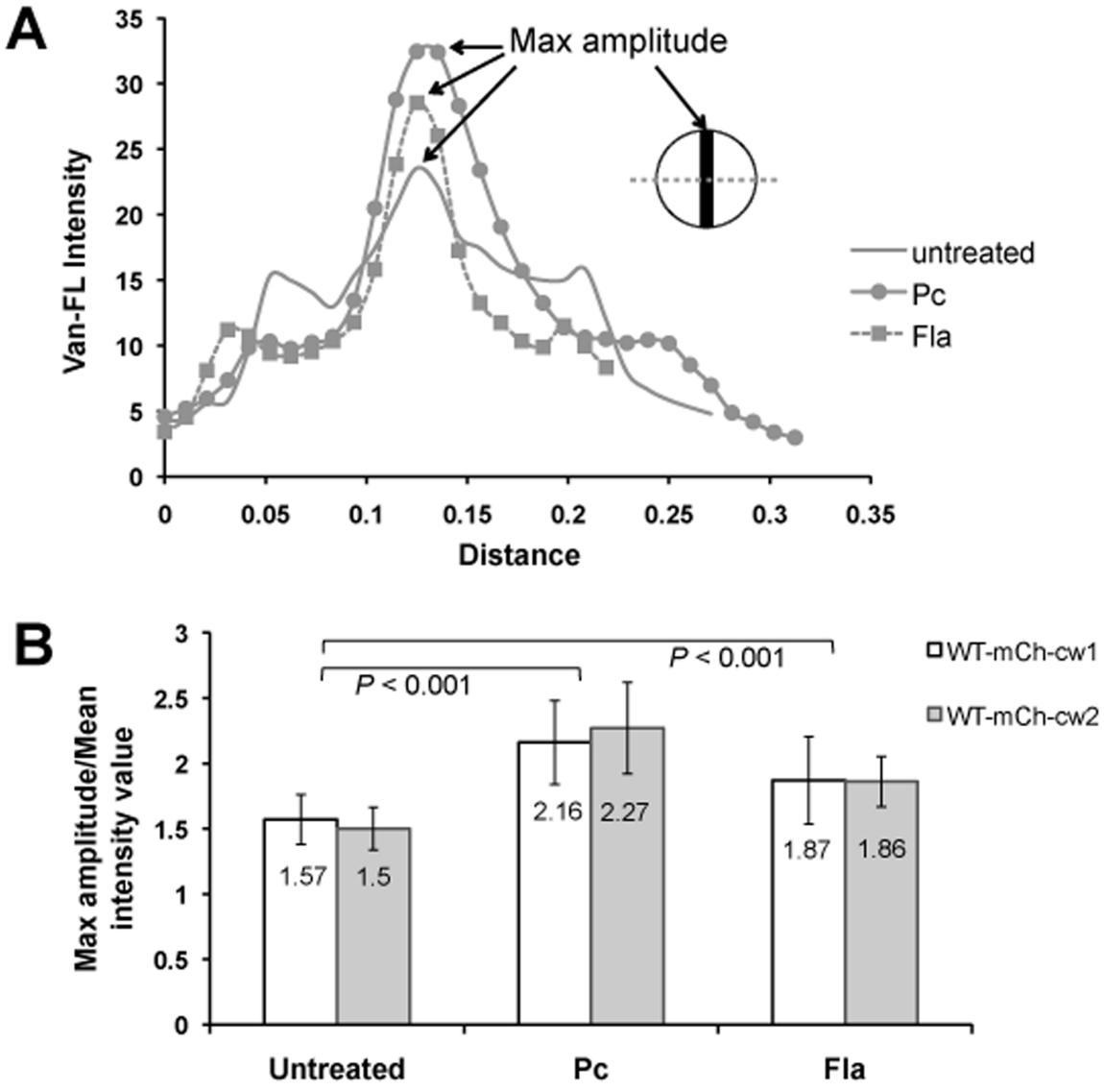

Fig. II-10. Penicillin and moenomycin treatment led to enrichment of Van-FL at the cross wall. (A) Fluorescence intensity profile of Van-FL staining from a line perpendicular to the cross wall and across the middle point of the cross wall. Simple line, untreated cell; dotted line with filled squares, moenomycin (Fla) treated cell; line with filled circles, penicillin (Pc) treated cell. Max amplitude represented the cross wall intensity. Note that the figure was remade using ImageJ software from the microscopy images; the intensity and distance values were not the same as the original data from Leica AF software; but represented the same profile distribution pattern. **(B)** Comparative Van-FL intensity at the cross wall among untreated, penicillin (Pc) treated, and moenomycin (Fla) treated cells. The cross wall Van-FL intensity values were calculated by the ratio of max amplitude against mean fluorescence intensity (generated by Leica AF software) from the same cell. The average ratio of 150 cells from three independent experiments of each group was shown in the bars. White bar, SA113 (pCX-mCh-cw1); gray bar, SA113 (pCX-mCh-cw2).

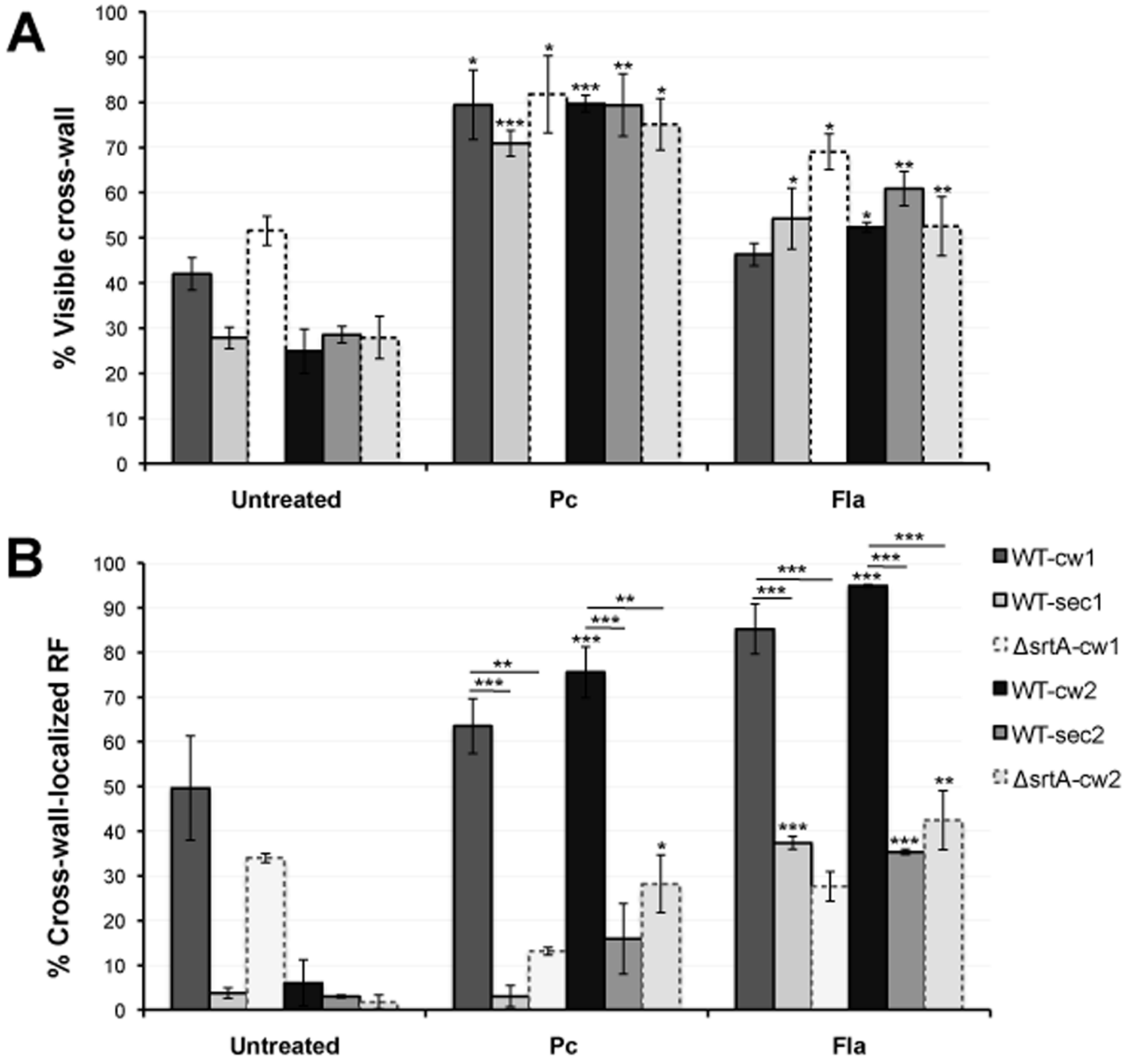

Fig. II-11. Quantification of visible cross walls and cross wall localized RF in the presence of penicillin or moenomycin. (A) Percentage of visible cross walls. The percentage was the ratio of visible cross wall numbers in a cell population versus the total cell numbers of the same cell population. Cross wall numbers were counted when Van-FL staining appeared as a line at the septum before daughter cells split (closed cross wall). More than 1000 cells from three independent experiments were counted. **(B)** Percentage of cross wall localized RF. The percentage was the ratio of numbers of line-like cross wall localized RF versus line-like cross walls (visible by Van-FL staining) in the same cell population. The total cells numbers counted were above 1000 from three independent experiments for every bar. Statistical analysis was performed using Student's *t*-test. *P*-values of statistic analysis between treated and untreated cells (inter-group comparison) were marked above the bar of the corresponding treated group; *P*-values of intra-group comparison were marked on the horizontal line. **P*<0.05, ***P* <0.01, ****P*<0.005.

In penicillin or moenomycin treated cells, Van-FL staining at the cross wall was significantly higher than that in the untreated cells, indicating that free D-Ala-D-Ala residues were enriched, which resulted from a decrease in murein cross-linking and an increase of lipid II molecules. In both scenarios, uncross-linked pentaglycines (SrtA substrates), the anchoring sites for mCh-cw, should also be increased. Thus, we assume that the increased availability of anchoring sites favors the anchoring of surface proteins, thus causing the observed incorporation and accumulation at the cross wall. This assumption was confirmed by the finding that antibiotic driven accumulation of mCh-cw at the cross wall required SrtA.

6. Antibiotic induced accumulation of mCh-cw at the cross wall requires SrtA

As shown above, penicillin and moenomycin impelled the accumulation of mCh-cw at the cross wall, irrespective of SP type. The question is: does the accumulation require SrtA mediated anchoring? To verify this question, we examined the influence of penicillin and moenomycin on Δ*srtA* (pCX-mCh-cw). In Δ*srtA,* mCh-cw cannot be anchored to the cell wall due to the absence of SrtA; therefore, mCh-cw was partially released into the supernatant and partially retained in the membrane via the C-terminal CWS domain. In the presence of penicillin or moenomycin, mCh-cw was largely dispersed over the entire cell wall (both cross wall and side wall), irrespective of the SP-types **(Fig. II-12)**. There was no RF accumulation at the cross wall as was seen for the SA113 WT (**Fig. II-8BC**), indicating that SrtA was necessary for the accumulation of mCh-cw at the cross wall.

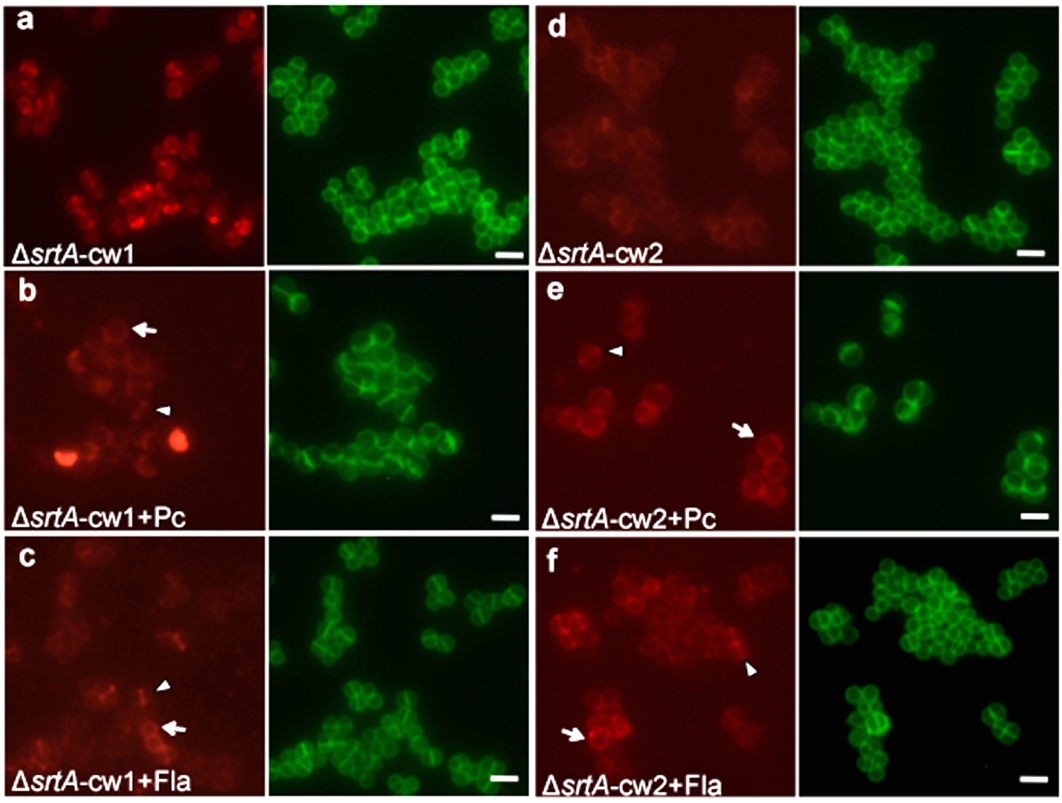

Fig. II-12. Localization patterns of Δ*srtA* (pCX-mCh-cw1&2) in the presence of penicillin or moenomycin. Arrows, mCh-cw dispersed over the entire cell; arrowheads, the cross wall localized mCh-cw. Scale bar, 2 μm.

Unpublished Results:

7. The localization of Sortase A is not altered by penicillin and moenomycin treatment

The above observation led us to the next question: if the SrtA localized and accumulated to the septum upon the cell wall antibiotics treatment? Until now several papers have reported the subcelullar localization of SrtA. The first report shows that SrtA localizes as several foci in *S. pyogenes* (Raz & Fischetti, 2008). The foci are cell cycle dependant, frequently found at the septum and to a less frequency at the cell poles. The SrtA localization seems to be differed in different bacteria. Apart from that in *S. pyogenes,* SrtA is found as single foci and colocalize with SecA in *S. mutans* and *Enterococcus faecalis* (Kline *et al.*, 2009, Hu *et al.*, 2008). However, in *S. peumonea* SrtA localizes over the entire cell and does not colocalize with SecA (Tsui *et al.*, 2011). A very recent report shows that SrtA localizes as short helical arcs in *B. subtilis* (Liew *et al.*, 2012). There is no report on SrtA localization in *Staphylococcus* yet.

To address the question of the SrtA localization in *S. aureus*, several fusions were constructed (**Fig. II-13**). It has been reported that a linker between the protein of interest and the fusion partner is important for the functionality of the fusions (Margolin, 2000, Volkov et al., 2003). To test the influence of the linker, different linkers composed of 5 aa (GGAAG), 6 aa (GSAGSA) and 14 aa (GSAGSAAGSGEFLE) were used in the fusions. To obtain a clear picture of SrtA localization and to avoid artifacts, mCherry or gpmCherry (coden usage optimized according to gram-positive bacteria) and sfGFP were adopted for both N- and C-terminal fusion with SrtA (**Fig. II-13**). The resulted constructs were transformed into SA113 Δ*srtA*. After 0.25% xylose induction for 1 h, samples were collected for microscopy analysis.
In the case of all the C-terminal SrtA-mCh fusions, SrtA showed an overall homogeneous localization pattern **(Fig. II-14A, C, E**). At the early stage of cell division, SrtA-mCh slightly enriched to the site where the new division septum was forming **(Fig. II-14A, C, arrowheads)**. At the late stage of cell division, SrtA-mCh distributed over the entire cell, with slight brightness at the septum due to two membrane layers before cell division (**Fig. II-14A, C, arrows**). When we compared the results with different linkers, fusions with short linkers (5 aa -GGAAG and 6 aa - GSAGSA) displayed brighter fluorescence than that with 14

aa. The same was observed with C-terminal sfGFP fusions **(Fig. II-14G, H)**. However, compared to SrtA-5-mCh, SrtA-5-sfGFP showed strong fluorescence at the septum (**Fig. II-14G**, arrow). SrtA-14-sfGFP also showed highlighted septum localization, but to a less extent **(Fig. II-14H, arrow)**. When SrtA-14-sfGFP was expressed from *srtA* original locus in the chromosome, the fluorescence was very weak but apparently was homogeneous all over the entire cell **(Fig. II-14I)**. It is likely that the highlight at the septum shown by plasmid encoded SrtA-5/14-sfGFP was artifact due to over-expression. The last construct sfGFP-5-SrtA provided a similar distribution pattern like SrtA-6-mCh, in which fluorescence of the fusions were found over the cell and colocalized with the membrane staining **(Fig. II-14L)**. The spot-like foci often represented the site for the future septum formation **(Fig. II-14L, arrowhead)**. At the late stage of the cell cycle, sfGFP-5-SrtA localized all over the cell **(Fig. II-14L**, **arrow)**. After the penicillin or moenomycin treatment, there was no accumulation of any SrtA fusions at the septum **(Fig. II-14B, D, F, J, K, M)**. Rather, the fluorescence of the fusions was distributed all over the cell. Sometimes it was ring-like **(Fig. II-14B, M, arrows)** and spot-like **(Fig. II-14B, M, arrowheads)**.

In conclusion, SrtA very likely localized over the entire membrane of the staphylococcal cell. The antibiotic treatment did not alter its localization. The best fusion for SrtA localization was sfGFP-5-SrtA.

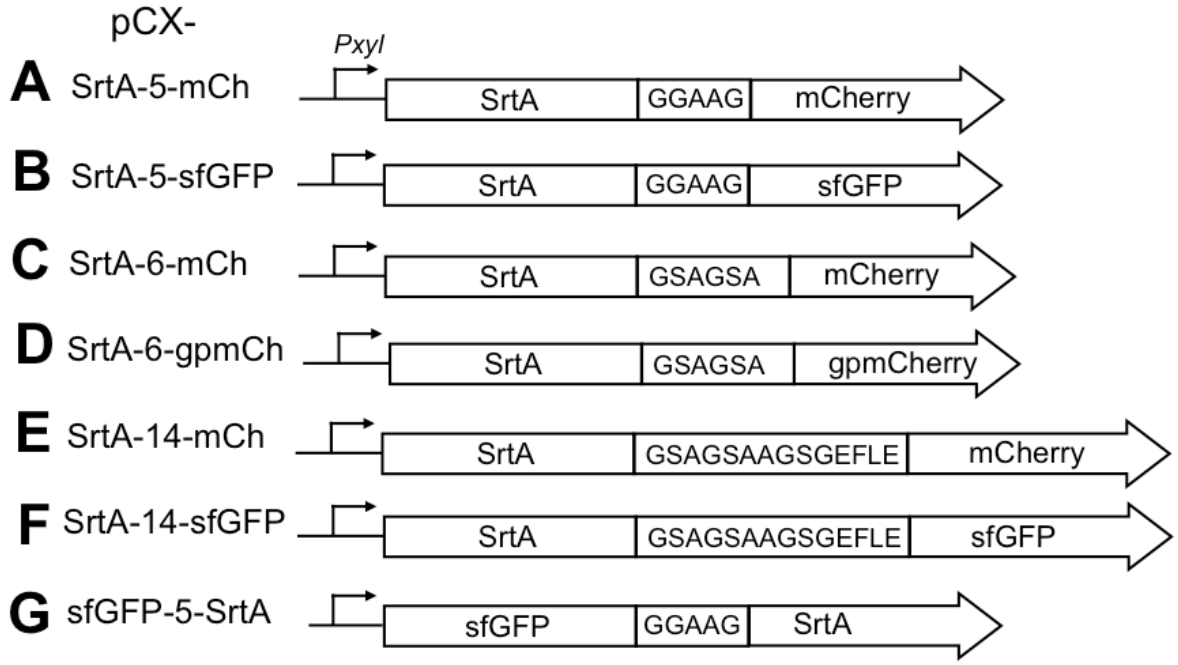

Fig. II-13. Schematic representation of SrtA-mCh/GFP fusions. The amino acids compositions of the linker domain were indicated.

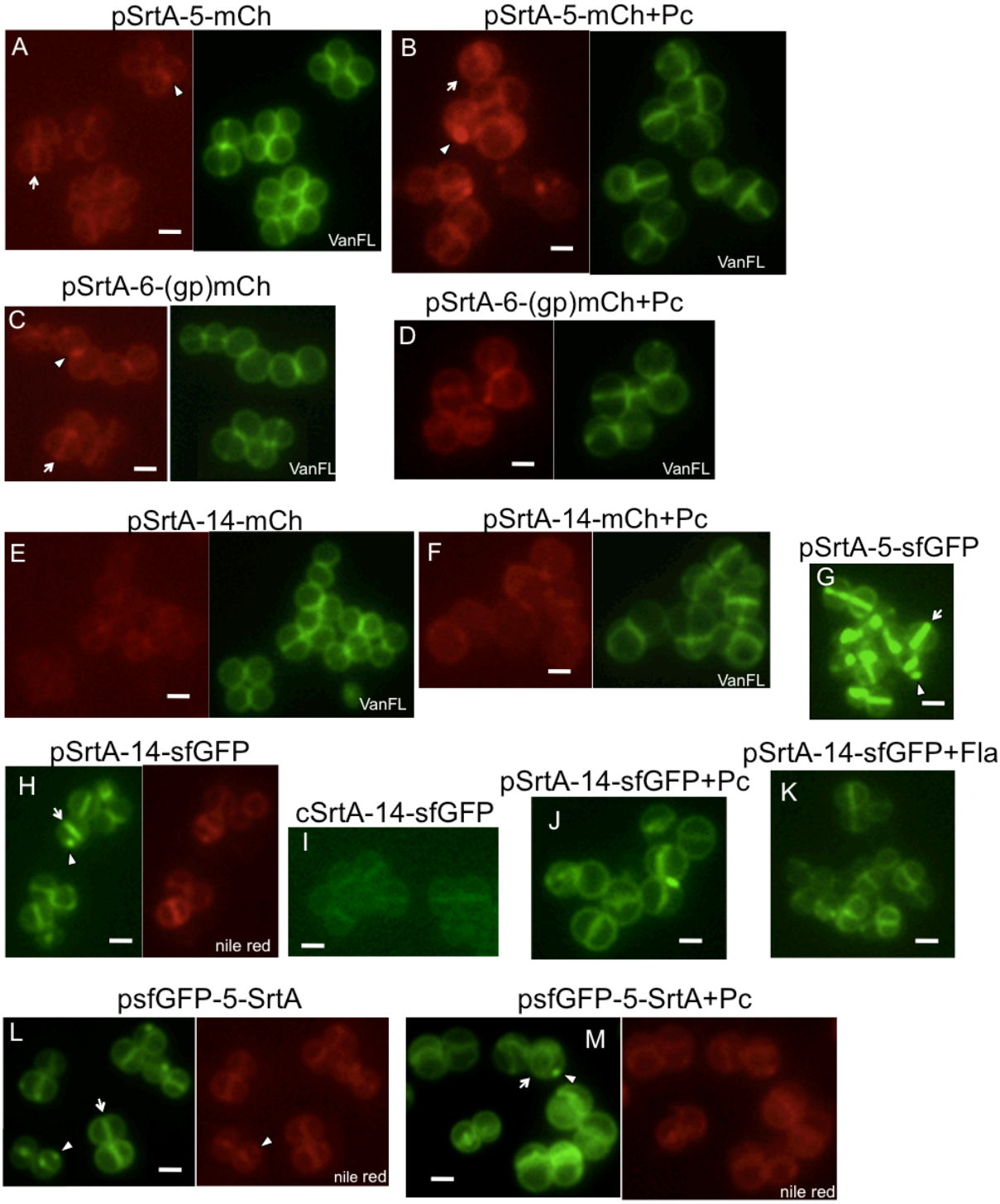

Fig. II-14. Localization of *S. aureus* SrtA. SA113 Δ*srtA* harboring various pCX-SrtA-mCh/GFP fusion plasmids were grown to the mid-log phase in the absence or presence of antibiotics before xylose induction. Samples were collected for microscopy analysis after 0.25% xylose induction for 1 h. The chromosomal fusion of SrtA-14-sfGFP (I) was integrated at *srtA* original locus under its native promoter; sample for this strain was taken from mid-log phase growth in TSB. The cell wall (Van-FL) or membrane (nile red) staining was indicated correspondingly. Arrowheads indicated spot-like localization, arrows indicated cross wall and ring-like distribution. Scale bar=1 μm.

8. Influence of penicillin on the membrane composition

Protein secretion is one of the cellular processes that are closely related with the cytoplasmic membrane. Several studies have demonstrated that the anionic phospholipids play important roles in regulating the activity and subcellular localization of Sec secretory translocon (Campo *et al.*, 2004, Gold *et al.*, 2010, Rosch *et al.*, 2007, Tsui et al., 2011). Phosphatidylglycerol (PG) and cardiolipin (CL) are the major anionic phospholipid components in the membrane. Visualization of anionic lipids using the fluorescent dye NAO (10-*N*-nonyl-acridine orange) revealed that *E. coli* and *B. subtilis* membranes contain anionic lipid-rich domains at the septum and cell poles (Kawai *et al.*, 2004, Mileykovskaya & Dowhan, 2000). In *S. pyogenes,* anionic lipids are enriched as single microdomain and colocalize with the 'ExPortal' Sec tranlocon (Rosch et al., 2007). The fluorescent dye NAO binds to anionic phospholipids and is CL specific (Mileykovskaya *et al.*, 2001). When NAO binds to anionic phospholipids due to the interaction between its quaternary amine and the phosphate residue of phospholipids, it gives green fluorescence (emission peak 525 nm). The binding of NAO to CL that has two phosphate groups per molecule leads to the dimerization of the dye, which shifts its fluorescence from green to red (emission peak 640 nm). In comparison, nile red is a nonpolar lipid staining dye.

The over-all localization pattern of mCh-cw in Δ*srtA* after antibiotic treatment **(Fig. II-12)** let us to speculate if the antibiotics exert side effect on protein secretion by affecting membrane composition. In the following study, *S. aureus* SA113 cells growing in the absence and presence of penicillin (0.02 μg/ml) for two hours were collected and subjected to nile red and NAO staining. In the absence of penicillin, both nile red and NAO stained the whole cell homogeneously **(Fig. II-15A, C, arrows)**. Moreover, foci-like staining was also frequently observed, which localized at the septum region or the future division sites **(Fig. II-15A, C, arrowheads)**. The foci appeared similar to the 'microdomain' found in *S. pyogenes* (Rosch et al., 2007). Yet in *S. pyogenes,* the foci are only found with NAO staining, not with nile red. The red fluorescence of NAO staining was fairly weak, indicting that the amount of CL was low and PG was the major anionic phospholipids in *S. aureus* **(Fig. II-15C)**. After penicillin treatment, the membrane staining appeared less homogeneous while the majority of the cells still had the normal membrane structure and septum **(Fig. II-15B, D, arrows)**. Foci were also observed **(Fig. II-15B, D, arrowheads)**. The interesting observation was that the red fluorescence of NAO was increased after penicillin treatment, showing an increased amount of CL in the membrane **(Fig. II-15D)**. An earlier study has reported similar result (Kariyama,

1982). Whether this change in membrane composition influenced the protein secretion affords future investigation.

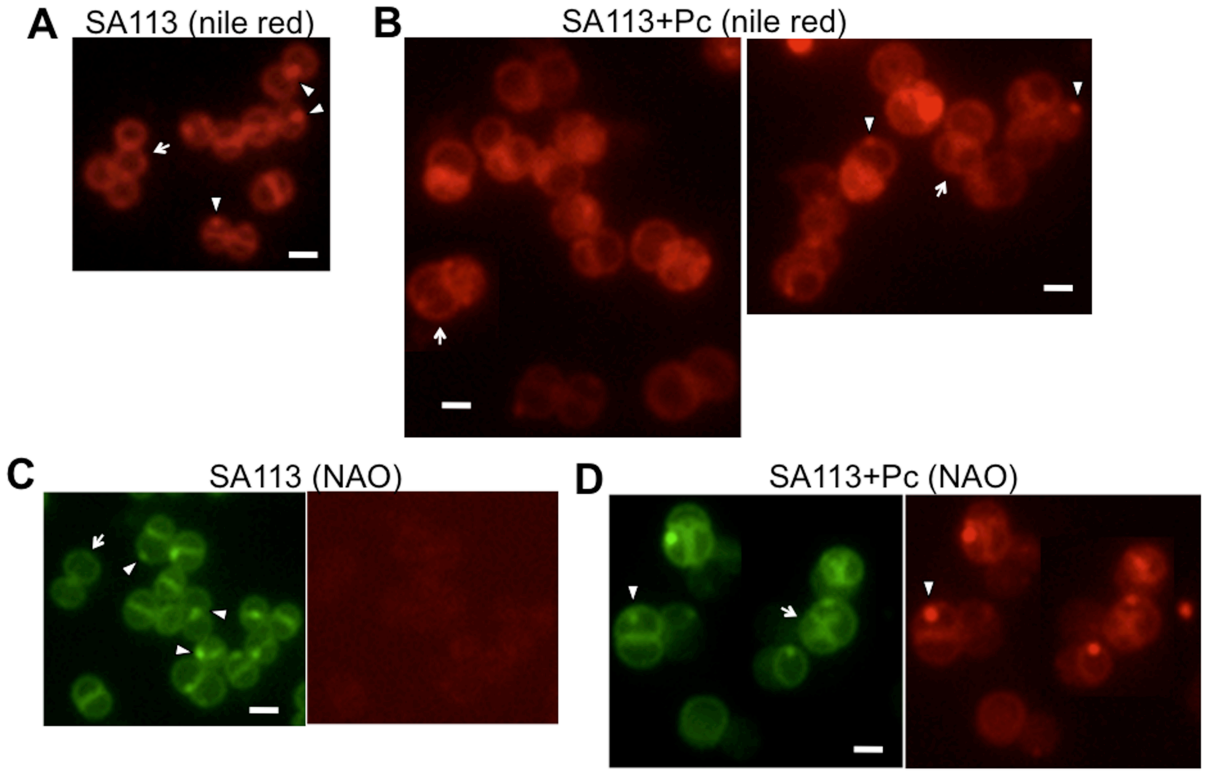

Fig. II-15. Membrane staining of *S. aureus* by nile red and NAO. SA113 grown in the absence or presence of penicillin to the mid-log phase was stained by nile red (5 μg/ml) or NAO (1 μM). Arrowheads indicated spot-like localization; arrows indicated the overall distribution. Scale bar, 1 μm.

9. Some other intriguing observations from the current study

The pioneering work in 1970s by using light microscopy and electron microscopy has demonstrated that staphylococci divide in successive perpendicular planes in all three dimensions (Tzagoloff & Novick, 1977). The new septum plane is at right angles to the previous one. After the septum formation and splitting catalyzed by cell wall hydrolase, the two daughter cells divide with 'abrupt popping motion' due to the internal pressure (Previc, 1970). After division, the staphylococcal cells form irregular clusters due to post-fissional movement (Koyama *et al.*, 1977). This post-fissional movement involves slight rotation so that the two daughter cells are attached to each other at or near the center of the previous division disk (Tzagoloff & Novick, 1977). The effects of cell wall antibiotics on the cell morphology and cell division have been examined by electron microscopy (Greenwood & O'Grady, 1972, Lorian, 1975, Lorian & Atkinson, 1976) Interestingly, the perpendicular

division mode is also found in a spherical *E. coli* (*rodA ftsA* mutant) (Begg & Donachie, 1998).

During the current studies, some intriguing images were obtained with respect to the cell division and separation of staphylococcal cells. A series of images demonstrated the cell cycle of *Staphylococcus* **(Fig. II-16A)**. The septum formation initiated as a ring and later became a flat disk that was visualized as a line in the middle of the cell **(Fig. II-16A-a, b)**. Two pairs of images **(Fig. II-16A-c, d and e, f)** showed the division event, in which the flat septum disk of the daughter cell rapidly became hemispherical. After division, the daughter cells were still connected to each other at the center of division plane **(Fig. II-16A-f)** or at its proximity **(Fig. II-16A-g)**.

It is well known that cell wall antibiotics trigger morphological changes. Penicillin is one of the intensively studied antibiotics. Yet it was still inspiring to observe that upon penicillin treatment, the septum ring formation was frequently and clearly visible by Van-FL staining. The two septum-rings from the two daughter cells looked like a pair of eyes with glasses **(Fig. II-16B-a)**. But they were not always horizontal within one plane **(Fig. II-16B-b, c)**, indicating that new division plane could be any plane in the three dimensions as long as it is perpendicular to the old one. The septum formation was often asymmetrical **(Fig. II-16B-c, d)**. A thicker ring or a half disk could also be visualized **(Fig. II-16B-e, f)**. A clear perpendicular conformation between two successive division planes was shown in the upper cell of **Fig. II-16B-e**.

Another interesting observation was from tunicamycin (1 μg/ml) treated cells. Because low concentrations of tunicamycin is known to preferentially inhibit TagO, one of the first enzymes of wall teichoic acid synthesis (Hancock *et al.*, 1976, Pooley & Karamata, 2000); its treatment led to very similar morphological phenotype as the *ΔtagO*. As shown in **Fig. II-16C**, the septum ring formation in *ΔtagO* or tunicamycin treated cell (data not shown) was much less visible compared to the penicillin treated cells **(Fig. II-16C-a, arrows)**. The cell clusters composed of unseparated tetrads or trimers of staphylococci were predominant **(Fig. II-16C)**. The Van-FL staining between the daughter cells was intensified **(Fig. II-16C-b, arrowheads)**.

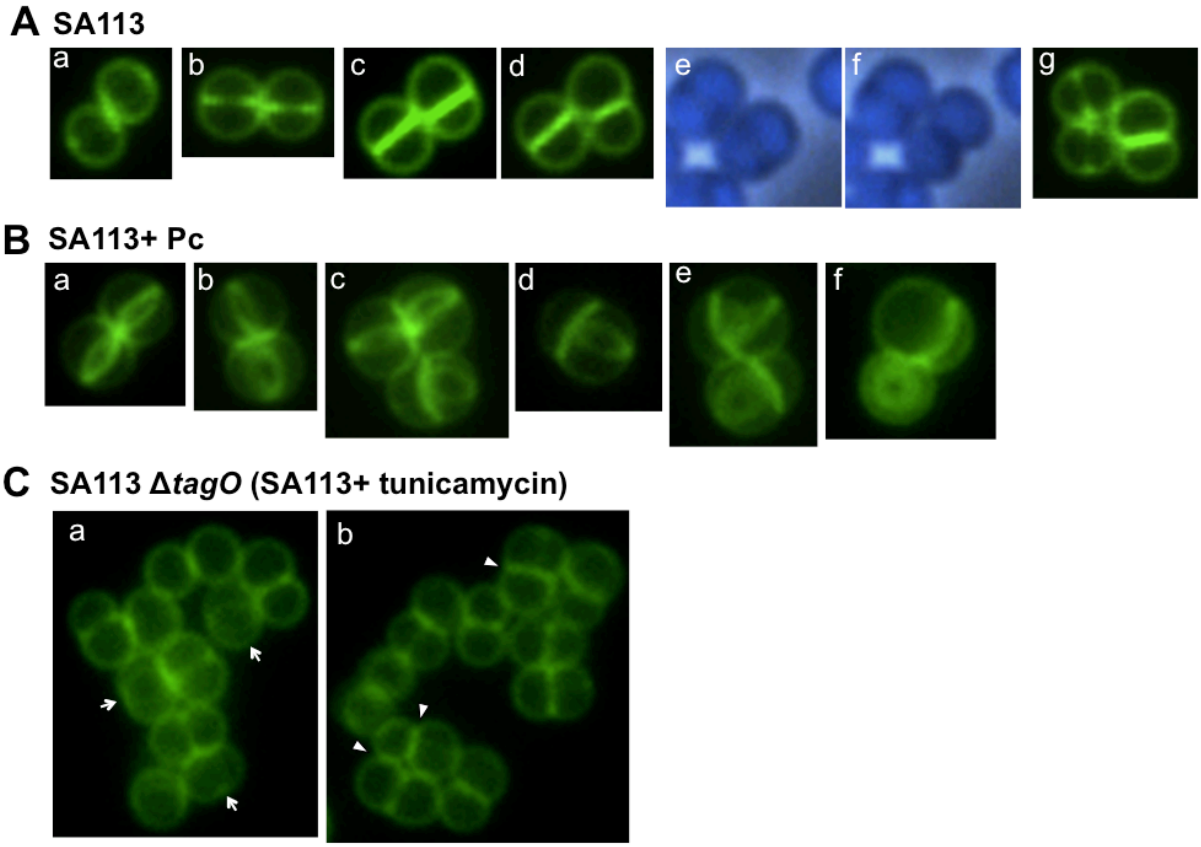

Fig. II-16. Van-FL and DAPI staining of *S. aureus* from mid-log phase showing septum formation and cell division. (A) SA113 grown in the absence of antibiotics. **(B)** SA113 grown in the presence of penicillin (0.02 μg/ml). **(C)** SA113 *ΔtagO*. Green, Van-FL staining; Blue, DAPI staining (A-e, f). Arrows in (C-a) indicated the ring-like pattern; arrowheads in (C-b) indicated enhanced Van-FL staining between the daughter cells.

Discussion

So far, immunofluorescence microscopy and immunoelectron microscopy have been used for surface proteins localization studies in the last decades. To our knowledge, there is no direct visualization method to be applied in this field yet. In this study, we aimed to develop a direct method for monitoring surface proteins' subcellular distribution. The recently developed fluorescent protein mCherry, the monomeric derivative of *Discosoma* sp. fluorescent protein 'DsRed' (Shaner *et al.*, 2004), provided us with an ideal tool. MCherry was found fully fluorescent after secretion through the Sec secretory pathway and was fluorescent in the membrane as well (Chen *et al.*, 2005, Lewenza *et al.*, 2006). Here we show that mCherry can be secreted and anchored to staphylococcal cell wall while maintaining stable fluorescence. The mCh-hybrids constructed in this study enabled us to observe and follow the subcellular (especially the cross wall) localization of anchored proteins. Meanwhile, we were also fully aware of the limitation of the system, as it was based on plasmid-encoded genes, by which the

proteins were higher expressed. Yet, prolonged protein expression only enhanced the fluorescent signals; it did not alter the distribution patterns within the time period tested, one and two hours after induction. Therefore, we can make at least statements as to the tendency of protein localization.

Apart from the influence of SPs (+/−YSIRK) on the localization of secretion, we also found that in the presence of the YSIRK-motif the RF intensity of mCh-fusion proteins was significantly increased. As shown in **Fig. II-7C,** mCh-sec1 exhibited spot-like bright foci at or near the division septum, which very likely resulted from the highly expressed proteins that exceeded the capability of protein transport. Indeed, mCh-sec1 showed higher RF than mCh-sec2 in both the supernatant and the cell pellet **(Fig. II-3A)**, implying that mCh-sec1 was expressed in a higher amount than mCh-sec2. The tendency that proteins fused with SP_{lip} (+YSIRK) were always higher expressed was observed in all mCh-constructs as well as in all GFP-fusions **(Fig. II-6B**). The difference in protein expression was most likely due to different SPs, as the plasmid, promoter, and RBS were identical in all constructs. Whether transcriptional or post-transcriptional regulation was responsible for the positive effect of the SP (+YSIRK) needs to be verified. In principle, we could confirm earlier results that *S. aureus* distinguishes between SPs to either direct (+YSIRK)-proteins to the cross wall (cell division site) or (-YSIRK)-proteins to the side wall (DeDent et al., 2008). How the targeting is accomplished is still unknown, but one cannot rule out that the different expression levels of +/−YSIRK-motif proteins played a role in the different targeting.

One of the most interesting findings of our study was the effect of sub-lethal concentrations of penicillin or moenomycin. These two antibiotics provoke concentration of cell wall-anchored mCh-cw1&2 at the cross wall, irrespective of their SP-type (**Fig. II-8B, C**). We also addressed the question of which role SrtA might play in targeting. In Δ*srtA,* proteins remain at least transiently in the membrane via their C-terminal CWS domain. In the absence of antibiotics a similar distribution of mCh-cw was observed in Δ*srtA,* as in WT. In Δ*srtA*-mCh-cw1, mCh was more accumulated in the cross wall and in Δ*srtA*-mCh-cw2, mCh was more abundant in the side wall (**Fig. II-12a, d**). The effect of penicillin and moenomycin in the Δ*srtA* was, however, not as pronounced as in the WT. In the presence of penicillin or moenomycin, not only mCh-cw but also Van-FL was concentrated in the cross wall, indicating that there is an increased content of free D-Ala-D-Ala residues (e.g., uncross-linked pentaglycine bridges or lipid II molecules), which represent the substrates for the SrtA

transpeptidation reaction. Such an accumulation of uncross-linked peptidoglycan precursors can be postulated since penicillin and moenomycin are known to bind to the active site of penicillin binding proteins, thus blocking the transpeptidation and transglycosylation, respectively (Izaki *et al.*, 1966, van Heijenoort *et al.*, 1987). It was surprising that vancomycin had little effect on mCh-cw distribution, as theoretically vancomycin inhibits both transpeptidation and transglycosylation. The previously described inhibiting effect of vancomycin is most likely due to the 10-times higher concentration used in their studies causing a complete inhibition of transpeptidation or transglycosylation (Perry et al., 2002, Ton-That & Schneewind, 1999).

Our preliminary data showed that SrtA localized all over the staphylococcal cell including both septum and side wall **(Fig. II-14L)**. The antibiotics did not cause an enrichment of SrtA localizing to the septum. Rather, SrtA always co-localized with the membrane; sometimes it formed septum-ring in the prescence of penicillin **(Fig. II-14B, M)**. This implies that SrtA can catalyze the sorting reaction quite efficiently even with increased amount of substrates. SrtA is a membrane protein with its N terminus inside the cytoplasm and the C-terminal enzymatic part located across the plasma membrane (Marraffini et al., 2006). Conventionally, GFP is used for the cytoplasmic fusion while mCherry could be used for membrane protein localization. We have also tested GFPmut3 in the fusion with SrtA, which turned out to be hardly visible. Fusion with sfGFP significantly improved the fluorescence performance. Yet the over-expression also caused some artifact **(Fig. II-14G).** It is necessary to analyze the functionality of the SrtA-fusion proteins in the future.

In sum, this study is more than the introduction of a new experimental approach. We used this new tool to directly follow the targeting and anchoring of various mCh-hybrid constructs. We have found that different SP types affect the expression and targeting of the fusion proteins. In the presence of sub-lethal concentrations of penicillin and moenomycin the cell wall anchored mCherry was concentrated at the cross wall. We assume that the antibiotics cause accumulation of SrtA substrates at the cross wall, which attract SrtA to incorporate the mCh-cw almost exclusively at the cross wall, irrespective of SP type. With this study we contribute to better understanding the influence of different signal peptide types in targeting anchored and secreted proteins, the role of cell wall antibiotics as well as the application of different fluorescent proteins in staphylococci.

Part III *Staphylococcus aureus* invasion of host cells triggering autophagy induction

Introduction

Staphylococcus aureus has been for a long time regarded as an extracellular pathogen, but later it was found that *S. aureus* could also survive intracellularly. It is now clear that *S. aureus* is able to survive in both professional phagocytes and non-phagocytic host cells such as keratinocytes, fibroblasts, endothelial cells and epithelial cells (Foster, 2005). The internalization to the non-phagocytes is mediated by the bacterial fibronectin-binding proteins forming fibronectin bridge to the α5β1 integrin on the host cell surface (Sinha *et al.*, 1999, Schwarz-Linek *et al.*, 2004). Hiding inside the host cell is considered as a strategy of the bacteria to proliferate and avoid the attack from the immune system and extracellular antibiotics (Sinha & Fraunholz, 2010, Garzoni & Kelley, 2009).

Autophagy is a cellular degradation/recycling system for turning over cellular constituents in eukaryotic cells to keep the cell clean and healthy (Deretic & Levine, 2009). Under stress conditions, such as starvation, the autophagy is induced to compensate the nutrient shortage. Apart from its cellular function, autophagic degradation is also a previously unrecognized effector of host innate immunity, which can eliminate the invading bacteria. The autophagosomes that are generated from the phagophore can engulf the bacteria and subsequently fuse with the lysosomes to degrade the bacteria.

In cooperation with the research group of Dr. Proikas-Cezanne (Autophagy Laboratory, Interfaculty Institute for Cell Biology, University of Tübingen), we addressed the questions of whether the invasion of *S. aureus* would trigger autophagy induction in the non-phagocytic host cells, and what would be the consequent fate for *S. aureus*.

Results and Discussion

To visualize the internalization of staphylococci to the host cells, several staphylococcal strains were transformed with a plasmid, pC-tuf-ppmch, in which the red fluorescent protein mCherry fused with lipase propeptide was constitutively expressed under the native EF-Tu promotor. The stains studied were *S. carnosus* TM300, an apathogenic staphylococcal species, *S. aureus* SA113 (MSSA, *agr* −), *S. aureus* HG001 (MSSA, *agr* +) and *S. aureus* USA300 (CA-MRSA, *agr* +). The human WIPI-1 protein specially localizes at the phagophore and at the autophagosomes upon the initiation of autophagy, therefore it is a marker protein for

monitoring autophagy induction. The research group of Dr. Proikas-Cezanne has previously set up the human osteosarcoma U2OS cell line stably expressing GFP-WIPI-1 (Proikas-Cezanne *et al.*, 2007). Upon infection of staphylococci for 0.5, 1 or 2 h, the induction of autophagy, which was indicated by GFP-WIPI-1 puncta formation, was automatically imaged and analyzed using the *In Cell Analyzer 1000* (GE Healthcare).

As presented in **Fig. III-1A-C,** *S. aureus* infection of GFP-WIPI-1 expressing U2OS cells resulted in an increase in the number of GFP-WIPI-1 puncta-positive cells (green in the left panel) as well as in the number of cells with GFP-WIPI-1 positive autophagosome-like vesicles entrapping *S. aureus* (middle and right panel). Among the three *S. aureus* strains tested, infections of *agr*-positive strains USA300 and HG001 triggered appr. 70%-76% GFP-WIPI-1 puncta-positive cells, higher than *agr*-negative strain SA113 (appr.60%) (left panel). Further, the percentage of cells displaying GFP-WIPI-1 positive autophagosome-like vesicles entrapping *S. aureus* was prominently higher with USA300 and HG001 invasion (appr. 40%) than with SA113 (appr. 18%) (right panel). In contrast, the infection of the non-pathogenic *S. carnosus* TM300 did not result in an invasion of host cells; accordingly, GFP-WIPI-1 positive autophagosome-like vesicles were not induced (**Fig. III-1D,** middle and right panel). Interestingly, after 2 h of incubation with *S. carnosus* TM300, the number of GFP-WIPI-1 puncta-positive cells increased (appr. 45%) (**Fig. III-1D**, left panel).

Further, by electron microscopy we found that the intracellular *S. aureus* USA300 cells were entrapped in vesicles with either one single cell (**Fig. III-2A**) or multiple cells (**Fig. III-2B**). In both cases, intracellular *S. aureus* USA300 cells showed clear signs of ongoing cell division (red arrows).

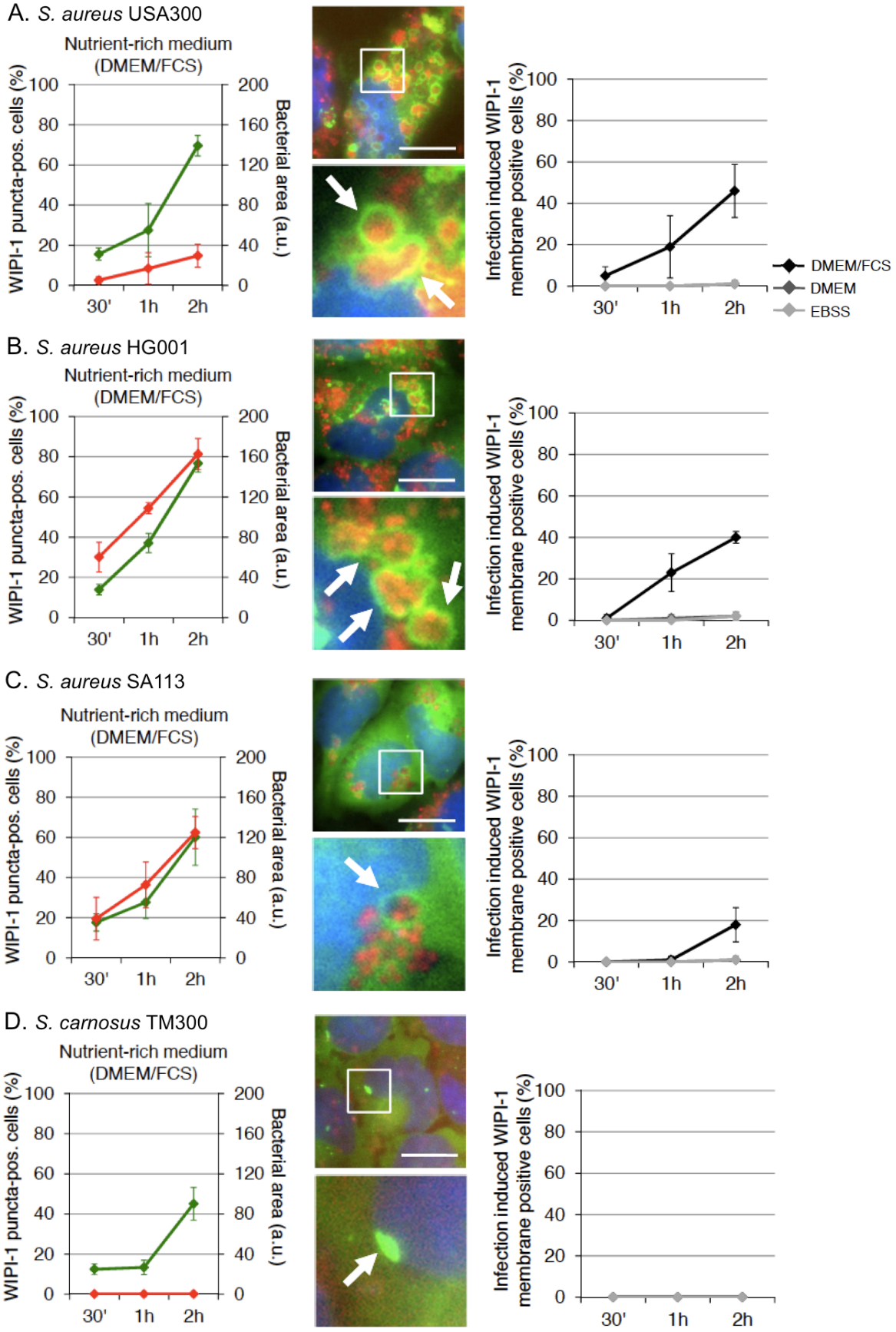

Fig. III-1. Pathogenic *S. aureus* induces GFP-WIPI-1 puncta formation and becomes entrapped in GFP-WIPI-1 positive circular membrane structures. GFP-WIPI-1 U2OS cells were infected with mCherry-expressing *S. aureus* USA300, HG001, SA113 and *S. carnosus* TM300 for 0.5, 1 and 2 h. The quantification of GFP-WIPI-1 puncta formation

(green) and intracellular bacteria load (red) is presented in the left panel. Representative images of 2 h infection are shown in the middle panel. Scale bars: 20µm. The number of cells displaying GFP-WIPI-1 positive autophagosomal-like vesicles entrapping staphylococci using nutrient-rich medium DMEM/FCS, serum-free medium DMEM, or serum- and amino acid-free medium EBSS medium was determined and presented in the right panel.

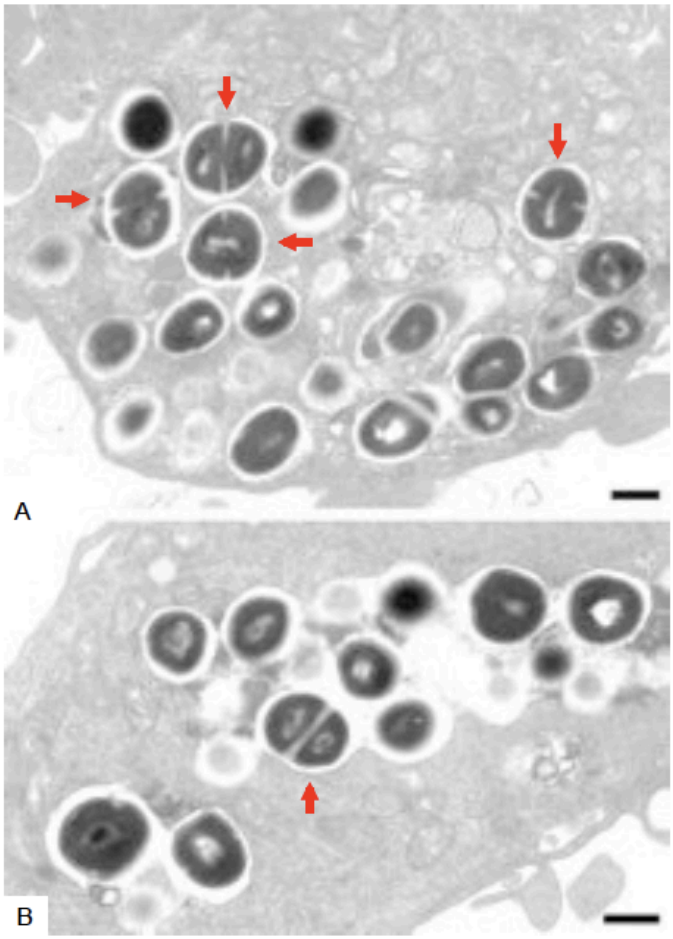

Fig. III-2. Electron microscopy *S. aureus* USA300 infected GFP-WIPI-1 expressing U2OS cells. GFP-WIPI-1 U2OS cells were infected with *S. aureus* USA300 in DMEM/FCS and examined by conventional electron microscopy. Either single *S. aureus* USA300 cells were found to reside within a vesicle **(A)**, or multiple cells were found in enlarged vesicles **(B)**. Red arrows indicated dividing staphylococcal cells. Scale bars: 500 nm.

Thus, our data demonstrated clearly that *S. aureus* could invade non-phagocytic host tumor cells and trigger autophagy induction. Interestingly, the host cells were more or less simultaneously invaded by quite a number of staphylococcal cells. This was hitherto not so clear. During this process of autophagy, several steps are involved and are probably very interesting for the further investigation. As mentioned in the introduction, the invasion of *S. aureus* to the non-phagocytes is mediated by a fibronectin-dependent bridging between fibronectin-binding protein and α5β1 integrins on the host cell surface. Apart from that, a

recent report showed that *S. aureus* could also be taken up by endothelial cells via the interaction between the staphylococcal major autolysin (Atl) and heat shock cognate protein Hsc70 of the host cells (Hirschhausen *et al.*, 2010). In our study, the invasion of three *S. aureus* strains to the host U2OS cells is very likely also due to these two pathways. Yet the autophagy induction is not strictly dependent on bacterial internalization, as the non-invasive *S. carnosus* stain could also triggered a mild GFP-WIPI-1 puncta formation in a time-delayed manner **(Fig. III-1D, left panel)**. We have to verify whether the induction by *S. carnosus* is directly due to certain bacterial components or just because that elongated incubation with bacteria induces stress on host cells unspecifically. To answer this question, we could test defined staphylococcal mutants and purified staphylococcal cell components.

After being taken up, the intracellular *S. aureus* are entrapped in the autophagosome-like vesicles **(Fig. III-1)**. Would the bacteria then be degraded or survive? Our data showed that the bacteria were still alive at least in the autophagosome-like vesicles (**Fig. III-2**). There are only a few data from the literatures so far. One previous study reported that autophagic degradation was induced against *S. aureus*, but the methicillin-resistant *S. aureus* were resistant to autophagic degradation (Amano *et al.*, 2006). Another report has suggested a model that the autophagic response is connected with *S. aureus agr* global regulator (Schnaith *et al.*, 2007). In their model, *agr*-positive *S. aureus* become entrapped and replicate in autophagosome-like vesicles and subsequently escape into the cytoplasm to promote host cell death, but *agr*-deficient *S. aureus* are subjected to lysosomal degradation (Schnaith et al., 2007). However, detailed and complete studies are missing. In our lab we have the advantage of owning a collection of staphylococcal mutants. In the future we could deepen our understanding of the combat between *S. aureus* and the host autophagic response by using different staphylococcal mutants.

Reference

Amano, A., I. Nakagawa & T. Yoshimori, (2006) Autophagy in innate immunity against intracellular bacteria. *J Biochem* 140: 161-166.

Bae, T. & O. Schneewind, (2003) The YSIRK-G/S motif of staphylococcal protein A and its role in efficiency of signal peptide processing. *J Bacteriol* 185: 2910-2919.

Bae, T. & O. Schneewind, (2006) Allelic replacement in *Staphylococcus aureus* with inducible counter-selection. *Plasmid* 55: 58-63.

Becker, K., G. Bierbaum, C. von Eiff, S. Engelmann, F. Götz, J. Hacker, M. Hecker, G. Peters, R. Rosenstein & W. Ziebuhr, (2007) Understanding the physiology and adaptation of staphylococci: a post-genomic approach. *Int J Med Microbiol* 297: 483-501.

Begg, K. J. & W. D. Donachie, (1998) Division planes alternate in spherical cells of *Escherichia coli*. *J Bacteriol* 180: 2564-2567.

Bernhardt, T. G. & P. A. de Boer, (2005) SlmA, a nucleoid-associated, FtsZ binding protein required for blocking septal ring assembly over Chromosomes in *E. coli*. *Mol Cell* 18: 555-564.

Biller, S. J. & W. F. Burkholder, (2009) The *Bacillus subtilis* SftA (YtpS) and SpoIIIE DNA translocases play distinct roles in growing cells to ensure faithful chromosome partitioning. *Mol Microbiol* 74: 790-809.

Britton, R. A. & A. D. Grossman, (1999) Synthetic lethal phenotypes caused by mutations affecting chromosome partitioning in *Bacillus subtilis*. *J Bacteriol* 181: 5860-5864.

Britton, R. A., D. C. Lin & A. D. Grossman, (1998) Characterization of a prokaryotic SMC protein involved in chromosome partitioning. *Genes Dev* 12: 1254-1259.

Brötz, H., M. Josten, I. Wiedemann, U. Schneider, F. Götz, G. Bierbaum & H. G. Sahl, (1998) Role of lipid-bound peptidoglycan precursors in the formation of pores by nisin, epidermin and other lantibiotics. *Mol Microbiol* 30: 317-327.

Burton, B. M., K. A. Marquis, N. L. Sullivan, T. A. Rapoport & D. Z. Rudner, (2007) The ATPase SpoIIIE transports DNA across fused septal membranes during sporulation in *Bacillus subtilis*. *Cell* 131: 1301-1312.

Campo, N., H. Tjalsma, G. Buist, D. Stepniak, M. Meijer, M. Veenhuis, M. Westermann, J. P. Muller, S. Bron, J. Kok, O. P. Kuipers & J. D. Jongbloed, (2004) Subcellular sites for bacterial protein export. *Mol Microbiol* 53: 1583-1599.

Carlsson, F., M. Stalhammar-Carlemalm, K. Flardh, C. Sandin, E. Carlemalm & G. Lindahl, (2006) Signal sequence directs localized secretion of bacterial surface proteins. *Nature* 442: 943-946.

Chen, J. C., P. H. Viollier & L. Shapiro, (2005) A membrane metalloprotease participates in the sequential degradation of a *Caulobacter* polarity determinant. *Mol Microbiol* 55: 1085-1103.

Cho, H., H. R. McManus, S. L. Dove & T. G. Bernhardt, (2011) Nucleoid occlusion factor SlmA is a DNA-activated FtsZ polymerization antagonist. *Proc Natl Acad Sci U S A* 108: 3773-3778.

Cormack, B. P., R. H. Valdivia & S. Falkow, (1996) FACS-optimized mutants of the green fluorescent protein (GFP). *Gene* 173: 33-38.

Danilova, O., R. Reyes-Lamothe, M. Pinskaya, D. Sherratt & C. Possoz, (2007) MukB colocalizes with the oriC region and is required for organization of the two *Escherichia coli* chromosome arms into separate cell halves. *Mol Microbiol* 65: 1485-1492.

DeDent, A., T. Bae, D. M. Missiakas & O. Schneewind, (2008) Signal peptides direct surface proteins to two distinct envelope locations of *Staphylococcus aureus*. *EMBO J* 27: 2656-2668.

DeDent, A. C., M. McAdow & O. Schneewind, (2007) Distribution of protein A on the surface of *Staphylococcus aureus*. *J Bacteriol* 189: 4473-4484.

Demleitner, G. & F. Götz, (1994) Evidence for importance of the *Staphylococcus hyicus* lipase pro-peptide in lipase secretion, stability and activity. *FEMS Microbiol Lett* 121: 189-197.

Deretic, V. & B. Levine, (2009) Autophagy, immunity, and microbial adaptations. *Cell Host Microbe* 5: 527-549.

Dervyn, E., M. F. Noirot-Gros, P. Mervelet, S. McGovern, S. D. Ehrlich, P. Polard & P. Noirot, (2004) The bacterial condensin/cohesin-like protein complex acts in DNA repair and regulation of gene expression. *Mol Microbiol* 51: 1629-1640.

Dinh, T. & T. G. Bernhardt, (2011) Using superfolder green fluorescent protein for periplasmic protein localization studies. *J Bacteriol* 193: 4984-4987.

Draper, G. C. & J. W. Gober, (2002) Bacterial chromosome segregation. *Annu Rev Microbiol* 56: 567-597.

Dworkin, J. & R. Losick, (2002) Does RNA polymerase help drive chromosome segregation in bacteria? *Proc Natl Acad Sci U S A* 99: 14089-14094.

Errington, J., H. Murray & L. J. Wu, (2005) Diversity and redundancy in bacterial chromosome segregation mechanisms. *Philos Trans R Soc Lond B Biol Sci* 360: 497-505.

Fedtke, I., F. Götz & A. Peschel, (2004) Bacterial evasion of innate host defenses--the *Staphylococcus aureus* lesson. *Int J Med Microbiol* 294: 189-194.

Feilmeier, B. J., G. Iseminger, D. Schroeder, H. Webber & G. J. Phillips, (2000) Green fluorescent protein functions as a reporter for protein localization in *Escherichia coli*. *J Bacteriol* 182: 4068-4076.

Fleury, B., W. L. Kelley, D. Lew, F. Götz, R. A. Proctor & P. Vaudaux, (2009) Transcriptomic and metabolic responses of *Staphylococcus aureus* exposed to supra-physiological temperatures. *BMC Microbiol* 9: 76.

Foster, T. J., (2005) Immune evasion by staphylococci. *Nat Rev Microbiol* 3: 948-958.

Foster, T. J. & M. Höök, (1998) Surface protein adhesins of *Staphylococcus aureus*. *Trends Microbiol* 6: 484-488.

Frankel, M. B., B. M. Wojcik, A. C. DeDent, D. M. Missiakas & O. Schneewind, (2010) ABI domain-containing proteins contribute to surface protein display and cell division in *Staphylococcus aureus*. *Mol Microbiol* 78: 238-252.

Garzoni, C. & W. L. Kelley, (2009) *Staphylococcus aureus*: new evidence for intracellular persistence. *Trends Microbiol* 17: 59-65.

Giesbrecht, P., T. Kersten, H. Maidhof & J. Wecke, (1998) Staphylococcal cell wall: morphogenesis and fatal variations in the presence of penicillin. *Microbiol Mol Biol Rev* 62: 1371-1414.

Gitai, Z., (2005) The new bacterial cell biology: moving parts and subcellular architecture. *Cell* 120: 577-586.

Gitai, Z., N. A. Dye, A. Reisenauer, M. Wachi & L. Shapiro, (2005) MreB actin-mediated segregation of a specific region of a bacterial chromosome. *Cell* 120: 329-341.

Gold, V. A., A. Robson, H. Bao, T. Romantsov, F. Duong & I. Collinson, (2010) The action of cardiolipin on the bacterial translocon. *Proc Natl Acad Sci U S A* 107: 10044-10049.

Gordon, G. S., D. Sitnikov, C. D. Webb, A. Teleman, A. Straight, R. Losick, A. W. Murray & A. Wright, (1997) Chromosome and low copy plasmid segregation in *E. coli*: visual evidence for distinct mechanisms. *Cell* 90: 1113-1121.

Götz, F., (2004) Staphylococci in colonization and disease: prospective targets for drugs and vaccines. *Curr Opin Microbiol* 7: 477-487.

Götz, F., Bannerman, T., and Schleifer, K.H., (2006) The Genera *Staphylococcus* and *Macrococcus* In: The Procaryotes. M. Dworkin (ed). New York, NY: Springer, pp. 5-75.

Graumann, P. L., (2000) *Bacillus subtilis* SMC is required for proper arrangement of the chromosome and for efficient segregation of replication termini but not for bipolar movement of newly duplicated origin regions. *J Bacteriol* 182: 6463-6471.

Greenwood, D. & F. O'Grady, (1972) Scanning electron microscopy of *Staphyloccus aureus* exposed to some common anti-staphylococcal agents. *J Gen Microbiol* 70: 263-270.

Gruber, S. & J. Errington, (2009) Recruitment of condensin to replication origin regions by ParB/SpoOJ promotes chromosome segregation in *B. subtilis*. *Cell* 137: 685-696.

Hahn, J. J. & R. M. Cole, (1963) Streptococcal M Antigen Location and Synthesis, Studied by Immunofluorescence. *J Exp Med* 118: 659-666.

Hancock, I. C., G. Wiseman & J. Baddiley, (1976) Biosynthesis of the unit that links teichoic acid to the bacterial wall: inhibition by tunicamycin. *FEBS Lett* 69: 75-80.

Hayama, R. & K. J. Marians, (2010) Physical and functional interaction between the condensin MukB and the decatenase topoisomerase IV in *Escherichia coli*. *Proc Natl Acad Sci U S A* 107: 18826-18831.

Haydon, D. J., N. R. Stokes, R. Ure, G. Galbraith, J. M. Bennett, D. R. Brown, P. J. Baker, V. V. Barynin, D. W. Rice, S. E. Sedelnikova, J. R. Heal, J. M. Sheridan, S. T. Aiwale, P. K. Chauhan, A. Srivastava, A. Taneja, I. Collins, J. Errington & L. G. Czaplewski, (2008) An inhibitor of FtsZ with potent and selective anti-staphylococcal activity. *Science* 321: 1673-1675.

Herbert, S., A. Bera, C. Nerz, D. Kraus, A. Peschel, C. Goerke, M. Meehl, A. Cheung & F. Götz, (2007) Molecular basis of resistance to muramidase and cationic antimicrobial peptide activity of lysozyme in staphylococci. *PLoS Pathog* 3: e102.

Hirano, M. & T. Hirano, (2002) Hinge-mediated dimerization of SMC protein is essential for its dynamic interaction with DNA. *EMBO J* 21: 5733-5744.

Hirano, T., (2006) At the heart of the chromosome: SMC proteins in action. *Nat Rev Mol Cell Biol* 7: 311-322.

Hirschhausen, N., T. Schlesier, M. A. Schmidt, F. Gotz, G. Peters & C. Heilmann, (2010) A novel staphylococcal internalization mechanism involves the major autolysin Atl and heat shock cognate protein Hsc70 as host cell receptor. *Cell Microbiol* 12: 1746-1764.

Hu, P., Z. Bian, M. Fan, M. Huang & P. Zhang, (2008) Sec translocase and sortase A are colocalised in a locus in the cytoplasmic membrane of *Streptococcus mutans*. *Arch Oral Biol* 53: 150-154.

Hu, Z. & J. Lutkenhaus, (1999) Topological regulation of cell division in *Escherichia coli* involves rapid pole to pole oscillation of the division inhibitor MinC under the control of MinD and MinE. *Mol Microbiol* 34: 82-90.

Izaki, K., M. Matsuhashi & J. L. Strominger, (1966) Glycopeptide transpeptidase and D-alanine carboxypeptidase: penicillin-sensitive enzymatic reactions. *Proc Natl Acad Sci U S A* 55: 656-663.

Jacob F, B. S., Cuzin F., (1963) On the Regulation of DNA Replication in Bacteria. *Cold Spring Harbor Symp Quant Biol* 28: 329-348.

Jensen, R. B. & L. Shapiro, (1999) The *Caulobacter* crescentus smc gene is required for cell cycle progression and chromosome segregation. *Proc Natl Acad Sci U S A* 96: 10661-10666.

Jun, S. & A. Wright, (2010) Entropy as the driver of chromosome segregation. *Nat Rev Microbiol* 8: 600-607.

Kaimer, C., J. E. González-Pastor & P. L. Graumann, (2009) SpoIIIE and a novel type of DNA translocase, SftA, couple chromosome segregation with cell division in *Bacillus subtilis*. *Mol Microbiol* 74: 810-825.

Kariyama, R., (1982) Increase of cardiolipin content in *Staphylococcus aureus* by the use of antibiotics affecting the cell wall. *J Antibiot (Tokyo)* 35: 1700-1704.

Kawai, F., M. Shoda, R. Harashima, Y. Sadaie, H. Hara & K. Matsumoto, (2004) Cardiolipin domains in *Bacillus subtilis* marburg membranes. *J Bacteriol* 186: 1475-1483.

Kellner, R., G. Jung, T. Hörner, H. Zähner, N. Schnell, K. D. Entian & F. Götz, (1988) Gallidermin: a new lanthionine-containing polypeptide antibiotic. *Eur J Biochem* 177: 53-59.

Kline, K. A., A. L. Kau, S. L. Chen, A. Lim, J. S. Pinkner, J. Rosch, S. R. Nallapareddy, B. E. Murray, B. Henriques-Normark, W. Beatty, M. G. Caparon & S. J. Hultgren, (2009) Mechanism for sortase localization and the role of sortase localization in efficient pilus assembly in Enterococcus faecalis. *J Bacteriol* 191: 3237-3247.

Koyama, T., M. Yamada & M. Matsuhashi, (1977) Formation of regular packets of *Staphylococcus aureus* cells. *J Bacteriol* 129: 1518-1523.

Kruse, T., B. Blagoev, A. Lobner-Olesen, M. Wachi, K. Sasaki, N. Iwai, M. Mann & K. Gerdes, (2006) Actin homolog MreB and RNA polymerase interact and are both required for chromosome segregation in *Escherichia coli*. *Genes Dev* 20: 113-124.

Kubitschek, H. E., (1990) Cell volume increase in *Escherichia coli* after shifts to richer media. *J Bacteriol* 172: 94-101.

Kuroda, M., T. Ohta, I. Uchiyama, T. Baba, H. Yuzawa, I. Kobayashi, L. Cui, A. Oguchi, K. Aoki, Y. Nagai, J. Lian, T. Ito, M. Kanamori, H. Matsumaru, A. Maruyama, H. Murakami, A. Hosoyama, Y. Mizutani-Ui, N. K. Takahashi, T. Sawano, R. Inoue, C. Kaito, K. Sekimizu, H. Hirakawa, S. Kuhara, S. Goto, J. Yabuzaki, M. Kanehisa, A. Yamashita, K. Oshima, K. Furuya, C. Yoshino, T. Shiba, M. Hattori, N. Ogasawara, H. Hayashi & K. Hiramatsu, (2001) Whole genome sequencing of meticillin-resistant *Staphylococcus aureus*. *Lancet* 357: 1225-1240.

Lambert, M. P. & F. C. Neuhaus, (1972) Mechanism of D-cycloserine action: alanine racemase from *Escherichia coli* W. *J Bacteriol* 110: 978-987.

Lau, I. F., S. R. Filipe, B. Soballe, O. A. Okstad, F. X. Barre & D. J. Sherratt, (2003) Spatial and temporal organization of replicating *Escherichia coli* chromosomes. *Mol Microbiol* 49: 731-743.

Leibig, M., B. Krismer, M. Kolb, A. Friede, F. Götz & R. Bertram, (2008) Marker removal in staphylococci via Cre recombinase and different lox sites. *Appl Environ Microbiol* 74: 1316-1323.

Lemon, K. P. & A. D. Grossman, (2001) The extrusion-capture model for chromosome partitioning in bacteria. *Genes Dev* 15: 2031-2041.

Lenarcic, R., S. Halbedel, L. Visser, M. Shaw, L. J. Wu, J. Errington, D. Marenduzzo & L. W. Hamoen, (2009) Localisation of DivIVA by targeting to negatively curved membranes. *EMBO J* 28: 2272-2282.

Lewenza, S., D. Vidal-Ingigliardi & A. P. Pugsley, (2006) Direct visualization of red fluorescent lipoproteins indicates conservation of the membrane sorting rules in the family *Enterobacteriaceae*. *J Bacteriol* 188: 3516-3524.

Li, Y., N. K. Stewart, A. J. Berger, S. Vos, A. J. Schoeffler, J. M. Berger, B. T. Chait & M. G. Oakley, (2010) *Escherichia coli* condensin MukB stimulates topoisomerase IV activity by a direct physical interaction. *Proc Natl Acad Sci U S A* 107: 18832-18837.

Liew, P. X., C. L. Wang & S. L. Wong, (2012) Functional characterization and localization of a *Bacillus subtilis* sortase and its substrate and use of this sortase system to covalently anchor a heterologous protein to the *B. subtilis* cell wall for surface display. *J Bacteriol* 194: 161-175.

Lindow, J. C., R. A. Britton & A. D. Grossman, (2002) Structural maintenance of chromosomes protein of *Bacillus subtilis* affects supercoiling in vivo. *J Bacteriol* 184: 5317-5322.

Lorian, V., (1975) Some effect of subinbilitory concentrations of penicillin on the structure and division of staphylococci. *Antimicrob Agents Chemother* 7: 864-867.

Lorian, V. & B. Atkinson, (1976) Effects of subinhibitory concentrations of antibiotics on cross walls of cocci. *Antimicrob Agents Chemother* 9: 1043-1055.
Margolin, W., (2000) Green fluorescent protein as a reporter for macromolecular localization in bacterial cells. *Methods* 20: 62-72.
Marraffini, L. A., A. C. Dedent & O. Schneewind, (2006) Sortases and the art of anchoring proteins to the envelopes of gram-positive bacteria. *Microbiol Mol Biol Rev* 70: 192-221.
Marston, A. L. & J. Errington, (1999) Selection of the midcell division site in *Bacillus subtilis* through MinD-dependent polar localization and activation of MinC. *Mol Microbiol* 33: 84-96.
Marston, A. L., H. B. Thomaides, D. H. Edwards, M. E. Sharpe & J. Errington, (1998) Polar localization of the MinD protein of *Bacillus subtilis* and its role in selection of the mid-cell division site. *Genes Dev* 12: 3419-3430.
Mascarenhas, J., J. Soppa, A. V. Strunnikov & P. L. Graumann, (2002) Cell cycle-dependent localization of two novel prokaryotic chromosome segregation and condensation proteins in *Bacillus subtilis* that interact with SMC protein. *EMBO J* 21: 3108-3118.
Mazmanian, S. K., G. Liu, H. Ton-That & O. Schneewind, (1999) *Staphylococcus aureus* sortase, an enzyme that anchors surface proteins to the cell wall. *Science* 285: 760-763.
Mileykovskaya, E. & W. Dowhan, (2000) Visualization of phospholipid domains in *Escherichia coli* by using the cardiolipin-specific fluorescent dye 10-N-nonyl acridine orange. *J Bacteriol* 182: 1172-1175.
Mileykovskaya, E., W. Dowhan, R. L. Birke, D. Zheng, L. Lutterodt & T. H. Haines, (2001) Cardiolipin binds nonyl acridine orange by aggregating the dye at exposed hydrophobic domains on bilayer surfaces. *FEBS Lett* 507: 187-190.
Mohl, D. A. & J. W. Gober, (1997) Cell cycle-dependent polar localization of chromosome partitioning proteins in *Caulobacter crescentus*. *Cell* 88: 675-684.
Moriya, S., E. Tsujikawa, A. K. Hassan, K. Asai, T. Kodama & N. Ogasawara, (1998) A *Bacillus subtilis* gene-encoding protein homologous to eukaryotic SMC motor protein is necessary for chromosome partition. *Mol Microbiol* 29: 179-187.
Müller-Anstett, M. A., P. Müller, T. Albrecht, M. Nega, J. Wagener, Q. Gao, S. Kaesler, M. Schaller, T. Biedermann & F. Götz, (2010) Staphylococcal peptidoglycan co-localizes with Nod2 and TLR2 and activates innate immune response via both receptors in primary murine keratinocytes. *PLoS One* 5: e13153.
Nielsen, H. J., Y. Li, B. Youngren, F. G. Hansen & S. Austin, (2006a) Progressive segregation of the *Escherichia coli* chromosome. *Mol Microbiol* 61: 383-393.
Nielsen, H. J., J. R. Ottesen, B. Youngren, S. J. Austin & F. G. Hansen, (2006b) The *Escherichia coli* chromosome is organized with the left and right chromosome arms in separate cell halves. *Mol Microbiol* 62: 331-338.
Niki, H., A. Jaffe, R. Imamura, T. Ogura & S. Hiraga, (1991) The new gene mukB codes for a 177 kd protein with coiled-coil domains involved in chromosome partitioning of *E. coli*. *EMBO J* 10: 183-193.
Pedelacq, J. D., S. Cabantous, T. Tran, T. C. Terwilliger & G. S. Waldo, (2006) Engineering and characterization of a superfolder green fluorescent protein. *Nat Biotechnol* 24: 79-88.
Perry, A. M., H. Ton-That, S. K. Mazmanian & O. Schneewind, (2002) Anchoring of surface proteins to the cell wall of *Staphylococcus aureus*. III. Lipid II is an in vivo peptidoglycan substrate for sortase-catalyzed surface protein anchoring. *J Biol Chem* 277: 16241-16248.
Peschel, A., B. Ottenwalder & F. Gotz, (1996) Inducible production and cellular location of the epidermin biosynthetic enzyme EpiB using an improved staphylococcal expression system. *FEMS Microbiol Lett* 137: 279-284.

Petrushenko, Z. M., Y. Cui, W. She & V. V. Rybenkov, (2010) Mechanics of DNA bridging by bacterial condensin MukBEF in vitro and in singulo. *EMBO J* 29: 1126-1135.
Petrushenko, Z. M., C. H. Lai & V. V. Rybenkov, (2006) Antagonistic interactions of kleisins and DNA with bacterial Condensin MukB. *J Biol Chem* 281: 34208-34217.
Petrushenko, Z. M., W. She & V. V. Rybenkov, (2011) A new family of bacterial condensins. *Mol Microbiol* 81: 881-896.
Pilavtepe-Çelik, M., M. O. Balaban, H. Alpas & A. E. Yousef, (2008) Image analysis based quantification of bacterial volume change with high hydrostatic pressure. *J Food Sci* 73: M423-429.
Pinho, M. G. & J. Errington, (2004) A divIVA null mutant of *Staphylococcus aureus* undergoes normal cell division. *FEMS Microbiol Lett* 240: 145-149.
Pooley, H. M. & D. Karamata, (2000) Incorporation of [2-3H]glycerol into cell surface components of *Bacillus subtilis* 168 and thermosensitive mutants affected in wall teichoic acid synthesis: effect of tunicamycin. *Microbiology* 146 (Pt 4): 797-805.
Previc, E. P., (1970) Biochemical determination of bacterial morphology and the geometry of cell division. *J Theor Biol* 27: 471-497.
Proctor, R. A., C. von Eiff, B. C. Kahl, K. Becker, P. McNamara, M. Herrmann & G. Peters, (2006) Small colony variants: a pathogenic form of bacteria that facilitates persistent and recurrent infections. *Nat Rev Microbiol* 4: 295-305.
Proikas-Cezanne, T., S. Ruckerbauer, Y. D. Stierhof, C. Berg & A. Nordheim, (2007) Human WIPI-1 puncta-formation: a novel assay to assess mammalian autophagy. *FEBS Lett* 581: 3396-3404.
Ptacin, J. L., S. F. Lee, E. C. Garner, E. Toro, M. Eckart, L. R. Comolli, W. E. Moerner & L. Shapiro, (2010) A spindle-like apparatus guides bacterial chromosome segregation. *Nat Cell Biol* 12: 791-798.
Ramamurthi, K. S. & R. Losick, (2009) Negative membrane curvature as a cue for subcellular localization of a bacterial protein. *Proc Natl Acad Sci U S A* 106: 13541-13545.
Raskin, D. M. & P. A. de Boer, (1999) MinDE-dependent pole-to-pole oscillation of division inhibitor MinC in *Escherichia coli*. *J Bacteriol* 181: 6419-6424.
Raz, A. & V. A. Fischetti, (2008) Sortase A localizes to distinct foci on the *Streptococcus pyogenes* membrane. *Proc Natl Acad Sci U S A* 105: 18549-18554.
Rosch, J. W., F. F. Hsu & M. G. Caparon, (2007) Anionic lipids enriched at the ExPortal of *Streptococcus pyogenes*. *J Bacteriol* 189: 801-806.
Rosenstein, R. & F. Götz, (2000) Staphylococcal lipases: biochemical and molecular characterization. *Biochimie* 82: 1005-1014.
Schnaith, A., H. Kashkar, S. A. Leggio, K. Addicks, M. Kronke & O. Krut, (2007) *Staphylococcus aureus* subvert autophagy for induction of caspase-independent host cell death. *J Biol Chem* 282: 2695-2706.
Schneewind, O., P. Model & V. A. Fischetti, (1992) Sorting of protein A to the staphylococcal cell wall. *Cell* 70: 267-281.
Schwarz-Linek, U., M. Hook & J. R. Potts, (2004) The molecular basis of fibronectin-mediated bacterial adherence to host cells. *Mol Microbiol* 52: 631-641.
Shaner, N. C., R. E. Campbell, P. A. Steinbach, B. N. Giepmans, A. E. Palmer & R. Y. Tsien, (2004) Improved monomeric red, orange and yellow fluorescent proteins derived from *Discosoma* sp. red fluorescent protein. *Nat Biotechnol* 22: 1567-1572.
Sharpe, M. E. & J. Errington, (1995) Postseptational chromosome partitioning in bacteria. *Proc Natl Acad Sci U S A* 92: 8630-8634.
She, W., Q. Wang, E. A. Mordukhova & V. V. Rybenkov, (2007) MukEF Is required for stable association of MukB with the chromosome. *J Bacteriol* 189: 7062-7068.
Sinha, B., P. P. Francois, O. Nusse, M. Foti, O. M. Hartford, P. Vaudaux, T. J. Foster, D. P. Lew, M. Herrmann & K. H. Krause, (1999) Fibronectin-binding protein acts as

Staphylococcus aureus invasin via fibronectin bridging to integrin alpha5beta1. *Cell Microbiol* 1: 101-117.

Sinha, B. & M. Fraunholz, (2010) *Staphylococcus aureus* host cell invasion and post-invasion events. *Int J Med Microbiol* 300: 170-175.

Soppa, J., K. Kobayashi, M. F. Noirot-Gros, D. Oesterhelt, S. D. Ehrlich, E. Dervyn, N. Ogasawara & S. Moriya, (2002) Discovery of two novel families of proteins that are proposed to interact with prokaryotic SMC proteins, and characterization of the *Bacillus subtilis* family members ScpA and ScpB. *Mol Microbiol* 45: 59-71.

Soufo, H. J. & P. L. Graumann, (2003) Actin-like proteins MreB and Mbl from *Bacillus subtilis* are required for bipolar positioning of replication origins. *Curr Biol* 13: 1916-1920.

Strauss, A. & F. Götz, (1996) In vivo immobilization of enzymatically active polypeptides on the cell surface of *Staphylococcus carnosus*. *Mol Microbiol* 21: 491-500.

Sturmfels, A., F. Götz & A. Peschel, (2001) Secretion of human growth hormone by the food-grade bacterium *Staphylococcus carnosus* requires a propeptide irrespective of the signal peptide used. *Arch Microbiol* 175: 295-300.

Sullivan, N. L., K. A. Marquis & D. Z. Rudner, (2009) Recruitment of SMC by ParB-parS organizes the origin region and promotes efficient chromosome segregation. *Cell* 137: 697-707.

Surtees, J. A. & B. E. Funnell, (2003) Plasmid and chromosome traffic control: how ParA and ParB drive partition. *Curr Top Dev Biol* 56: 145-180.

Tadesse, S., J. Mascarenhas, B. Kosters, A. Hasilik & P. L. Graumann, (2005) Genetic interaction of the SMC complex with topoisomerase IV in *Bacillus subtilis*. *Microbiology* 151: 3729-3737.

Tavares, J. R., R. F. de Souza, G. L. Meira & F. J. Gueiros-Filho, (2008) Cytological characterization of YpsB, a novel component of the *Bacillus subtilis* divisome. *J Bacteriol* 190: 7096-7107.

Teleman, A. A., P. L. Graumann, D. C. Lin, A. D. Grossman & R. Losick, (1998) Chromosome arrangement within a bacterium. *Curr Biol* 8: 1102-1109.

Thanbichler, M., (2009) Closing the ring: a new twist to bacterial chromosome condensation. *Cell* 137: 598-600.

Ton-That, H. & O. Schneewind, (1999) Anchor structure of staphylococcal surface proteins. IV. Inhibitors of the cell wall sorting reaction. *J Biol Chem* 274: 24316-24320.

Toro, E. & L. Shapiro, (2010) Bacterial chromosome organization and segregation. *Cold Spring Harb Perspect Biol* 2: a000349.

Trevors, J. T., (1996) Genome size in bacteria. *Antonie Van Leeuwenhoek* 69: 293-303.

Tsui, H. C., S. K. Keen, L. T. Sham, K. J. Wayne & M. E. Winkler, (2011) Dynamic distribution of the SecA and SecY translocase subunits and septal localization of the HtrA surface chaperone/protease during *Streptococcus pneumoniae* D39 cell division. *MBio* 2.

Tzagoloff, H. & R. Novick, (1977) Geometry of cell division in *Staphylococcus aureus*. *J Bacteriol* 129: 343-350.

van Heijenoort, Y., M. Leduc, H. Singer & J. van Heijenoort, (1987) Effects of moenomycin on *Escherichia coli*. *J Gen Microbiol* 133: 667-674.

Veiga, H., A. M. Jorge & M. G. Pinho, (2011) Absence of nucleoid occlusion effector Noc impairs formation of orthogonal FtsZ rings during *Staphylococcus aureus* cell division. *Mol Microbiol* 80: 1366-1380.

Viollier, P. H., M. Thanbichler, P. T. McGrath, L. West, M. Meewan, H. H. McAdams & L. Shapiro, (2004) Rapid and sequential movement of individual chromosomal loci to specific subcellular locations during bacterial DNA replication. *Proc Natl Acad Sci U S A* 101: 9257-9262.

Volkov, A., J. Mascarenhas, C. Andrei-Selmer, H. D. Ulrich & P. L. Graumann, (2003) A prokaryotic condensin/cohesin-like complex can actively compact chromosomes from a single position on the nucleoid and binds to DNA as a ring-like structure. *Mol Cell Biol* 23: 5638-5650.

Wang, X., X. Liu, C. Possoz & D. J. Sherratt, (2006) The two *Escherichia coli* chromosome arms locate to separate cell halves. *Genes Dev* 20: 1727-1731.

Webb, C. D., A. Teleman, S. Gordon, A. Straight, A. Belmont, D. C. Lin, A. D. Grossman, A. Wright & R. Losick, (1997) Bipolar localization of the replication origin regions of chromosomes in vegetative and sporulating cells of *B. subtilis*. *Cell* 88: 667-674.

Wieland, K. P., B. Wieland & F. Götz, (1995) A promoter-screening plasmid and xylose-inducible, glucose-repressible expression vectors for *Staphylococcus carnosus*. *Gene* 158: 91-96.

Woldringh, C. L., (2002) The role of co-transcriptional translation and protein translocation (transertion) in bacterial chromosome segregation. *Mol Microbiol* 45: 17-29.

Wu, L. J. & J. Errington, (1994) *Bacillus subtilis* SpoIIIE protein required for DNA segregation during asymmetric cell division. *Science* 264: 572-575.

Wu, L. J. & J. Errington, (2004) Coordination of cell division and chromosome segregation by a nucleoid occlusion protein in *Bacillus subtilis*. *Cell* 117: 915-925.

Wu, L. J. & J. Errington, (2011) Nucleoid occlusion and bacterial cell division. *Nat Rev Microbiol* 10: 8-12.

Yu, X. C., E. K. Weihe & W. Margolin, (1998) Role of the C terminus of FtsK in *Escherichia coli* chromosome segregation. *J Bacteriol* 180: 6424-6428.

Zapun, A., T. Vernet & M. G. Pinho, (2008) The different shapes of cocci. *FEMS Microbiol Rev* 32: 345-360.

Curriculum Vitae

Personal Information

Name: Wenqi Yu

Date of Birth: 12/09/1980

Place of Birth: Shanghai, P. R. China

Education

05/2007-12/2011	PhD study, Supervisor Prof. Dr. Friedrich Götz, Dept. Microbial Genetics, University of Tübingen, Germany
09/2004-04/2007	Graduate Study, Supervisor Prof. Dr. Di Qu, Key Laboratory of Medical Molecular Virology, Ministry of Education and Ministry of Public Health; Institute of Medical Microbiology and Institute of Biomedical Sciences, Fudan University, China Project: "Biochemical characterization and inhibitors screening of peptide deformylase of *Staphylococcus epidermidis* "
09/1999-07/2004	Bachelor, Shanghai Medical College of Fudan University, China Major subject: Clinical Medicine Minor subject: Public Health Administration Honor of "First-Class Student" and "Excellent Bachelor Thesis" of Fudan University (Thesis title: 'Investigation and evaluation of different procedures in diagnosing *Mycobacterium tuberculosis* infection')
09/1996-07/1999	Shanghai Anshan High School (No. 1 High School Affiliated to Tongji University), Shanghai, China
09/1995-07/1996	Shanghai Huimin Middle School, Shanghai, China
09/1993-07/1995	Wu Xi Chang'an Middle School, Jiangsu Province, China
09/1987-07/1993	Wu Xi Chang'an Primary School, Jiangsu Province, China

Acknowledgements

In the end, I am closing this thesis with my deep gratitude to all of the people who have helped me, encouraged me and supported me during the last years. I thank my former supervisor Prof. Dr. Di Qu in Fudan University, who has enlightened me and opened the door for a scientific pursuit in microbiology for me. I owe my great appreciation to my supervisor Prof. Dr. Friedrich Götz, who has offered me the opportunity and freedom to approach the scientific topics that I am interested in. His wealth of knowledge and profound expertise provide me with a solid platform and guidance to conduct staphylococcal research. I thank Tobias Knust, Dr. Joel Defeu Soufo and Prof. Dr. Peter Graumann in Freiburg University. It was only with their great help and valuable suggestions that I could finish the first part of the thesis. I thank Josef Lehner, Maximilian Schlebusch, Dr. Iris Maldener and Prof. Dr. Karl Forchhammer. It would be impossible for me to finish the thesis without their expertise and technical assistance in microscopy. I am also very grateful for our fruitful cooperation with Mario Mauthe and Dr. Tassula Proikas-Cezanne.

No stranger to the frustration and disappointment inherent in the research work, I am very grateful that I have a stimulating and collaborative scientific environment in our lab. Martin Schlag, Till Albrecht, Ya-Yun Chu, Xiangyan Li, Rosmarie Gaupp, Mulugeta Nega, Julia Buschman, Ute Bertsche, Ralph Bertram, Linda Dube, Martina Leibig, Ralf Rosenstein, Silvia Herbert, Anne-Kathrin Ziebandt, Patrick Müller, Maria Müller-Anstett, Ursula Theurer, Regine Stemmler, Vera Augsburger, Lalitha Biswas, Raja Biswas, Jongkon Saising, Minh Thu Nguyen, Dogan Doruk Demircioglu, Daniel Kühner, Tobias Roth, Silvana Perconti, Maja Urbanczyk, Julia Deibert, Felix Weihs, Peter Popella... I am indebted to all of my lovely colleagues who are always ready to help me whenever I need help.

Last but not least, many thanks to my dearest parents and friends. Their endless encouragement and constant support enabled me to be strong and brave to confront every obstacle that I have ever encountered.

Appendix: Publications from the current thesis

JOURNAL OF BACTERIOLOGY, Aug. 2010, p. 4067–4073 Vol. 192, No. 15
0021-9193/10/$12.00 doi:10.1128/JB.00010-10

Contribution of SMC (Structural Maintenance of Chromosomes) and SpoIIIE to Chromosome Segregation in Staphylococci[▽]

Wenqi Yu,[1] Silvia Herbert,[1] Peter L. Graumann,[2] and Friedrich Götz[1]*

Microbial Genetics, University of Tübingen, Auf der Morgenstelle 28E, D-72076 Tübingen, Germany,[1] and Mikrobiologie, Fachbereich für Biologie, Universität Freiburg, Schänzle Straße 1, 79104 Freiburg, Germany[2]

Received 5 January 2010/Accepted 17 May 2010

In contrast to rod-shaped bacteria, little is known about chromosomal maintenance and segregation in the spherical *Staphylococcus aureus*. The analysis of chromosomal segregation in *smc* (structural maintenance of chromosomes) and *spoIIIE* single and double mutants unravels differences in the chromosome dynamics in the spherical staphylococcal cells compared to the model in rods.

In bacteria, studies on chromosome dynamics are mainly focused on model organisms such as *Escherichia coli*, *Bacillus subtilis*, and *Caulobacter crescentus* (8, 28). However, in staphylococci, with their spherical cell shape and their special consecutive perpendicular mode of division (34), little is known about chromosome organization and dynamics so far. Moreover, the important status of *Staphylococcus aureus* as one of the most prominent human pathogens highlights the significance of studying essential cellular processes that could serve as a basis for antibiotic target development (11, 15).

SMC (*s*tructure *m*aintenance of *c*hromosomes) protein is one of the crucial factors involved in various aspects of chromosome dynamics, such as chromosome condensation, packaging, partitioning, and DNA repair (4, 6, 13, 22, 24, 30). *B. subtilis* SMC and its homolog, MukB, in *E. coli* are composed of two head regions at N and C termini, setting up an ATPase domain separated by two heptad-rich regions forming a single internal long coiled coil that are connected by a flexible hinge domain in the middle. Homodimerized SMC proteins linked by the hinge domain (17) form a complex with ScpA and ScpB (*s*egregation and *c*ondensation *p*roteins A and B) (23), while MukB interacts with MukF and MukE in *E. coli* correspondingly (27). The *B. subtilis smc* mutant shows a severe temperature-sensitive lethal phenotype with irregular chromosome organization and chromosome segregation defects (4, 24). It was proposed that the pleiotropic phenotype of the *smc* mutant was primarily due to its function in chromosome condensation (4). Interestingly, a recent report described that the mycobacterial *smc* deletion mutant was still proficient in DNA repair and long-term survival (14).

The involvement of SpoIIIE in chromosome segregation was first identified during sporulation in *B. subtilis* (32). It is required for active translocation of the bulk chromosome into the forespore across the fused septal membranes (5). SpoIIIE consists of an N-terminal transmembrane domain responsible for membrane anchoring and the C-terminal ATPase and DNA translocation domain. The function of SpoIIIE in postseptational chromosome partitioning renders it as a backup mechanism to rescue the nucleoids that have been trapped by the division septum when chromosome segregation was perturbed in vegetative cells (26). Consequently, the *smc* and *spoIIIE* double mutant had a synergistic lethal phenotype in *B. subtilis* (3). The combination of the *E. coli mukB* null mutation and truncation of *ftsK* encoding the homolog protein to SpoIIIE resulted in a similar synergistic lethal phenotype (33).

Genome analysis revealed that there was a single *smc* gene locus present in all of the staphylococcal genomes available so far. *S. aureus smc* (SAOUHSC_01204) encodes a 1,188-amino-acid polypeptide with a calculated molecular mass of 136.7 kDa that shares 42.8% similarity with *B. subtilis* SMC and consists of the typical domain structures of the SMC protein family analyzed by ClustalW2 alignment and SMART (Simple Modular Architecture Research Tool). During our previous work, a transposon Tn*917* mutagenesis library was constructed in an *S. aureus* double-knockout strain (DKO1) in which two genes encoding "lipopolysaccharide modification acyltransferase" and "acyltransferase" were deleted (16). One insertion mutant (DKO1.6) was identified that carried Tn*917* at nucleotides 1078 to 1087 within the *smc* gene. In order to study the function of SMC involved in chromosome organization and segregation, *smc*::Tn*917* was phage transduced into wild-type (WT) *S. aureus* strain SA113, generating a single *smc*::Tn*917* mutant (Fig. 1A). Phage transductions were performed at 23°C to decrease the probability of suppressor mutations. Isolated mutants were confirmed by sequencing. Surprisingly, SA113 *smc*::Tn*917* showed similar growth behavior to WT cells both on tryptic soy agar (TSA) plates and in tryptic soy broth (TSB) liquid medium at all three temperatures (30°C, 37°C, and 42°C) tested (Fig. 2A and B). These observations were in contrast to the previous findings in *B. subtilis.* The *B. subtilis* Δ*smc* mutant was temperature sensitive, the mutation was lethal in rich medium, and the mutant could only grow at 23°C in this medium (4, 24).

Next, we sought to verify if the loss of functional SMC would affect chromosome segregation in *S. aureus*. Samples were taken from exponentially growing cultures at three temperatures for fluorescent microscopy examination (Leica DM5500B). DNA was stained with DAPI (4′,6-diamidino-2-phenylindole), the cell membrane was labeled with FM1-43,

* Corresponding author. Mailing address: Mikrobielle Genetik, Universität Tübingen, Auf der Morgenstelle 28E, D-72076 Tübingen, Germany. Phone: (49) 7071-2974636. Fax: (49) 7071-295039. E-mail: friedrich.goetz@uni-tuebingen.de.

▽ Published ahead of print on 4 June 2010.

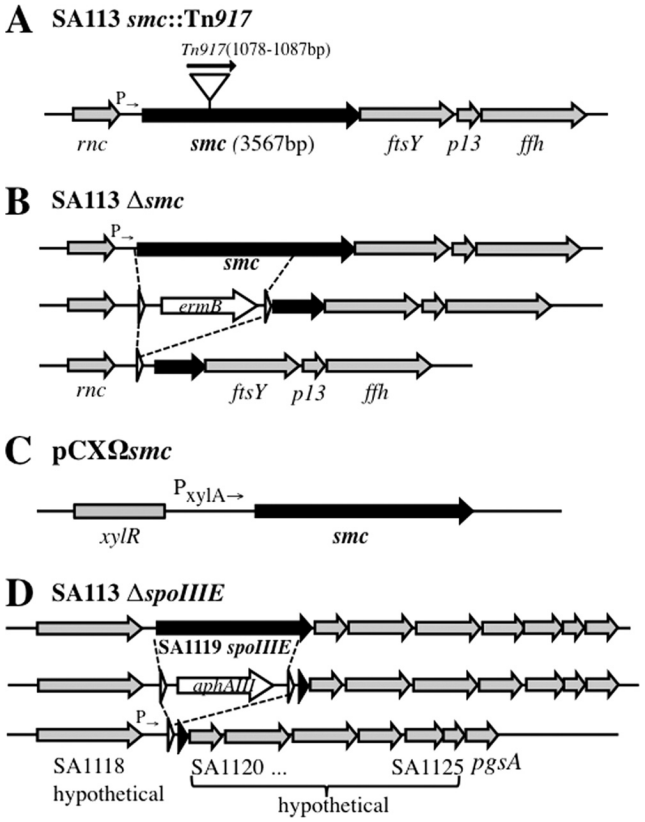

FIG. 1. (A) Tn*917* insertion site in SA113 *smc*::Tn*917*. (B) Construction of SA113 Δ*smc*. The *smc* coding sequence, except for 1,294 bp at the 3′ end, was replaced by *ermB* cassette flanked with *lox* sites that was further removed by Cre recombinase. (C) Scheme of pCXΩ*smc*. The *smc* gene was cloned into pCX15 (31), under the transcriptional control of the xylose promoter/operator system. (D) Construction of SA113 Δ*spoIIIE*. The *spoIIIE* coding sequence, except for 68 bp at the 3′ end, was replaced by an *aphAIII* cassette flanked with *lox* sites and further removed by Cre recombinase; white arrowheads represent *lox* sites.

and the cell wall was labeled with BODIPY (boron-dipyrromethene)-vancomycin (Van-FL) to visualize different cellular structures. While in the rod-shaped cells of *E. coli* and *B. subtilis*, the chromosome seems to occupy approximately three-fourths of the cell volume (4, 24), in *S. aureus* the chromosome almost fills the entire cell compartment, as demonstrated by DAPI staining (Fig. 3A). In SA113 *smc*::Tn*917*, about 10% of the cells were devoid of nucleoids; they appeared as anucleate cells ("black cells" stained with DAPI) that indicated defects in chromosome segregation (Fig. 3B). The anucleate cells were also observed in SA113-DKO1.6 that carried *smc*::Tn*917* but not in SA113-DKO1, confirming that the chromosome segregation defect was due to the mutation in the *smc* gene. In SA113 *smc*::Tn*917*, "half-black cells" were observed (2% of 911 cells counted at 30°C) which were composed of one anucleate hemisphere and one normal hemisphere with regular chromosome content and morphology (Fig. 3B, arrow). We assume that this kind of "half-black cell" would be able to further divide into one anucleate daughter cell and one normal daughter cell as the cross wall could correctly form in the middle of the cell (Fig. 3B; staining with Van-FL [green]) and single spherical anucleate cells were observed frequently (Table 1). Furthermore, anucleate diplococci (Fig. 4B, yellow arrow) were observed, although at a low rate of 0.12% (2 pairs of black diplococci out of 1,634 cells counted). It is yet difficult to distinguish whether these anucleate diplococci were divided from one anucleate cell or were divided from two "half-black cells" and afterwards detached from tetrads composing two normal cells and these two anucleate cells. Intriguingly, quantitative analysis revealed that the percentage of anucleate cells decreased by 3-fold at 42°C in the *smc*::Tn*917* strain (Table 1), suggesting that the defect of chromosome segregation caused by SMC mutation could be relieved by higher growth rate, probably due to the accelerated

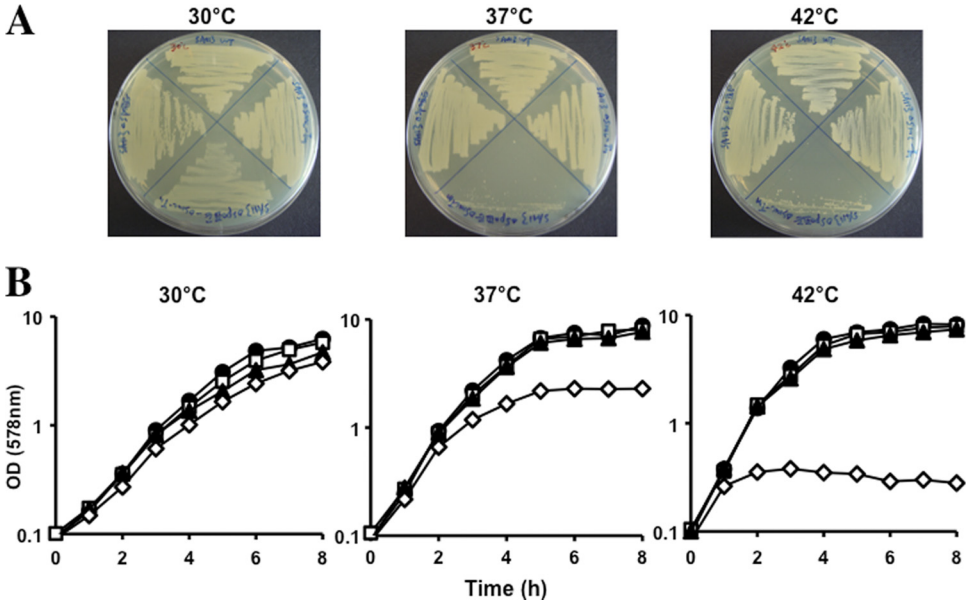

FIG. 2. (A) Growth comparison of the SA113 WT (top) and *smc*::Tn*917* (right), Δ*spoIIIE* (left), and *smc*::Tn*917* Δ*spoIIIE* (bottom) mutants on TSB agar plates at 30°C, 37°C, and 42°C for 24 h. (B) Growth in TSB rich medium. ●, WT; □, *smc*::Tn*917* mutant; □, Δ*spoIIIE* mutant; ◇, *smc*::Tn*917* Δ*spoIIIE* mutant.

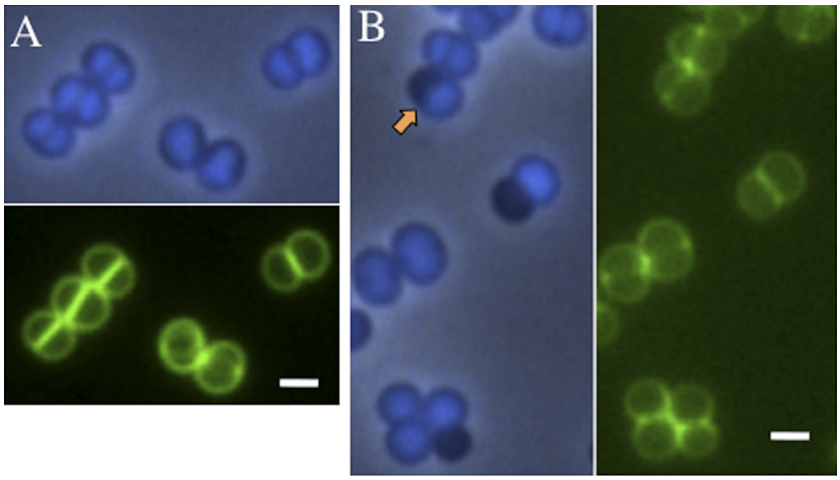

FIG. 3. Chromosome distribution in the SA113 WT and SA113 *smc*::*Tn917* mutant from mid-log-phase TSB cultures at 30°C. (A) SA113 WT. Newly formed equatorial rings could be visualized in two tilted cells. (B) SA113 *smc*::Tn*917*. The orange arrow indicates the "half-black cell." The cell wall was stained with Van-FL (green), and the chromosome was stained with DAPI (blue) and visualized in the phase-contrast–fluorescent merging mode. Scale bar, 1 μm.

chromosome replication which was assumed to be one of the driving forces for chromosome segregation (7). Notably, no other aberrant chromosome distribution or abnormal cell shape could be found in *S. aureus smc*::Tn*917* mutants, except for the anucleate cells (Table 1). Thus, SMC's function as condensin appeared to be less critical in *S. aureus* in contrast to *B. subtilis* SMC or *E. coli* MukB. Furthermore, the chromosome segregation defect in the *S. aureus smc*::Tn*917* strain could be partially complemented by plasmid-encoded SMC, which is controlled by xylose inducible promoter (pCXΩ*smc*) (31) (Fig. 1C and Table 1).

In the genome of *S. aureus*, *smc* is located directly upstream of *ftsY*, *p13*, and *ffh*, the genes encoding components of the signal recognition particle protein translocation system. In order to rule out the possible polar effect of Tn*917* on the downstream genes' expression, a markerless partial deletion *smc* mutant was constructed (Fig. 1B). A 1.3-kb fragment of *smc* gene at its 3′ was left intact due to the consideration that it

TABLE 1. Quantitive analysis of irregular chromosome appearance from mid-log-phase culture[a]

Temp and strain genotype	Total no. of cells counted	% of cells:				
		Anucleate	With "CUT" phenotype	With uneven chromosome distribution	With increased/decreased DNA content	Big/small[b]
30°C						
WT	911	0.3	NO[c]	NO	0.2/NO	NO
Δ*smc*	1,258	9.4	NO	0.3	0.3/NO	NO
smc::Tn*917*	881	10.4	NO	0.3	0.3/NO	NO
smc::Tn*917* pCXΩ*smc*	1,316	2.3	NO	0.5	0.3/NO	0.1/NO
Δ*spoIIIE*	975	0.7	NO	0.4	0.5/NO	NO/0.1
smc::Tn*917* Δ*spoIIIE*	802	4.8	1.9	10.7	3.2/6.1	1.6/4.5
37°C						
WT	1,023	0.3	NO	0.7	0.6/NO	NO
Δ*smc*	1,144	7.9	NO	0.7	0.5/NO	NO/0.3
smc::Tn*917*	851	7.2	NO	0.8	0.7/0.2	NO/0.2
smc::Tn*917* pCXΩ*smc*	1,216	1.8	NO	0.7	0.7/0.3	NO/0.3
Δ*spoIIIE*	732	0.4	NO	0.7	0.8/NO	NO/0.1
smc::Tn*917* Δ*spoIIIE*	826	6.4	1.7	20.8	5.3/6.2	2.9/4.5
42°C						
WT	987	0.3	NO	1.5	1.5/0.8	NO/0.7
Δ*smc*	1,240	2.5	NO	1.4	1.8/1.0	NO/0.9
smc::Tn*917*	922	3.5	NO	1.5	2.0/0.9	NO/1.1
smc::Tn*917* pCXΩ*smc*	1,232	1.7	NO	1.5	1.9/1.2	0.3/1.1
Δ*spoIIIE*	890	0.3	NO	1.6	2.1/1.0	NO/0.9
smc::Tn*917* Δ*spoIIIE*	681	6.2	2.0	28.5	5.3/11.2	4.0/7.0

[a] Data were summarized from three independent experiments.
[b] Big cells are ≥1.5 μm in diameter, and small cells are ≤0.5 μm in diameter.
[c] NO, not observed within the total number of cells counted.

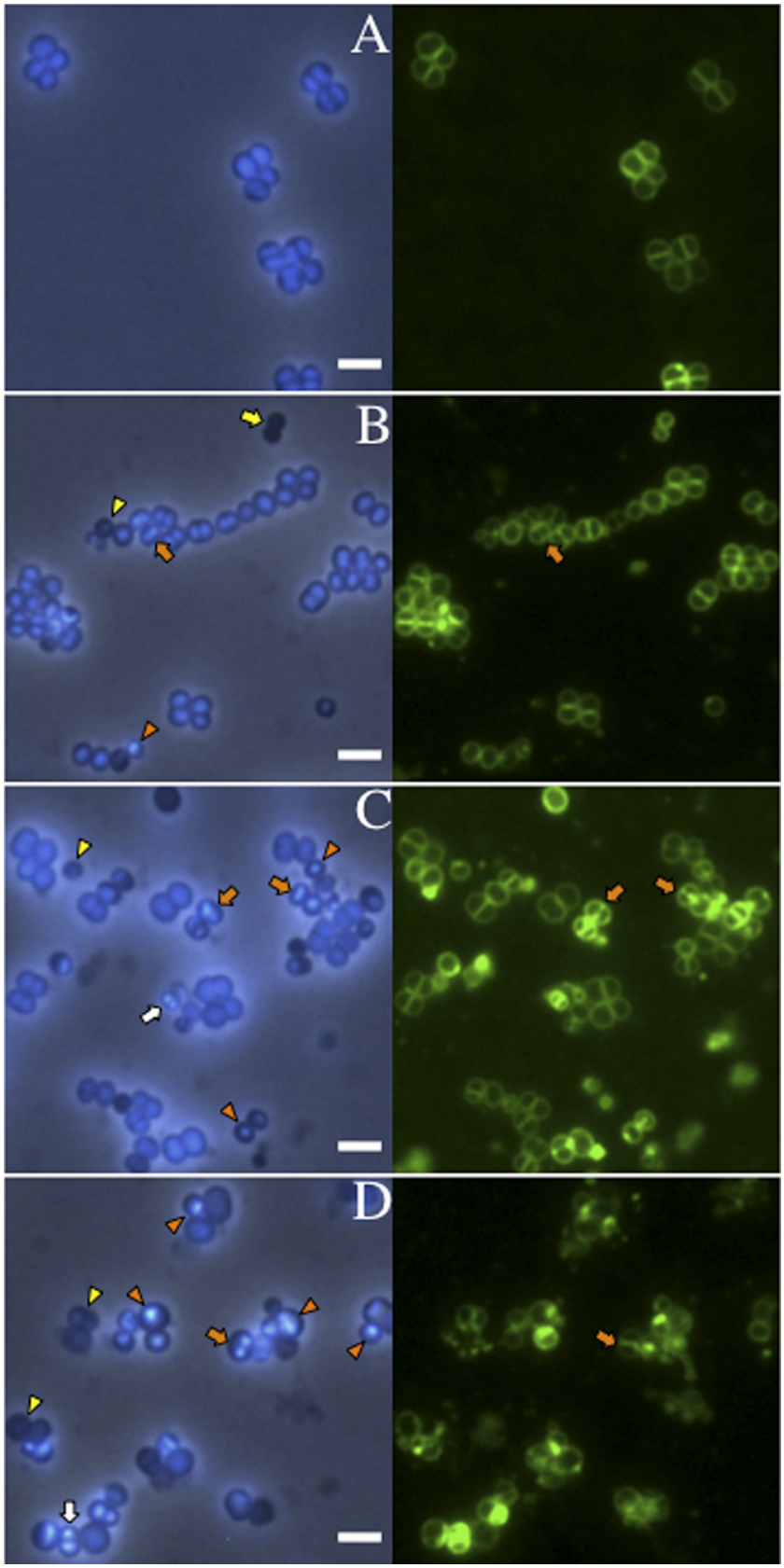

FIG. 4. Altered chromosome morphology aggravated at higher temperatures in SA113 *smc*::Tn*917* Δ*spoIIIE*. (A) SA113 WT grown for 1.5 h at 42°C. (B to D) SA113 *smc*::Tn*917* Δ*spoIIIE* grown for 1.5 h after dilution of the overnight culture into fresh TSB medium at 30°C, 37°C, and 42°C respectively. DNA was stained with DAPI (blue), and the cell membrane was labeled with FM1-43 (green). Orange arrows indicate examples of the "guillotine effect," or 'CUT' phenotype; yellow arrows indicate anucleate diplococci; white arrows indicate increased DNA content; yellow arrowheads indicate decreased DNA content; and orange arrowheads show the unevenly distributed nucleoid. Scale bar, 2 μm.

contains a potential promoter controlling the downstream genes' expression. SA113 Δ*smc* exhibited the same growth curve as SA113 *smc*::Tn*917* (data not shown) and a similar rate of chromosome segregation deficiency (Table 1).

Why is the effect of *smc* mutation in staphylococci less severe than that in rod-shaped bacteria? First, the discrepancy could be explained partially by the morphological difference between rods and cocci. Given that *E. coli* or *B. subtilis* cells are 1.1 to 1.5 μm wide and 2.0 to 6.0 μm long, the staphylococcal cell is only half the size (0.5 to 1.5 μm in diameter) of a bacillus cell (12). Besides, *S. aureus* has a much smaller cell volume of 0.15 μm^3 compared to *E. coli* with 0.5 to 0.7 μm^3 (19, 25). Despite different genome sizes between *B. subtilis* and *S. aureus* (4.1 Mbp versus 2.9 Mbp, respectively) (20, 29), the small staphylococcal cell size becomes spatially limiting for the nucleoids; therefore, decondensed chromosomes were not observed in *S. aureus smc* mutant cells. Second, as chromosome segregation is one of the most important cellular processes, bacteria must have employed redundant mechanisms. Other factors may play a more important role during chromosome segregation in the spherical cells.

Earlier studies showed that the DNA translocase SpoIIIE could rescue the trapped chromosome from septum membrane during vegetative growth in *B. subtilis* (26). In order to evaluate the function of SpoIIIE in *S. aureus*, an SA113 *spoIIIE* deletion mutant was constructed via double-cross homologous recombination by using a counterselection vector, pKOR1 (1). A majority of the *spoIIIE* reading frame, except for 68 bp at the 3′ end (which contains the Shine-Dalgarno sequence of the downstream gene), was replaced with an *aphAIII* cassette that renders kanamycin resistance (Fig. 1D). The *aphAIII* cassette was flanked with *lox* sites and was further removed by Cre recombinase (21). Afterwards, *smc*::Tn*917* was transduced into SA113Δ*spoIIIE*, resulting in the SA113 *smc spoIIIE* double mutant. Consistent with previous findings in *B. subtilis* (26), *S. aureus spoIIIE* single mutant cells had neither a significant growth disadvantage (Fig. 2A and B) nor an obvious defect in chromosome distribution compared to the WT (data not shown).

However, distinct from *B. subtilis*, in *S. aureus* a viable *smc spoIIIE* double mutant could be isolated. Growth curves showed that the SA113 *smc spoIIIE* double mutants were temperature sensitive (Fig. 2A and B). Colonies can only be formed at low temperatures on TSA plates. In liquid medium, the SA113 *smc spoIIIE* double mutant could grow to an optical density at 578 nm (OD_{578}) of 2.2 after 8 h at 30°C, whereas the growth ceased after only two generations (growing for 2 h to an OD_{578} of 0.4) at 42°C. Shifting the culture from 24°C to 42°C resulted in rapid growth cessation. To examine the morphological changes in the SA113 *smc spoIIIE* double mutant, samples were taken at early (1.5 h) and late (5 h) growth phases after dilution of overnight cultures into fresh TSB medium and incubated at various temperatures. At the early growth phase, the SA113 *smc spoIIIE* double mutant had distorted chromosome organization and heterogeneous cell sizes, as depicted in Fig. 4B to D and quantified in Table 1. Approximately 2% of the cells showed the so-called "guillotine effect" or "CUT" phenotype that occurred when the chromosome was bisected by the septal membrane (Fig. 4, orange arrows; Table 1), which was not observed in WT cells or *smc* single mutants. The percentage could not be exactly counted due to the limitations of the two-dimensional microscopy technique. Four to 6% of the double mutant cells were anucleate, which did not increase significantly compared to the *smc* single mutant (Table 1). While the same staining method was always applied, 3-fold more mutant cells appeared to contain an increased amount of DNA compared to WT (bright blue cells in Fig. 4C and D [white arrows]). More significantly, about 11% of the mutant cells showed decreased content of DNA (Fig. 4, yellow arrowheads), which was 10 fold higher than WT or the single mutants. The most severe irregular morphology is the unevenly distributed chromosomes that were no more homogeneous but rather accumulated punctately in nearly 30% of the mutant cells (Fig. 4, orange arrowheads). These aberrant chromosomal morphological changes suggested that the *smc spoIIIE* double mutant was greatly deficient not only in chromosome segregation but also in chromosome structure maintenance, and the defect in chromosome structure appeared even more severe than the segregation defect. The SA113 *smc spoIIIE* double mutant also had heterogeneous cell sizes; cells appeared as big (≥1.5 μm in diameter) as well as small (≤0.5 μm in diameter) (Table 1). The heterogeneous cell sizes are probably an indirect consequence of the *smc spoIIIE* mutations, since (i) there is no significant correlation between cell size change and the degree of chromosomal disorder (Table 1) and (ii) the defect in chromosome structure and segregation may interfere with many other cellular processes that affect cell size. At the late growth stage, the chromosome structure was severely disrupted, the cells eventually lysed, and more cell debris was produced at 42°C (data not shown). However, at 30°C, although the irregular chromosome disorder was aggravated and the cell size differentiated more obviously than during the earlier growth phase, there were still considerable amounts of normal cells with regular chromosome structure (data not shown).

Thus, compared to SA113 *smc* and *spoIIIE* single mutants, the highly distorted chromosome arrangement in *S. aureus smc spoIIIE* double mutants indicated that SpoIIIE compensated for SMC's function in chromosome segregation to a certain extent. The aggravated chromosome segregation defect in the *smc spoIIIE* double mutant disclosed the chromosome maintenance deficiency in the *smc* single mutant, since it is unlikely that SpoIIIE had a direct role in chromosome organization. In other words, the optimal chromosome segregation facilitates proper chromosome organization in *S. aureus*. While the number of anucleate cells decreased with increased temperature in the *smc* single mutant, the effect was reversed in the *smc spoIIIE* double mutant, where the number of anuclate cells was slightly increased at higher temperature. Interestingly, earlier transcriptomic data for the heat shock response in *S. aureus* showed that *spoIIIE* was transcribed 2.15-fold higher at 48°C (9). This finding could explain that the defect in the *smc* single mutant is in part compensated for by overexpression of SpoIIIE. Distinct from *B. subtilis* or *E. coli*, *S. aureus smc spoIIIE* double mutants are viable at low temperature, although possible suppressor mutations could not be excluded. The distinction underlies a different mechanism for guaranteeing maximum chromosome segregation in staphylococci. Presumably, besides the difference in cell shape,

other factors that play more significant roles in chromosome partitioning in cocci than in rods need to be identified.

Recently it has been found in *B. subtilis* that a second FtsK/SpoIIIE-like protein, SftA (*s*eptum-associated *F*tsK-like *t*ranslocase of DNA), coordinates chromosome translocation to ensure maximum chromosome segregation, however, at a different stage of cell division from SpoIIIE (2, 18). SftA contains the C-terminal DNA binding and ATPase domain, but instead of the N-terminal transmembrane domain in SpoIIIE, it has a soluble domain. SftA translocates chromosomes before septation, while SpoIIIE comes into play postseptationally when chromosomes are trapped by the septal membrane. Like *B. subtilis spoIIIE* mutants, the *sftA* mutants had a synergistic lethal defect with an *smc* deletion (18). The *B. subtilis sftA spoIIIE* double mutant undergoes normal growth, while the defect in chromosome segregation is exacerbated significantly compared to that in both single mutants. A protein homologous to *B. subtilis* SftA with conserved domain structures is encoded in all staphylococcal genomes, and the homologs share 33.3% identity. It is highly interesting to evaluate the function of SftA in staphylococci for future investigation.

Another aspect that should be considered about staphylococcal chromosome segregation is the specific cell division mode of staphylococci. In contrast to *B. subtilis* or *E. coli*, where division always takes place in the middle of the longitudinal cell, in *S. aureus* the division plane shifts by 90° to the previous one (10). Accordingly, the chromosome replication and segregation that occur prior to cell division must occur perpendicularly as well. Theoretically, in the spherical cell, there are infinite numbers of future division planes that are perpendicular to the previous division disc. The flexibility in shifting the orientation of chromosome replication and segregation might allow staphylococci to cope with the deficiency of chromosome segregation in *smc spoIIIE* double mutants. The regulation of setting the division plane and chromosome segregation direction in staphylococci is totally unknown yet.

Taken together, we have obtained a first insight into chromosome segregation in *Staphylococcus* and presented intriguing results regarding the genetic interaction of SMC and SpoIIIE, two critical factors involved in chromosomal dynamics. These findings shed light on different mechanisms of chromosome dynamics in the spherical staphylococcal cells, in contrast to the model in rods, which definitely deserves future investigation.

We thank Karl Forchhammer, Department of Organismic Interactions, University of Tübingen, for assistance with the microscopy studies.

This work was supported by DFG, graduate college GK 685, and SFB 766.

REFERENCES

1. **Bae, T., and O. Schneewind.** 2006. Allelic replacement in *Staphylococcus aureus* with inducible counter-selection. Plasmid **55:**58–63.
2. **Biller, S. J., and W. F. Burkholder.** 2009. The *Bacillus subtilis* SftA (YtpS) and SpoIIIE DNA translocases play distinct roles in growing cells to ensure faithful chromosome partitioning. Mol. Microbiol. **74:**790–809.
3. **Britton, R. A., and A. D. Grossman.** 1999. Synthetic lethal phenotypes caused by mutations affecting chromosome partitioning in *Bacillus subtilis*. J. Bacteriol. **181:**5860–5864.
4. **Britton, R. A., D. C. Lin, and A. D. Grossman.** 1998. Characterization of a prokaryotic SMC protein involved in chromosome partitioning. Genes Dev. **12:**1254–1259.
5. **Burton, B. M., K. A. Marquis, N. L. Sullivan, T. A. Rapoport, and D. Z. Rudner.** 2007. The ATPase SpoIIIE transports DNA across fused septal membranes during sporulation in *Bacillus subtilis*. Cell **131:**1301–1312.
6. **Dervyn, E., M. F. Noirot-Gros, P. Mervelet, S. McGovern, S. D. Ehrlich, P. Polard, and P. Noirot.** 2004. The bacterial condensin/cohesin-like protein complex acts in DNA repair and regulation of gene expression. Mol. Microbiol. **51:**1629–1640.
7. **Draper, G. C., and J. W. Gober.** 2002. Bacterial chromosome segregation. Annu. Rev. Microbiol. **56:**567–597.
8. **Errington, J., R. A. Daniel, and D. J. Scheffers.** 2003. Cytokinesis in bacteria. Microbiol. Mol. Biol. Rev. **67:**52–65.
9. **Fleury, B., W. L. Kelley, D. Lew, F. Gotz, R. A. Proctor, and P. Vaudaux.** 2009. Transcriptomic and metabolic responses of Staphylococcus aureus exposed to supra-physiological temperatures. BMC Microbiol. **9:**76.
10. **Giesbrecht, P., T. Kersten, H. Maidhof, and J. Wecke.** 1998. Staphylococcal cell wall: morphogenesis and fatal variations in the presence of penicillin. Microbiol. Mol. Biol. Rev. **62:**1371–1414.
11. **Götz, F.** 2004. Staphylococci in colonization and disease: prospective targets for drugs and vaccines. Curr. Opin. Microbiol. **7:**477–487.
12. **Götz, F., T. Bannerman, and K. H. Schleifer.** 2006. The genera *Staphylococcus* and *Macrococcus*, p. 5–75. *In* M. Dworkin (ed.), The procaryotes, vol. 4. Springer, New York, NY.
13. **Graumann, P. L.** 2000. *Bacillus subtilis* SMC is required for proper arrangement of the chromosome and for efficient segregation of replication termini but not for bipolar movement of newly duplicated origin regions. J. Bacteriol. **182:**6463–6471.
14. **Güthlein, C., R. M. Wanner, P. Sander, E. C. Böttger, and B. Springer.** 2008. A mycobacterial *smc* null mutant is proficient in DNA repair and long-term survival. J. Bacteriol. **190:**452–456.
15. **Haydon, D. J., N. R. Stokes, R. Ure, G. Galbraith, J. M. Bennett, D. R. Brown, P. J. Baker, V. V. Barynin, D. W. Rice, S. E. Sedelnikova, J. R. Heal, J. M. Sheridan, S. T. Aiwale, P. K. Chauhan, A. Srivastava, A. Taneja, I. Collins, J. Errington, and L. G. Czaplewski.** 2008. An inhibitor of FtsZ with potent and selective anti-staphylococcal activity. Science **321:**1673–1675.
16. **Herbert, S., A. Bera, C. Nerz, D. Kraus, A. Peschel, C. Goerke, M. Meehl, A. Cheung, and F. Götz.** 2007. Molecular basis of resistance to muramidase and cationic antimicrobial peptide activity of lysozyme in staphylococci. PLoS Pathog. **3:**e102.
17. **Hirano, M., and T. Hirano.** 2002. Hinge-mediated dimerization of SMC protein is essential for its dynamic interaction with DNA. EMBO J. **21:**5733–5744.
18. **Kaimer, C., J. E. González-Pastor, and P. L. Graumann.** 2009. SpoIIIE and a novel type of DNA translocase, SftA, couple chromosome segregation with cell division in *Bacillus subtilis*. Mol. Microbiol. **74:**810–825.
19. **Kubitschek, H. E.** 1990. Cell volume increase in *Escherichia coli* after shifts to richer media. J. Bacteriol. **172:**94–101.
20. **Kuroda, M., T. Ohta, I. Uchiyama, T. Baba, H. Yuzawa, I. Kobayashi, L. Cui, A. Oguchi, K. Aoki, Y. Nagai, J. Lian, T. Ito, M. Kanamori, H. Matsumaru, A. Maruyama, H. Murakami, A. Hosoyama, Y. Mizutani-Ui, N. K. Takahashi, T. Sawano, R. Inoue, C. Kaito, K. Sekimizu, H. Hirakawa, S. Kuhara, S. Goto, J. Yabuzaki, M. Kanehisa, A. Yamashita, K. Oshima, K. Furuya, C. Yoshino, T. Shiba, M. Hattori, N. Ogasawara, H. Hayashi, and K. Hiramatsu.** 2001. Whole genome sequencing of meticillin-resistant Staphylococcus aureus. Lancet **357:**1225–1240.
21. **Leibig, M., B. Krismer, M. Kolb, A. Friede, F. Götz, and R. Bertram.** 2008. Marker removal in staphylococci via Cre recombinase and different *lox* sites. Appl. Environ. Microbiol. **74:**1316–1323.
22. **Lindow, J. C., R. A. Britton, and A. D. Grossman.** 2002. Structural maintenance of chromosomes protein of *Bacillus subtilis* affects supercoiling in vivo. J. Bacteriol. **184:**5317–5322.
23. **Mascarenhas, J., J. Soppa, A. V. Strunnikov, and P. L. Graumann.** 2002. Cell cycle-dependent localization of two novel prokaryotic chromosome segregation and condensation proteins in *Bacillus subtilis* that interact with SMC protein. EMBO J. **21:**3108–3118.
24. **Moriya, S., E. Tsujikawa, A. K. Hassan, K. Asai, T. Kodama, and N. Ogasawara.** 1998. A *Bacillus subtilis* gene-encoding protein homologous to eukaryotic SMC motor protein is necessary for chromosome partition. Mol. Microbiol. **29:**179–187.
25. **Pilavtepe-Çelik, M., M. O. Balaban, H. Alpas, and A. E. Yousef.** 2008. Image analysis based quantification of bacterial volume change with high hydrostatic pressure. J. Food Sci. **73:**M423–M429.
26. **Sharpe, M. E., and J. Errington.** 1995. Postseptational chromosome partitioning in bacteria. Proc. Natl. Acad. Sci. U. S. A. **92:**8630–8634.
27. **She, W., Q. Wang, E. A. Mordukhova, and V. V. Rybenkov.** 2007. MukEF Is required for stable association of MukB with the chromosome. J. Bacteriol. **189:**7062–7068.
28. **Thanbichler, M., and L. Shapiro.** 2006. MipZ, a spatial regulator coordinating chromosome segregation with cell division in *Caulobacter*. Cell **126:**147–162.

29. **Trevors, J. T.** 1996. Genome size in bacteria. Antonie Van Leeuwenhoek **69:**293–303.
30. **Volkov, A., J. Mascarenhas, C. Andrei-Selmer, H. D. Ulrich, and P. L. Graumann.** 2003. A prokaryotic condensin/cohesin-like complex can actively compact chromosomes from a single position on the nucleoid and binds to DNA as a ring-like structure. Mol. Cell. Biol. **23:**5638–5650.
31. **Wieland, K. P., B. Wieland, and F. Götz.** 1995. A promoter-screening plasmid and xylose-inducible, glucose-repressible expression vectors for *Staphylococcus carnosus*. Gene **158:**91–96.
32. **Wu, L. J., and J. Errington.** 1994. *Bacillus subtilis* SpoIIIE protein required for DNA segregation during asymmetric cell division. Science **264:**572–575.
33. **Yu, X. C., E. K. Weihe, and W. Margolin.** 1998. Role of the C terminus of FtsK in *Escherichia coli* chromosome segregation. J. Bacteriol. **180:**6424–6428.
34. **Zapun, A., T. Vernet, and M. G. Pinho.** 2008. The different shapes of cocci. FEMS Microbiol. Rev. **32:**345–360.

OPEN ACCESS Freely available online

PLoS one

Cell Wall Antibiotics Provoke Accumulation of Anchored mCherry in the Cross Wall of *Staphylococcus aureus*

Wenqi Yu, Friedrich Götz*

Microbial Genetics, University of Tübingen, Tübingen, Germany

Abstract

A fluorescence microscopy method to directly follow the localization of defined proteins in *Staphylococcus* was hampered by the unstable fluorescence of fluorescent proteins. Here, we constructed plasmid (pCX) encoded red fluorescence (RF) mCherry (mCh) hybrids, namely mCh-cyto (no signal peptide and no sorting sequence), mCh-sec (with signal peptide), and mCh-cw (with signal peptide and cell wall sorting sequence). The *S. aureus* clones targeted mCh-fusion proteins into the cytosol, the supernatant and the cell envelope respectively; in all cases mCherry exhibited bright fluorescence. In staphylococci two types of signal peptides (SP) can be distinguished: the +YSIRK motif SP_{lip} and the −YSIRK motif SP_{sasF}. mCh-hybrids supplied with the +YSIRK motif SP_{lip} were always expressed higher than those with −YSIRK motif SP_{sasF}. To study the location of the anchoring process and also the influence of SP type, mCh-cw was supplied on the one hand with +YSIRK motif (mCh-cw1) and the other hand with -YSIRK motif (mCh-cw2). MCh-cw1 preferentially localized at the cross wall, while mCh-cw2 preferentially localized at the peripheral wall. Interestingly, when treated with sub-lethal concentrations of penicillin or moenomycin, both mCh-cw1 and mCh-cw2 were concentrated at the cross wall. The shift from the peripheral wall to the cross wall required Sortase A (SrtA), as in the *srtA* mutant this effect was blunted. The effect is most likely due to antibiotic mediated increase of free anchoring sites (Lipid II) at the cross wall, the substrate of SrtA, leading to a preferential incorporation of anchored proteins at the cross wall.

Citation: Yu W, Götz F (2012) Cell Wall Antibiotics Provoke Accumulation of Anchored mCherry in the Cross Wall of *Staphylococcus aureus*. PLoS ONE 7(1): e30076. doi:10.1371/journal.pone.0030076

Editor: Ben Adler, Monash University, Australia

Received September 30, 2011; **Accepted** December 13, 2011; **Published** January 10, 2012

Funding: This work was supported by DFG (Deutsche Forschungsgemeinschaft), SFB (Sonderforschungsbereich) 766. The funders had no role in study design, data collection and analysis, decision to publish, or preparation of the manuscript.

Competing Interests: The authors have declared that no competing interests exist.

* E-mail: friedrich.goetz@uni-tuebingen.de

Introduction

Surface anchored proteins of *Staphylococcus aureus* represent a group of proteins that are exposed on the bacterial cell envelope and covalently anchored to the staphylococcal cell wall peptidoglycan [1]. Many of the surface proteins belong to the MSCRAMM family (microbial surface components recognizing adhesive matrix molecules), which play key roles in colonization and adhesion of *S. aureus* [2].

The process of anchoring surface proteins to the staphylococcal cell wall, termed the 'sorting pathway', includes three steps [3]: translocation, sorting and incorporation into mature peptidoglycan. Anchored proteins are distinguished by a C-terminal cell wall sorting signal (CWS). The N-terminal signal peptide directs the polypeptide into the Sec secretory translocon. Sortase A (SrtA) [4], a membrane-bound transpeptidase, performs the sorting reaction by cleaving the amide bond between threonine and glycine within the LPXTG motif, which results in the acyl intermediate. The peptidoglycan precursor, Lipid II, serves as the substrate for the sorting reaction, which is the tethering of the C-terminal threonine of the surface protein to lipid II by an amide bond. Lipid II tethered with the surface proteins is finally incorporated into mature peptidoglycan [5].

Previously, we have described that the N-terminal signal peptides of staphylococcal lipases harbor a conserved motif - Ser, Ile, Arg and Lys - designated as the SIRK-motif [6]. This motif (termed as YSIRK/GS) is later found conserved in many, but not all surface proteins. SP with the YSIRK/GS motif promotes the secretion of surface proteins [7]. In *Streptococcus pyogenes* [8] and in *S. aureus* [9], the SP (+YSIRK-motif) has a function in directing surface proteins to different surface localizations. In *S. aureus*, SP (+YSIRK) directs the secretion and anchoring of surface proteins at septum (cross wall), while the SP (−YSIRK) leads the secretion and anchoring of surface proteins more to the cell pole [9]. It has also been shown that three transmembrane proteins, namely Spd (surface protein display) proteins, are involved in the surface display of protein A, one of the predominant surface proteins carrying SP (+YSIRK) [10]. The expression level and surface display of protein A are largely reduced in each *spd* mutant. Moreover, *spd* mutants affect the expression of surface proteins with SP (+YSIRK). Interestingly, the *spd* mutants exhibit an increased abundance of visible cross walls and thickened cross walls. Yet, how cross wall formation affects the surface display of surface proteins remains unclear.

Conventionally, immunofluorescence microscopy has been applied to surface proteins localization studies, as the cell surface immobilized proteins have relatively easy and stable access to antibodies [11,12]. However, immunofluorescence microscopy has a certain intrinsic limitation that especially impedes the subcellular and high throughput studies. For example, antibodies cannot penetrate into the septum without cell wall permeabilization; yet cell wall permeabilization using cell wall hydrolase or detergents

often leads to the release of surface proteins with the risk of artifacts. Further, a large numbers of specific antibodies are needed in order to study various surface proteins' localization, which is laborious and time consuming. Particularly in *S. aureus* immunofluorescence is extremely hindered by protein A, the IgG binding protein.

In this study, we developed a direct visualization method for monitoring the surface proteins anchoring process. The red fluorescent protein mCherry was fused with different signal sequences and targeted as cytoplasmic, secreted, and cell wall anchored. Cell wall anchored mCherry (mCh-cw) enabled us to visualize the cross and peripheral wall localization pattern rather than using immunofluorescence microscopy. Intriguingly, independent of different signal peptides, treatment with sub-lethal concentrations of cell wall biosynthesis antibiotics led to strong accumulation of mCh-cw at the cross wall which correlated with the increased Van-FL binding at the cross wall. Our results show that mCherry is a useful tool to localize and follow the anchoring or secretion processes in staphylococci.

Results

Defined mCh-fusion proteins are targeted in an active form (maintaining RF) to distinct subcellular compartments

Previously, we have anchored staphylococcal lipase to staphylococcal cell wall in an active form [13]. Anchored lipase could be extracted from the cell wall, together with covalently tethered peptidoglycan [14]. Based on these results, we asked if mCherry could be immobilized to staphylococcal peptidoglycan while maintaining stable fluorescence. The mature lipase was replaced by mCherry in pCX30Δ82, generating pCXmCh-cw1 (**Fig. 1A**). The protein domain order in this construct was, the N-terminal signal peptide (SP_{lip}) and propeptide (PP_{lip}) of lipase, mCherry, and the C-terminal cell wall sorting sequence (CWS) of FnBPB (fibronectin binding protein B). CWS consisted of the LPXTG motif, followed by a hydrophobic domain and a positively charged tail [13]. To differentiate the effect of SP (+/−YSIRK), the signal peptide of surface protein SasF (SP_{sasF}), a non-YSIRK SP was used to substitute SP_{lip}, resulting in pCXmCh-cw2 (**Fig. 1B**). Moreover, hybrids mCh-sec1&2 lacking C-terminal CWS, as well as hybrid mCh-cyto lacking both SP and CWS, were constructed (**Fig. 1C, 1D, 1E**). All the fusions were carried out under the xylose inducible and glucose repressible *Pxyl* promoter of the pCX30 vector backbone [15]. Importantly, it was necessary to keep the PP_{lip} in the fusion with mCherry in all the constructs, since PP_{lip} significantly promotes the fusion partners' secretion, stability and activity [16,17]. Expressing mCherry without PP_{lip} showed drastically reduced fluorescence (data not shown).

To test if mCh-hybrids were functional, the plasmids were transformed into *S. aureus* SA113 (WT) and its SrtA mutant (Δ*srtA*). After xylose induction, different cell fractions were collected for mCherry expression (indicated by RF measurement). As shown in **Fig. 2A**, the supernatant of WT-sec1 exhibited the highest RF signals, which were set as 100%. WT-sec2 showed the second highest RF intensity of about 50%. WT-cw1, WT-cw2 and WT-cyto had little RF in the supernatant**,** while the Δ*srtA*-cw1 or Δ*srtA*-cw2 showed 10–15% RF intensity (**Fig. 2A**). All constructs (anchored or secreted mCh-hybrids) with SP_{lip} (+YSIRK motif) exhibited significantly higher fluorescence intensity than those with SP_{sasF} (-YSIRK motif). The same results were obtained in SA113 Δ*spa* (data not shown), where the protein levels could be accessed by Western blotting without the interference of protein A. The protein level of different constructs (**Fig. 2B**) correlated with their fluorescence profiles, except for Δ*srtA*-cw1 and Δ*srtA*-cw2 where mCh-cw was released into the supernatant with the unprocessed C-terminal CWS. Possibly, the unprocessed CWS interfered with the correct folding of mCherry; therefore, the fluorescence emission was reduced to some extent. Once covalently anchored to peptidoglycan, surface proteins are immobilized and can only be released by peptidoglycan hydrolyses [3,13]. Lysostaphin, the glycyl-glycine endopeptidase, cleaves specifically the pentaglycine cross bridges in staphylococcal peptidoglycan, and thereby releases the surface proteins that are linked to pentaglycine bridges. WT-cw1 released the highest amount of RF by lysostaphin treatment, indicating that mCherry was largely peptidoglycan-immobilized. In WT-cw2 five-fold less RF was released (**Fig. 2A**). In the pellet fraction after lysostaphin treatment, WT-cyto displayed the highest fluorescence, indicating that without SPs, mCh-fusion proteins were not secreted but remained in the cytosol (**Fig. 2A**). SA113 WT (pCX30Δ82) showed no fluorescence in all cell fractions, like the negative controls, which were SA113 without plasmid or the BO medium (data not shown). To test if mCh-hybrids were functional in

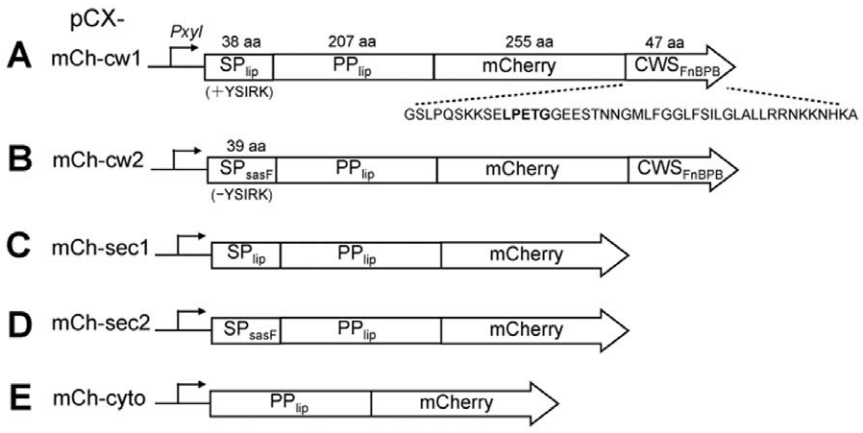

Figure 1. Schematic representation of mCh-hybrids. SP, signal peptide; PP, propeptide; CWS, cell wall sorting signal; mCh: mCherry; lip, lipase. The amino acid sequence of CWS was indicated. The parent plasmid was pCX30 and all mCh-fusion constructs were under control of the xylose-inducible promoter, P*xyl*.
doi:10.1371/journal.pone.0030076.g001

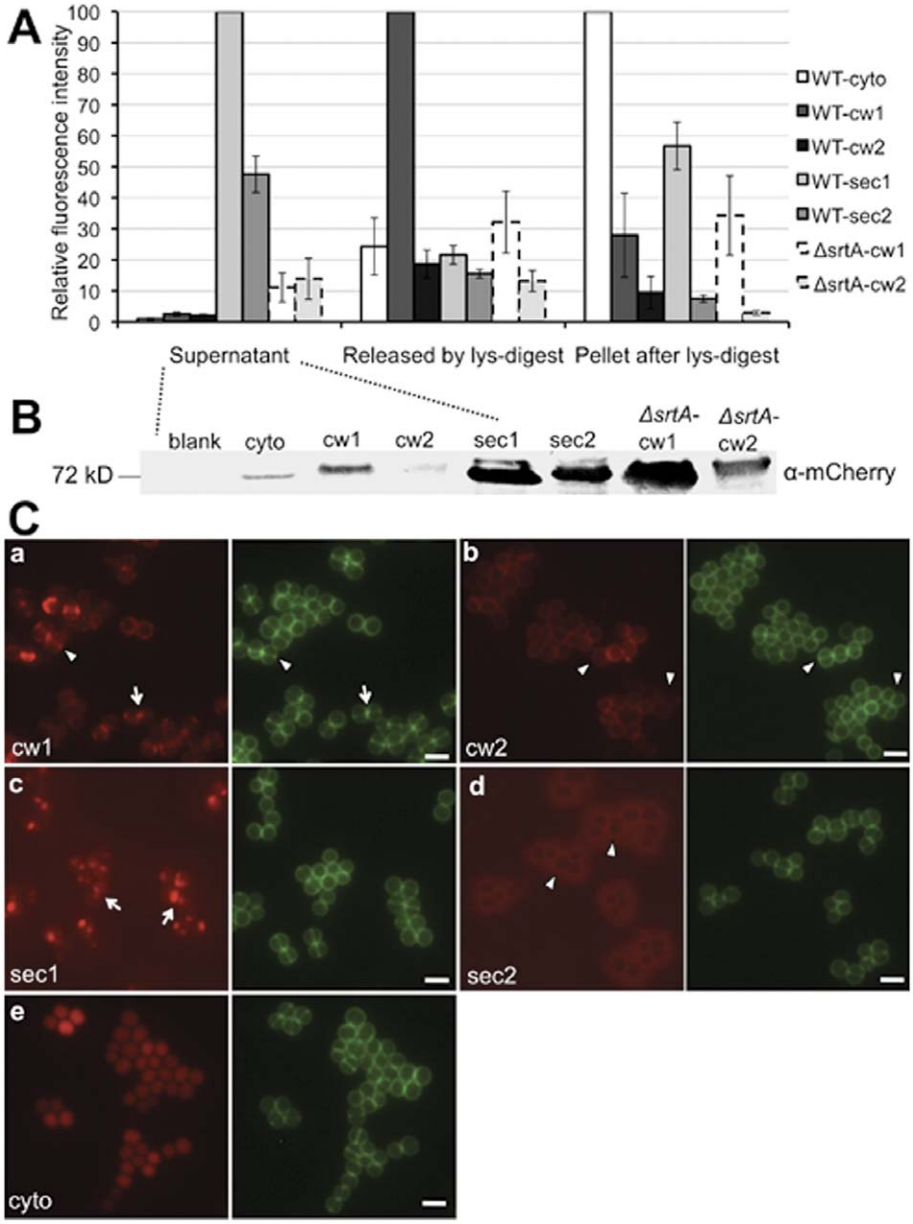

Figure 2. Monitoring mCh-hybrids. A. Fluorescence intensity comparison of mCh-hybrids from different cell fractions. WT-cyto, SA113 (pCXmCh-cyto); WT-cw1 or 2, SA113 (pCXmCh-cw1) or (pCXmCh-cw2); WT-sec1 or 2, SA113 (pCXmCh-sec1) or (pCXmCh-sec2); Δ*srtA*-cw1 or 2, SA113 Δ*srtA* (pCXmCh-cw1) or (pCXmCh-cw2); lys, lysostaphin. **B.** Western blotting of mCh-hybrid proteins in the culture supernatant of protein A deficient mutant SA113 Δ*spa*. Blank, SA113 Δ*spa* without plasmid; cyto, SA113 Δ*spa* (pCXmCh-cyto); cw1 or 2, SA113 Δ*spa* (pCXmCh-cw1) or (pCXmCh-cw2); sec1 or 2, SA113 Δ*spa* (pCXmCh-sec1) or (pCXmCh-sec2); Δ*srtA*-cw1 or 2, SA113 Δ*spa*Δ*srtA* (pCXmCh-cw1) or (pCXmCh-cw2). **C.** Subcellular localization of mCh-hybrid proteins in SA113. **a.** pCXmCh-cw1; **b.** pCXmCh-cw2; **c.** pCXmCh-sec1; **d.** pCXmCh-sec2; **e.** pCXmCh-cyto. Arrowheads in **a** and **b**, fluorescence localized at the cross wall in **a**, but absent from the cross wall in **b**; arrows in **a** and **c,** RF foci close to the initial sites of the cross walls; arrowheads in **d,** halo-like RF distribution absent from the cross wall. Images **a, c,** and **e** were taken after one hour of xylose induction; images **b** and **d** were taken after two hours of induction. Green: Van-FL staining (cell wall); scale bar, 2 μm.
doi:10.1371/journal.pone.0030076.g002

different staphylococcal species, all constructs were transformed into *S. carnosus* TM300 and its *srtA* deletion mutant; we obtained similar results as with *S. aureus* strains (data not shown).

mCh-hybrids provide useful tools to visualize the effect of SP (+/− YSIRK-motif)

In earlier studies it was suggested that SP (+YSIRK) directs the secretion and anchoring of surface proteins at the division septum, whereas the surface proteins with SP (−YSIRK) are secreted and incorporated at the cell pole [8,9]. To test if the spatial difference of SP (+/−YSIRK) can be visualized by mCh-hybrids, we compared the mCh-fusions with SP_{lip} (+YSIRK) and SP_{sasF} (−YSIRK). Indeed, the localization patterns of the SA113 (pCXmCh-cw1) and SA113 (pCXmCh-cw2) clones differed from each other. The mCh-cw1 clone exhibited patchy circumferential RF and especially bright RF at the cross wall (**Fig. 2Ca, arrowheads**); often, two foci adjacent to the new cross wall were

observed **(Fig. 2Ca, arrows).** In contrast, in the mCh-cw2 clone RF distributed homogeneously at the peripheral cell wall; little RF was seen in the cross wall, even after two daughter cells split **(Fig. 2Cb, arrowheads).** Quantification of colocalization analysis of Van-FL (green fluorescence of cell wall staining) and mCh-cw (RF) revealed that mCh-cw1 colocalized with nearly 50% of the total cross walls, while mCh-cw2 colocalized with only 6% of total visible cross walls **(Fig. S1B)**.

The effect of SPs (+/−YSIRK) can also be visualized by the secretion patterns of SA113 (pCXmCh-sec1) and SA113 (pCXmCh-sec2). In mCh-sec2, most of RF was outside and surrounding the cells as a diffuse halo while absent at the cross walls **(Fig. 2Cd, arrowheads)**, which indicated a peripheral secretion pattern. In contrast, mCh-sec1 exhibited spot-like foci particularly at or near the (future) division septum **(Fig. 2Cc, arrows)**. The different localization pattern between SA113 (pCXmCh-sec1) and SA113 (pCXmCh-sec2) was in agreement with earlier observations that SPs (+/−YSIRK) probably direct the secretion of surface proteins to different sites [8,9]. In the cytoplasmic expressed mCh-hybrids of SA113 (pCXmCh-cyto), RF was uniformly distributed within the cells **(Fig. 2Ce)**.

Penicillin and moenomycin direct mCh-cw to the cross wall, irrespective of SP type

Several cell wall biosynthesis antibiotics interfere with the protein anchoring reaction [5,18]. It has been shown that for example penicillin G, vancomycin, moenomycin, bacitracin and tunicamycin inhibit the tethering of surface proteins with lipid II. Considering that the surface proteins anchoring process is closely related to both protein secretion and cell wall biosynthesis, we examined whether these cell wall antibiotics effect the localization of secretion or anchoring. Gallidermin [19], a lantibiotic that specifically binds to lipid II [20], and D-cycloserine, which prevents D-Ala-D-Ala terminus synthesis of the muropeptides [21], were also tested. As shown in **Fig. 3A**, overnight cultures of SA113 (pCXmCh-cw) were diluted into fresh BO medium. Antibiotics were added at 0.1 OD_{578}, followed by two hours of incubation before xylose induction. Samples for microscopy examination were collected after one and two hours of xylose induction. The sub-lethal concentrations of various antibiotics were determined experimentally when the bacterial growth was slightly retarded but not completely inhibited, allowing protein synthesis to proceed.

Among all of the antibiotics tested, penicillin G (Pc) and moenomycin (synonym: flavomycin, Fla) triggered a strikingly altered localization pattern compared to the untreated cells. In **Fig. 3B** the results of two hours' xylose induction were shown (the results of one hour xylose induction looked essentially the same, only fluorescence intensity was less). The most striking difference between untreated (**Fig. 3Ba,d**) and penicillin G or moenomycin treated clones (**Fig. 3Bb,c,e,f, arrowheads**) was that mCh-cw became almost exclusively localized at the cross wall. The antibiotics provoked an accumulation of anchored mCherry in the cross wall of *S. aureus*.

Penicillin and moenomycin also cause Van-FL accumulation at the cross wall

In the presence of penicillin or moenomycin, we found that not only mCh-cw but also Van-FL that recognizes free -D-Ala-D-Ala of lipid II or uncrosslinked murein in the cell wall was accumulated at the cross wall while simultaneously disappearing from the side wall. We tried to quantify the percentage of Van-FL stained cross wall and the rate of cross wall localized mCh-cw (RF) in antibiotic treated and untreated cells (**Fig. S1**). The percentage of visible cross walls was the ratio of visible cross wall numbers (when Van-FL staining appeared as a line at the septum before daughter cells split) in a cell population versus the total cell numbers of the same cell population. Percentage of cross wall localized RF was the ratio of numbers of line-like cross wall localized RF versus line-like cross walls (visible by Van-FL staining) in the same cell population. Both penicillin and moenomycin treatment led to a significantly higher percentage of visible cross wall formation and an increased percentage of RF localizing at the cross wall in SA113 carrying either pCXmCh-cw1 or pCXmCh-cw2 (**Fig. S1A, B**). The effect was more pronounced in the mCh-cw2 clone. In the untreated cells, mCh-cw2 colocalized with only 6% of the cross walls, while in penicillin or moenomycin treated cells, the percentage rose to 76% and 95% respectively, implying that mCh-cw2 colocalized with almost every visible cross wall in moenomycin treated cells.

The relative fluorescence intensity of Van-FL at the cross wall was also quantified. The fluorescence profile of a line that is perpendicular to the cross wall and across its middle point was compared between untreated and antibiotics treated cells (**Fig. 4A**). Only cells with a 'cross wall line' (a closed septum before cell split) were measured. The max amplitude (the major peak) indicated the fluorescence intensity at the cross wall. The two small peaks indicated the peripheral (side) wall fluorescence intensity. Generally, penicillin- or moenomycin-treated cells displayed higher fluorescence (RF and VanFL) at the cross wall and lower fluorescence at the peripheral wall when compared to untreated cells (**Fig. 4A**). To quantify the significance and avoid the error of staining or imaging difference, the value of max amplitude was divided by the mean Van-FL fluorescence intensity value of the same cell. **Fig. 4B** showed the average ratio (cross wall intensity/mean intensity) of 150 cells from three independent experiments in each group. The data showed that both penicillin and moenomycin significantly intensified Van-FL staining at the cross wall compared to the untreated cells. Of all cell wall antibiotics tested, penicillin and moenomycin induced the most obvious phenotype. Bacitracin and gallidermin triggered the accumulation of mCh-cw at the cross wall to a certain extent, whereas vancomycin and D-cycloserine had little influence. Under all situations, an increased Van-FL staining at the cross wall correlated with an increased mCh-cw colocalization.

In penicillin or moenomycin treated cells, Van-FL staining at the cross wall was significantly higher than that in the untreated cells, indicating that free D-Ala-D-Ala residues were enriched, which resulted from a decrease in murein cross-linking and an increase of lipid II molecules. In both scenarios, uncross-linked pentaglycines (SrtA substrates), the anchoring sites for mCh-cw, should also be increased. Thus, we assume that the increased availability of anchoring sites favors the anchoring of surface proteins, thus causing the observed incorporation and accumulation at the cross wall. This assumption was confirmed by the finding that antibiotic driven accumulation of mCh-cw at the cross wall required SrtA.

Antibiotic induced accumulation of mCh-cw at the cross wall requires SrtA

As shown above, penicillin and moenomycin impelled the accumulation of mCh-cw at the cross wall, irrespective of SP type. The question is: does the accumulation require SrtA mediated anchoring? To verify this question, we examined the influence of penicillin and moenomycin on Δ*srtA* (pCXmCh-cw) as well as SA113 (pCXmCh-sec).

In Δ*srtA* (pCXmCh-cw), mCh-cw cannot be anchored to the cell wall due to the absence of SrtA; therefore, mCh-cw was partially

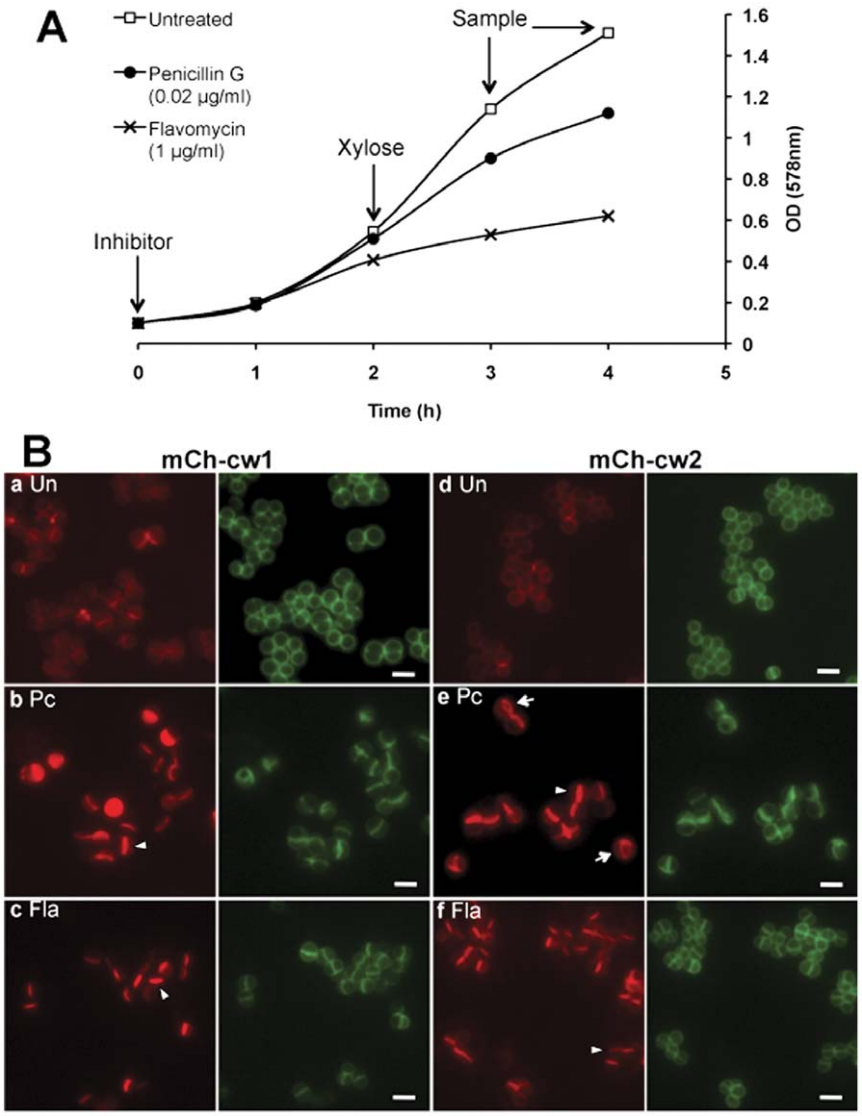

Figure 3 Penicillin and moenomycin direct mCh-cw to the cross wall, irrespective of SP type. A. Schematic representation of antibiotics treatment assay. Untreated (□); treated with penicillin (0.02 μg/ml) (●); treated with moenomycin (flavomycin) (1 μg/ml) (×). **B.** Influence of penicillin (Pc) and moenomycin (Fla) on the subcellular localization of mCh-cw hybrid proteins. Arrowheads indicated the cross wall accumulation of mCh-cw; arrows indicated the ring-like distribution; scale bar, 2 μm.
doi:10.1371/journal.pone.0030076.g003

released into the supernatant and partially retained in the membrane via the C-terminal CWS domain. In the presence of penicillin or moenomycin, mCh-cw was largely dispersed over the entire cell wall (both cross wall and side wall), irrespective of the SP-types (**Fig. 5**). There was no RF accumulation at the cross wall as was seen for the SA113 WT (**Fig. 4B**), indicating that SrtA was necessary for the accumulation of mCh-cw at the cross wall.

Discussion

So far, immunofluorescence microscopy and immunoelectron microscopy have been used for surface proteins localization studies in the last decades. To our knowledge, there is no direct visualization method to be applied in this field yet. In this study, we aimed to develop a direct method for monitoring surface proteins' subcellular distribution. The recently developed fluorescent protein mCherry, the monomeric derivative of *Discosoma* sp. fluorescent protein 'DsRed' [22], provided us with an ideal tool. mCherry was found fully fluorescent after secretion through the Sec secretory pathway and was fluorescent in the membrane as well [23,24]. Here we show that mCherry can be secreted and anchored to staphylococcal cell wall while maintaining stable fluorescence.

Our trial with GFPmut3 [25] failed, because GFPmut3 lost fluorescence when it was translocated via the Sec secretory pathway (**Fig. S3A**), similar to the observation with GFPuv in *Escherichia coli* [26]. It has been reported recently that a new GFP variant, the super-folder GFP (sfGFP) [27], can be translocated through the Sec secretory pathway in *E. coli* while maintaining fluorescence [28]. However, in *S. aureus*, the fluorescence of secreted sfGFP-fusions was still fairly low, although the sfGFP-fusions were secreted in a higher amount than the GFPmut3-fusions (**Fig. S3**). In comparison, the secreted mCh-fusions showed 7–13 fold higher fluorescence intensity than GFP-fusions while the difference in the protein amount was not that remarkable (**Fig. S3**). Western blotting results revealed that

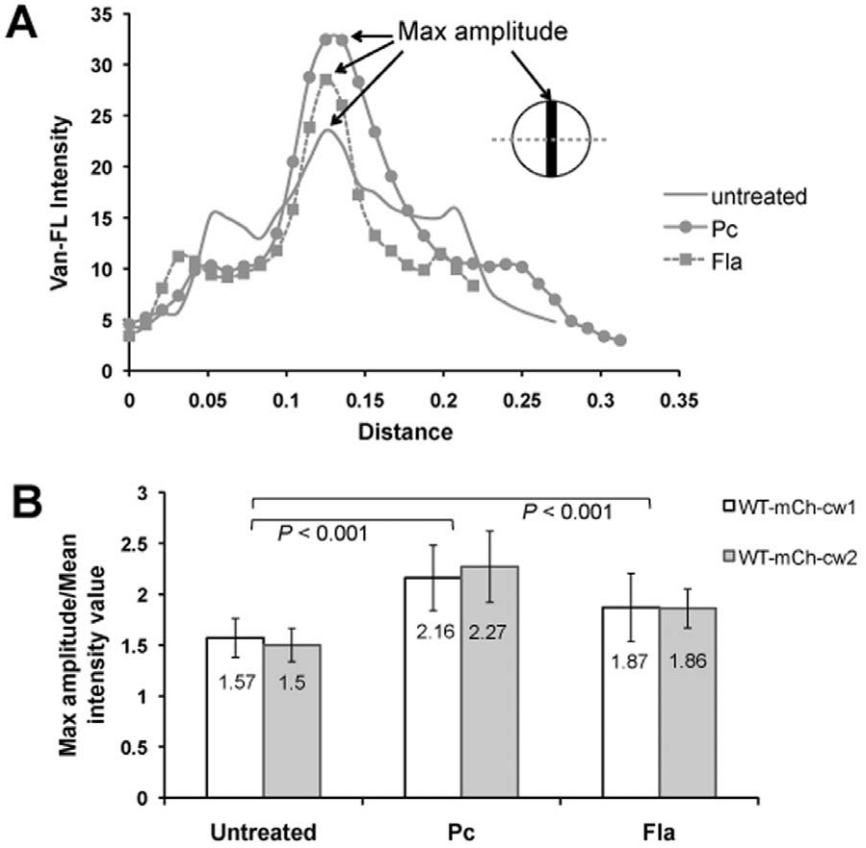

Figure 4. Penicillin and moenomycin treatment led to enrichment of Van-FL at the cross wall. A. Fluorescence intensity profile of Van-FL staining from a line perpendicular to the cross wall and across the middle point of the cross wall. Simple line, untreated cell; dotted line with filled squares, moenomycin (Fla) treated cell; line with filled circles, penicillin (Pc) treated cell. Max amplitude represented the cross wall intensity. Note that the figure was remade using ImageJ software from the microscopy images; the intensity and distance values were not the same as the original data from Leica AF software; but represented the same profile distribution. **B.** Comparative Van-FL intensity at the cross wall among untreated, penicillin (Pc) treated, and moenomycin (Fla) treated cells. The cross wall Van-FL intensity values were calculated by the ratio of max amplitude against mean fluorescence intensity (generated by Leica AF software) from the same cell. The average ratio of 150 cells from three independent experiments of each group was shown in the bars. White bar, SA113 (pCXmCh-cw1); gray bar, SA113 (pCXmCh-cw2).
doi:10.1371/journal.pone.0030076.g004

different from the secreted mCh-fusions, the secreted GFP-fusions (ppGFP-sec1, ppGFP-sec2, ppsfGFP-sec1, and ppsfGFP-sec2) migrated slightly higher than ppGFP or ppsfGFP (**Fig. S3B, arrows**), which indicated that the majority of the secreted GFP-fusions were still tethered with signal peptides. It appeared that the secreted GFP-fusions could not be processed and fold correctly to be fluorescent after Sec-dependent secretion. The mCh-hybrids constructed in this study enabled us to observe and follow the subcellular (especially the cross wall) localization of anchored proteins. Meanwhile, we were also fully aware of the limitation of the system, as it was based on plasmid-encoded genes, by which the proteins were higher expressed. Yet, prolonged protein expression only enhanced the fluorescent signals; it did not alter the distribution patterns within the time period tested, one and two hours after induction. Therefore, we can make at least statements as to the tendency of protein localization.

Apart from the influence of SPs (+/−YSIRK) on the localization of secretion, we also found that in the presence of the YSIRK-motif the RF intensity of mCh-fusion proteins was significantly increased. As shown in **Fig. 2Cc,** mCh-sec1 exhibited spot-like bright foci at or near the division septum, which very likely resulted from the highly expressed proteins that exceeded the capability of protein transport. Indeed, mCh-sec1 showed higher RF than mCh-sec2 in both the supernatant and the cell pellet (**Fig. 2A**), implying that mCh-sec1 was expressed in a higher amount than mCh-sec2. The tendency that proteins fused with SP_{lip} (+YSIRK) were always higher expressed was observed in all mCh-constructs as well as in all GFP-fusions (**Fig. S3B**). The difference in protein expression was most likely due to different SPs, as the plasmid, promoter, and RBS were identical in all constructs. Whether transcriptional or post-transcriptional regulation was responsible for the positive effect of the SP (+YSIRK) needs to be verified. In principle, we could confirm earlier results that *S. aureus* distinguishes between SPs to either direct (+YSIRK)-proteins to the cross wall (cell division site) or (-YSIRK)-proteins to the side wall [9]. How the targeting is accomplished is unknown, but one cannot rule out that the different targeting is due to the different expression levels of +/−YSIRK-motif proteins. It is worthwhile to investigate the influence of expression rate on targeting.

One of the most interesting findings of our study was the effect of sub-lethal concentrations of penicillin or moenomycin. These two antibiotics provoke concentration of cell wall-anchored mCh-cw1&2 at the cross wall, irrespective of their SP-type (**Fig. 3B**). The antibiotics also had an effect on secreted mCh-sec1&2; here it looked as if the release of mCh-sec was retarded, leading to an

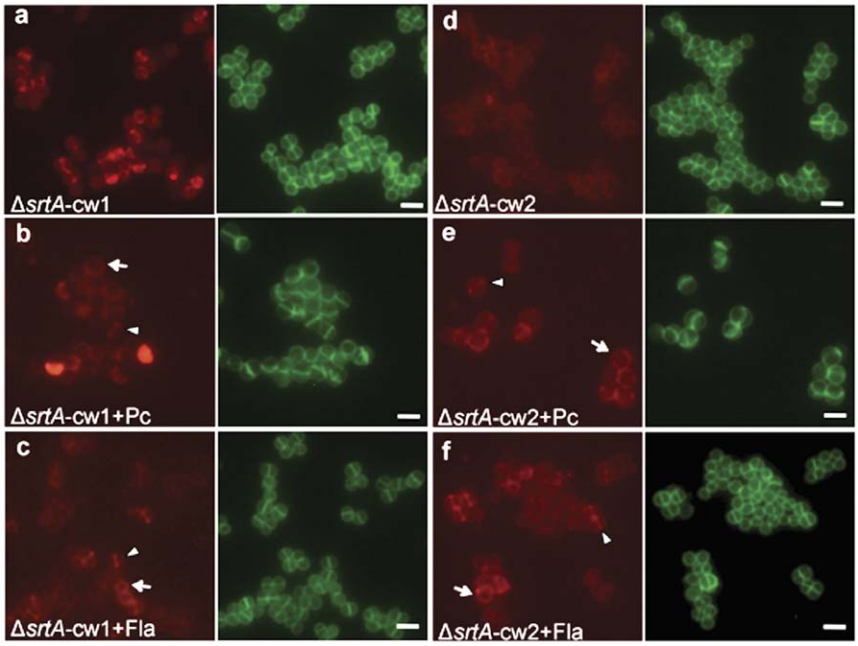

Figure 5. Localization patterns of Δ*srtA* (pCXmCh-cw1&2) in the presence of penicillin or moenomycin. Arrows, mCh-cw dispersed over the entire cell; arrowheads, the cross wall localized mCh-cw. Scale bar, 2 μm.
doi:10.1371/journal.pone.0030076.g005

accumulation at or near cross wall sites of the cell envelope (**Fig. S2**). We also addressed the question of which role SrtA might play in targeting. In Δ*srtA*, proteins remain at least transiently in the membrane via their C-terminal CWS domain. In the absence of antibiotics a similar distribution of mCh-cw was observed in Δ*srtA*, as in WT. In Δ*srtA*-mCh-cw1, mCh was more accumulated in the cross wall and in Δ*srtA*-mCh-cw2, mCh was more abundant in the side wall (**Fig. 5a,d**). The effect of penicillin and moenomycin in the Δ*srtA* mutant was, however, not as pronounced as in the WT.

In the presence of penicillin or moenomycin, not only mCh-cw but also Van-FL was concentrated in the cross wall, indicating that there is an increased content of free D-Ala-D-Ala residues (e.g., uncross-linked pentaglycine bridges or lipid II molecules), which represent the substrates for the SrtA transpeptidation reaction. Such an accumulation of uncross-linked peptidoglycan precursors can be postulated since penicillin and moenomycin are known to bind to the active site of PBPs, thus blocking the transpeptidation and transglycosylation, respectively [29,30]. It was surprising that vancomycin had little effect on mCh-cw distribution, as theoretically vancomycin inhibits both transpeptidation and transglycosylation. The previously described inhibiting effect of vancomycin is most likely due to the 10-times higher concentration used in their studies causing a complete inhibition of transpeptidation or transglycosylation [5,18].

This paper is more than the introduction of a new experimental approach. We used this new tool to directly follow the targeting and anchoring of various mCh-hybrid constructs. We found that the SPs with or without YSIRK motif targeted proteins to different subcellular localizations. However, in the presence of sub-lethal concentrations of penicillin and moenomycin the influence of SP in targeting was abrogated as all anchored mCh-cw was concentrated at the cross wall. We assume that the antibiotics cause accumulation of SrtA substrates at the cross wall, which attract SrtA to incorporate the mCh-cw almost exclusively at the cross wall, irrespective of SP type. With this study we contribute to better understanding the influence of different signal peptide types in targeting anchored and secreted proteins and the role of cell wall antibiotics.

Materials and Methods

Bacterial stains and growth conditions

The bacteria strains used were *S. aureus* SA113, SA113 Δ*srtA* [31], *S. carnosus* TM300, and *S. carnosus* TM300 Δ*srtA* [32]. To perform Western blotting analysis und avoid the interference of protein A in SA113 Δ*srtA*, SA113 Δ*spa*Δ*srtA* was generated by transducing Δ*srtA*::erm to a marker-less SA113 Δ*spa* strain (this study). Generally, pre-cultures of staphylococci were cultivated at 37°C in Basic Medium (BM) composed of 1% peptone, 0.5% yeast extract, 0.5% NaCl, 0.1% glucose and 0.1% K_2HPO_4. Overnight pre-cultures were diluted to $OD_{578} = 0.1$ in fresh BO medium (BM without glucose); 0.5% xylose was added at $OD_{578} = 0.5$ to induce genes' expression, if not stated specifically. When necessary, cultures were supplemented with chloramphenicol 10 μg/ml (Sigma), erythromycin 5 μg/ml (Sigma).

Construction of plasmids

Standard techniques were used for DNA manipulation and polymerase chain reaction (PCR) [33]. Electroporation of staphylococci was performed as described previously [34]. Plasmids isolation and DNA fragments purification were done using commercial kits from Qiagen. Enzymes used to manipulate DNA were from New England BioLabs or Fermentas. Oligonucleotides were synthesized from biomers.net GmbH (Ulm, Germany). DNA sequencing was performed by GATC Biotech AG (Konstanz, Germany).

The backbone for plasmid construction was pCX30 and its derivatives pCX30Δ82 [13]. pCXmCh-cw1 was constructed by the replacement of the mature *lipase* gene fragment with *mCherry* in pCX30Δ82. The *mCherry* gene without stop codon was amplified from plasmid pJCL61 (a gift from P. L. Graumann) by using primers mch1 (ATACCGCCTAGGATGGTGAGCAAGGGC-

GAGGAGGATA) and mch2 (TTATGCAAGCTTCCCTTG-TACAGCTCGTCCATGCCGCCGGT). The PCR product was digested with AvrII-HindIII and cloned into pCX30Δ82, resulting in an in-frame fusion of mCherry with the N-terminal lipase signal peptide (SP_{lip}) and propeptide (PP_{lip}), together with the C-terminal cell wall sorting sequence (CWS). To construct pCXmCh-cw2, the signal peptide sequence of *sasF* (SP_{sasF}) was amplified from the chromosomal DNA of SA113 by using primers mch3 (CGCGGATCCGAGGAGGTTTAATTAATGTTGAT-GGCTAAATATCGAGGGAAACCGTTT) and mch4 (CTC-GCATGCAGCTTGGGCATCGTACGGCAAGATATTC). Primers mch5 (CTCGCATGCAATGATTCGACAACACAAAC-AACGA) and mch2 were used to amplify *pp-mCherry* fragment from pCXmCh-cw1. The PCR products of SP_{sasF} and *pp-mCherry* were digested with SphI and ligated together. The ligation mixture was used as the template for another round of PCR using primers mch3 and mch2 to produce the SP_{sasF}-*pp-mCherry* fusion. SP_{sasF}-*pp-mCherry* fusion was restricted by BamHI-HindIII and cloned into the same digested pCX30Δ82. To construct pCXmCh-cyto, the *pp-mCherry* fragment containing the Shine-Dalgarno sequence and the stop codon was amplified from pCXmCh-cw1 by primers mch6 (TATGCGGATCCTATCTAGGAGGTATTAATTAT-GAATGATTCGACAACACAAACAACGACA) and mch7 (TT-ATGCTCTAGACTACTTGTACAGCTCGTCCATGCCGCC-GGT), digested with BamHI-XbaI and ligated with BamHI-XbaI restricted pCX30Δ82. To construct pCXmCh-sec1, the DNA fragment of *mCherry* amplified by primers mch1 and mch7 was restricted with AvrII-XbaI and cloned into pCX30Δ82. pCXmCh-sec2 was constructed by digesting SP_{sasF}-*pp-mCherry* PCR product from primers mch3 and mch7 with BamHI-XbaI, and subsequent ligation with similarly digested pCX30Δ82.

Enzymatic release, fluorescence measurement and Western blotting

Cultures of *S. aureus* SA113 harboring pCX30Δ82 and mCh-hybrid plasmids were un-induced (as control) and induced with xylose followed by two hours of continued growth. Cells were harvested by centrifugation at 13,000×*g* for 15min. Supernatant was filtered before fluorescence measurement. Cell pellets were washed three times with Tris buffer (50 mM Tris, 150 mM NaCl, pH 7.5). Afterwards, cells were resuspended in Tris buffer supplemented with 0.5 M sucrose and normalized to the same $OD_{578} = 1$. 200 µl of the cell suspensions were treated with 25 µg/ml lysostaphin (Genmedics, Reutlingen, Germany) at 37°C for 10 min followed by immediate centrifugation at 13,000×*g* for 15min. The supernatant and the cell pellet after digestion were collected separately for fluorescence measurement. mCherry's RF signals were measured at 580nm excitation and 630nm emission wavelength by Tecan infinite 200 Microplate Reader (Tecan Group Ltd., Männedorf, Switzerland). SA113 without plasmids or the BO medium served as negative controls. The fluorescence intensity of supernatant was divided by the OD of the harvesting time. To perform the Western blotting analysis, mCh-hybrids were transformed into SA113 Δ*spa* and SA113 Δ*spa*Δ*srtA*. After the same induction procedure as for SA113 WT, the filtered culture supernatant was collected and normalized according to the OD of the harvesting time. Proteins were precipitated with 10% trichloroacetic acid (TCA), washed in acetone and dried in SpeedVac for 1 min. The pellet was resuspended in 1× loading buffer for SDS-PAGE and Western blotting. Hybrid proteins were detected by a rabbit polyclonal anti-mCherry antibody (Antibodies-online GmbH, Aachen, Germany).

Antibiotics treatment and growth curve monitoring

To optimize the concentration of each antibiotic used in this study, series dilutions from 0 to 10×MIC of antibiotics was added into cultures of SA113 at $OD_{578} = 0.1$ in the BO medium. 0.5% xylose was added at $OD_{578} = 0.5$. OD_{578} was measured every hour. The final concentration was determined as the growth of bacteria was partially inhibited but still viable. The final concentrations used were: penicillin G 0.02 µg/ml (Serva, Heidelberg, Germany), moenomycin (flavomycin) 1 µg/ml (Sigma), bacitracin 2 µg/ml (Sigma), vancomycin 0.5 µg/ml (Sigma), tunicamycin 1 µg/ml (Serva, Heidelberg, Germany), gallidermin 0.1 µg/ml (Genmedics, Reutlingen, Germany), D-cycloserine 20 µg/ml (Sigma).

Fluorescence microscopy

Cell wall and cross walls were visualized by fluorescence labeled vancomycin (BODIPY® FL vancomycin, Van-FL) staining [35] Cell samples taken at desired times were mixed with 1 µg/ml Van-FL (Invitrogen) and incubated for 5 min in the dark. 10 µl cell suspension was applied to the glass slide covered with 2% agarose. Fluorescent microscopy was performed with Leica DM5500 B Upright microscope. Images were captured with Leica DFC360 FX high-sensitivity monochrome digital camera. 504 ms exposure time was used for mCherry RF images. Fluorescence quantification was performed using Leica Application Suite Advanced Fluorescence software and ImageJ software.

Supporting Information

Figure S1 Quantification of visible cross walls and cross wall localized RF in the presence of penicillin or moenomycin. A. Percentage of visible cross walls. The percentage was the ratio of visible cross wall numbers in a cell population versus the total cell numbers of the same cell population. Cross wall numbers were counted when Van-FL staining appeared as a line at the septum before daughter cells split (closed cross wall). More than 1000 cells from three independent experiments were counted. **B.** Percentage of cross wall localized RF. The percentage was the ratio of numbers of line-like cross wall localized RF versus line-like cross walls (visible by Van-FL staining) in the same cell population. The total cells numbers counted were above 1000 from three independent experiments for every bar. Statistical analysis was performed using Student's *t*-test. *P*-values of statistic analysis between treated and untreated cells (inter-group comparison) were marked above the bar of the corresponding treated group; *P*-values of intra-group comparison were marked on the horizontal line. $*P<0.05$, $**P<0.01$, $***P<0.005$.
(TIF)

Figure S2 Localization patterns of SA113 (pCXmCh-sec1&2) in the presence of penicillin or moenomycin. Arrows in **b** and **e** indicted half-moon distribution of mCh-sec; arrows in **c** and **f** indicated dispersed mCh-sec over the entire cell; arrowheads, cross wall localized mCh-sec.
(TIF)

Figure S3 Fluorescence intensity and Western blotting comparison between secreted GFP- and mCh-hybrids. A. Fluorescence intensity of the culture supernatant from GFP/mCh-hybrids. The vertical axis indicated the ratio of the fluorescence intensity compared to the blank. **B.** Western blotting of the culture supernatant from GFP/mCh-hybrids. All of the GFP-hybrid plasmids were constructed in the same way as the mCh-hybrids and expressed in the protein A deficient mutant SA113 Δ*spa*. Blank, SA113 Δ*spa* without plasmid; GFP, SA113

Δ*spa* (pCX-*gfpmut3*); ppGFP, SA113 Δ*spa* (pCX-pp_{lip}*gfpmut3*); ppGFP-sec1, SA113 Δ*spa* (pCX-$sp_{lip}pp_{lip}$*gfpmut3*); ppGFP-sec2, SA113 Δ*spa* (pCX-$sp_{sasF}pp_{lip}$*gfpmut3*); sfGFP, SA113 Δ*spa* (pCX-*sfgfp*); ppsfGFP, SA113 Δ*spa* (pCX-pp_{lip}*sfgfp*); ppsfGFP-sec1, SA113 Δ*spa* (pCX-$sp_{lip}pp_{lip}$*sfgfp*); ppsfGFP-sec2, SA113 Δ*spa* (pCX-$sp_{sasF}pp_{lip}$*sfgfp*); ppmCh, SA113 Δ*spa* (pCXmCh-cyto); ppmCh-sec1, SA113 Δ*spa* (pCXmCh-sec1); ppmCh-sec2, SA113 Δ*spa* (pCXmCh-sec2). Arrows indicated the unprocessed (upper band) or the processed (lower band) form of the secreted GFP/mCh fusions.
(TIF)

Acknowledgments

We thank Prof. Karl Forchhammer for his assistance in microscopy analysis.

Author Contributions

Conceived and designed the experiments: WY FG. Performed the experiments: WY. Analyzed the data: WY FG. Contributed reagents/materials/analysis tools: WY FG. Wrote the paper: WY FG.

References

1. Schneewind O, Model P, Fischetti VA (1992) Sorting of protein A to the staphylococcal cell wall. Cell 70: 267–281.
2. Foster TJ, Höök M (1998) Surface protein adhesins of *Staphylococcus aureus*. Trends Microbiol 6: 484–488.
3. Marraffini LA, Dedent AC, Schneewind O (2006) Sortases and the art of anchoring proteins to the envelopes of gram-positive bacteria. Microbiol Mol Biol Rev 70: 192–221.
4. Mazmanian SK, Liu G, Ton-That H, Schneewind O (1999) *Staphylococcus aureus* sortase, an enzyme that anchors surface proteins to the cell wall. Science 285: 760–763.
5. Perry AM, Ton-That H, Mazmanian SK, Schneewind O (2002) Anchoring of surface proteins to the cell wall of *Staphylococcus aureus*. III. Lipid II is an in vivo peptidoglycan substrate for sortase-catalyzed surface protein anchoring. J Biol Chem 277: 16241–16248.
6. Rosenstein R, Götz F (2000) Staphylococcal lipases: biochemical and molecular characterization. Biochimie 82: 1005–1014.
7. Bae T, Schneewind O (2003) The YSIRK-G/S motif of staphylococcal protein A and its role in efficiency of signal peptide processing. J Bacteriol 185: 2910–2919.
8. Carlsson F, Stalhammar-Carlemalm M, Flardh K, Sandin C, Carlemalm E, et al. (2006) Signal sequence directs localized secretion of bacterial surface proteins. Nature 442: 943–946.
9. DeDent A, Bae T, Missiakas DM, Schneewind O (2008) Signal peptides direct surface proteins to two distinct envelope locations of *Staphylococcus aureus*. EMBO J 27: 2656–2668.
10. Frankel MB, Wojcik BM, DeDent AC, Missiakas DM, Schneewind O (2010) ABI domain-containing proteins contribute to surface protein display and cell division in *Staphylococcus aureus*. Mol Microbiol 78: 238–252.
11. DeDent AC, McAdow M, Schneewind O (2007) Distribution of protein A on the surface of Staphylococcus aureus. J Bacteriol 189: 4473–4484.
12. Hahn JJ, Cole RM (1963) Streptococcal M Antigen Location and Synthesis, Studied by Immunofluorescence. J Exp Med 118: 659–666.
13. Strauss A, Götz F (1996) In vivo immobilization of enzymatically active polypeptides on the cell surface of *Staphylococcus carnosus*. Mol Microbiol 21: 491–500.
14. Müller-Anstett MA, Müller P, Albrecht T, Nega M, Wagener J, et al. (2010) Staphylococcal peptidoglycan co-localizes with Nod2 and TLR2 and activates innate immune response via both receptors in primary murine keratinocytes. PLoS One 5: e13153.
15. Wieland KP, Wieland B, Götz F (1995) A promoter-screening plasmid and xylose-inducible, glucose-repressible expression vectors for *Staphylococcus carnosus*. Gene 158: 91–96.
16. Demleitner G, Götz F (1994) Evidence for importance of the *Staphylococcus hyicus* lipase pro-peptide in lipase secretion, stability and activity. FEMS Microbiol Lett 121: 189–197.
17. Sturmfels A, Götz F, Peschel A (2001) Secretion of human growth hormone by the food-grade bacterium *Staphylococcus carnosus* requires a propeptide irrespective of the signal peptide used. Arch Microbiol 175: 295–300.
18. Ton-That H, Schneewind O (1999) Anchor structure of staphylococcal surface proteins. IV. Inhibitors of the cell wall sorting reaction. J Biol Chem 274: 24316–24320.
19. Kellner R, Jung G, Hörner T, Zähner H, Schnell N, et al. (1988) Gallidermin: a new lanthionine-containing polypeptide antibiotic. Eur J Biochem 177: 53–59.
20. Brötz H, Josten M, Wiedemann I, Schneider U, Götz F, et al. (1998) Role of lipid-bound peptidoglycan precursors in the formation of pores by nisin, epidermin and other lantibiotics. Mol Microbiol 30: 317–327.
21. Lambert MP, Neuhaus FC (1972) Mechanism of D-cycloserine action: alanine racemase from *Escherichia coli* W. J Bacteriol 110: 978–987.
22. Shaner NC, Campbell RE, Steinbach PA, Giepmans BN, Palmer AE, et al. (2004) Improved monomeric red, orange and yellow fluorescent proteins derived from *Discosoma* sp. red fluorescent protein. Nat Biotechnol 22: 1567–1572.
23. Chen JC, Viollier PH, Shapiro L (2005) A membrane metalloprotease participates in the sequential degradation of a *Caulobacter* polarity determinant. Mol Microbiol 55: 1085–1103.
24. Lewenza S, Vidal-Ingigliardi D, Pugsley AP (2006) Direct visualization of red fluorescent lipoproteins indicates conservation of the membrane sorting rules in the family *Enterobacteriaceae*. J Bacteriol 188: 3516–3524.
25. Cormack BP, Valdivia RH, Falkow S (1996) FACS-optimized mutants of the green fluorescent protein (GFP). Gene 173: 33–38.
26. Feilmeier BJ, Iseminger G, Schroeder D, Webber H, Phillips GJ (2000) Green fluorescent protein functions as a reporter for protein localization in *Escherichia coli*. J Bacteriol 182: 4068–4076.
27. Pedelacq JD, Cabantous S, Tran T, Terwilliger TC, Waldo GS (2006) Engineering and characterization of a superfolder green fluorescent protein. Nat Biotechnol 24: 79–88.
28. Uehara T, Parzych KR, Dinh T, Bernhardt TG (2010) Daughter cell separation is controlled by cytokinetic ring-activated cell wall hydrolysis. EMBO J 29: 1412–1422.
29. Izaki K, Matsuhashi M, Strominger JL (1966) Glycopeptide transpeptidase and D-alanine carboxypeptidase: penicillin-sensitive enzymatic reactions. Proc Natl Acad Sci U S A 55: 656–663.
30. van Heijenoort Y, Leduc M, Singer H, van Heijenoort J (1987) Effects of moenomycin on *Escherichia coli*. J Gen Microbiol 133: 667–674.
31. Weidenmaier C, Kokai-Kun JF, Kulauzovic E, Kohler T, Thumm G, et al. (2008) Differential roles of sortase-anchored surface proteins and wall teichoic acid in *Staphylococcus aureus* nasal colonization. Int J Med Microbiol 298: 505–513.
32. Leibig M, Krismer B, Kolb M, Friede A, Götz F, et al. (2008) Marker removal in staphylococci via Cre recombinase and different lox sites. Appl Environ Microbiol 74: 1316–1323.
33. Sambrook J, Fritsch, E. F, Maniatis, T (1989) Molecular Cloning: a Laboratory Manual. New York: Cold Spring Harbor Laboratory Press.
34. Löfblom J, Kronqvist N, Uhlen M, Stahl S, Wernerus H (2007) Optimization of electroporation-mediated transformation: *Staphylococcus carnosus* as model organism. J Appl Microbiol 102: 736–747.
35. Pinho MG, Errington J (2003) Dispersed mode of *Staphylococcus aureus* cell wall synthesis in the absence of the division machinery. Mol Microbiol 50: 871–881.

WIPI-1 positive autophagosome-like vesicles entrap pathogenic *Staphylococcus aureus* for lysosomal degradation

Mario Mauthe[1], Wenqi Yu[2], Oleg Krut[3], Martin Krönke[3], Friedrich Götz[2], Horst Robenek[4], and Tassula Proikas-Cezanne[1]*

[1]Autophagy Laboratory, Interfaculty Institute for Cell Biology, University of Tübingen; [2]Microbial Genetics, Interfaculty Institute for Microbiology and Infectious Medicine, University of Tübingen; [3]Institute for Medical Microbiology, Immunology and Hygiene, University of Cologne; [4]Leibniz Institute for Arteriosclerosis Research, University of Münster, Germany.

*Corresponding author: Tassula Proikas-Cezanne, Autophagy Laboratory, Interfaculty Institute for Cell Biology, Eberhard Karls University Tübingen, Auf der Morgenstelle 15, 72076 Tübingen, Germany, Phone: +49 7071 2978895, FAX: +49 7071 295359, Email: tassula.proikas-cezanne@uni-tuebingen.de

Abstract

Invading pathogens provoke the autophagic machinery and in a process termed xenophagy, the host cell survives because autophagy is employed as a safeguard for pathogens that escaped phagosomes. However, some pathogens can manipulate the autophagic pathway and replicate within the niche of generated autophagosome-like vesicles. By automated, fluorescence-based high content analyses, we demonstrate that *Staphylococcus aureus* strains (USA300, HG001, SA113) stimulate autophagy, and become entrapped in intracellular PtdIns(3)P-enriched vesicles that are decorated with human WIPI-1, an essential PtdIns(3)P effector of canonical autophagy and membrane protein of both phagophores and autophagosomes. Further, *agr*-positive *S. aureus* (USA300, HG001) strains were more efficiently entrapped in WIPI-1 positive autophagosome-like vesicles when compared to *agr*-negative cells (SA113). By confocal and electron microscopy we provide evidence that single and multiple Staphylococci entrapped undergo cell division. Moreover, the number of WIPI-1 positive autophagosome-like vesicles entrapping Staphylococci significantly increased upon i) lysosomal inhibition by bafilomycin A_1 and ii) blocking PIKfyve-mediated PtdIns(3,5)P_2 generation by YM201636. In summary, our results provide evidence that the PtdIns(3)P effector function of WIPI-1 is utilized during xenophagy of *Staphylococcus aureus*. We suggest that invading *S. aureus* cells become entrapped in autophagosome-like WIPI-1 positive vesicles targeted for lysosomal degradation in non-professional host cells.

Keywords: WIPI-1, Atg18, *Staphylococcus aureus*, PtdIns(3)P, autophagy.

Introduction

Macroautophagy (hereafter autophagy) is a cytoprotective, cellular degradation mechanism for long-lived proteins and organelles [1]. Autophagy is specific to eukaryotic cells and important for cellular survival by enabling a constitutive clearance and recycling of cytoplasmic material (basal autophagy). Crucial to the process of autophagy is the fact, that cytoplasmic material is stochastically degraded. Portions of the cytoplasm become randomly sequestered in unique, double-membrane vesicles, autophagosomes. Autophagosomes are generated by elongation and closure of a membrane precursor, the phagophore. Subsequently, autophagosomes fuse with lysosomes to acquire acidic hydrolases for cargo degradation [2]. This stochastic, constitutive form of autophagy provides constant clearance of the cytoplasm. Upon stress, such as starvation, the autophagic activity is induced above basal level to compensate nutrient shortage by providing monomeric constituents, such as amino acids, and energy. Conversely, under nutrient-rich conditions autophagy is suppressed by the mTORC1 signaling circuit [3]. Importantly, autophagy is also activated in a specific manner and targets damaged organelles, protein aggregates or pathogens for degradation [4]. Both, stochastic and specific autophagy are crucial to secure cellular homeostasis [5].

Prerequisite for the formation of autophagosomes is the generation of an essential phospholipid, phosphatidylinositol 3-phosphate (PtdIns(3)P), a result of the activity of the phosphatidylinositol 3-kinase class III (PtdIns3KC3) in complex with Beclin 1, p150 and Atg14L [6, 7]. The PtdIns(3)P signal is decoded through PtdIns(3)P-binding effectors specific to autophagy, such as the human WIPI proteins [8]. WIPI-1 (Atg18 in yeast) specifically binds PtdIns(3)P at the phagophore and fosters the recruitment of two ubiquitin-like conjugation systems, Atg12 and LC3, involved in autophagosome elongation and closure [9]. Subsequently, WIPI-1 becomes a membrane protein of autophagosomes where it localizes at both the inner and outer membrane [10, 11]. Hence the specific localization of WIPI-1 at the phagophore and at autophagosomes upon the initiation of autophagy can monitor the process of canonical autophagy, as it is dependent on the PtdIns(3)P signal [11].

The process of autophagy is closely connected with a variety of diseases such as tumor development, neurodegeneration, and with cellular responses to pathogens, including viral infection and bacterial cell invasion [5, 12]. *Staphylococcus aureus*, a major pathogen for nosocomial infectious diseases was initially characterized as an extracellular pathogen, but was later found to also target non-professional host cells like keratinocytes, fibroblasts, endothelial cells and epithelial cells where invading *S. aureus* liberates from the endosomal compartment [13]. In HeLa cells, *S. aureus* was found to become sequestered and to

replicate in autophagosome-like vesicles as a result of autophagosome/lysosome fusion block, which ultimately leads to cell death [14].

Here, we visualized the invasion of mCherry-expressing *S. aureus* strains USA300, HG001, SA113 in human U2OS tumor cells that stably express GFP-WIPI-1 for automated, fluorescence-based high content analyses, a procedure that monitors the autophagic process and that we have established earlier [15]. We provide evidence that *S. aureus* stimulates canonical autophagy in non-professional host cells, and become entrapped in non-canonical WIPI-1 positive autophagosome-like vesicles. Time course experiments showed that the number of tumor cells that contain such WIPI-1 positive autophagosome-like vesicles with entrapped *S. aureus* cells increased over time (30 min – 2 h). After an infection period of 2 h, 40 – 50% of the cells harbored WIPI-1 positive autophagosome-like vesicles sequestering *agr*-positive *S. aureus* (USA300, HG001), and 20% of the tumor cells contained entrapped *agr*-negative *S. aureus* (SA113). Importantly, we demonstrate that the number of WIPI-1 positive autophagosome-like vesicles harboring *S. aureus* significantly increased upon lysosomal inhibition, strongly arguing for the degradation of *S. aureus* through xenophagy. In addition, by employing GFP-FYVE and a selective PIKfyve inhibitor (YM201636) we further demonstrate the requirement of PtdIns(3)P-enriched membranes during the process of entrapping invading *S. aureus*.

Material and methods

Eukaryotic cell culture. The human osteosarcoma cell line U2OS (ATCC) was cultured in DMEM (Invitrogen) supplemented with 10% FCS (PAA), 100 U/ml penicillin/ 100 µg/ml streptomycin (Invitrogen), 5µg/ml plasmocin (Invivogen) at 37°C, 5% CO_2. Monoclonal human U2OS cell clones stably expressing either GFP-WIPI-1 [15, 16] or GFP-2xFYVE [9] were cultured in DMEM (Invitrogen) supplemented with 10% FCS (PAA), 100 U/ml penicillin/ 100 µg/ml streptomycin (Invitrogen), 5µg/ml plasmocin (Invivogen), 0.6 mg/ml G418 (Invitrogen) at 37°C, 5% CO_2. The following media were used for treatments: DMEM/FCS (DMEM supplemented with 10% FCS), DMEM (DMEM without FCS), EBSS (Sigma-Aldrich).

Bacterial strains. *S. aureus* USA300, HG001, SA113 or *S. carnosus* TM300 [17] were electroporated with the pCtuf-*ppmch* plasmid. The pCtuf-*ppmch* plasmid encoded mCherry fused with the propeptide of lipase for fluorescence enhancement, and *ppmch* expression was controlled by the native constitutive EF-Tu promotor. Electroporated bacterial strains were grown in Basic medium (1% peptone, 0.5% yeast extract, 0.5% NaCl, 0.1% glucose, 0.1% K_2HPO_4) at 37°C to an OD_{600} of 0.8, and harvest by centrifugation.

Bacterial infection of eukaryotic host cells. GFP-WIPI-1 expressing U2OS cells were seeded in 96-well plates (Brand) in DMEM/10% FCS 20 hours before bacterial infection. *S. aureus* (USA300, HG001, SA113) or *S. carnosus* carrying the pCtuf-*ppmch* plasmid, were diluted in DMEM, DMEM/10% FCS or EBSS (SIGMA-Aldrich) to an m.o.i of 100, added to the GFP-WIPI-1 U2OS cells and incubated for 0.5, 1 or 2 hours at 37°C, 5% CO_2. Alternatively, *S. aureus* USA300 cells were diluted (m.o.i of 100) in DMEM/FCS supplemented with either bafilomycin A_1 (200 nM, Sigma-Aldrich) or YM201636 (800 nM, Cayman Chemicals) or with both and used to infect GFP-WIPI-1 expressing U2OS cells for 2 hours at 37°C, 5% CO_2. Alternatively, GFP-2xFYVE expressing U2OS cells [15, 16] were infected with *S. aureus* USA300 (in DMEM/FCS) for 2 hours at 37°C, 5% CO_2.

Autophagy assay. GFP-WIPI-1 expressing U2OS cells, seeded in 96-well plates, were treated with nutrient-rich culture medium (DMEM/10% FCS), culture medium lacking serum (DMEM) or medium lacking serum and amino acids (EBSS) for 0.5, 1 or 2 hours. After fixation with 3.7% paraformaldehyde for 30 minutes, autophagy was accessed by WIPI-1 puncta formation analysis [11, 18] (see below).

Confocal laser scanning microscopy. Confocal microscopy was conducted as previously described [8]. Images were acquired using a LSM510 microscope (Zeiss) and a 63 x 1.4 DIC Plan-Apochromat oil-immersion objective. 8-10 optical sections (0.5µm) were acquired. Both, single optical sections as well as projections from 8-10 optical sections are presented.

Automated fluorescence image acquisition and analysis. Stable GFP-WIPI-1 U2OS cells were automatically imaged and analysed using the *In Cell Analyzer 1000* (GE Healthcare) as described earlier [9, 15]. Cells exposed to bacteria (see above) were stained with DAPI (5 µg/ml; Applichem). Fluorescence images were automatically acquired with a Nikon 40x Planfluor objective and the excitation/emission filter D360_40X/HQ460_40M (DAPI), HQ535_50X/HQ620_60M (mCherry) and S475_20X/HQ535_50M (GFP). GFP-WIPI-1 puncta were automatically analysed as previously described [15] and the number of GFP-WIPI-1 puncta-positive cells as well as the number of GFP-WIPI-1 puncta per cell was determined. Red fluorescent bacteria were automatically analysed by using the *Dual Area Object Analysis*. The algorithms *Inclusion* and *Multiscale Top Hat* were applied and the total area of bacterial fluorescence within the cell was determined. To determine the number of cells containing GFP-WIPI-1 positive autophagosome-like vesicles sequestering bacteria, automatically acquired fused images (DAPI, GFP, mCherry) of 100 individual cells for each treatment were analyzed.

Electron microscopy. Stable GFP-WIPI-1 U2OS cells were infected with *S. aureus* USA300 (m.o.i of 100) in DMEM/FCS and fixed in 2% glutaraldehyde and 0.5% osmium tetroxide in 0.1 M PBS, dehydrated with ethanol, and embedded in Epon using standard

procedures as previously described [19]. Thin sections were cut using an ultramicrotome and contrasted with uranyl acetate and lead citrate. Thin sections were examined in an EM410 electron microscope (Philipis) and documented digitally (Ditabis).

Statistical analysis. Statistical significance was evaluated using two-tailed heteroscedastic *t*-testing and *p*-values were calculated.

Results

Visualizing basal and induced autophagy by automated GFP-WIPI-1 image acquisition and analysis. The WIPI-1 puncta-formation assay allows the assessment of the evolutionarily conserved, PtdIns(3)P-dependent initiation of autophagy on the basis of fluorescence microscopy, previously employed by using confocal microscopy or automated image acquisition and analysis [11, 15]. Thereby, endogenous WIPI-1 can be visualized by indirect immunofluorescence, or alternatively by introducing GFP-WIPI-1 as conducted in the present study. Fluorescent WIPI-1 puncta reflect the accumulation of WIPI-1 at membranes via its specific binding to PtdIns(3)P, found to represent phagophores and autophagosomes [10, 11]. In addition, WIPI-1 binds to PtdIns(3)P at the endoplasmic reticulum and at the plasma membrane upon the induction of autophagy, indicative for membrane origins where phagophore/autophagosome formation is initiated by unknown mechanisms [10]. Here, we employed automated GFP-WIPI-1 image acquisition and analysis as follows. Human U2OS cells that stably express GFP-WIPI-1 were seeded in 96-well plates and basal autophagy, and starvation-induced autophagy was monitored in up to 3000 individual cells per treatment over time (Figure 1). After an incubation period of 0.5, 1 or 2 h with nutrient-rich culture medium (DMEM/FCS), basal autophagic activity was found in appr. 10% of the cells (Figure 1A, 1D). Serum starvation (DMEM) elevated the number of GFP-WIPI-1 puncta-positive cells to appr. 50% (Figure 1B, 1D), and both serum- and amino acid starvation (EBSS) further elevated this number to appr. 85% (Figure 1C, 1D). In addition, we demonstrate that with regard to nutrient-rich medium (DMEM/FCS), the number of GFP-WIPI-1 puncta per cell also increased upon either serum (DMEM) and prominently upon both serum- and amino acid starvation (EBSS) (Figure 1E). These culture media (DMEM/FCS, DMEM, EBSS) were used in the following experiments to infect GFP-WIPI-1 expressing U2OS cells with mCherry-expressing Staphylococci.

Formation of GFP-WIPI-1 positive autophagosome-like vesicles upon *Staphylococcus aureus* infection. Upon infection of GFP-WIPI-1 U2OS cells with pathogenic Staphylococci, here *S. aureus* HG001, in nutrient-rich medium (DMEM/FCS) we identified canonical, autophagosomal GFP-WIPI-1 membranes (Figure 2A, 2B) and new

GFP-WIPI-1 autophagosome-like vesicles that were both larger in diameter with decreased fluorescence intensity (Figure 2C) when compared to the canonical GFP-WIPI-1 puncta. GFP-WIPI-1 autophagosome-like vesicles (Figure 2C) were rarely observed when starvation media (DMEM, EBSS) were used during the infection with *S. aureus* HG001 (Suppl. Figure 1).

To monitor and quantify this particular GFP-WIPI-1 response upon mCherry-expressing Staphylococci in an automated fashion (Figure 3), cells were stained with DAPI and by using three different excitation/emission filters. DAPI, GFP and mCherry fluorescence images were acquired (Figure 3). Up to 2723 individual cells per treatment were automatically analysed and recognized by both DAPI and the overall cellular GFP fluorescence. GFP images were used to automatically detect and determine the number of cells harboring GFP-WIPI-1 puncta by applying a decision tree as previously described [15]. Additionally, mCherry fluorescence was used to automatically determine the fluorescence area, reflecting the amount of intracellular Staphylococci. For the quantification of cells harboring GFP-WIPI-1 positive autophagosome-like vesicles entrapping Staphylococci, fused images (DAPI, GFP, mCherry) of 100 individual cells were used (Figure 3).

Pathogenic *Staphylococcus aureus* USA300, HG001 and SA113 stimulated canonical autophagosome formation and became entrapped in GFP-WIPI-1 positive autophagosome-like vesicles. In the following experiment, GFP-WIPI-1 expressing U2OS cells were infected for 0.5, 1 and 2 h with mCherry-expressing *S. aureus* USA300 (Figure 4, Suppl. Figure 2), HG001 (Figure 5, Suppl. Figure 3) or SA113 (Figure 6, Suppl. Figure 4) either in nutrient-rich medium (DMEM/FCS), serum-free medium (DMEM) or serum- and amino acid-free medium (EBSS). Subsequently, fluorescence images (appr. 2000 individual cells per treatment) were automatically acquired and analyzed as described (Figure 3). Please note that the control experiments in Figure 1 were conducted in parallel to the experiments presented in Figure 4 – 7 hence provide the comparison for conditions without (Figure 1) and with (Figures 4 – 7, Suppl. Figures 2 – 5) Staphylococci.

As shown in Figure 1, under nutrient rich conditions (DMEM/FCS) the number of GFP-WIPI-1 puncta-positive cells is low (appr. 10%), reflecting cells that undergo basal autophagy. Interestingly, upon infection of GFP-WIPI-1 expressing U2OS cells with *S. aureus* USA300 in DMEM/FCS, a prominent increase of GFP-WIPI-1 puncta-positive cells (up to appr. 70% within 2 h of infection) was observed (Figure 4A, in green). In addition, the number of GFP-WIPI-1 puncta per individual cell also increased upon *S. aureus* USA300 infection in DMEM/FCS (Suppl. Figure 6B). The elevated number of GFP-WIPI-1 puncta-positive cells and GFP-WIPI-1 puncta per cell correlated with an increase of intracellular *S. aureus* USA300 (Figure 4A, in red). Using serum-free conditions either in the presence (DMEM, Figure 4B, in red) or absence of amino acids (EBSS, Figure 4C, in red), no increase

of intracellular *S. aureus* USA300 was observed. However, infection of *S. aureus* USA300 in DMEM also resulted in an increase (up to appr. 70%) of GFP-WIPI-1 puncta-positive cells (Figure 4B, in green), whereas *S. aureus* USA300 in EBSS (Figure 4C) did not trigger a further increase of the number of GFP-WIPI-1 positive cells when compared to EBSS treatment alone (Figure 1).

Next, we determined the number of cells displaying entrapped *S. aureus* USA300 within GFP-WIPI-1 positive autophagosome-like vesicles (Figure 4D, 4E). In line with the increased number of cells carrying intracellular *S. aureus* USA300 when nutrient-rich medium (DMEM/FCS) was used (Figure 4A), the number of cells with GFP-WIPI-1 positive autophagosome-like vesicles that entrap *S. aureus* USA300 (appr. 40%) also increased (Figure 4E). This was not observed by using DMEM or EBSS (Figure 4E). We also provide the control images corresponding to *S. aureus* USA300 infections using either DMEM or EBSS (Suppl. Figure 2).

The infection of stably expressing GFP-WIPI-1 U2OS cells with *S. aureus* HG001 in DMEM/FCS also triggered an elevation of GFP-WIPI-1 puncta-positive cells (up to 76%) (Figure 5A, in green) and of GFP-WIPI-1 puncta per cell (Suppl. Figure 6C). Again, the increased number of GFP-WIPI-1 puncta-positive cells correlated with an increased bacterial load (Figure 5A, in red), and the increase in the number of cells displaying GFP-WIPI-1 positive autophagosome-like vesicles entrapping *S. aureus* HG001 (appr. 40%) (Figure 5D, 5E). Also in this case, this feature was not observed by using DMEM or EBSS (Figure 5E), but DMEM conditions still triggered an increase of GFP-WIPI-1 puncta formation (Figure 5B, Suppl. Figure 6C) when compared with control setting (Figure 1, Suppl. Figure 6A). Control images corresponding to *S. aureus* HG001 infections using either DMEM or EBSS are also provided (Suppl. Figure 3).

Next, we employed the *agr*-deficient *S. aureus* strain SA113 and infected stably expressing GFP-WIPI-1 U2OS cells. Clearly, upon infection in DMEM/FCS the number of GFP-WIPI-1 puncta-positive cells increased over time to up to 60% (Figure 6A, in green), which correlated with an increasing bacterial load (Figure 6A, in red). See also the increased number of GFP-WIPI-1 puncta per cell upon *S. aureus* SA113 infection in DMEM/FCS (Suppl. Figure 6D). In contrast to the effect of the employed *agr*-positive *S. aureus* strains USA300 (Figure 4) and HG001 (Figure 5), the number of cells displaying *S. aureus* SA113 entrapped in GFP-WIPI-1 positive autophagosome-like vesicles was prominently lower (appr. 18%) (Figure 6D, 6E). However, the presence of *S. aureus* SA113 in DMEM also triggered an increase of GFP-WIPI-1 puncta-positive cells (Figure 6B) when compared to control setting (Figure 1), whereas in EBSS no further elevation was achieved (Figure 6C), and in both cases, cells did not display entrapped *S. aureus* SA113 (Figure 6E). Control images of *S. aureus* SA113 infections with either DMEM or EBSS are also provided (Suppl. Figure 4).

Apathogenic *Staphylococcus carnosus* TM300 cells were not entrapped in intracellular GFP-WIPI-1 positive autophagosome-like vesicles. In contrast to the pathogenic *S. aureus* strains (see above), infection of stably expressing GFP-WIPI-1 U2OS cells with the apathogenic *S. carnosus* TM300 did not result in an invasion of host cells in either of the used media (Figure 7A – C), in line, GFP-WIPI-1 positive autophagosome-like vesicles were not induced (Figure 7D, 7E). Control images for *S. carnosus* TM300 in DMEM or EBSS are provided (Suppl. Figure 5). Interestingly, within 2 h of incubation with *S. carnosus* TM300 in DMEM/FCS, the number of GFP-WIPI-1 puncta-positive cells increased (appr. 45%) (Figure 7A) when compared to the control setting (Figure 1), which was not observed by using DMEM (Figure 7B) or EBSS (Figure 7C). However, the number of GFP-WIPI-1 puncta per individual cell did not increase upon infection of *S. carnosus* TM300 in DMEM/FCS (Suppl. Figure 6E) when compared to uninfected condition (Suppl. Figure 6A).

Both inhibition of PtdIns(3,5)P_2 production and lysosomal inhibition increased the number of WIPI-1 positive autophagosome-like vesicles entrapping *Staphylococcus aureus*. Next, we questioned whether pathogenic *S. aureus* cells entrapped in GFP-WIPI-1 positive autophagosomal-like vesicles are degraded in the lysosome. We employed the lysosomal inhibitor bafilomycin A_1 (Baf A_1) to block autophagsosome/lysosome fusion events upon infection of GFP-WIPI-1 expressing U2OS cells with *S. aureus* USA300 in DMEM/FCS. Upon Baf A_1 addition the number of cells harboring GFP-WIPI-1 positive autophagosomal-like vesicles entrapping *S. aureus* USA300 (Figure 8A, left panel) significantly increased. And, the number of GFP-WIPI-1 positive autophagosomal-like vesicles per individual cell also significantly increased (Figure 8B, left panel). In this situation (Figure 8A, left panel; Figure 8B, left panel) we found that the bacterial load did not significantly change (Suppl. Figure 7).

Further, during infection of GFP-WIPI-1 expressing U2OS cells with *S. aureus* USA300 in DMEM/FCS we employed YM201636 (YM), a specific PIKfyve inhibitor that blocks PtdIns(3,5)P_2 production from PtdIns(3)P [20]. Upon YM treatment the number of cells harboring GFP-WIPI-1 positive autophagosomal-like vesicles (Figure 8A, left panel) and the number of the vesicles per cell (Figure 8B, left panel) significantly increased. Again, the intracellular bacterial load within the cells did not change (Suppl. Figure 7). Baf A_1/YM cotreatment had an additive effect (Figure 8A, 8B left panels). The corresponding automated GFP-WIPI-1 puncta formation analysis is also provided (Figure 8A, 8B right panels).

Confocal and electron microscopy of intracellular *Staphylococcus aureus* USA300. To achieve more image resolution, we infected GFP-WIPI-1 expressing U2OS cells with *S. aureus* USA300 in DMEM/FCS followed by confocal laser scanning microscopy (Figure 9A). Clearly, GFP-WIPI-1 positive autophagosome-like vesicles harbored multiple *S.*

aureus USA300 cells and the analysis of individual confocal sections confirmed that these vesicles are found in the cytoplasm (Figure 9A, 1 – 4).

It has been shown that *S. aureus* invading HeLa cells become sequestered in Rab7-positive endosomes [14]. As Rab7 marks late endosomes, we here used GFP-2xFYVE to visualize early endosomes. We used GFP-2xFYVE expressing U2OS cells for infection with with *S. aureus* USA300 in DMEM/FCS. Indeed, we also found, that *S. aureus* USA300 cells were entrapped in GFP-2xFYVE positive endosomes (Figure 9B, 1 – 4).

Further, by electron microscopy we found that intracellular *S. aureus* USA300 cells are entrapped in vesicles with a single *S. aureus* USA300 cell (Figure 10A), or in vesicles harboring multiple *S. aureus* USA300 cells (Figure 10B). In both cases, intracellular *S. aureus* USA300 cells showed clear signs of ongoing cell division (red arrows).

Discussion

Autophagy is considered as an ancient eukaryotic pathway for cellular self-digestion that evolved with the endomembrane system [21]. As the endomembrane system provided an opportunity for invading pathogens to manipulate the host cell, it is further considered that the autophagic response to pathogen invasion may have also evolved as an early host defense program of eukaryotic cells [21, 22]. Interestingly enough, this hypothesis explains that (i) autophagy is in part a stochastic degradation pathway to clear the cytoplasm, thereby securing the functionality of both proteins and the endomembrane system, but is also (ii) a specific response triggered by certain stress exposures, such as pathogen invasion. In fact, the autophagic response to pathogen invasion has been identified because autophagy-related proteins (ATG) essential to the stochastic process of autophagy, such as Atg5 and LC3, have also been found to decorate membranes harboring intracellular pathogens, and to be functionally involved in the cellular response to pathogens [4, 23]. Still, molecular mechanisms of autophagic responses to pathogen exposure are insufficiently understood.

Bacterial pathogens employ a variety of mechanisms to manipulate host cell membranes [24, 25]. Commonly, many bacteria interfere with the phosphoinositide metabolism that is often targeted by bacterial virulence factors [26]. Among the phosphoinositides, PtdIns(3)P is the essential variant for the forming autophagosomal membrane, hence it can be anticipated that PtdIns(3)P might commonly interconnect bacterial infection with the autophagic pathway. In fact, it has been shown that PtdIns(3)P is involved in the formation of Salmonella-containing vacuoles serving as a niche in host cells, and that PtdIns(3)P is targeted by *M. tuberculosis* to inhibit phagosome maturation [27].

Here, we addressed this question by investigating the process of *S. aureus* invasion of tumor cells.

A study by Schnaith and coworkers suggested a model that connected the autophagic response with *S. aureus* infection via the bacterial *agr* virulence factor [14]. In this model, late phagosomes with (i) *agr*-positive *S. aureus* become entrapped in autophagosome-like vesicles, where *S. aureus* replicate and subsequently escape into the cytoplasm to promote host cell death, but (ii) *agr*-deficient *S. aureus* are subjected to lysosomal degradation [14].

We here provide evidence, that exposure of non-professional host cells (tumor cells) to Staphylococci stimulates the canonical WIPI-1 response at the onset of autophagy, which is to bind to PtdIns(3)P at the phagophore to foster the recruitment of downstream ATGs, such as Atg5 and LC3 [9, 28]. Interestingly, this response is attributable to the interaction of Staphylococci with the host cell membrane, as we found WIPI-1 to become stimulated upon both non-invasive and invasive Staphylococci. In line, WIPI-1 was also stimulated upon peptidoglycan treatment (data not shown). By further analyzing invasive *S. aureus* strains in this study, we identified new WIPI-1 positive autophagosome-like vesicles that entrapped multiple *S. aureus* particles. And moreover, *agr*-positive *S. aureus* strains were more efficiently entrapped when compared to *agr*-deficient *S. aureus* cells. Our results demonstrate that WIPI-1, a principal PtdIns(3)P effector at the onset of stochastic, canonical autophagy, is also involved in selective engagement of the autophagic pathway, moreover underscored by the notion that Staphylococci prominently stimulated WIPI-1 in nutrient-rich conditions. And, our results demonstrate that *S. aureus* (i) stimulates autophagy and (ii) in addition, becomes entrapped in WIPI-1 positive autophagosome-like vesicles.

The most compelling explanation would be that WIPI-1 becomes stimulated upon *S. aureus* interaction with the plasma membrane, subsequently WIPI-1 positive phagophore membranes, e.g. originated from the endoplasmic reticulum, are utilized to sequester *S. aureus* where bacterial replication occurs. In addition, we also found *S. aureus* particles sequestered in phagosomes, marked by the FYVE domain [29], which are intended for phagocytosis. Hence our results can be viewed as host cell response to *S. aureus*, critically involving PtdIns(3)P membranes that either serve as phagosome membranes, or that are utilized to further sequester *S. aureus*, thereby generating a replication niche. Evidence that bacterial replication occurs is given by our electron microscopy analysis showing dividing *S. aureus* cells within the sequestering vesicle. The importance of PtdIns(3)P-enriched membranes during sequestration of invading *S. aureus* is further emphazised by our finding that more WIPI-1 positive autophagosome-like vesicles entrap *S. aureus* cells when phosphorylation of PtdIns(3)P to PtdIns(3,5)P_2 by PIKfyve was specifically blocked.

PtdIns(3)P-enriched membranes promote vesicle fusion with lysosomes. In line, FYVE domain marked phagosomes that carry *S. aureus* would be subjected to phagocytosis as suggested [14]. If WIPI-1 positive autophagosome-like vesicles entrapping *S. aureus* identified in this study, would reflect cytoplasmic sequestration of invaded *S. aureus* with PtdIns(3)P-enriched WIPI-1 positive phagophores, the resulting autophagosome-like vesicles should become subjected to fusion with the lysosomal compartment, because they are enriched in PtdIns(3)P. But, it was shown that lysosomal fusion is blocked upon *S. aureus* invasion [14]. To address this question we employed bafilomycin A_1 to inhibit the functionality of the lysosomal compartment. Clearly, lysosomal inhibition significantly increased the number of WIPI-1 positive autophagosome-like vesicles harboring *agr*-positive Staphylococci. This demonstrates that non-professional host cells employ autophagy as a defense response with regards to *S. aureus* infection, in line with previous suggestions [30]. However, under some circumstances [14] bacterial replication and vesicle escape might override this cellular defense program.

Acknowledgements. We kindly thank Marianne Opalka for technical assistance. This work was supported by grants from the Federal Ministry for Education and Science (BMBF, BioProfile) and the German Research Society (DFG, SFB 773) to TP-C.

References

1. Z. Yang and D.J. Klionsky, "Eaten alive: a history of macroautophagy," *Nature Cell Biology,* vol. 12,no. 9, pp. 814-822, 2010.
2. Z. Yang and D.J. Klionsky, "Mammalian autophagy: core molecular machinery and signaling regulation," *Current Opinion in Cell Biology,* vol. 22,no. 2, pp. 124-131, 2010.
3. J. Kim, M. Kundu, B. Viollet and K.L. Guan, "AMPK and mTOR regulate autophagy through direct phosphorylation of Ulk1," *Nature Cell Biology,* vol. 13,no. 2, pp. 132-141, 2011.
4. A. van der Vaart, M. Mari and F. Reggiori, "A picky eater: exploring the mechanisms of selective autophagy in human pathologies," *Traffic,* vol. 9,no. 3, pp. 281-289, 2008.
5. N. Mizushima, B. Levine, A.M. Cuervo and D.J. Klionsky, "Autophagy fights disease through cellular self-digestion," *Nature,* vol. 451,no. 7182, pp. 1069-1075, 2008.
6. T. Noda, K. Matsunaga and T. Yoshimori, "Atg14L recruits PtdIns 3-kinase to the ER for autophagosome formation," *Autophagy,* vol. 7,no. 4, pp., 2011.
7. T. Proikas-Cezanne and P. Codogno, "Beclin 1 or not Beclin 1," *Autophagy,* vol. 7,no. 7, pp. 671-672, 2011.

8. T. Proikas-Cezanne, S. Waddell, A. Gaugel et al., "WIPI-1alpha (WIPI49), a member of the novel 7-bladed WIPI protein family, is aberrantly expressed in human cancer and is linked to starvation-induced autophagy," *Oncogene,* vol. 23,no. 58, pp. 9314-9325, 2004.
9. M. Mauthe, A. Jacob, S. Freiberger et al., "Resveratrol-mediated autophagy requires WIPI-1 regulated LC3 lipidation in the absence of induced phagophore formation," *Autophagy,* vol. 7,no. 12, pp., 2011.
10. T. Proikas-Cezanne and H. Robenek, "Freeze-fracture replica immunolabelling reveals human WIPI-1 and WIPI-2 as membrane proteins of autophagosomes," *Journal of Cellular and Molecular Medicine,* vol. 15,no. 9, pp. 2007-2010, 2011.
11. T. Proikas-Cezanne, S. Ruckerbauer, Y.D. Stierhof, C. Berg and A. Nordheim, "Human WIPI-1 puncta-formation: a novel assay to assess mammalian autophagy," *FEBS Letters,* vol. 581,no. 18, pp. 3396-3404, 2007.
12. B. Levine, N. Mizushima and H.W. Virgin, "Autophagy in immunity and inflammation," *Nature,* vol. 469,no. 7330, pp. 323-335, 2011.
13. I. Fedtke, F. Gotz and A. Peschel, "Bacterial evasion of innate host defenses--the Staphylococcus aureus lesson," *International Journal of Medical Microbiology,* vol. 294,no. 2-3, pp. 189-194, 2004.
14. A. Schnaith, H. Kashkar, S.A. Leggio et al., "Staphylococcus aureus subvert autophagy for induction of caspase-independent host cell death," *Journal of Biological Chemistry,* vol. 282,no. 4, pp. 2695-2706, 2007.
15. S.G. Pfisterer, M. Mauthe, P. Codogno and T. Proikas-Cezanne, "Ca2+/Calmodulin-dependent Kinase Signaling via CaMKI and AMPK Contributes to the Regulation of WIPI-1 at the Onset of Autophagy," *Molecular Pharmacology,* vol.,no., 2011.
16. A. Grotemeier, S. Alers, S.G. Pfisterer et al., "AMPK-independent induction of autophagy by cytosolic Ca2+ increase," *Cellular Signalling,* vol. 22,no. 6, pp. 914-925, 2010.
17. R. Rosenstein and F. Götz, "Genomic differences between the food-grade Staphylococcus carnosus and pathogenic staphylococcal species," *International Journal of Medical Microbiology,* vol. 300,no. 2-3, pp. 104-108, 2010.
18. T. Proikas-Cezanne and S.G. Pfisterer, "Assessing mammalian autophagy by WIPI-1/Atg18 puncta formation," *Methods in Enzymology,* vol. 452,no. 247-260, 2009.
19. H. Robenek, M.J. Robenek, I. Buers et al., "Lipid droplets gain PAT family proteins by interaction with specialized plasma membrane domains," *The Journal of biological chemistry,* vol. 280,no. 28, pp. 26330-26338, 2005.

20. H.B. Jefferies, F.T. Cooke, P. Jat et al., "A selective PIKfyve inhibitor blocks PtdIns(3,5)P(2) production and disrupts endomembrane transport and retroviral budding," *EMBO reports,* vol. 9,no. 2, pp. 164-170, 2008.
21. B. Levine, "Eating oneself and uninvited guests: autophagy-related pathways in cellular defense," *Cell,* vol. 120,no. 2, pp. 159-162, 2005.
22. R. Sumpter, Jr. and B. Levine, "Autophagy and innate immunity: triggering, targeting and tuning," *Seminars in Cell and Developmental Biology,* vol. 21,no. 7, pp. 699-711, 2010.
23. M.C. Lerena, C.L. Vazquez and M.I. Colombo, "Bacterial pathogens and the autophagic response," *Cellular Microbiology,* vol. 12,no. 1, pp. 10-18, 2010.
24. S. Shahnazari and J.H. Brumell, "Mechanisms and consequences of bacterial targeting by the autophagy pathway," *Current Opinion in Microbiology,* vol. 14,no. 1, pp. 68-75, 2011.
25. H. Ham, A. Sreelatha and K. Orth, "Manipulation of host membranes by bacterial effectors," *Nature Reviews: Microbiology,* vol. 9,no. 9, pp. 635-646, 2011.
26. J. Pizarro-Cerda and P. Cossart, "Subversion of phosphoinositide metabolism by intracellular bacterial pathogens," *Nature Cell Biology,* vol. 6,no. 11, pp. 1026-1033, 2004.
27. T. Noda and T. Yoshimori, "Molecular basis of canonical and bactericidal autophagy," *International Immunology,* vol. 21,no. 11, pp. 1199-1204, 2009.
28. E. Itakura and N. Mizushima, "Characterization of autophagosome formation site by a hierarchical analysis of mammalian Atg proteins," *Autophagy,* vol. 6,no. 6, pp. 764-776, 2010.
29. J.M. Gaullier, A. Simonsen, A. D'Arrigo et al., "FYVE fingers bind PtdIns(3)P," *Nature,* vol. 394,no. 6692, pp. 432-433, 1998.
30. S. Kageyama, H. Omori, T. Saitoh et al., "The LC3 recruitment mechanism is separate from Atg9L1-dependent membrane formation in the autophagic response against Salmonella," *Molecular Biology of the Cell,* vol. 22,no. 13, pp. 2290-2300, 2011.
31. L.K. McDougal, C.D. Steward, G.E. Killgore et al., "Pulsed-field gel electrophoresis typing of oxacillin-resistant Staphylococcus aureus isolates from the United States: establishing a national database," *Journal of Clinical Microbiology,* vol. 41,no. 11, pp. 5113-5120, 2003.
32. S. Herbert, A.K. Ziebandt, K. Ohlsen et al., "Repair of global regulators in Staphylococcus aureus 8325 and comparative analysis with other clinical isolates," *Infection and Immunity,* vol. 78,no. 6, pp. 2877-2889, 2010.

33. S. Iordanescu and M. Surdeanu, "Two restriction and modification systems in Staphylococcus aureus NCTC8325," *Journal of General Microbiology,* vol. 96,no. 2, pp. 277-281, 1976.

34. R. Rosenstein, C. Nerz, L. Biswas et al., "Genome analysis of the meat starter culture bacterium Staphylococcus carnosus TM300," *Applied and Environment Microbiology,* vol. 75,no. 3, pp. 811-822, 2009.

Tables

Table 1. Bacterial strains used in this study.

Bacterial strain	Relevant properties	Relevant genotype	Reference
S. aureus USA300	Pathogenic, community-associated methicillin-resistant *S. aureus* (CA-MRSA)	*agr* $^{+}$	[31]
S. aureus HG001	Pathogenic, methicillin-sensitive *S. aureus* (MSSA)	*agr* $^{+}$	[32]
S. aureus SA113	Pathogenic, methicillin-sensitive *S. aureus* (MSSA)	*agr* $^{-}$	[33]
S. carnosus TM300	Apathogenic, food grade staphylococcal species		[34]

Figure legends

Figure 1. GFP-WIPI-1 puncta formation upon serum- and amino acid starvation. GFP-WIPI-1 U2OS cells were treated with nutrient-rich culture medium (DMEM/FCS), serum-free culture medium (DMEM) or with medium lacking both serum and amino acids (EBSS) for 0.5, 1 and 2 h. Fluorescence images were automatically acquired and 2 h treatment images are shown (A – C). The numbers of GFP-WIPI-1 puncta-positive cells (D) and number of GFP-WIPI-1 puncta per cell (E) was automatically determined. Each measure point represents mean values from up to 3000 individually analyzed cells per treatment condition ± SD (n=2, each in triplicates). Scale bars: 20 µm.

Figure 2. GFP-WIPI-1 images upon infection of U2OS cells with *S. aureus* HG001. GFP-WIPI-1 U2OS cells were infected with *S. aureus* HG001 in DMEM/FCS for 2 h and images were automatically acquired. GFP-WIPI-1 fluorescence of the cells (indicated with the black dashed line) is shown, and cell nuclei are indicated (red dashed line) according to DAPI staining (not shown). Highlighted are the different GFP-WIPI-1 structures observed: large perinuclear GFP-WIPI-1 positive membranes (A) and cytoplasmic GFP-WIPI-1 puncta (B), reflecting canonical autophagosomal membranes. In addition, GFP-WIPI-1 positive autophagosomal-like vesicles appeared specifically upon infection (C). Scale bars: 20 µm. Supplementary information is provided (Suppl. Figure 1).

Figure 3. Automated image acquisition and analysis of stably expressing GFP-WIPI-1 U2OS cells with mCherry-expressing Staphylococci. Fluorescence images (middle panel) were automatically acquired using different emission/excitation filters for DAPI, GFP and mCherry (left panel). DAPI and GFP images were used to automatically detect individual cells, and GFP images were used for detecting and analyzing GFP-WIPI-1 puncta formation (indicated in the right panel). Additionally, for each of the individual cells the bacterial area was determined (indicated in the right panel) and a fused image was further used to determine the number of cells harboring WIPI-1 positive autophagosome-like vesicles entrapping Staphylococci.

Figure 4. Pathogenic *S. aureus* USA300 induces GFP-WIPI-1 puncta formation and becomes entrapped in GFP-WIPI-1 positive autophagosome-like vesicles. GFP-WIPI-1 U2OS cells were infected with mCherry-expressing *S. aureus* USA300 for 0.5, 1 and 2 h in DMEM/FCS, DMEM or EBSS. Automated image acquisition and analysis was conducted as described in Figure 3. The quantification of up to 2000 individual cells is presented for GFP-WIPI-1 (in green) and *S. aureus* USA300 (in red) using either DMEM/FCS (A), DMEM (B), or

EBSS (C) for infection ± SD (n=2, in duplicates). Representative images (2 h infection in DMEM/FCS) are shown (D). Scale bars: 20µm. From 100 infected cells for each of the treatment condition, the number of cells displaying GFP-WIPI-1 positive autophagosomal-like vesicles entrapping *S. aureus* USA300 was determined (E) ± SD (n=2, in duplicates).

Figure 5. **Pathogenic *S. aureus* HG001 induces GFP-WIPI-1 puncta formation and becomes entrapped in GFP-WIPI-1 positive autophagosome-like vesicles.** According to Figure 4, GFP-WIPI-1 U2OS cells were infected with mCherry-expressing *S. aureus* HG001 in DMEM/FCS (A), DMEM (B) and EBSS (C) and up to 2000 individual cells were analyzed. Images (2 h, DMEM/FCS) are shown (D). Scale bars: 20 µm. The number of cells displaying GFP-WIPI-1 positive autophagosomal-like vesicles entrapping *S. aureus* HG001 was determined (E) ± SD (n=2, in duplicates).

Figure 6. **Pathogenic *S. aureus* SA113 induces GFP-WIPI-1 puncta formation and becomes entrapped in GFP-WIPI-1 positive autophagosome-like vesicles.** According to Figure 4 and 5, GFP-WIPI-1 U2OS cells were infected with mCherry-expressing *S. aureus* SA113 in DMEM/FCS (A), DMEM (B) and EBSS (C) and analyzed (up to 2000 individual cells), representative images (2 h, DMEM/FCS) are shown (D, scale bars: 20µm) and the quantification of cells displaying GFP-WIPI-1 positive autophagosomal-like vesicles entrapping *S. aureus* SA113 is presented (E) ± SD (n=2, in duplicates).

Figure 7. Apathogenic *S. carnosus* TM300 cells are not entrapped in GFP-WIPI-1 positive autophagosome-like vesicles. According to Figure 4 – 6, GFP-WIPI-1 U2OS cells were infected with mCherry-expressing *S. carnosus* TM300 in DMEM/FCS (A), DMEM (B) and EBSS (C) and analyzed (up to 2000 individual cells). Representative images (2 h, DMEM/FCS) are presented (D, scale bars: 20µm). The number of cells with GFP-WIPI-1 positive autophagosomal-like vesicles entrapping *S. carnosus* TM300 is presented (E) ± SD (n=2, in duplicates).

Figure 8. **Bafilomycin A_1 and YM201636 treatments increased the number of GFP-WIPI-1 positive autophagosome-like vesicles entrapping Staphylococci.** GFP-WIPI-1 U2OS cells were infected with *S. aureus* USA300 in DMEM/FCS in the absence (control) or presence of 200 nM bafilomycin A_1 (Baf A_1), 800 nM YM201636 (YM), or with both (200 nM Baf A_1/ 800 nM YM) for 2 h. Images were automatically acquired (not shown). The number of GFP-WIPI-1 puncta-positive cells (A, right panel) and the number of GFP-WIPI-1 puncta per cell (B, right panel) was determined. From 100 infected cells for each of the treatment condition, the number of cells displaying GFP-WIPI-1 positive autophagosomal-like vesicles

entrapping *S. aureus* USA300 (A, left panel) and the number of GFP-WIPI-1 autophagosomal-like vesicles entrapping *S. aureus* USA300 per cell (B, left panel) was determined (n=3). *p<0.05, **p<0.01, ns: not significant.

Figure 9. Confocal laser scanning microscopy of *S. aureus* USA300 infected GFP-WIPI-1 or GFP-2xFYVE expressing U2OS cells. GFP-WIPI-1 (A) or GFP-2xFYVE (B) expressing U2OS cells were infected with *S. aureus* USA300 for 2 h in DMEM/FCS. Representative images (n=3) are shown. Magnifications display individual LSM sections (1-4). Scale bars: 20 µm.

Figure 10. Electron microscopy *S. aureus* USA300 infected GFP-WIPI-1 expressing U2OS cells. GFP-WIPI-1 U2OS cells were infected with *S. aureus* USA300 in DMEM/FCS followed by conventional electron microscopy. Either single *S. aureus* USA300 cells were found to reside within a vesicle (A), or multiple cells were found in enlarged vesicles (B). Red arrows indicate dividing Staphylococci. Scale bars: 500 nm.

Supplementary figure legends

Suppl. Figure 1. GFP-WIPI-1 images upon infection of U2OS cells with Staphylococci. Panel DMEM/FCS is presented as Figure 2. GFP-WIPI-1 U2OS cells were infected with *S. aureus* HG001 in DMEM/FCS, DMEM or EBSS for 2 h and images were automatically acquired. Black dashed lines: GFP-WIPI-1 fluorescence. Red dashed lines according to DAPI staining (not shown): cell nuclei. Scale bars: 20 µm.

Suppl. Figure 2. *S. aureus* USA300 infection of GFP-WIPI-1 expressing U2OS cells. Control images corresponding to Figure 4D. Scale bars: 20 µm.

Suppl. Figure 3. *S. aureus* HG001 infection of GFP-WIPI-1 expressing U2OS cells. Control images corresponding to Figure 5D. Scale bars: 20 µm.

Suppl. Figure 4. *S. aureus* SA113 infection of GFP-WIPI-1 expressing U2OS cells. Control images corresponding to Figure 6D. Scale bars: 20 µm.

Suppl. Figure 5. *S. carnosus* TM300 infection of GFP-WIPI-1 expressing U2OS cells. Control images corresponding to Figure 7D. Scale bars: 20 µm.

Suppl. Figure 6. Automated analysis of GFP-WIPI-1 puncta per cell numbers upon Staphylococci infection. This analysis corresponds to Figure 1E (A), Figure 4 (B), Figure 5 (C), Figure 6 (D) Figure 7 (E).

Suppl. Figure 7. Bacterial load of *S. aureus* USA300 infected GFP-WIPI-1 cells in the absence or presence of bafilomycin A_1 and YM201636. This analysis corresponds to Figure 8 (n=3). ns= not significant.

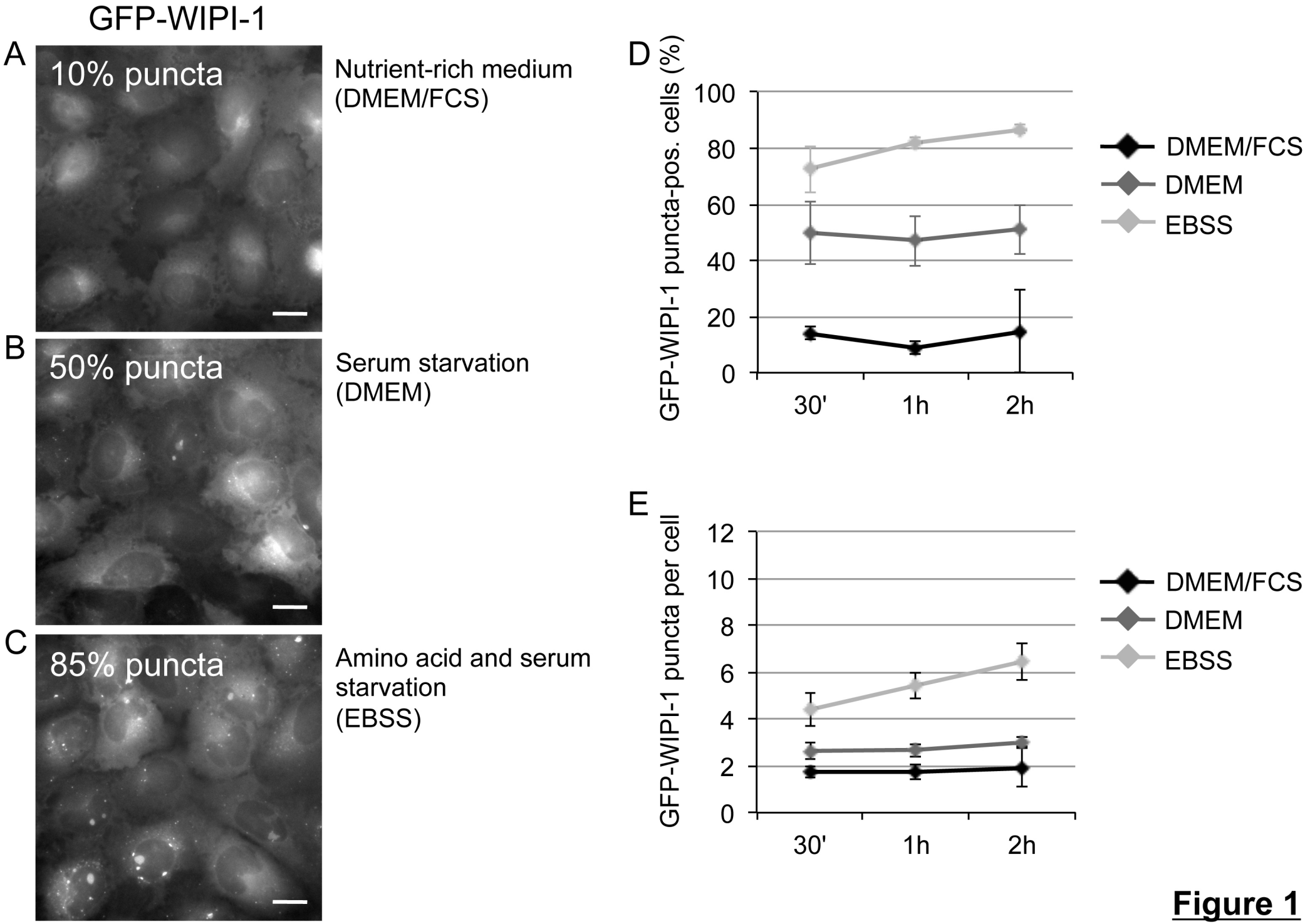
GFP-WIPI-1
A
10% puncta
Nutrient-rich medium
(DMEM/FCS)
B
50% puncta
Serum starvation
(DMEM)
C
85% puncta
Amino acid and serum
starvation
(EBSS)
D
GFP-WIPI-1 puncta-pos. cells (%)
100
80
60
40
20
0
30'
1h
2h
DMEM/FCS
DMEM
EBSS
E
GFP-WIPI-1 puncta per cell
12
10
8
6
4
2
0
30'
1h
2h
DMEM/FCS
DMEM
EBSS

Figure 1

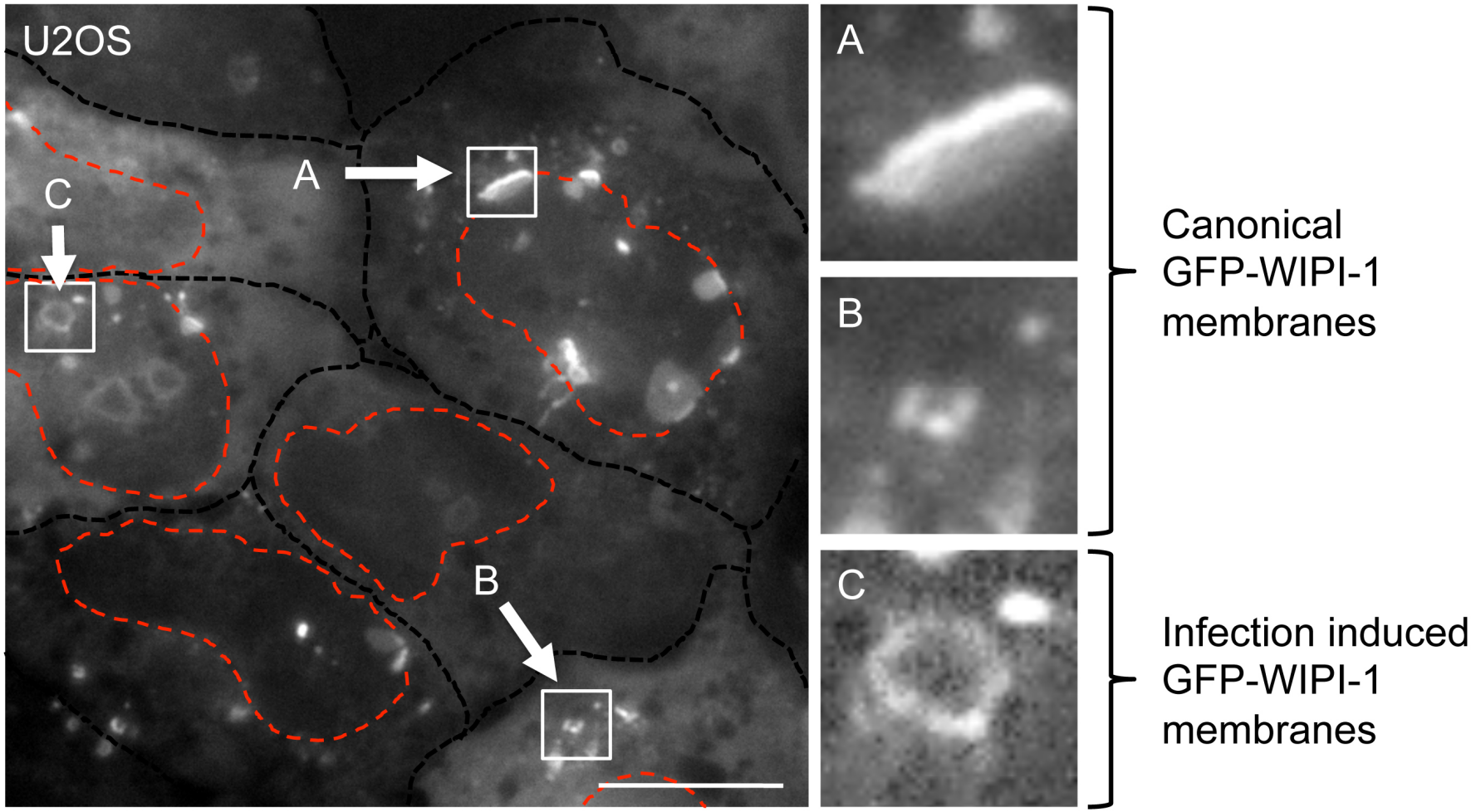
U2OS
A
B
C
A
B
C
Canonical
GFP-WIPI-1
membranes
Infection induced
GFP-WIPI-1
membranes

Figure 2

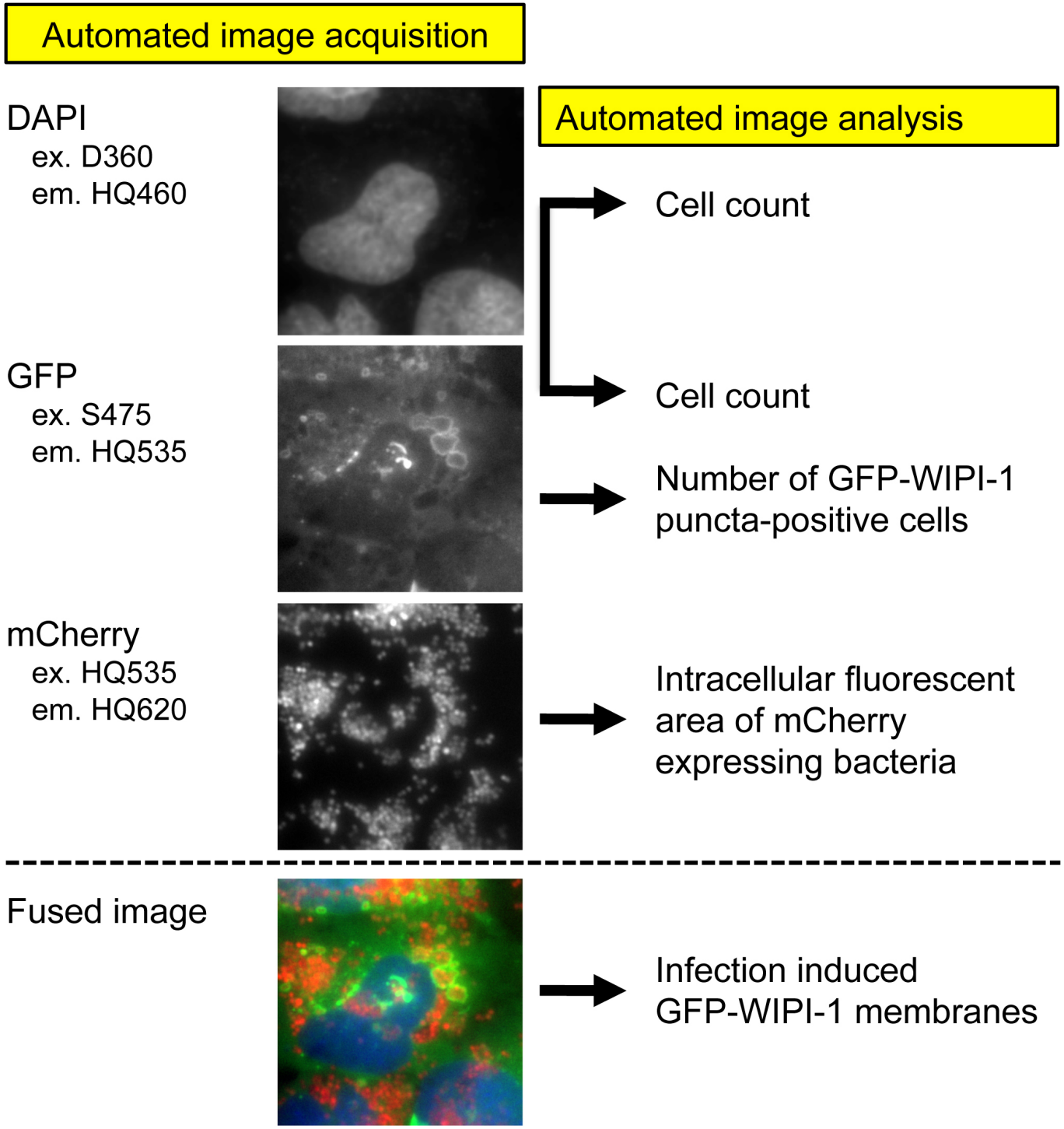
Automated image acquisition
DAPI
ex. D360
em. HQ460
GFP
ex. S475
em. HQ535
mCherry
ex. HQ535
em. HQ620
Fused image
Automated image analysis
Cell count
Cell count
Number of GFP-WIPI-1 puncta-positive cells
Intracellular fluorescent area of mCherry expressing bacteria
Infection induced GFP-WIPI-1 membranes

Figure 3

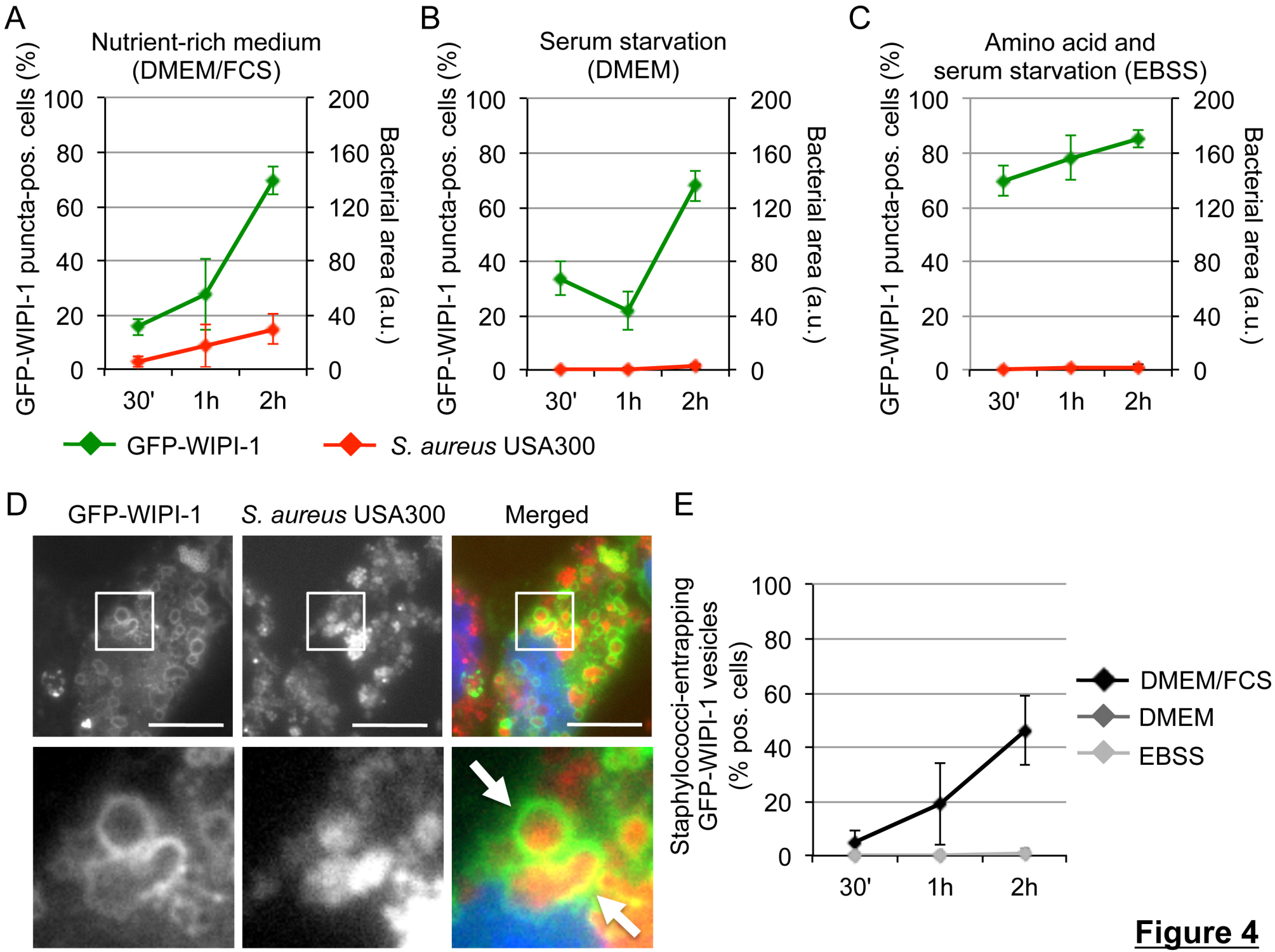
A
Nutrient-rich medium
(DMEM/FCS)
B
Serum starvation
(DMEM)
C
Amino acid and
serum starvation (EBSS)
GFP-WIPI-1 puncta-pos. cells (%)
Bacterial area (a.u.)
0
20
40
60
80
100
0
40
80
120
160
200
30'
1h
2h
GFP-WIPI-1
S. aureus USA300
D
GFP-WIPI-1
S. aureus USA300
Merged
E
Staphylococci-entrapping
GFP-WIPI-1 vesicles
(% pos. cells)
DMEM/FCS
DMEM
EBSS

Figure 4

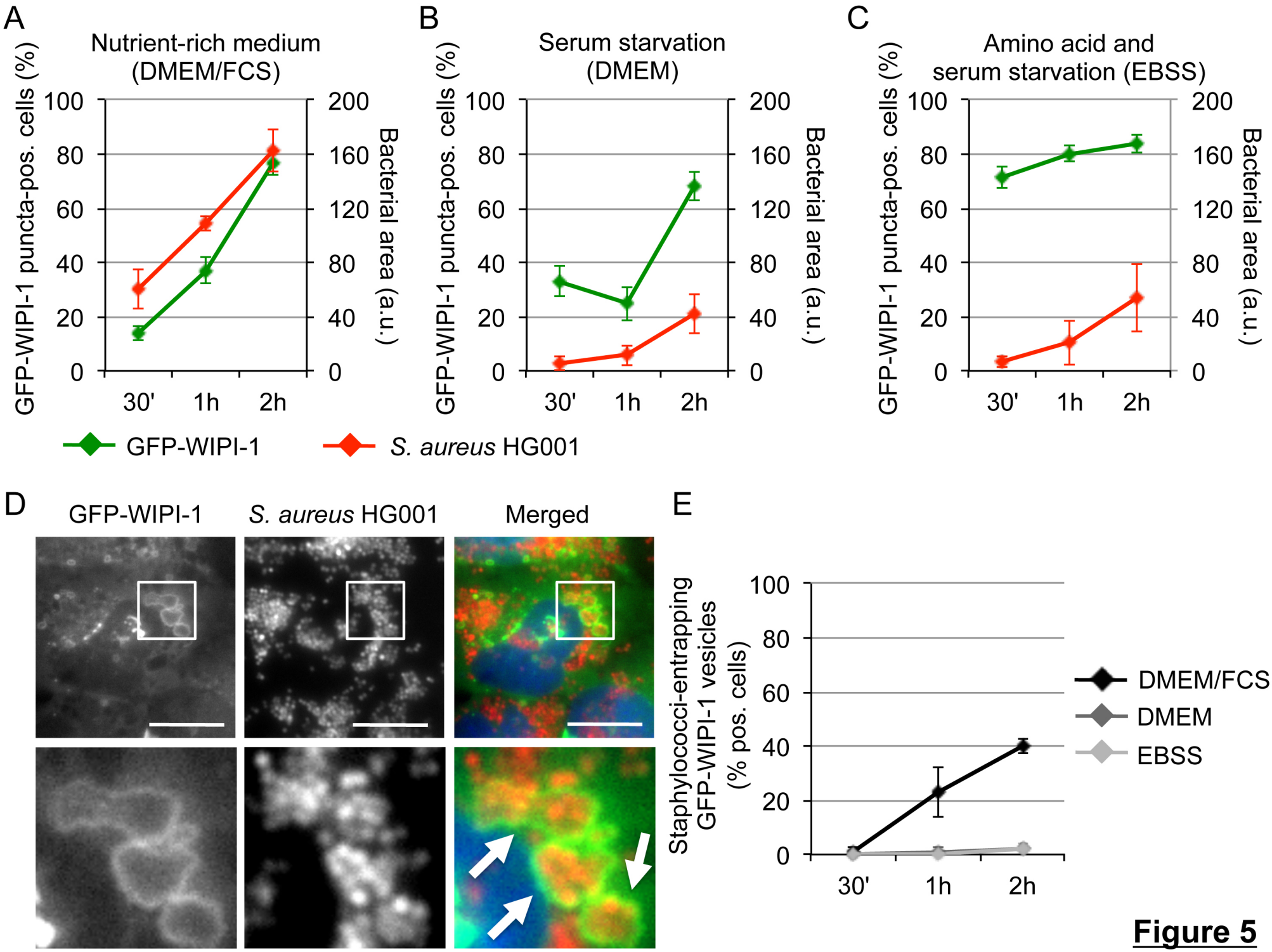
A
Nutrient-rich medium
(DMEM/FCS)
B
Serum starvation
(DMEM)
C
Amino acid and
serum starvation (EBSS)
GFP-WIPI-1 puncta-pos. cells (%)
Bacterial area (a.u.)
0
20
40
60
80
100
0
40
80
120
160
200
30'
1h
2h
GFP-WIPI-1
S. aureus HG001
D
GFP-WIPI-1
S. aureus HG001
Merged
E
Staphylococci-entrapping
GFP-WIPI-1 vesicles
(% pos. cells)
DMEM/FCS
DMEM
EBSS

Figure 5

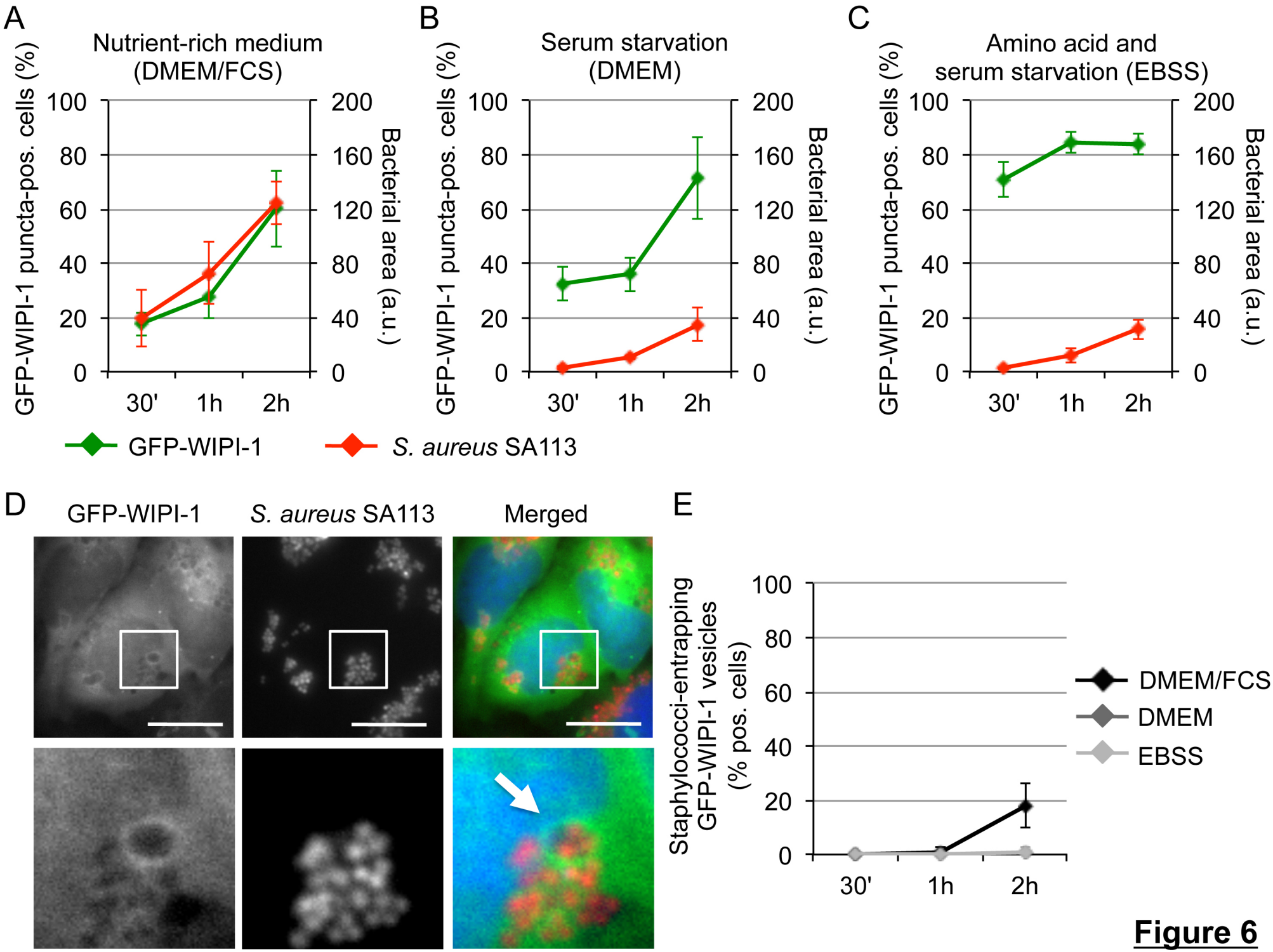
A
Nutrient-rich medium
(DMEM/FCS)
B
Serum starvation
(DMEM)
C
Amino acid and
serum starvation (EBSS)
GFP-WIPI-1 puncta-pos. cells (%)
Bacterial area (a.u.)
0
20
40
60
80
100
0
40
80
120
160
200
30'
1h
2h
GFP-WIPI-1
S. aureus SA113
D
GFP-WIPI-1
S. aureus SA113
Merged
E
Staphylococci-entrapping
GFP-WIPI-1 vesicles
(% pos. cells)
DMEM/FCS
DMEM
EBSS

Figure 6

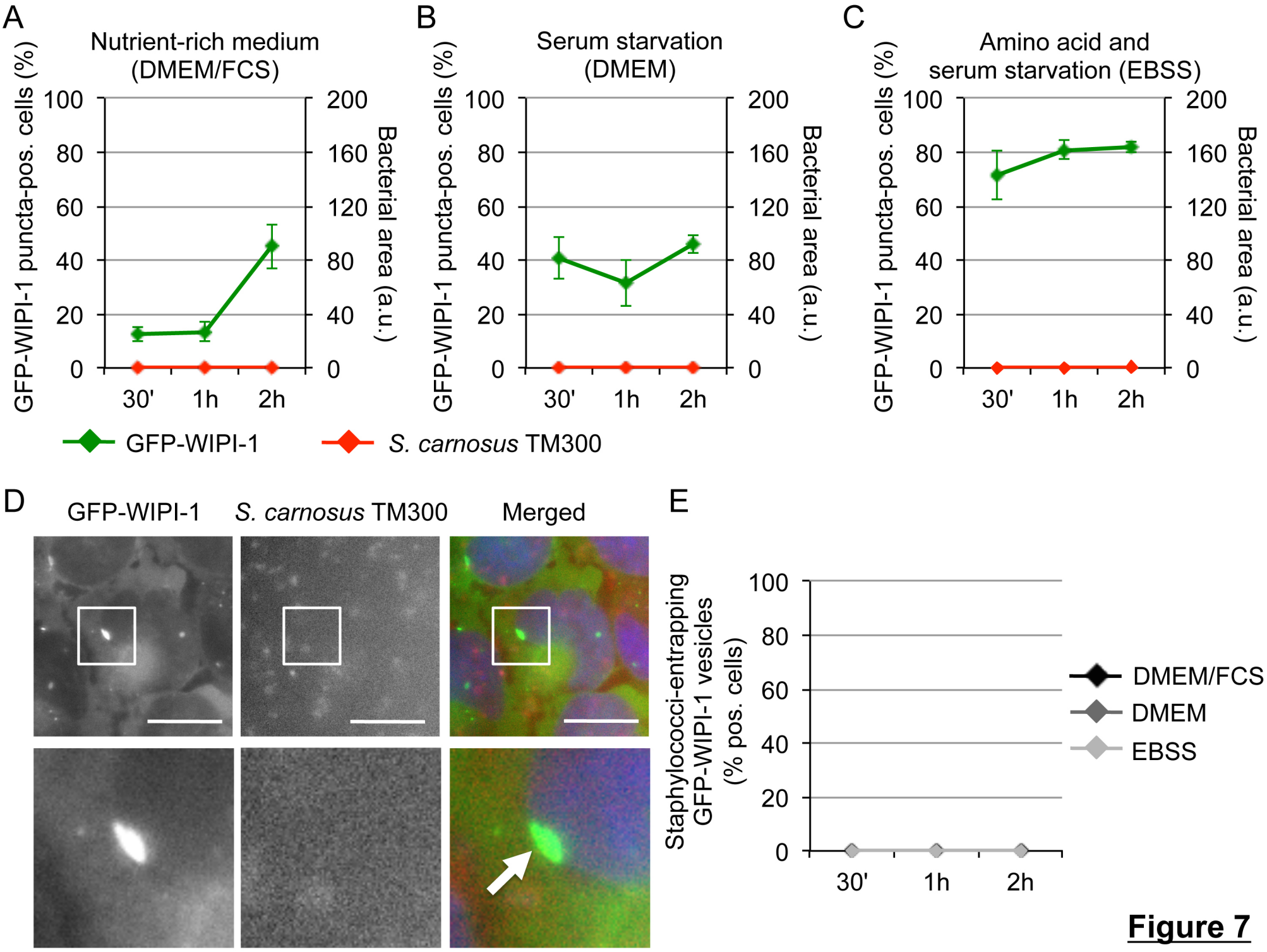
A
Nutrient-rich medium
(DMEM/FCS)
B
Serum starvation
(DMEM)
C
Amino acid and
serum starvation (EBSS)
GFP-WIPI-1 puncta-pos. cells (%)
Bacterial area (a.u.)
0
20
40
60
80
100
0
40
80
120
160
200
30'
1h
2h
GFP-WIPI-1
S. carnosus TM300
D
GFP-WIPI-1
S. carnosus TM300
Merged
E
Staphylococci-entrapping
GFP-WIPI-1 vesicles
(% pos. cells)
DMEM/FCS
DMEM
EBSS

Figure 7

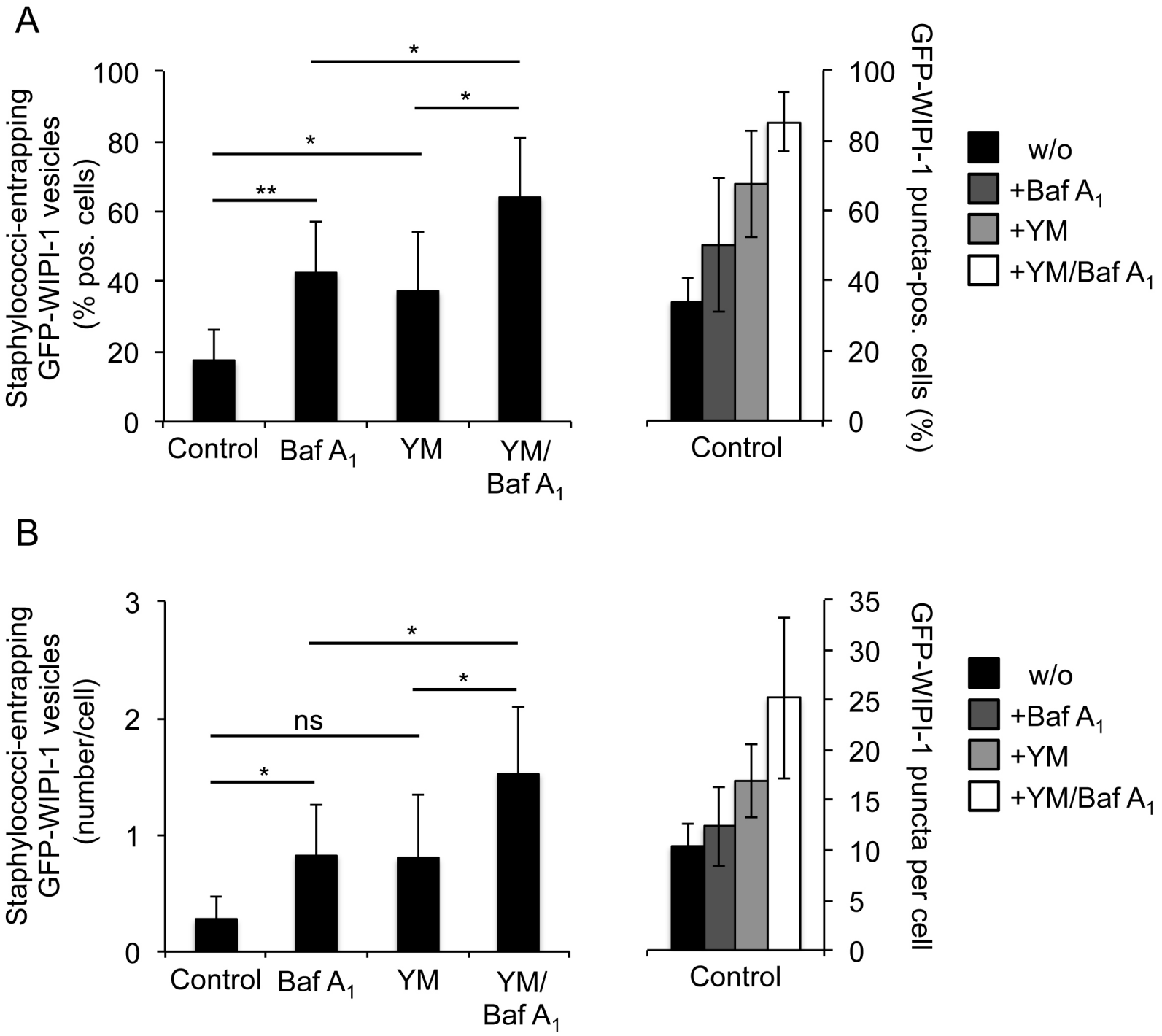
A
Staphylococci-entrapping GFP-WIPI-1 vesicles (% pos. cells)
100
80
60
40
20
0
*
*
*
**
Control
Baf A1
YM
YM/ Baf A1
GFP-WIPI-1 puncta-pos. cells (%)
Control
w/o
+Baf A1
+YM
+YM/Baf A1
B
Staphylococci-entrapping GFP-WIPI-1 vesicles (number/cell)
3
2
1
0
*
*
ns
*
Control
Baf A1
YM
YM/ Baf A1
GFP-WIPI-1 puncta per cell
35
30
25
20
15
10
5
0
Control
w/o
+Baf A1
+YM
+YM/Baf A1

Figure 8

A

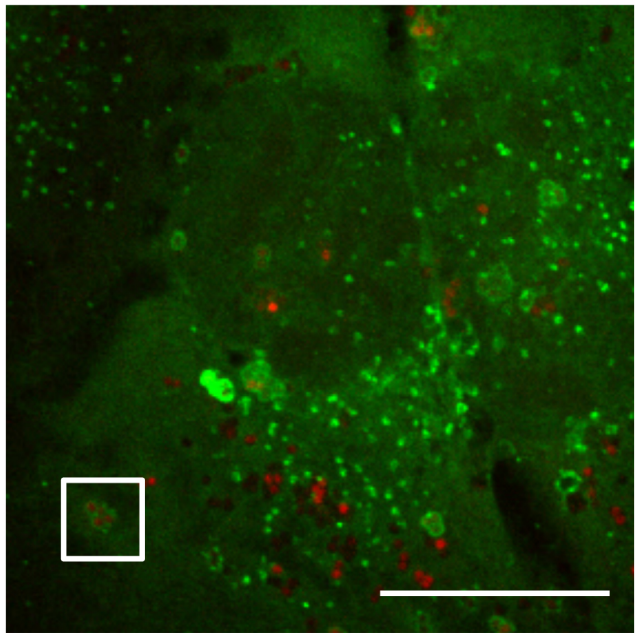

GFP-WIPI-1

Confocal LSM sections

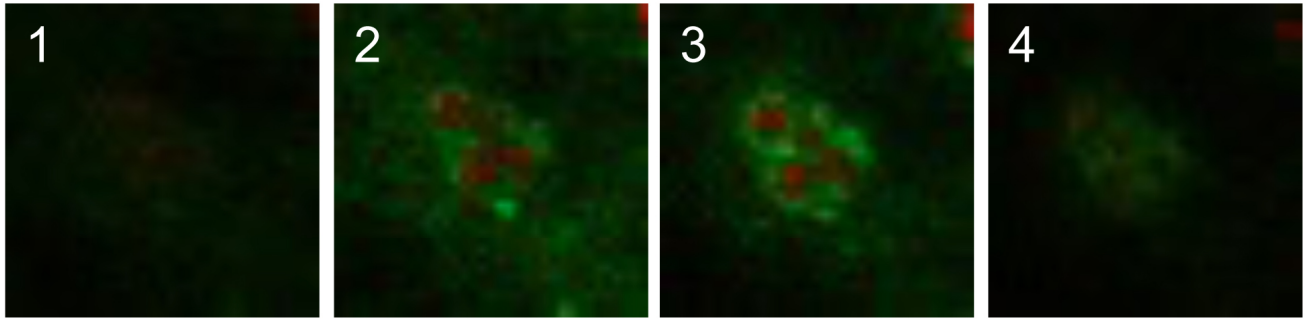

B

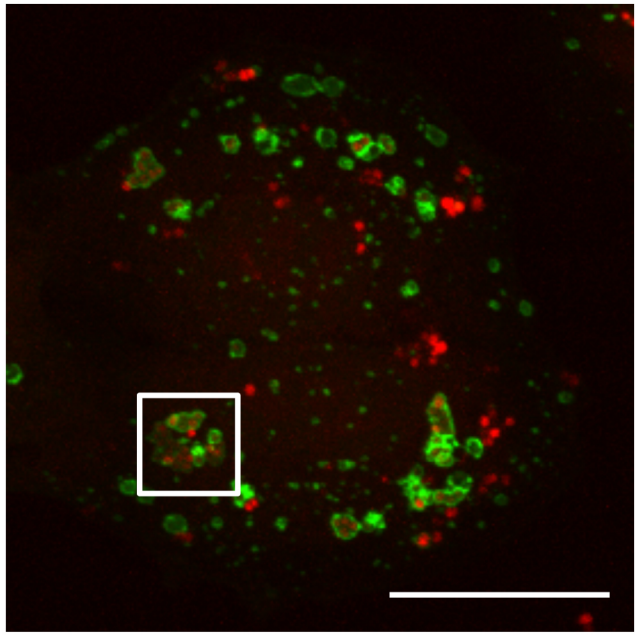

GFP-2xFYVE

Confocal LSM sections

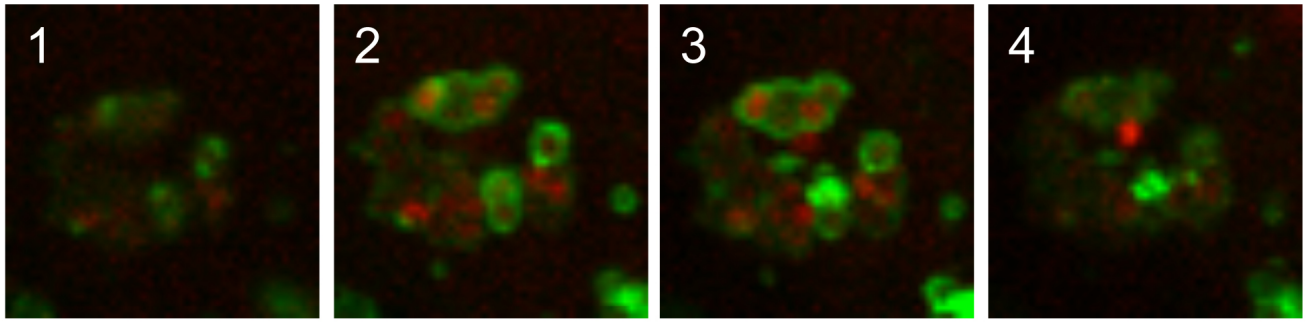

Figure 9

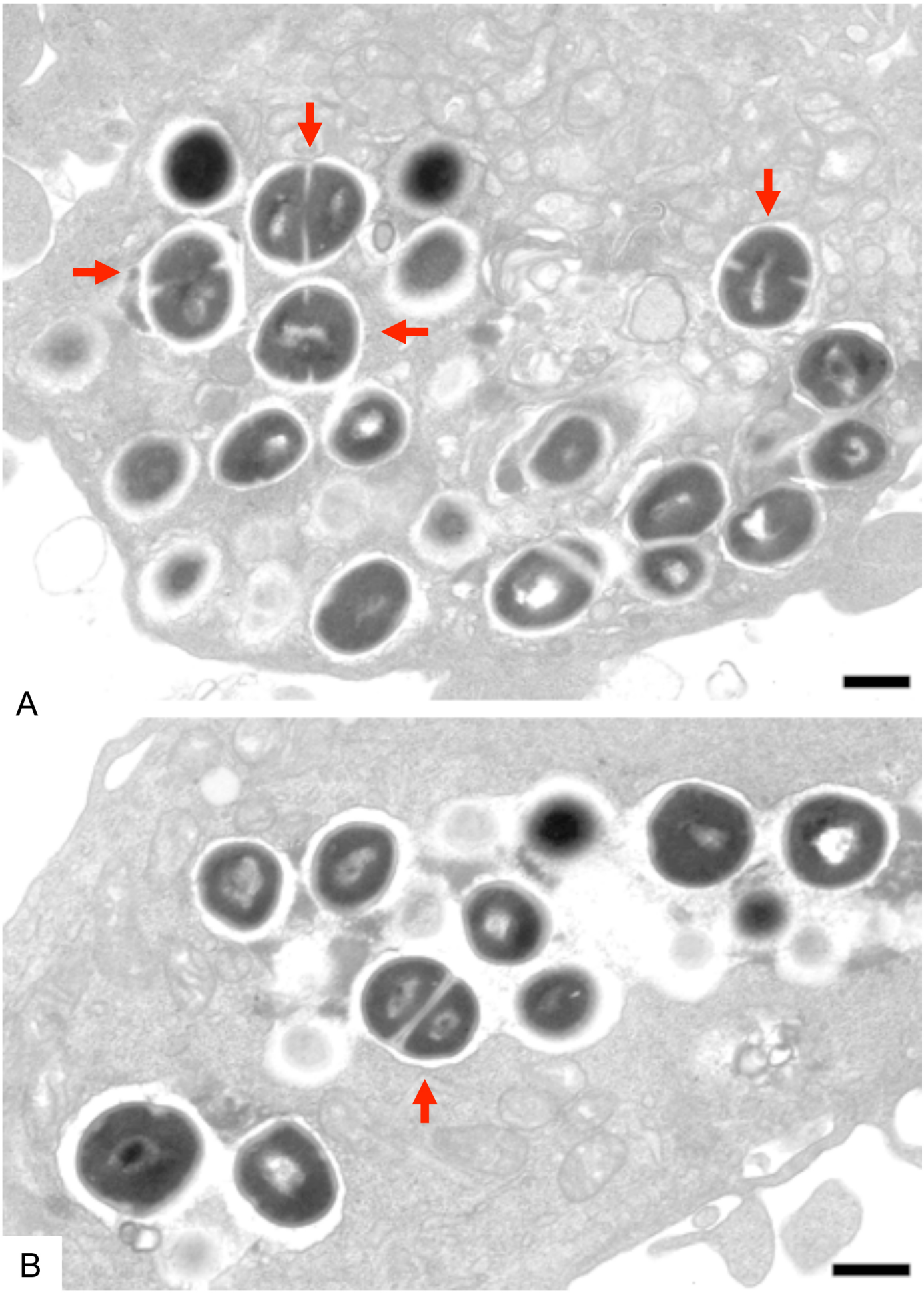

Figure 10

DMEM/FCS

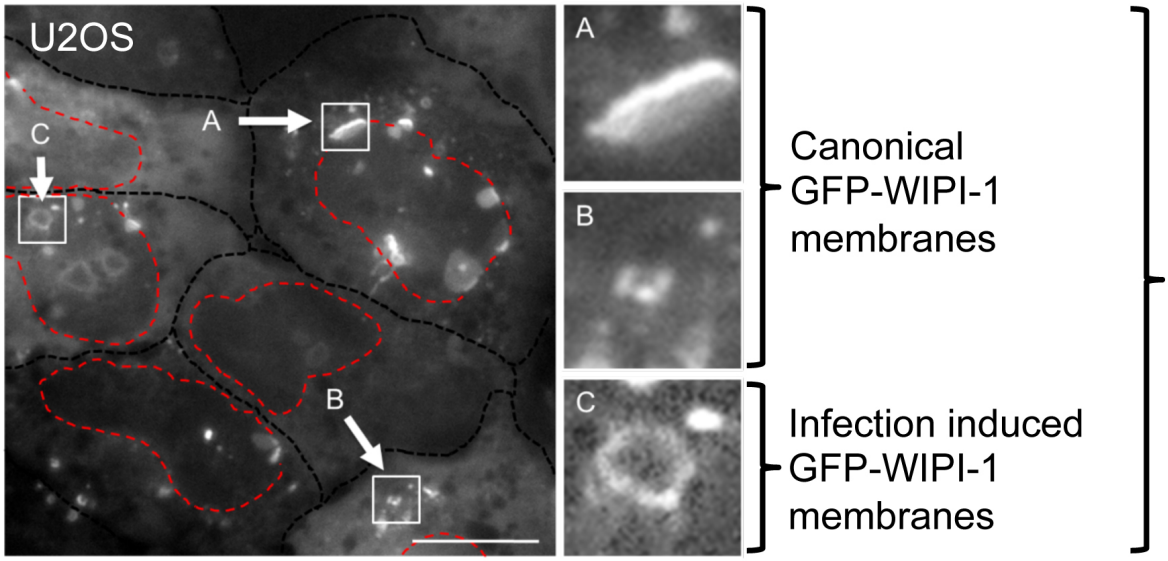

DMEM

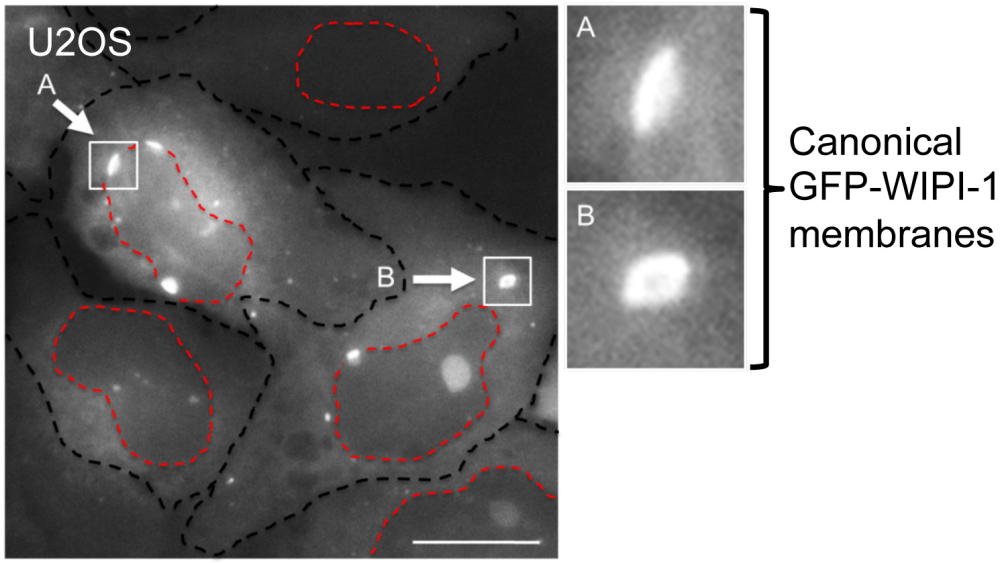

EBSS

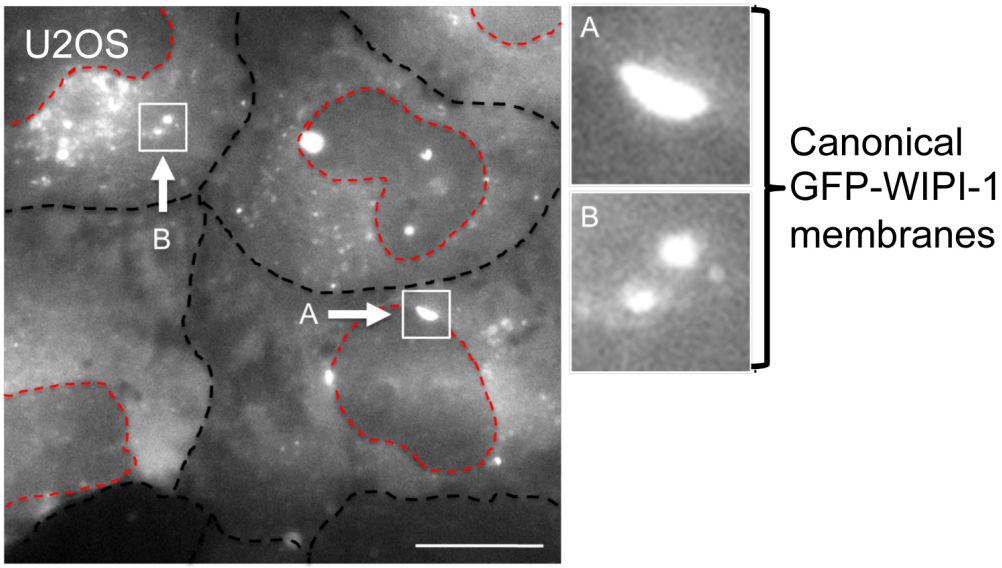

Suppl. Figure 1

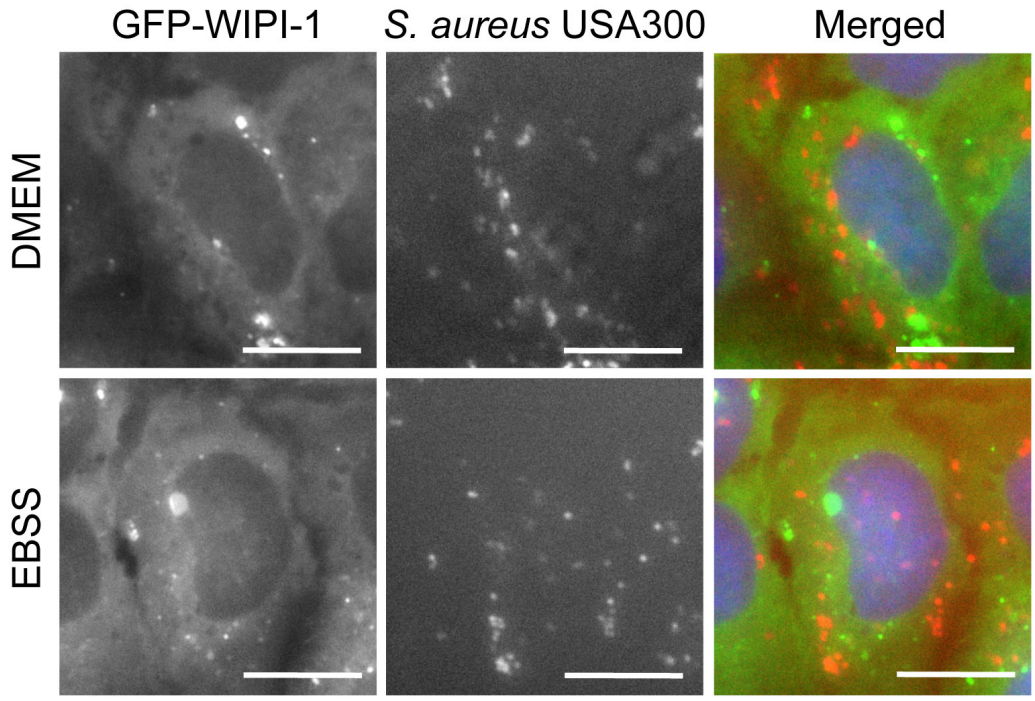

Suppl. Figure 2

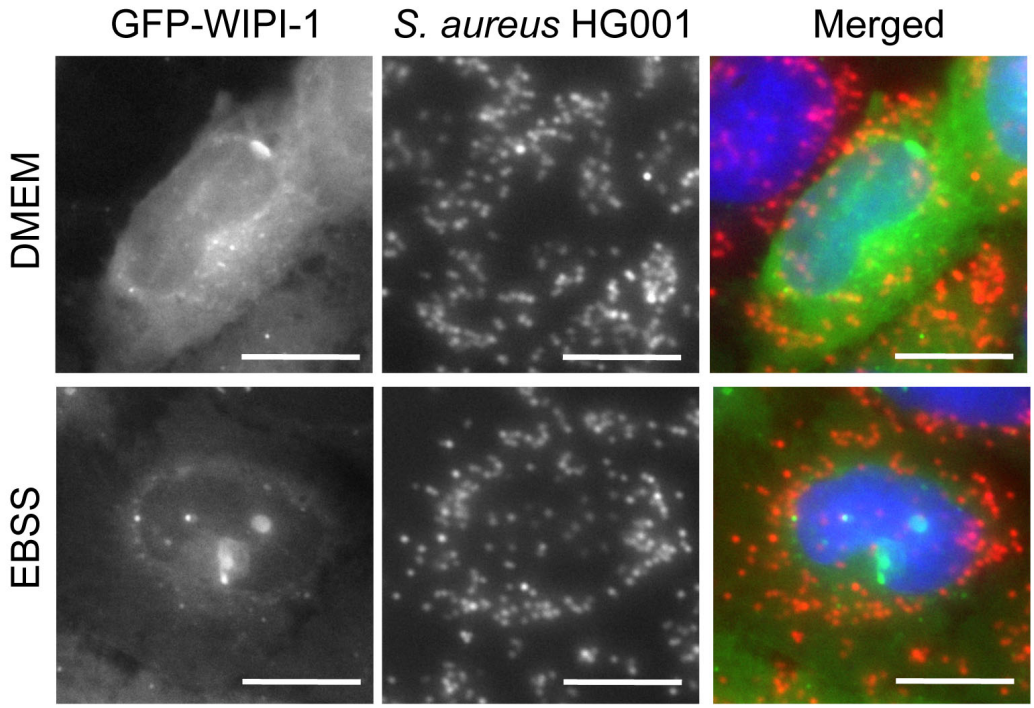

Suppl. Figure 3

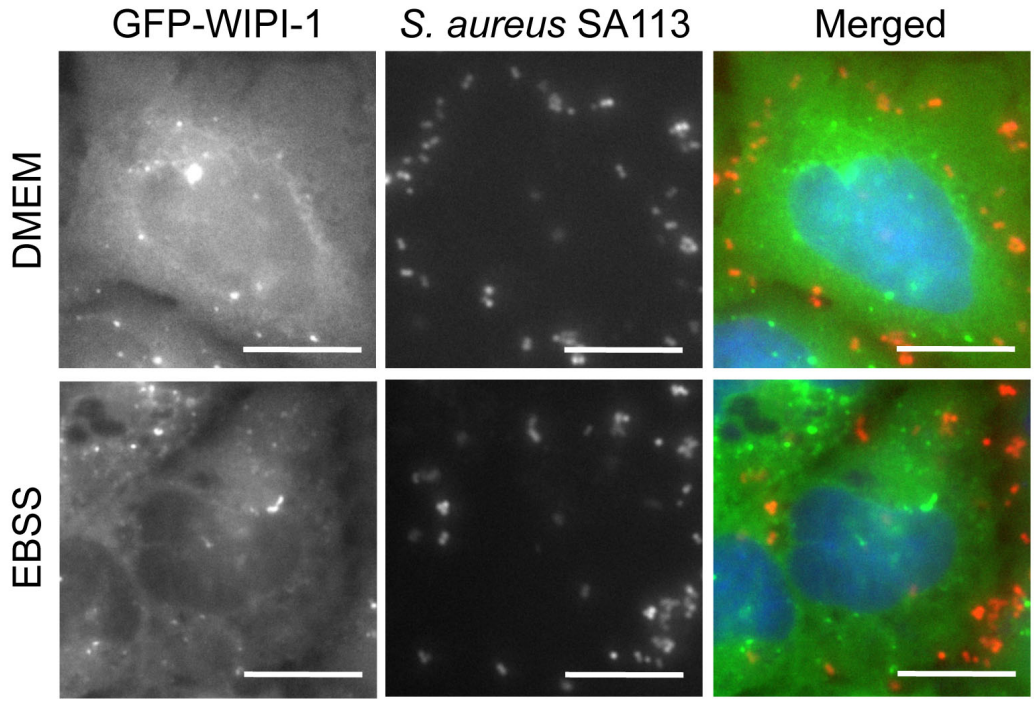

Suppl. Figure 4

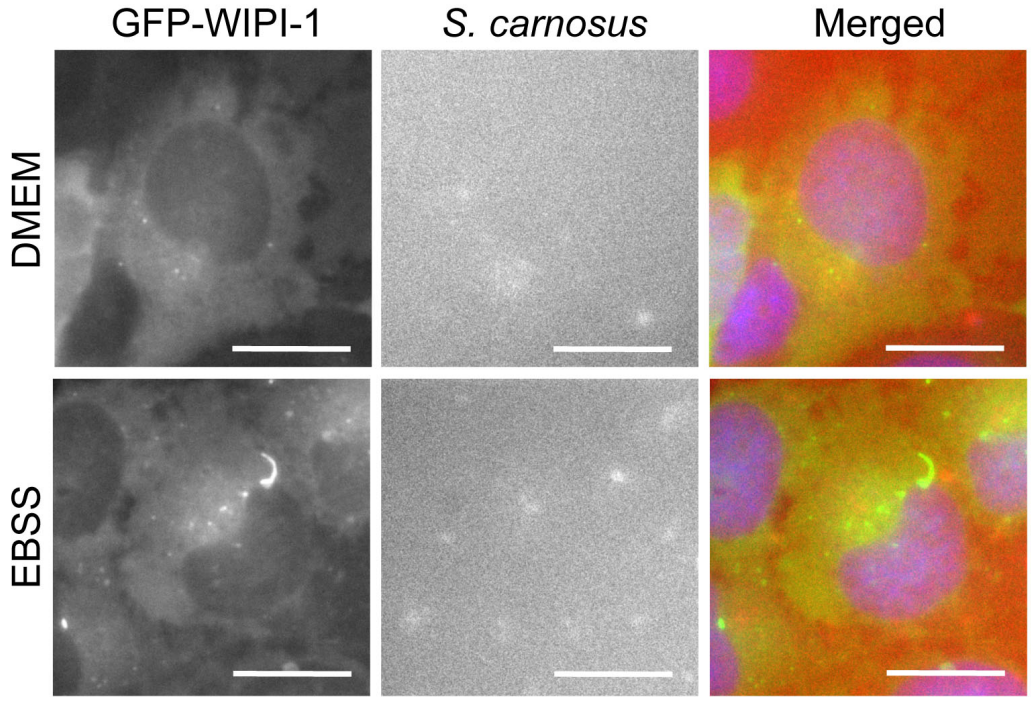

Suppl. Figure 5

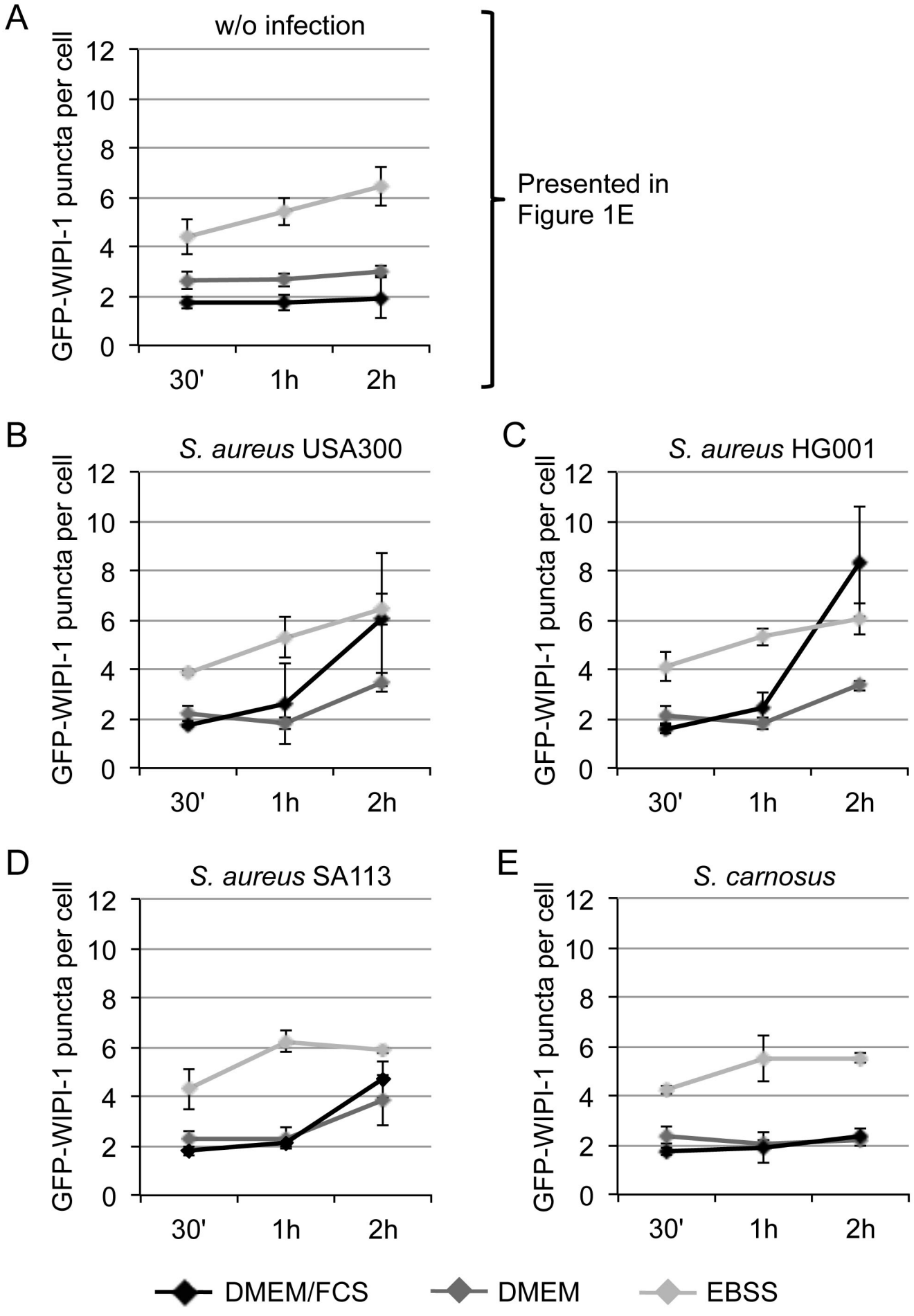

Suppl. Figure 6

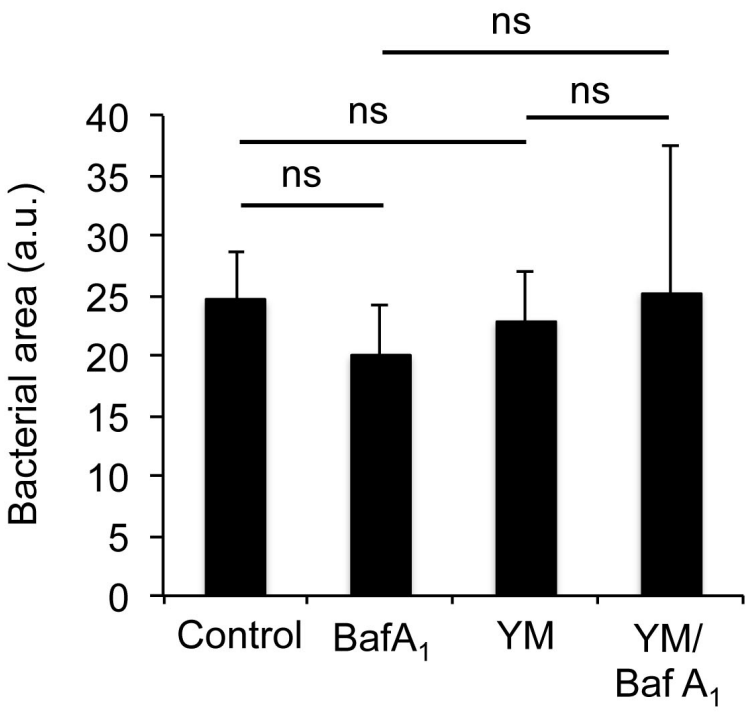

Suppl. Figure 7